PARAMETRIC ANALYSIS OF FIBRE LASER BEAM WELDING OF COPPER & SS 304

BY

AGNIBHA BANERJEE

B. TECH (MECHANICAL ENGINEERING), 2018

NIT DURGAPUR, W.B.

EXAMINATION ROLL NO. – M4PRD23005

THESIS

SUBMITTED IN PARTIAL FULFILLMENT OF THE REQUIREMENTS FOR THE AWARD OF THE DEGREE OF MASTER OF PRODUCTION ENGINEERING IN THE FACULTY OF ENGINEERING AND TECHNOLOGY

JADAVPUR UNIVERSITY

2023

DEPARTMENT OF PRODUCTION ENGINEERING

JADAVPUR UNIVERSITY

KOLKATA – 700032

INDIA

JADAVPUR UNIVERSITY

FACULTY OF ENGINEERING & TECHNOLOGY

Date:

CERTIFICATE OF RECOMMENDATION

I HEREBY RECOMMEND THAT THE THESIS ENTITLED **"PARAMETRIC ANALYSIS OF FIBRE LASER BEAM WELDING OF COPPER & SS 304"** CARRIED OUT UNDER MY/OUR GUIDANCE BY **MR. AGNIBHA BANERJEE** MAY BE ACCEPTED IN THE PARTIAL FULFILLMENT OF THE REQUIREMENTS FOR THE DEGREE OF **"MASTER OF PRODUCTION ENGINEERING".**

COUNTERSIGNED BY:

……

HEAD,

Dept. of Production Engineering
Jadavpur University
Kolkata-700032

……

DEAN,

Faculty of Engineering & Technology,
Jadavpur University
Kolkata-700032

THESIS ADVISOR:

……

(Prof. Arunanshu Shekhar Kuar)

Dept. of Production Engineering
Jadavpur University
Kolkata-700032

JADAVPUR UNIVERSITY

FACULTY OF ENGINEERING & TECHNOLOGY

CERTIFICATE OF APPROVAL*

The foregoing thesis is hereby approved as a creditable study of an engineering subject carried out and presented in a manner satisfactory to warrant its acceptance as a prerequisite to the degree for which it has been submitted. It is understood that by this approval, the undersigned do not necessarily endorse or approve any statement made, opinion expressed and conclusion drawn therein but thesis only for the purpose for which it has been submitted.

COMMITTEE ON FINAL EXAMINATION FOR EVALUATION OF THE THESIS

……
(External Examiner)

……..……..
(Internal Examiner)

*Only in case the recommendation is concurred in

ACKNOWLEDGEMENT

I would like to express my profound gratitude and thanks to my project guide Prof. Arunanshu Shekhar Kuar, Department of Production Engineering, Jadavpur University, Kolkata for introducing the present topic and intellectual support, inspiring guidance and his invaluable encouragement, suggestions and cooperation helps a lot to completion of my project work successfully.

I am also thankful to Prof. Bijoy Bhattacharyya, Former Head of Department, Production Engineering, Jadavpur University, Kolkata, for providing necessary information and guidance regarding the project. I would like to express my warmest gratitude to Prof. Bijan Sarkar, Head of Department, Production Engineering, Jadavpur University, Kolkata, for providing great support and guidance regarding the thesis. I am thankful to all respected professors and teachers of the department of Production Engineering who took keen interest in the work and gave their valuable suggestions.

I would also like to thank Mr. Dhiraj Kumar, Mr. Rajat Dutta, Mr. Kingshuk Mandal, Mr. Mohit Pandey, Research Scholars, Jadavpur University for their support and help throughout my thesis which made my work better.

I would like to convey my special thanks to my friends Somnath, Dwarika, Rajdeep, Arindam, Gourav and many more for their useful assistance, co-operation and constant support. I am also thankful to the librarian, technicians and other staff of our department for their cordial assistance throughout my thesis work.

I would like to thank Jadavpur University for providing me this wonderful opportunity and all my friends for their kind cooperation which helps me to complete my project.

I feel pleased and privileged to fulfil my parents' ambition, and I am greatly indebted to them for bearing the inconvenience during my M.Prod.E course. Thank you, my beloved parents.

.....

(AGNIBHA BANERJEE)

ABSTRACT

Copper and stainless-steel joints have a wide range of applications due to their excellent combination of strength and ductility, electrical and thermal conductivity, and excellent heat-transfer capability, such as fuel lines, brake systems, and electrical connections in the automotive industry, refrigeration units, aircraft components, missile systems, space vehicles, electrical transmission systems, electronic components, and so on. The current work used statistical design of experiments to conduct experimental examinations of continuous wave fibre laser beam welding of 1 mm thick commercially pure copper and stainless-steel grade 304 in butt configuration. Regression models are used to establish the relationship between process parameters such laser power, scanning speed, defocus distance, number of passes, & argon gas pressure and output responses like the width of the fusion zone and size of the heat impacted zone for both Cu and SS 304. ANOVA is used to calculate the percentage contributions of the most important process parameters and their optimum ranges on the output responses. It has been found that the welding process depends largely on the laser power, scanning speed, and defocus distance. The width of the fusion zone is also positively impacted by laser power, while all other parameters have a negative effect. While scanning speed and defocus distance have a detrimental effect on the width of the copper's heat-affected zone, laser power, the number of passes, and gas pressure have a favorable effect. The heat affected zone width of SS 304 is similarly affected positively by laser power and number of passes, while negatively by scanning speed, defocus distance, and gas pressure. The efficiency of the shielding gas is demonstrated by the decrease in the occurrence of longitudinal cracks caused by the production of brittle intermetallic compounds. ANOVA demonstrates the generated model's suitability in terms of accuracy. To achieve the best weld quality at the best process parameter setting, a single and multi-objective desirability function-based optimization technique is used. A comparison of optimization results obtained from PSO, TLBO and GWO is also carried out. The created model was found to be in good agreement with the outcomes of the validation experiment. The optimal parameter values are also used to create a set of samples for tensile and micro-hardness tests.

TABLE OF CONTENT

LIST OF FIGURES

LIST OF TABLES

CHAPTER 1

INTRODUCTION

1.1. Introduction

LASERS (Light Amplification by Stimulated Emission of Radiation) are optoelectronic devices which give a monochromatic beam of electromagnetic radiation with very low divergence. The 1954 invention MASER (Microwave Amplification by Stimulated Emission of Radiation) and the laser both work on the same principles. Around the time the laser was developed in 1960, the apparatus was known as an Optical MASER or an Infrared MASER. The term "LASER" has received broad popularity since around 1965. The development of high-power lasers is one of the important technological achievements. Focused high-power lasers have been very effectively used by material scientists and engineers as a unique wonder tool. Many metallurgical processes have been developed like laser welding, laser cutting, laser drilling, laser cladding, laser glazing etc. Laser welding is developing as a viable replacement for traditional welding processes due to its enhanced productivity and diversity.

Some lasers emit visible light, whereas others emit infrared or ultraviolet radiation that is invisible to the human eye. Although the wavelength of visible light is between 0.37 and 0.75μm, there are known lasers in the vacuum ultraviolet and microwave areas with wavelengths between 0.1 and 1 μm. Those with practical use have wavelengths between 0.2 and 500μm. Lasers come in a variety of sizes, from semiconductor lasers that are less than 1mm in diameter to those employed in nuclear fusion research that may be as large as 100m. But they fundamentally have the same core traits [1].

Lasers are currently being implemented in the automobile sector to make seam or stitch welds as a substitute for traditional resistance spot welding, which is commonly used to join auto-body panels to subassemblies, in the fields of biology, medicine, and even nuclear fusion. The benefits of laser welding over resistance spot welding stem from the small size of the laser spot, the weld's deep penetration into the material, and the demand for just single-sided access to the

workpiece [2]. Key advantages of laser welding include decreased flange widths, enhanced structural strength, and high-speed automated production.

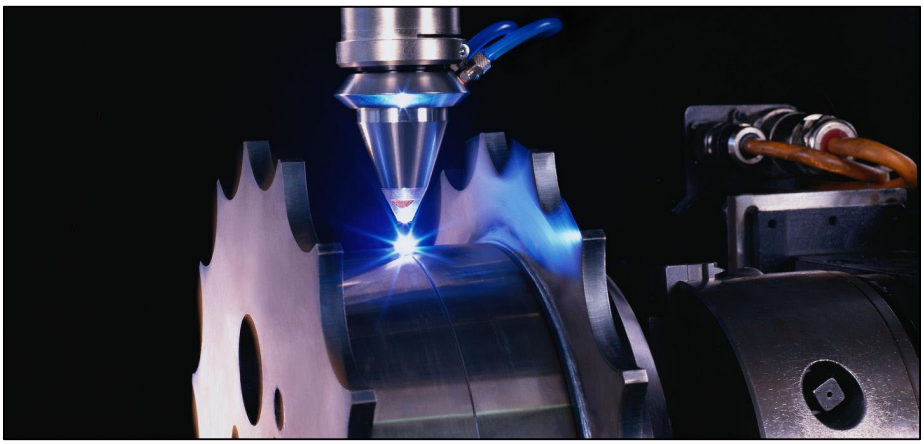

Fig. 1.1. Laser beam welding [3]

Traditionally CO2 lasers have been employed for car body applications. Significant breakthroughs have been achieved with Nd:YAG lasers, which are now capable of delivering beam strengths of more than 2 KW or more using a fibre optic connection. This is especially beneficial for robotic operations, when it is essential to control the laser beam around a fixed component. Lasers are also utilised in the fabrication of customised blanks, where adequately prepared sheet metal, including varying thickness and material combinations, are butt welded together prior to being pressed into the completed form. This leads in substantial cost and weight reductions and enhances structural rigidity [4]. Fibre lasers and Disk lasers are also very popular nowadays. In order to minimise weight, the usage of lighter materials like Al, Mg, and Ti will become more and more crucial in the automotive industry in the future. The capacity to create appropriate joints, nevertheless, will be necessary for this. Laser welding of Polymers, Composites and Ceramics have also become very prominent in Aerospace Industries applications.

1.2. Basic Principle of Laser

Laser light is created by amplifying stimulated emission. Since the emission energy is unique from its source and is a measurable amount, the light will have a single wavelength (monochromatic). The high-energy, single-wavelength light is converted into a spatially stable form (collimated or non-divergent), and the successive waveforms are in phase (coherent). The

coherence and collimation of the light therefore result in high energy density, and the monochromatic wavelength will identify specific target absorption [5].

1.2.1. Constituent elements of Laser

A laser is made up of three elements as shown in Fig. 1.2:

a) **Laser medium** – Material in which the laser is generated. It is positioned between two optically parallel, highly reflecting mirrors, one of which only partially reflects the beam. For solid state lasers the medium is typically comprised of a host material doped with active laser element.
b) **Pump Source** – Facilitates laser production by giving the laser medium the required activation energy. Electrical or optical pumping is possible, and the gain medium can be solid, liquid, or gas. It can enhance the amplitude of light waves passing through it via stimulated emission.
c) **Laser resonator** – Consists of a front half reflector and a rear 100% reflector, and regulates how the laser is produced in the laser medium. The gain medium is placed in such a fashion that light oscillating between the reflectors passes through it every time before emitting through the transmitting mirror after reaching adequate amplification.

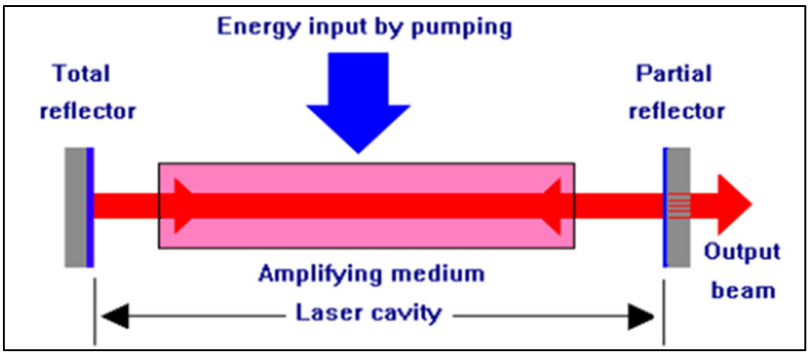

Fig. 1.2. Illustration of laser elements [6]

1.2.2. Principle of laser generation

The concept of energy level is important in laser emission, which takes place via transition between different energy levels of an atomic or molecular system. The interaction of light (laser) with tiny matters such as atoms, ions and molecules are understood by considering three

different processes: fluorescence or spontaneous emission, stimulated emission and amplification [7] and are depicted in Fig. 1.3.

a) **Spontaneous emission** – Upon stimulating the laser medium's atoms with energy (E = hv) from the pump source, the electrons in the excited atoms are momentarily raised to higher energy states. The electrons that are kept in this excited state eventually fall to a lower energy level since they can't stay there permanently. The electron in this activity emits a photon to release the extra energy it got from the pump energy. This phenomenon, known as spontaneous emission, generates the photons that set the foundation for laser production.

b) **Stimulated emission** – In the higher energy states, the photons released by spontaneous emission finally collide with other electrons. Due to the speed of light and density of excited atoms, this occurs in a remarkably little period of time. A new photon is produced when the incoming photon "knocks" the excited electron to a lower energy level. Because these two photons are coherent, they are moving in the same direction, at the same wavelength, and in phase. Stimulated emission is the name of this procedure.

c) **Amplification** - There is an all-around emission of photons. Some, though, pass through the laser medium and collide with the resonator mirrors before being reflected back into it. For stimulated emission, the favored amplification direction is determined by the resonator reflectors. The amplification requires that the proportion of atoms in the excited state exceed that of the lower energy levels. More atoms being in the excited state due to "population inversion" creates the environment required for laser production.

Lasing activity's basic premise is that an electron at a high energy level is compelled to transition to a lower energy level, resulting in the production of a photon with the same properties as the incoming photon that initiated the transition. Since the input photon must be absorbed, the higher state must contain more electrons than the lower state. This is referred to as a "population inversion" and is a rare occurrence because the thermal Boltzmann population distribution of an atom, which may contain ions and molecules, would have more electrons at the lower energy level.

By envisioning the most fundamental instance of a two-level atom, it is impossible to create a population inversion in this closed situation. Inverse correlations exist between the populations

at the lower and upper levels as well as the applied field's power and the rates of absorption and stimulated emission, respectively. This results in a maximum of 50% of the population in the upper state or no net change in the population at either level in the steady state. Since a population inversion cannot be established in a two-level system as a result, lasers need at least three participating energy levels [6].

The linewidth that corresponds to each laser wavelength is influenced by the gain bandwidth of the laser medium and the design of the optical resonator, which may include elements intended to purposely limit the linewidth, such as filters or etalons. If a laser can concurrently produce many lines, the first step in determining its operating wavelength is to use cavity mirrors that are highly reflecting only at the necessary wavelength. The low reflectivity of all the other lines' mirrors will prevent them from achieving the necessary laser activity. However, even a single laser line may effectively span a range of wavelengths. For instance, the "gain bandwidth" of a laser diode, which is several nanometers broad, corresponds to a range of wavelengths.

The electrons in the lasing material's atoms, ions, and molecules are typically at lower steady-state energies. The bulk of the lasing material's units are pumped with light energy from an excitation source, which causes them to become activated to higher energy levels. The situation when the population of the units in the higher level rises relative to its population at some adjacent lower level is known as a population inversion in the upper level with reference to the lower level. Right now, these units are in a dicey condition. They only hold onto this shape for a short period of time before deteriorating and reverting to their original energy state. There are two possible outcomes for this decay: stimulated emission, in which the photons create coherent light, and spontaneous emission, in which the units just decay to their ground state and produce random, directional light. During this stimulated transition, energy is released in the form of light photons that have the same direction and wavelength as the incoming photon. The intensity of the laser light is progressively increased until it is high enough to pass through the partly reflecting mirror.

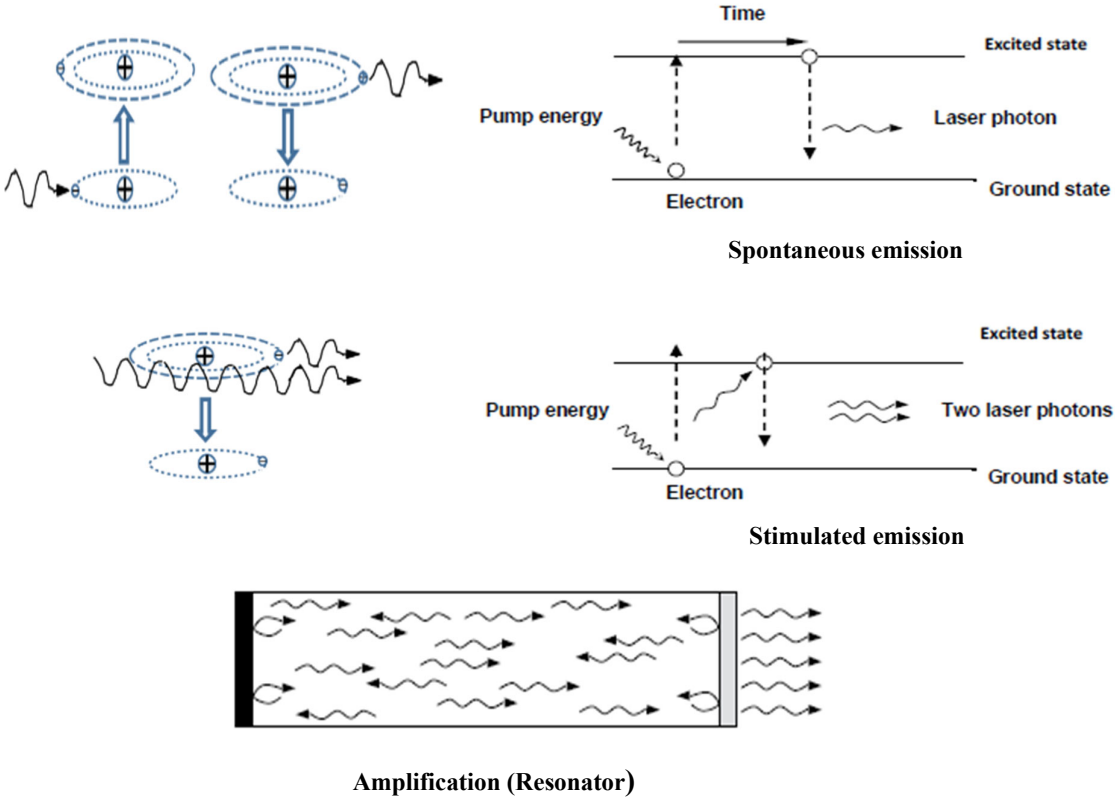

Fig. 1.3. Schematic illustration of stages of laser generation [8]

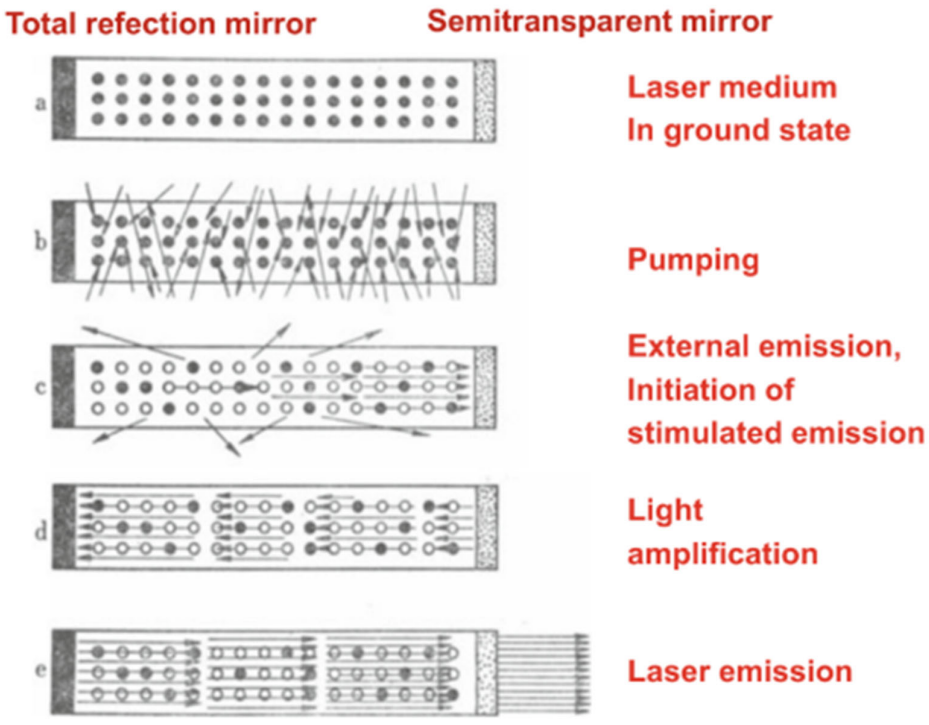

Fig. 1.4. Schematic representation of resonant cavity [7]

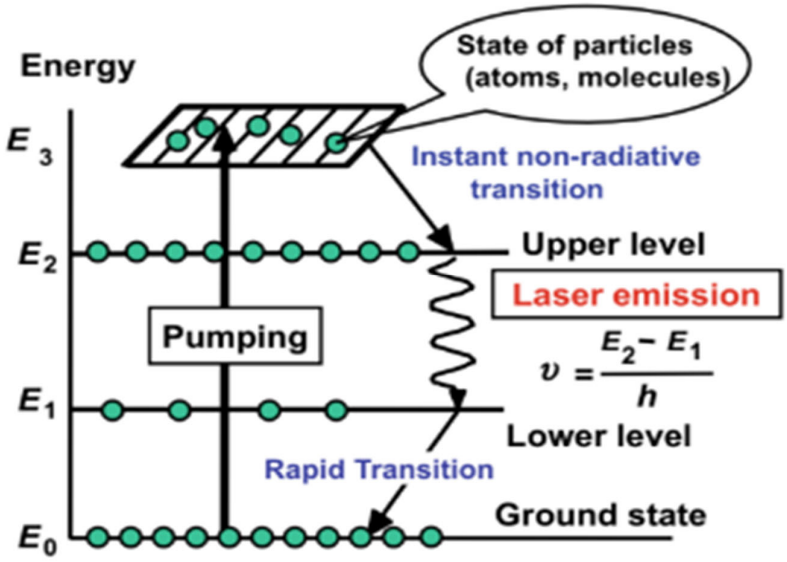

Fig. 1.5. Sketch of energy system of four levels for laser emission [7]

The deployment of energy systems with more than three levels, an optical resonator, or a resonant cavity with more than two reflecting mirrors should be necessary for the laser emission. The energy system of four levels for laser emission is sketched in Fig. 1.5 [7]. The laser with the frequency (ν) corresponding to the energy difference (E_2-E_1) is emitted. Light can be reflected back and forth many times by the mirrors and is amplified by stimulated emission in each pass-through active medium. As an example of resonant cavity with two mirrors, excitation and stimulated emission in a solid laser rod is schematically represented in Fig. 1.4 [8].

1.3. Laser as a heating source

The laser must increase the temperature of the material being fused in order to perform laser welding. To raise the temperature of the substance, the laser must be absorbed by it. In essence, the laser is concentrated onto the substance in a manner akin to how a magnifying glass may focus the sun. The laser's power density, which is about 106 watts per cubic centimeter (watts/cm^3), is significantly higher than that.

The method of laser absorption into the component and subsequent heating is shown in Fig. 1.6 (1) Laser light photons, which are packets of light energy that comprise the laser, impact

on the material and are partially or completely absorbed. The photon's energy is absorbed by the material lattice, resulting in phonons or "heating waves" inside the lattice. (2) Repetitive photon absorption raises vibrations in the lattice, causing bonds to dissolve and melting to occur.

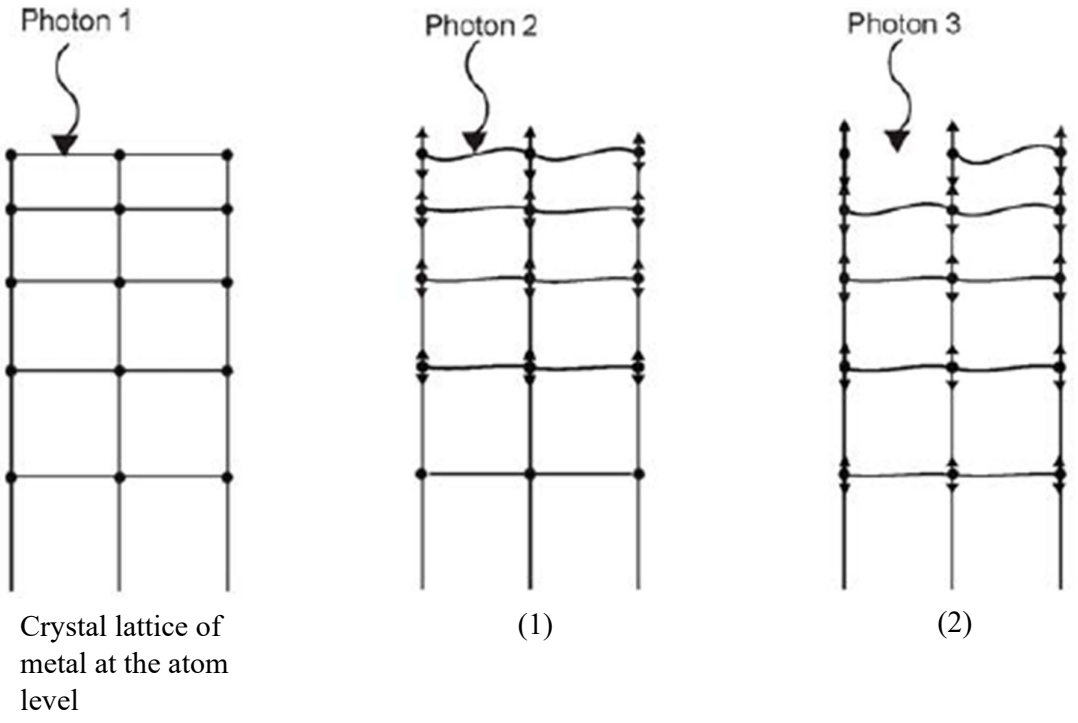

Fig. 1.6. Laser absorption and heating [9]

Even in absorbent metals like steel, the laser is first reflected. A little portion of the laser is absorbed, which heats the metal surface. The absorption of laser power increases as the surface temperature rises. This causes a snowball effect in which the laser quickly heats the material, causing melting and the production of the weld [9].

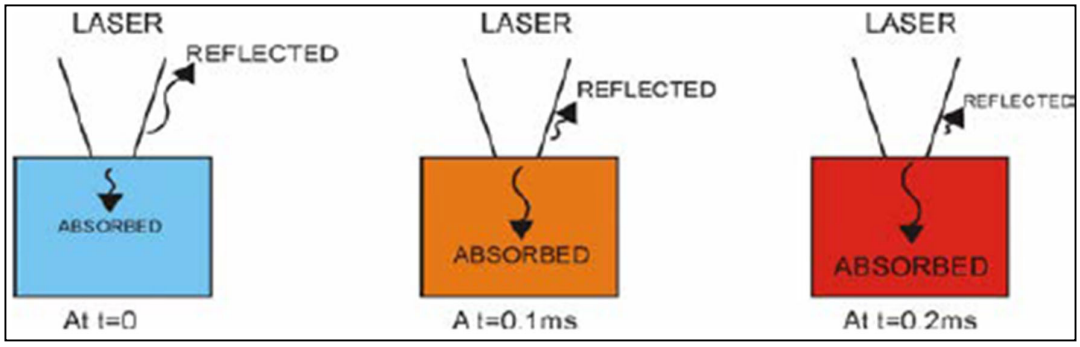

Fig. 1.7. Time-based schematic of laser absorption for welding [9]

1.4. Laser Welding modes

The laser is a method with a high-power density that offers a special welding capacity to enhance penetration with less heat input. The weld is created as the material is quickly heated by the powerful laser light, usually in a matter of milliseconds. There are three types of welds, based on the power density contained within the focus spot size: (1) conduction mode, (2) transmission mode, and (3) transition/penetration/keyhole mode, see Fig. 1.8 [8]–[10].

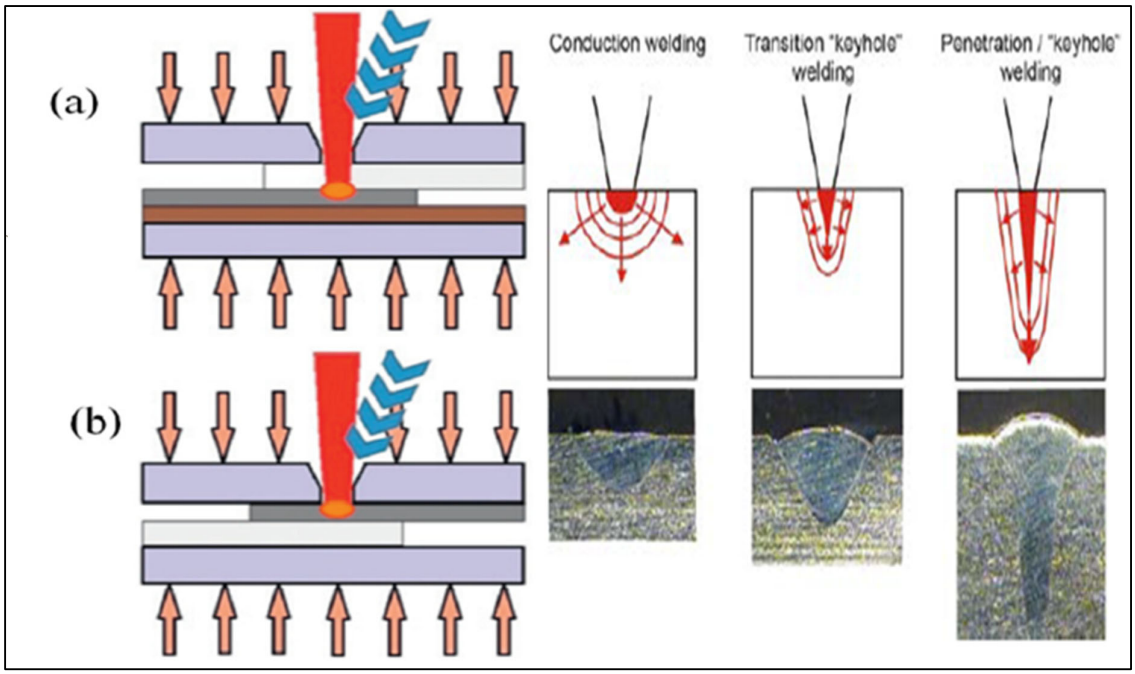

(a) Laser transmission welding

(b) Laser conduction welding

Fig. 1.8. Types of Laser welding mode [11]

1.4.1. Conduction mode

Low energy density (0.5 MW/cm2) and lesser power are used to create a conduction mode weld. The resultant weld, seen in Fig. 1.9, is shallow and broad, like a bowl. Simply heating the components in the conduction mode of welding causes the materials to melt, flow together, and solidify. The maximum weld depth in conduction mode welding, which normally varies from only a few tenths of a millimeter to 1 millimeter, is limited by the heat conductivity of the materials. Energy is transmitted into the workpiece exclusively by heat conduction. Rapid

(2.5 ms) steady state conditions are attained. Conduction welding is ideal for spot welding and bonding thin-wall materials since its breadth is always greater than its depth.

Applications that demand for an aesthetically pleasant weld might benefit from conduction welding; laser conduction welds generate rounded, smooth beads that frequently don't require additional grinding or polishing. On the exposed surfaces of electronics packages, corner welds are created via conduction mode welding. When particles may be an issue, battery sealing is another typical conduction mode weld application.

The processing temperature can exceed the vaporization temperature if the energy fed into a conduction weld doesn't vaporize rapidly enough. The weld depth rapidly rises as the material is evaporated, and penetration welding begins. This type of weld is called a "transition" weld, and its width to depth ratio is usually unity [12].

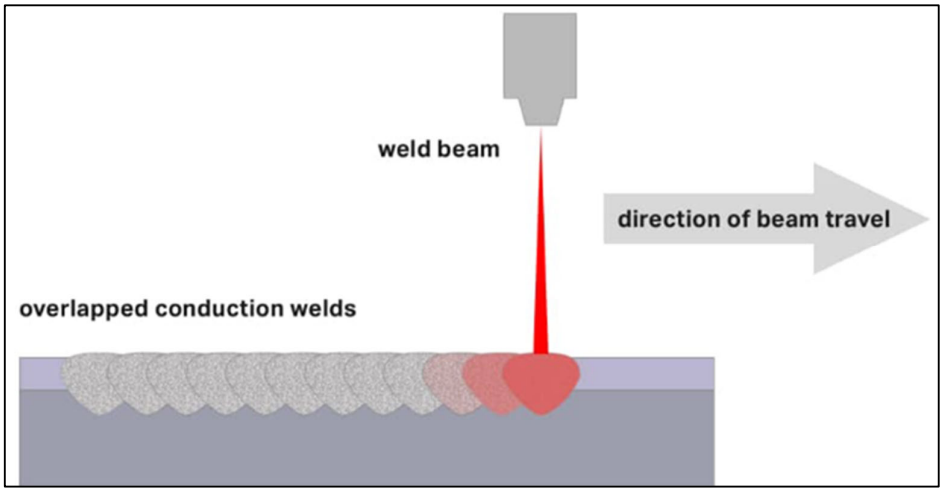

Fig. 1.9. Conduction mode weld [12]

1.4.2. Transmission mode

There are a few different names for laser transmission welding, such as laser plastic welding, through-transmission welding (TTLW), and laser polymer welding. Although the titles may vary, the idea remains the same. Fig. 1.10 [13] depicts the operation principle.

The phrase "laser plastic welding" is the one that is most frequently used to describe this technique, however "transmission welding" is a far more precise description of the procedure. This is because the fundamental idea behind this joining technique is to generate a weld by transmitting or passing laser energy through a single piece of plastic. Unlike traditional

welding, which applies energy to the materials' surfaces. The goal of transmission welding is to apply energy to the interface of two workpieces. It is vitally important for a transmission weld to have a transmissive top portion, an absorbing bottom part, clamping and contact force, and material compatibility.

Transmission welding has the following benefits: (1) low mechanical stress; (2) accurate energy management; and (3) strong and lasting welds. Four) Quick cycle times, etc. This form of weld is frequently used in the automotive sector (sensor housings, instrument clusters, interior panels, fluid control devices), as well as the medical business (catheters, fluid control). Polypropylene, polycarbonate, PMMA, and PTFE are examples of materials that are frequently welded [13].

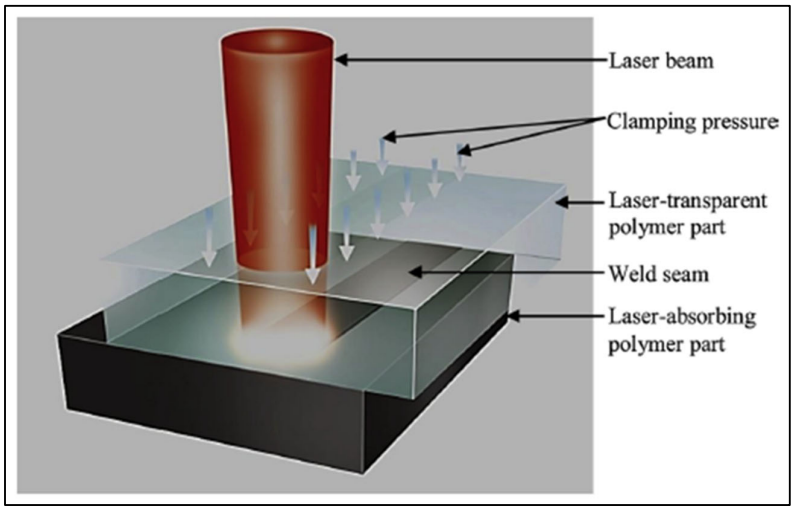

Fig. 1.10. Operating principle of transmission welding [13]

1.4.3. Transition/Keyhole mode

During the welding process, a high energy-density laser beam (1–1.5 MW/cm^2) vaporizes the workpiece to create a hole (keyhole), which enables the laser beam to pierce into the metal and build a deep, narrow melt pool. Once the keyhole has formed, the laser beam is far more quickly absorbed by the metal due to many laser-light reflections that take place there. Only a small portion (usually 50-80%) of the absorbed energy melts the metal; the remaining is lost by radiation, convection, or thermal conduction into the metal's base [14]. The fluid flow becomes shallower but quicker when beam power is increased. The flow deepens and accelerates as the beam diameter decreases [15]. The final penetration depth of the weld is affected by how much

heat is lost in various ways. Conduction loss through the base metal is quite high at low transit speeds [14].

While surface tension tends to seal the keyhole at the surface, the pressure of the vapor inside the keyhole aids in penetration by stabilizing the keyhole and keeping it open for more penetration. However, at slow travel speed, the vapor cavity has a tendency to collapse, which reduces penetration. The laser beam's interactions with the metal vapor and the atoms in the shielding gas cause a plasma to develop above the workpiece's surface. As a result of the laser beam's energy being absorbed, the maximum weld penetration is lowered. The laser beam's optical quality is diminished by the plasma's lens-like function [16].

It is only possible for a keyhole cavity to develop when the beam is powerful enough. As the material is continuously evaporated by the beam, it fills with gas or vapor. The amount of ionization, density, and therefore temperature all affect how much energy is absorbed. A keyhole mode weld has an aspect ratio larger than 1.5 and a deep, narrow profile. Fig. 1.11 depicts a keyhole mode weld schematically.

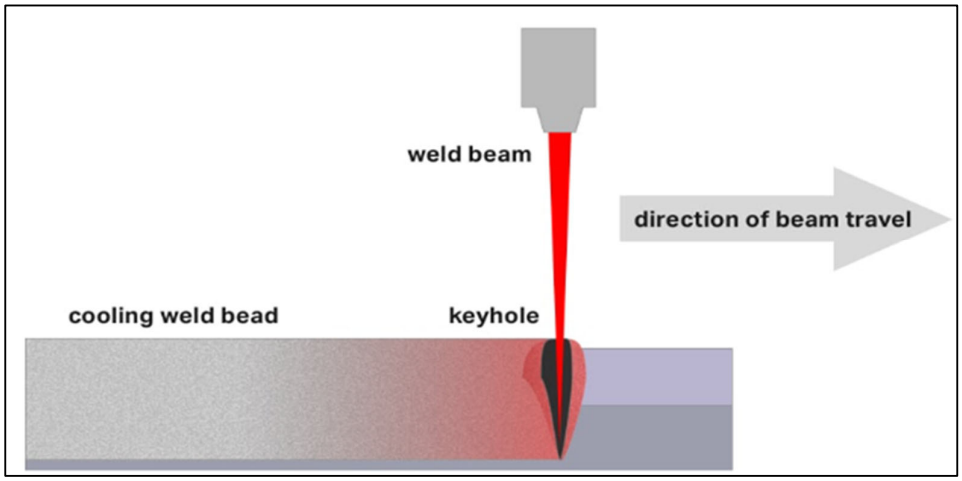

Fig. 1.11. Keyhole mode weld [12]

1.5. Pulsed and Continuous wave lasers

Either a seam weld or a single spot weld can be used to make a weld. There are two approaches to produce the laser output needed to produce these welds:

1.5.1. Pulsed lasers

Precisely at a predetermined width and frequency, pulsed lasers emit a succession of short pulses (a discrete packet of energy) until terminated. Because energy is held in capacitors until it is released, a pulsed laser can have a peak power that is higher than its average power. Very high peak powers are possible using pulsed lasers. A seam weld is produced using pulsed lasers by a succession of overlapping spot welds. Pulse laser welding is suitable for usage on heat-sensitive components and extremely thin-walled materials due to the short pulse length (usually a few milliseconds). Metals like copper (Cu) and aluminum (Al) that reflect light tend to function well with pulsed laser welding. These spot welds have an overlap of between 80 and 90% for hermetic sealing applications. Fig. 1.12 depicts the pulse power and pulsed laser weld bead [17]

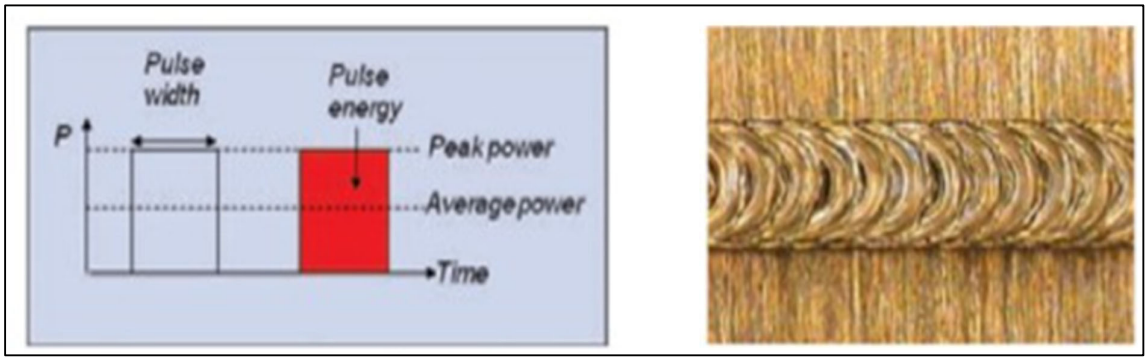

Fig. 1.12. Pulsed laser power and weld bead [17]

1.5.2. Continuous wave lasers

The term "continuous wave" (CW) laser refers to lasers that continuously emit a beam. Typically, these are fibre type lasers that excite a gain medium with on-turned-on diodes to produce laser light. For welding materials that are crack-sensitive, such as high carbon stainless steels, and for deep penetration welds (over 0.060" deep), CW lasers are particularly well suited.

CW lasers may be used at power levels ranging from 200 W to 100 KW. For the majority of metals, CW laser welding needs 200 watts or more to couple them. Metals with various thermal and reflectance properties can be fused with the help of this broad power range combined with high energy densities.

To avoid overheating the component, CW lasers typically operate at high feed rates. To get a weld with the desired penetration, power and feed speed must be carefully adjusted. The portion will be heated up more when the flow rate is slowed down, resulting in deeper penetration. Fig. 1.13 depicts a typical continuous wave weld power and weld bead [17].

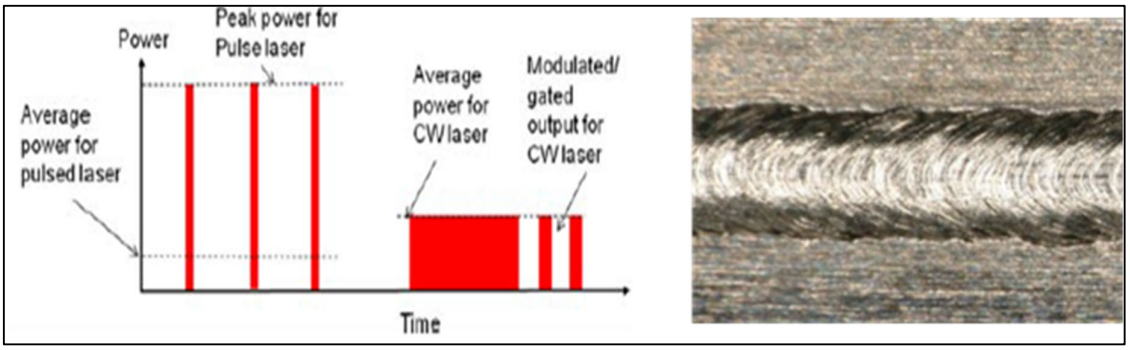

Fig. 1.13. Continuous wave laser power and weld bead [17]

A 25 W pulsed Nd:YAG laser, as an illustration, is capable of generating peak energies of up to 5 kW for short durations. As a result, it is capable of producing spot welds that would normally need a 5 kW CW laser.

1.6. Laser welding parameters

The quality, size, and characteristics of a laser weld are influenced by a variety of process factors. Both continuous wave lasers and pulsed lasers have been used in experiments.

The only variables that affect the laser beam in the case of CW lasers are the laser's power, the beam's size and shape on the workpiece, the position of the focal plane with respect to the workpiece's surface, the power density (power/beam size), the laser's wavelength, the beam's divergence (the focal length of the focusing lens), and the beam's intensity distribution.

There are more characteristics for pulsed lasers, including pulse energy, pulse repetition rate, pulse length, mean laser power (pulse energy x pulse repetition rate), average peak power (pulse energy/pulse duration), average peak power density (average peak power/spot area), and pulse shape.

Other critical criteria are welding speed (seam and stitch welds), welding duration (spot welds), and weld length (stitch welds). The amount of power in the incident laser beam that is absorbed (rather than reflected) by the material is determined by its surface qualities. The quantity

needed to create a melted weld pool is then determined by the heat capacity and flow parameters.

Material attributes include heat capacity, heat conductivity, surface reflectivity, melting temperature, material thickness, and weld physical orientation (vertical or horizontal).

Another set of characteristics is connected to the gas used to shield the welding process: the kind of gas, the flow rate of the gas, the angle of the gas flow to the workpiece, and the nozzle designs. A Fishbone diagram in Fig. 1.14 illustrates this. Also, the Table 1.1 gives a brief idea about characteristic variables involved in welding.

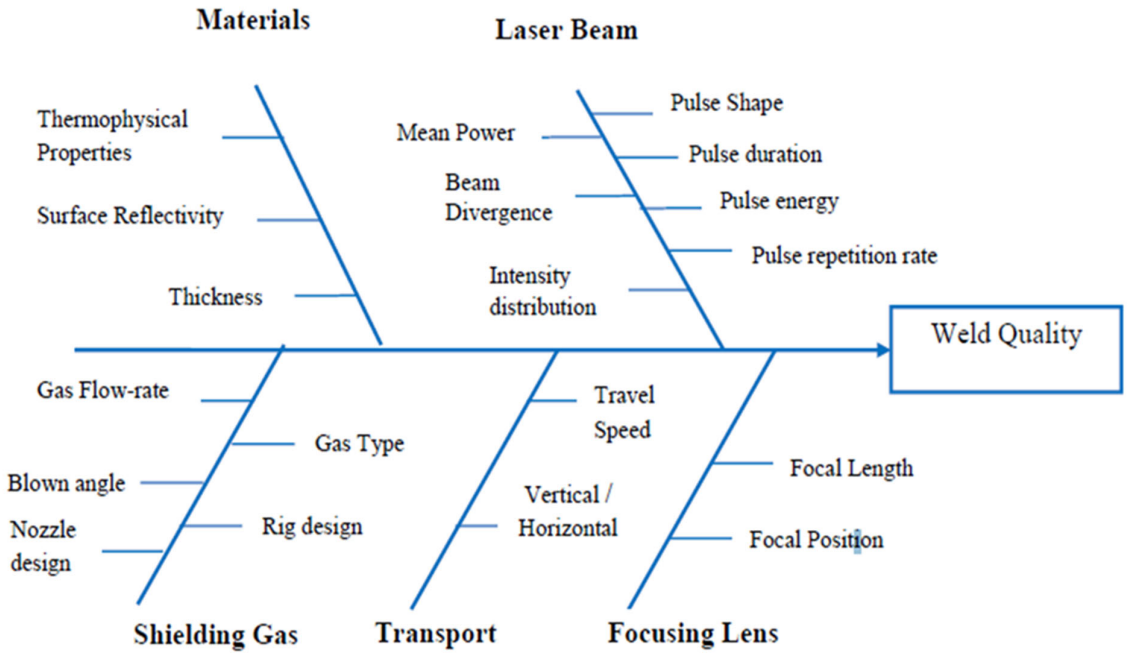

Fig. 1.14. Fishbone diagram of laser welding parameters [18]

Table 1.1. Characteristic variables involving in the laser welding

Operating factors	Phenomenological factors	Product factors
Power Source:		**Weld bead:**
Wavelength, Power, power Distribution (Pulsed/Continuous), Spot size, Focal point, Pulse		Geometry, Penetration depth, Bead shape, Bead height, Bead width, Width to penetration ratio, HAZ, Percentage dilution

shape, Pulse duration, Pulse frequency	Molten pool size, solidification speed, chemical composition, Shielding gas,	
Material: Chemical composition, Thermo-Physical property, Microstructure	Fluid flow dynamics, Cooling rate, Temperature distribution	
Shielding gas: Nature, chemical composition, Flow-rate, Position and angle **Position and movement:** Position of the beam, Weld direction, Weld speed, Gap between weld joints	------	**Mechanical and Metallurgical Properties:** Hardness, Yield strength, Residual stresses, Joint strength, Impact strength, Fatigue life, Creep strength, thermal and mechanical distortion

1.7. Laser welding systems

Many researchers and laser manufacturers have worked together to produce industrial lasers for actual material processing. As shown in Table 1.2 [19], [20], each laser is called based on their emitted medium or substance, shape, oscillation medium, wavelength, and pulsed width. The lasers are comprehended by categorizing them as gas, liquid, or solid lasers. In terms of ease of use, solid lasers are the best.

High-power lasers were initially produced in CO_2 lasers, then in YAG lasers. Excimer lasers were later created. Then there were high-power diode lasers. Furthermore, high-quality, high-power diode lasers for disc and fibre lasers were produced. High-power, high-quality, and high-efficiency disc and fibre lasers were created and widely utilized for welding in the twenty-first century. Ultrashort pulse lasers such as picosecond (10^{-12} sec) and femtosecond (10^{-15} sec) lasers, second harmonic lasers generating green light from YAG, disc and fibre lasers, and blue diode lasers have all been actively developed in recent years. Ultrashort pulse lasers were

primarily employed for glass lap joining. Green and blue lasers are intended to fuse copper (Cu) plates and sheets with consistency.

Recently improved fibre lasers provide tremendous flexibility in adjusting weld parameters as well as the best penetration per watt performance, enabling high speed seam welding. Diode lasers are another well-known laser technology for plastic welding applications.

Table 1.2. Names and characteristics of lasers for welding

	Wavelengths	**Ray**	**Laser Media**	**Avg. Power**	**Merits**
CO_2 laser	10.6 μm	Fair-infrared	CO_2-N_2-He mixed gas	0.5 – 12 KW	Easier high power
YAG laser	1.06 μm	Near-infrared	Nd^{3+}:$Y_3Al_5O_{12}$ garnet (Solid)	50W–5 KW	Good flexibility
Diode laser	0.8 – 1 μm	Near-infrared	Al(In)GaAs (Solid)	2 - 60 KW	Compact and high efficiency
Solid-state laser	1.06 μm	Near-infrared	Nd^{3+}:$Y_3Al_5O_{12}$ garnet (Solid)	6 KW-13.5KW	High brightness and efficiency
Disk laser	1.03 μm	Near-infrared	Yb^{3+}:YAG or YVO_4 (Solid)	16 KW	High brightness and efficiency
Fibre laser	1.07 μm	Near-infrared	Yb^{3+}:SiO_2 (Solid)	10 KW – 120 KW	Compact and high brightness and efficiency
Green laser	515, 532, 535 nm	Green	Nonlinear optical crystal from disk, YAG or Fibre laser	500 W – 3 KW	Short wavelength, High absorption for copper
Ultrashort pulse laser	0.8 – 1.6 μm	Near-infrared	Titanium-sapphire (solid)	1 – 1000 W	Ultrashort pulse, Narrow HAZ

1.7.1. CO_2 laser

Carbon dioxide (CO_2) lasers remain the most favoured alternative for industrial applications because they can supply high continuous power up to several kilowatts while remaining efficient. Simultaneously, their versatility has made them beneficial for non-industrial applications like as medical treatments and research, where their mid-infrared (IR) wavelengths are helpful. In recent years, this established technology has benefited from the development of innovative designs that result in more compact lasers with better output power per unit volume [21].

I. Construction

It consists of a tube with a diameter of 2 cm and a length of 5 m. The discharge is produced via D.C. excitation. Silicon mirrors with an aluminium coating make up the resonant cavity. Pressured He has three pressures: 7 Torr, 1.2 Torr, and 0.33 Torr. The large gain of the transition makes it possible to operate a laser oscillator at 10.6 m.

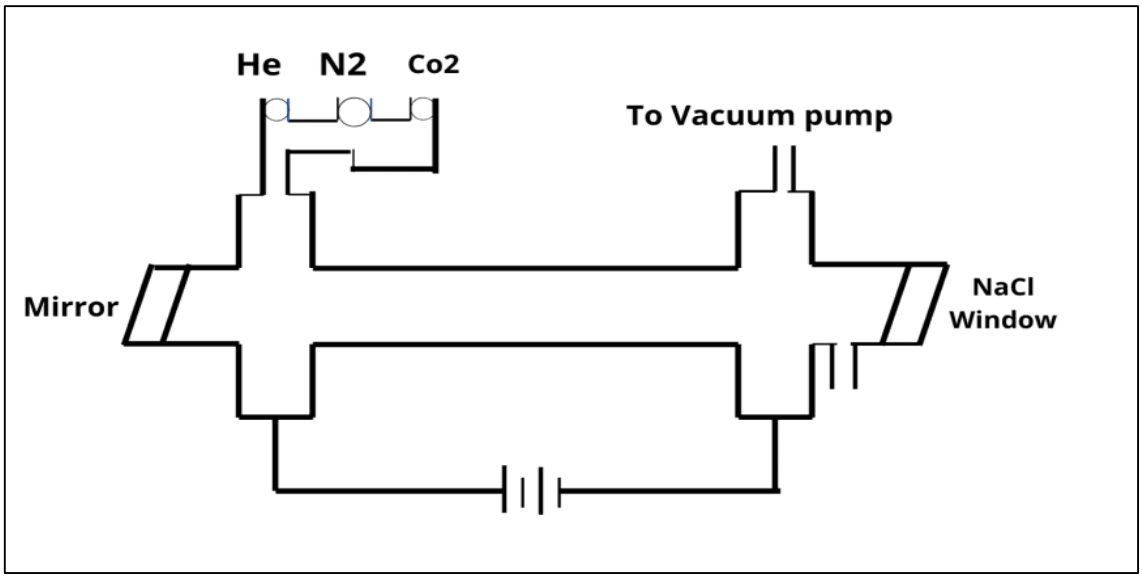

Fig. 1.15. CO_2 Laser [22]

A selective device, such as a diffraction grating, is put into the cavity to create a 9.0 m oscillation. The maximal power of this laser is between 50 and 60 w/m. CO_2 lasers are widely used in industry.

II. Working

To generate a CO_2 laser, a gas discharge tube is filled with a blend of CO_2 and N_2 in a about 0.8:1 ratio. Helium is also added to the mix. The combination has more helium than nitrogen. The CO_2 molecule works as an active or laser medium in the same manner as helium does in case of He-Ne lasers, while the N_2 molecule aids with population inversion.

A significant number of electrons are released when an electric discharge is transmitted through the tube, pumping nitrogen molecules into the V = 1 state. Because the difference in energy between the vibrational energy levels of nitrogen and carbon dioxide in a CO_2 laser is so minimal (about 0.3 eV), there are many electrons in the gas discharge tube with energies greater than 0.3 eV.

Although CO_2 lasers generally have a wavelength of 10.6 m, there are other spectral lines with wavelengths in the 9–11 m range, particularly at 9.6 m [22]. Most of the time, typical power outputs range from a few tens of watts to several kilowatts. The energy conversion efficiency may be much greater than 10%, which is notably higher than that of the majority of gas lasers (due to a particularly favourable excitation path). While many diodes have a lower efficiency, lamp-pumped semiconductor lasers are more efficient than many of them.

III. Advantages

1) The CO_2 laser is easy to manufacture.
2) The laser's output is continuous.
3) It is quite effective.
4) It produces a lot of electricity.
5) By increasing the length of the gas tube, the output power can be increased.

IV. Disadvantages

1) Carbon monoxide contamination of oxygen will have an influence on laser action.
2) The operating temperature has a significant impact on the laser's output power.
3) Corrosion of the reflecting plates is a problem.
4) Due to its invisible nature to naked eye (infrared range), accidental exposure may cause eye injury.

V. Applications

1) CO_2 lasers are often utilized in industrial fields, such as cutting and welding, because of their tremendous power.
2) It's a soft tissue surgery tool.
3) It is employed in the manufacturing processes.
4) Used to treat a variety of non-cancerous and cancerous skin conditions.

1.7.2. Solid State (Nd:YAG) laser

Solid-state lasers use the crystal Nd:YAG, also known as neodymium-doped yttrium aluminium garnet (Nd:$Y_3Al_5O_{12}$), as the lasing medium. Since the two ions are similar in size, the yttrium ions in the host crystal structure of the yttrium aluminium garnet are routinely replaced by a minimal percentage (about 1%) of the dopant, triply ionised neodymium, Nd(III) (YAG). The neodymium ion causes the lasing activity in the crystal, similar to how the red chromium ion in ruby lasers does [23].

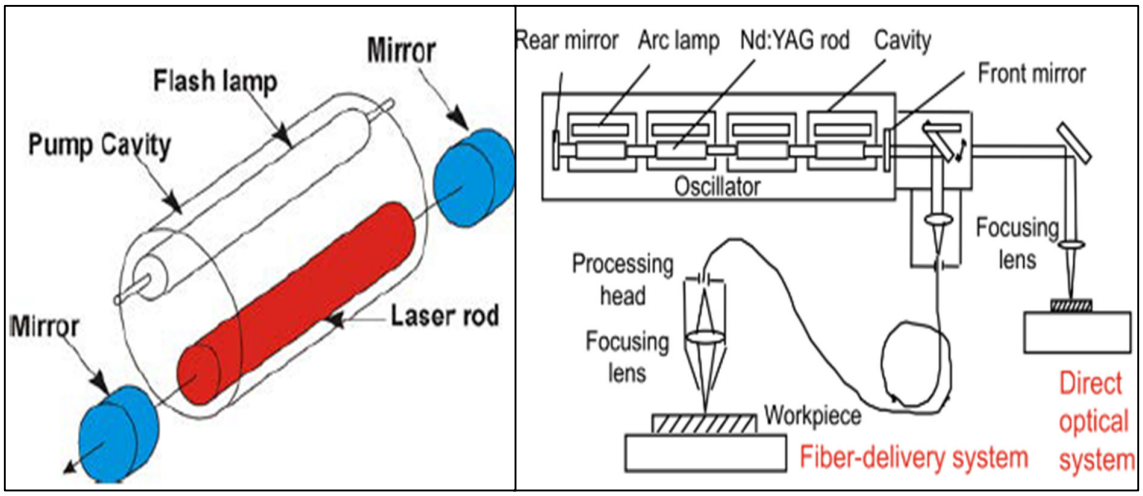

Fig. 1.16. Nd: YAG Laser [7]

I. Construction

The Nd:YAG laser is created as seen in Fig. 1.16. A small percentage of the Yttrium ions (Y^{3+}) in the Nd: YAG crystal's active component are replaced with Neodymium (Nd^{3+}). A cylindrical rod has been created out of this active component. The ends of the cylindrical rod have been extensively polished, making them parallel and visually smooth. Together with a pumping source (flash tube), this cylindrical rod (laser rod) is placed inside a cavity of a strong elliptical reflector [24]. The optical resonator is made up of two exterior reflecting mirrors. One mirror, M1, is entirely reflecting, whereas M2, it is just partially reflective.

II. Working

Nd: YAG rod is optically pumped by krypton flash tubes. Neodymium ions (Nd^{3+}) are stimulated to higher levels. The change from the meta stable to the ground state results in the emission of a laser beam with a wavelength of 1.064 m. Neodymium (Nd^{3+}) atoms are raised from the lower levels E0 to the upper levels E3 and E4 when the krypton flash lamp is turned on due to the absorption of light radiation with wavelengths of 0.73 and 0.8m (Pump bands).

Neodymium ions undergo a non-radiative transition from these energy levels E2. E2 is a metastable condition. Level E2 collects neodymium ions, with population inversion happening between E2 and E1. When an ion spontaneously transitions from E2 to E1, it emits a photon with certain energy. This emitted photon will initiate a chain of stimulated photons between E2 and E1.

The photons produced in this manner increase in strength as they bounce back and forth between two mirrors. After a period, the quantity of photons multiplies more quickly. Once sufficient strength is attained (the laser requirement has been satisfied), a powerful laser light with a wavelength of 1.064m is transmitted via the partial reflector. It relates to the transition from E2 to E1.

III. Advantages

1) It's ideal for thin materials that need to be processed quickly.
2) It has a high DPI resolution.
3) It's also handy for applications that require a lot of power, such as metal marking.

4) It produces more energy and has a high repeating rate.
5) Population inversion is fairly simple to do.
6) It can be Q-switched to operate in CW or pulse mode. This is useful for modest laser ablation.
7) Nd:YAG laser machines can cut highly reflective materials such as aluminium, copper, and non-ferrous metals that other laser cutting machines can't.
8) It is simple to use and maintain.
9) The cost of acquisition is lower.

IV. Disadvantages

1) It is not recommended to use with materials of moderate thickness.
2) This laser type allows for slower manufacturing of thicker materials. As a result, it has a reduced efficiency.
3) It exhibits a low absorption of lighter materials' radiation in the visible spectrum.
4) Despite high engraving resolutions, it will not allow for a longer scan gap. This slows down the procedure.
5) In YAG, the electron energy level structure of Nd^{3+} is complicated.

V. Applications

1) Laser designators and laser rangefinders employ Nd:YAG lasers. A laser designator is a light source that emits a laser beam that is used to target targets for assault. A laser rangefinder is a rangefinder that determines the distance to an object using laser light.

2) To treat posterior capsular opacification, Nd: YAG lasers are employed (a condition that may occur after a cataract surgery). Skin malignancies are removed using Nd:YAG lasers.

3) For etching or marking a range of polymers and metals, Nd:YAG lasers are employed. For cutting and welding steel, these are used.

1.7.3. Li Ion laser

LIBs are currently piquing interest as green energy sources in pollution-free electrical vehicles. Electro mobility appears to be a viable choice today for the conservation of energy resources and environmental preservation. It is quite evident that Lithium Ion Battery (LIB) technology is the energy storage concept that can meet the future energy and power density requirements of the automotive industry. Modern LIBs use thick-film electrodes (cathode, anode), which are complex multi-material systems with well-defined material components, grain sizes, porosities, and pore size distributions in the micrometre and sub-micrometre range. The thick-film electrode stacks used in contemporary prismatic or pouch batteries for high-power applications have a capacity of at least 60 Amp-hr [25].

I. Construction

The battery component consists of several cells that are maintained at a constant distance from one another to facilitate cooling and avoid overheating. In EV battery packs with many battery cells, a modular construction is necessary because of the electrochemical properties of the components. The cells are layered using metal or plastic support structures to allow for state-of-charge dependent swelling.

Common techniques for fastening the structure include gluing the cells together and/or encasing the cells in a metal frame. EV battery design guidelines can occasionally be debatable. Lightweight metal alloy or carbon fibre materials are recommended since the construction should be as strong and lightweight as feasible [26]. The UMW approach was employed to analyse both copper and aluminium because, in a typical large format lithium-ion battery, copper foil serves as the anode current collector and aluminium serves as the cathode current collector.

Only identical material stacks were allowed for the experimental joints, as can be seen in the figure below, with copper foils joining copper tabs and aluminium foils joining aluminium tabs. The tabs' thickness was maintained at 0.127 mm. Two foil thicknesses, 0.012 and 0.025 mm, and two foil stack heights, 20 and 60 layers, were studied in order to demonstrate feasibility and investigate the impacts on joint quality as the foil thickness and number of layers vary [27].

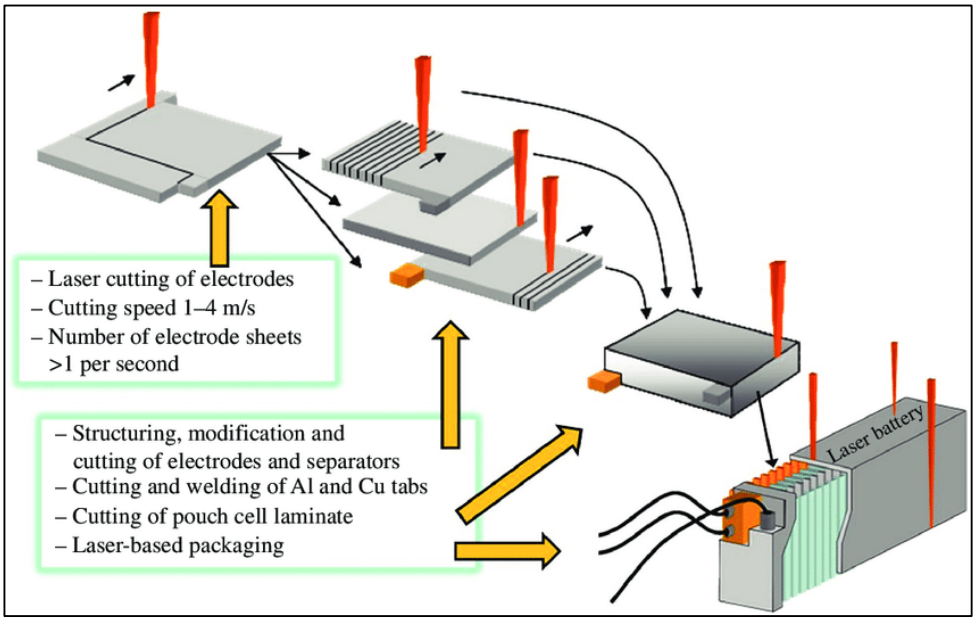

Fig. 1.17. Li Ion Laser [25]

II. Working

All lithium-ion batteries function similarly. A portion of the lithium ions on the positive lithium-cobalt oxide electrode are released during battery charging and go through the electrolyte to the negative graphite electrode, where they remain. The battery collects and stores energy throughout this process [28]. When the battery is discharging, the lithium ions move back across the electrolyte to the positive electrode, creating the energy that powers the battery.

Both times, the ions and electrons move in the opposite directions along the external circuit. The electrolyte acts as an insulator for electrons, preventing them from moving through it. Both the movement of electrons across the external circuit in the opposite direction and the movement of ions through the electrolyte are interdependent processes, and if one stops, the other will too. You lose power when the battery is fully depleted because ions cannot travel through the electrolyte and electrons cannot pass through the outer circuit. The flow of electrons and ions also ceases when you switch off the machine that the battery is powering.

While the battery is rapidly depleting, it essentially comes to an end (but it does keep on discharging, at a very slow rate, even with the machine disconnected). Unlike simpler batteries, LIBs have electronic controllers built-in that regulate how they charge and discharge [29]. Lithium-ion batteries are shielded from overcharging and overheating, which can occasionally

result in explosions. A positive electrode (linked to the battery's +ve terminal), a negative electrode (coupled to the battery's -ve terminal), and an electrolyte are the three components that make up each cell [30].

III. Advantages

1) As Lithium-Ion batteries have been around for a long time, the cost of manufacturing them has dropped dramatically. In addition, using a lithium-ion battery for a portable gadget is significantly more cost effective because they are readily available and cost much less.

2) Its high-power density with electric gadgets such as cell phones requiring longer battery life while still utilizing more power, there is always a demand for batteries with a higher power density.

3) Lithium-ion batteries are easy to maintain and care for because they don't require several complicated processes. Apart from that, there isn't a lot of money or effort required to keep these lithium-ion batteries running.

4) Another advantage of lithium-ion batteries is their ability to maintain a constant voltage. A lithium-ion battery will successfully maintain the voltage fixed no matter how heavy the usage or load is. This is due to the fact that the voltage created by each lithium-ion battery is around 3.6 volts, which is significantly higher than the voltage generated by its alternatives [31].

5) This advantage of lithium-ion batteries implies that the proper technology can be applied to the specific task at hand. Some lithium-ion batteries have a high-power density, making them ideal for customer mobile electronics. Other li-ion battery varieties may deliver far higher power levels, making them ideal for energy equipment and electric vehicles.

IV. Disadvantages

1) Lithium-ion batteries are less durable than other types of rechargeable batteries. They require protection from being severely overcharged and discharged. Apart from that, lithium-ion batteries need to be maintained in a safe manner. As a result, every lithium-ion battery requires protection circuitry that is a substantial drawback in order to maintain these safe limits.

2) Even though lithium-ion batteries have a lengthy life period, their performance changes with time. Lithium-ion batteries' effectiveness and performance also tend to deteriorate with time. Furthermore, whether or not they are in use, lithium-ion batteries can degrade their performance. The loss in capacity is caused by a time-related element in addition to utilization.

3) Lithium-ion batteries are not suitable for heavy-duty applications due to their lack of robust technology. Because Li-ion batteries contain liquid polymerized electrolytes, they can perforate quickly and with little force.

4) The disadvantage of lithium-ion batteries has become more pronounced. Many airlines prohibit the transport of lithium-ion batteries, limiting their cargo to ships [31]. These lithium-ion batteries must also be kept in carry-on luggage for flight passengers. Although, in the case of the safety position, this may change with time. The quantity of batteries available, on the other hand, remains restricted, which is the most significant disadvantage of lithium-ion batteries.

V. Applications

As mentioned before, there are many different sizes and forms of lithium-ion batteries. No of the size of the system, they are a great option for power requirements. Additionally, lithium-ion batteries offer a wide range of power options, from energy storage to portable energy. Applications for lithium-ion batteries are many [32]. i) Power backups/UPS, ii) Mobile, Laptops, and other commonly used consumer electronic goods, iii) Electric mobility, iv) Energy Storage Systems.

1.7.4. Semiconductor Diode laser

In diode laser, a current is directly flown in the forward direction against a semi-conductor of double hetero-junction structure from the outer side, and then the light is emitted by recombing electrons and positive holes at the active layer between an n-type and p-type semiconductor region. The photons move forth and back by the mirror and/or refraction rating, and the laser radiates due to amplification by stimulated emission. Diode lasers are called semiconductor lasers or laser diode (LD) [8].

I. Construction

Electrons from the n-region cross the junction and recombine with holes from the p-region when a p-n junction diode is forward biased. During the recombination process, a certain direct band gap semiconductor, such as Ga-As, emits light radiation (photons). The term "recombination radiation" refers to this particular kind of light. The photon emitted during recombination encourages the recombination of more electrons and holes [33]. Consequently, stimulated emission takes place, producing laser.

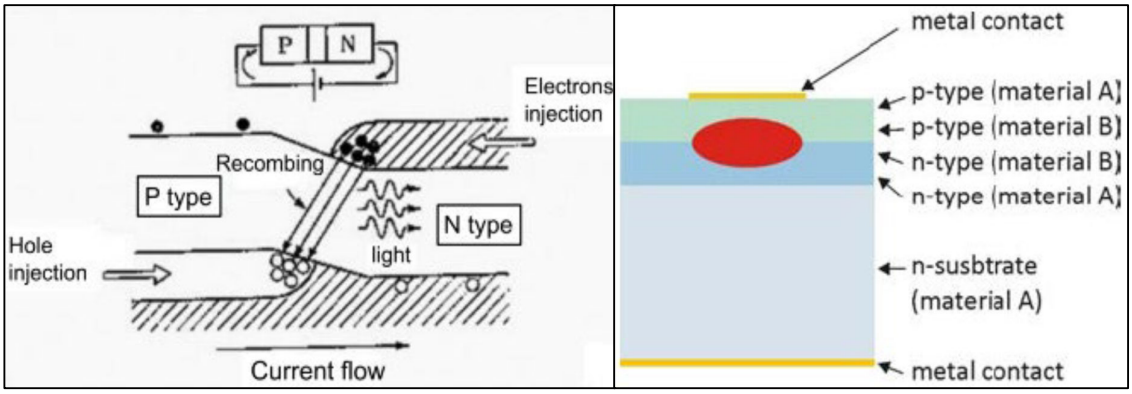

Fig. 1.18. Working of Diode laser [9]

II. Working

Countless electrons and holes are injected into the junction area when a p-n junction is forward biased with a high applied voltage [33]. In the vicinity of the junction, there are a lot of electrons in the conduction band and a lot of holes in the valence band. When the population density is

high, a population inversion occurs. Light-wave radiation is created when electrons and holes recombine.

More light photons are released and the light output becomes nearly instantly brighter as the forward-biased voltage is raised [33]. Phase photons will be released as a result of a series of induced recombination that these photons will trigger. Photons travelling in the plane of the junction are strengthened by reflection between two parallel and diametrically opposite sides. When it reaches a certain strength, a laser beam with a wavelength of 8400 is released.

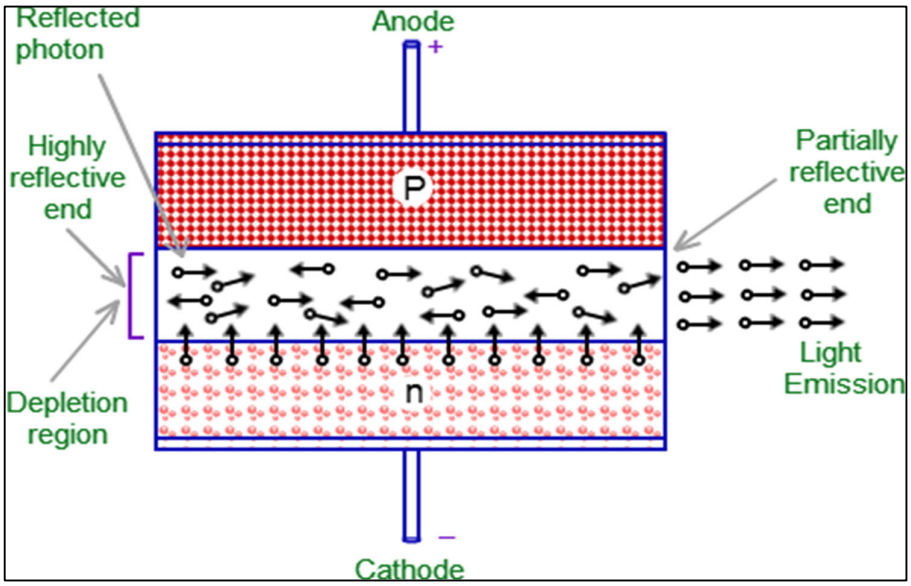

Fig. 1.19. Semiconductors Diode Laser [33]

III. Advantages

1) It is extremely little in size. The set-up is straightforward and compact.
2) It has a high level of efficiency.
3) Controlling the junction current allows the laser power to be readily raised.
4) It has a lower power output than ruby and CO_2 lasers.
5) It only necessitates a little amount of supplementary equipment.
6) It can emit a continuous wave or a pulsed wave.

IV. Disadvantages

1) Controlling the mode pattern and mode structure of a laser is tough.
2) The output is usually between 5 and 15 degrees, indicating that the laser beam has a considerable divergence.
3) The purity and monochromic of the laser are more powerful than other laser types.
4) The current density at the threshold is extremely high ($400A/mm^2$).
5) It has a low level of coherence and stability.

V. Applications

1) It's a common fibre optic communication technology.
2) It employs infrared radiation to aid in the healing of wounds.
3) It's also utilized as a pain reliever.
4) It is employed in laser printers as well as the writing and reading of CDs.

1.7.5. Fibre laser

Fibre lasers are a particular kind of solid-state laser in which the gain medium is an optical fibre. Fibre lasers have been an important development in the field of solid-state lasers since the idea of using an optical fibre as a mode converter for lasers was first proposed. In the modern world, fibre lasers are pervasive. They are often used in industrial applications to carry out cutting, marking, welding, cleaning, texturing, drilling, and a range of other operations because to the varied wavelengths they can produce [34]. Additionally, they work in fields like health and telecommunications.

I. Construction

Fibre lasers are solid-state lasers that employ optical fibres as their active gain medium. Raw light from the pump laser diodes is absorbed by a fibre made of silicate or phosphate glass, which then turns it into a laser beam of a certain wavelength in these lasers. To do this, the optical fibre is doped. Doping is the process of introducing a rare-earth element to a fibre. Using different doping components, laser beams with a wide range of wavelengths may be created [35].

A wide range of wavelengths enables the fibre lasers to be suited for a variety of applications such as laser cutting, texturing, cleaning, engraving, drilling, marking, and welding. Fibre lasers may now be employed in a variety of areas, including manufacturing, spectroscopy, power, transportation, medicine, and the military.

II. Working

In the laser material, a meta-stable state corresponding to an appropriate energy must exist. After being "pumped" to a higher state, the electron in laser material immediately slides down to a somewhat lower meta-stable state. We presently have a significant number of electrons with sufficient energy lying about, ready to be nudged into releasing that energy in the form of a photon [35].

The term "fibre laser" refers to the optical fibre that serves as the active gain medium in the device. Any fibre laser equipment that produces a high-power, well-collimated laser follows a five-step process. i) Production of pump light, ii) Collection and transport into the optical fibre, iii) Pump light travels via the optical fibre, iv) Stimulated emission in the laser cavity, and v) Amplification of raw laser light into a laser beam.

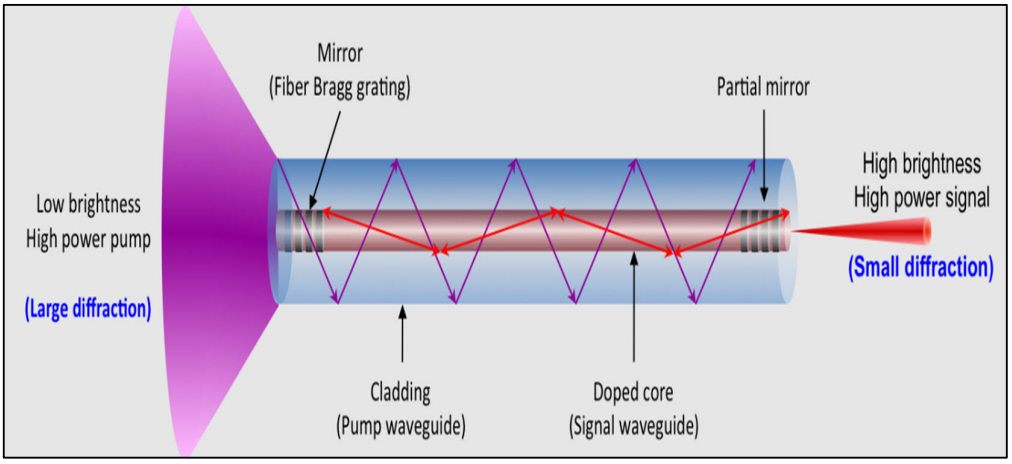

Fig. 1.20. Fibre Laser [35]

III. Advantages

Traditional welding requires a lot of work but is inefficient. High-efficiency fibre laser welding technology will eventually replace traditional welding techniques as fibre laser technology advances [36].

1) The benefits of intensification and miniaturization brought about by advanced technology, affordable glass optical fibre, and the availability of optical fibre.
2) Due to the non-uniform broadening brought on by the splitting of the glass matrix Stark, which results in a wide absorption band, the glass fibre does not require strict phase matching of the incident pump light like a crystal.
3) The glass material has a very low volume-to-area ratio, heat dissipation is quick, and loss is minimal, all of which contribute to a high up-conversion efficiency and a low laser threshold.
4) The output laser has a wide range of wavelengths; this is due to the rich energy level and variety of rare earth ions.
5) Both the glass fibre's fluorescence spectrum and the rare earth ion energy level are broad.
6) The fibre laser provides advantages of no adjustment, no maintenance, and excellent stability that are unmatched by conventional lasers because there is no optical lens in the cavity of the fibre laser.
7) Because the fibre is exported, a number of multi-dimensional arbitrary space processing applications may be handled by the laser easily, simplifying the mechanical system's design.
8) Capable of enduring abrasive working conditions and having a high tolerance for temperature, humidity, shock, and dust.

IV. Disadvantages

1) Expensive fibre.
2) It is simple to break the fibre substance.
3) Due to the tiny fibre core. Its single-pulse energy is low in comparison to a solid-state laser.

V. Applications

1) Fibre Laser marking and cutting give tremendous efficiency in the manufacture and cutting of sophisticated devices with very small parts. It is used in the medical industry to make easily traceable identification markings on medical equipment.

2) The jewellery industry is one of the most common applications for fibre laser marking machines. In the Jewellery & Gems Industry, fibre laser machines are commonly used to perform accurate and complicated markings and cuts, as well as obtain high production capacity in a short period of time.

3) Automotive, aviation, aerospace and manufacturing sectors are another sector where fibre laser marking machine is used.

4) When it comes to the sectors where the fibre laser marking machine is used, one of the most benefited sectors is the electronics sector.

1.7.6. Excimer laser

The two most prevalent gas lasers that create ultraviolet light are excimer lasers and nitrogen lasers. The active medium is composed of a noble gas, a halogen gas, and a buffer gas (often neon). The gas combination of a typical excimer laser comprises of 2-9% noble gas, 0.2% halogen gas, and 90-98% buffer gas, which acts as an energy delivery medium [35]. The combination is generally contained in a pressure vessel at 3500-5000 millibars and is induced by a short electric discharge lasting a few tens of nanoseconds.

I. Construction

Electric discharge pumping is employed in Excimer lasers to induce population inversion. Voltage is applied across the electrodes of the gas discharge tube, which is filled with a low-pressure gas mixture as the gain medium. The applied voltage generates an electric field within the tube. This electric field accelerates electrons in the gas. These electrons clash with the gas atom or gain medium, stimulating the atom to higher energy levels [37].

If an atom in a lower energy level transitions to an excited state quicker than an atom in a higher energy level moves to lower energy levels, the population of the higher energy level is greater than the population of the lower-lying energy levels. As a result, gas emissions are experiencing a demographic inversion.

II. Working

It consists of a tube with two electrodes that are connected to a discharge voltage source. The active medium exists between these two electrodes. A resonant cavity is formed around the arrangement by two planes and parallel mirrors M1 and M2. Mirror M1 is a completely reflecting mirror, whereas Mirror M2 is a partly reflecting mirror emitting pulse laser [36].

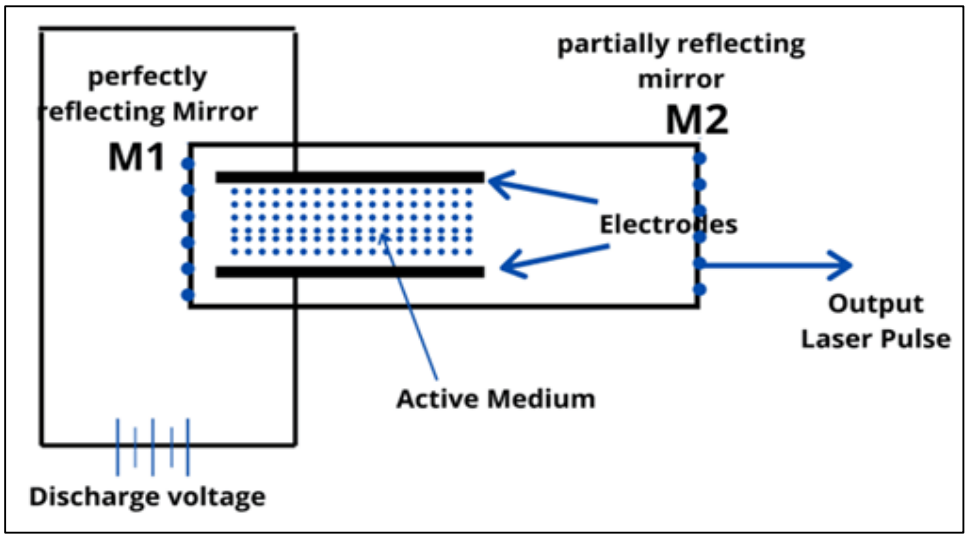

Fig. 1.21. Excimer Laser [37]

III. Advantages

Laser: 1) Capable of high powers.

2) Highly monochromatic.

3) Adaptable to various source fibres.

LED: 1) Small, adaptable.

2) Low cost.

3) Can be used directly for endoscopic/interstitial.

Lamp: 1) Simple design.

2) Low cost.

3) Broad field irradiation.

IV. Disadvantages

The number of problems related with the usage of excimer lasers has been decreased to less than 1%. There are minimal disadvantages to utilising an excimer laser. Excimer laser procedures are more costly than other surgeries [37]. If not done appropriately, it may create glare and night vision problems. Furthermore, no promise can be made that the surgery will be a total success. For example, simply because you get excimer laser surgery does not guarantee your eye problems will disappear. And, like with any other operation, there are risks associated.

V. Applications

1) Ophthalmology is the field of eyesight correction.
2) Microlithography.
3) Micromachining.

1.7.7. Disk laser

Following the creation of LD-pumped Nd^{3+}: YAG lasers, LD-pumped Yb^{3+}: YAG lasers have been produced. A thin disk-shaped YAG plate is put atop a coin-sized copper (Cu) plate, and an LD beam is irradiated many times onto the disk-shaped YAG plate. A designed resonant cavity and increased Yb^{3+} conversion efficiency has aided in the creation of high-quality, high-power, and high-efficiency lasers. Figure following depicts the emission mechanism of disc lasers.

For welding automobile bodywork and parts, fibre-delivered high-power disc lasers with a wavelength of 1.03 μm are employed. In shipbuilding, hybrid welding of thick steel plates with a high-power disc laser and MAG arc is used. In addition, high-power green lasers derived from high-power disc lasers have been produced for use in welding Cu sheets and plates [38].

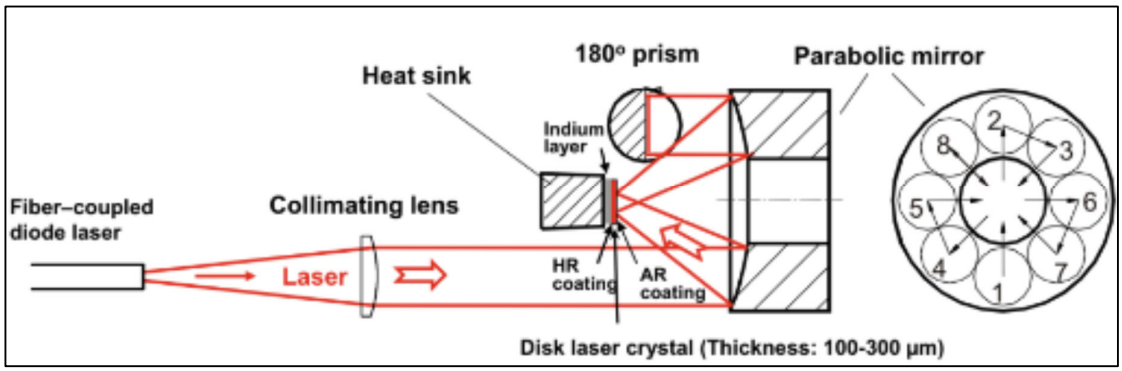

Fig. 1.22. Emission mechanism of disk laser apparatus [38]

1.8. Advantages of laser welding

a) Easily automated process.
b) Controllable process parameters.
c) The very narrow weld may be obtained.
d) High quality of the weld structure.
e) Very small heat-affected zone.
f) Welding of dissimilar materials is possible.
g) It is possible to weld very tiny, fragile workpieces.
h) No vacuum is necessary.
i) Minimal workpiece distortion.

1.9. Disadvantages of laser welding

a) The initial cost and maintenance cost is high.
b) Some metals might fracture as a result of the fast cooling.
c) LBW requires highly skilled labour.
d) 19 mm is the maximum welding thickness allowed.
e) Extremely poor energy conversion efficiency is seen in LBW. Typically, it is less than 10%.

1.10. Application areas

Laser welding may be used to address many technical problems, especially for parts that are delicate to the effects of high heat input, prone to deformation, or call for extremely accurate welding [37]. Laser welding provides a number of distinguishing benefits over other types of welding and have a wide variety of applications:

a) **Precision part:** Due to the low heat input, lasers are ideal for welding fine and fragile metal components with little internal tensions.

b) **Medical devices:** When welding medical equipment, non-contact welding and no welding splatter assure hygiene.

c) **Solenoids and machined items:** Due to the low heat input, lasers are perfect for combining machined components such as solenoids and produce minimum distortion.

d) **Aesthetics**: Laser welding produces outstanding results.

e) **Limited access:** Welding in otherwise inaccessible regions is possible thanks to the non-contact laser beam.

f) **Jewellery welding and high-value items:** It's a suitable choice for welding high-value, high-precision pieces, such as precious metals, because to its precise controllability and low heating impacts.

1.11. Optimization of process parameters

Optimization of process parameters in any manufacturing process, including laser welding, involves finding the best combination of parameters to achieve desired outcomes efficiently. Here are some general steps to optimize process parameters:

1. Define Objectives: Clearly define the goals and objectives of the welding process. This could include criteria such as weld strength, weld appearance, production speed, or cost efficiency.

2. Identify Key Parameters: Determine the process parameters that significantly influence the desired outcomes. These parameters can vary depending on the specific welding process and materials involved. Examples include laser power, welding speed, beam diameter, focal length, shielding gas, pulse frequency, and duration.

3. Design Experimental Plan: Develop a structured experimental plan to systematically vary the selected parameters. This could involve using techniques like Design of Experiments (DOE), where different combinations of parameter settings are tested to identify the most influential factors and their optimal levels.

4. Conduct Experiments: Perform the experiments according to the planned design. Ensure that the welding process is executed consistently and accurately. Collect relevant data, such as weld quality assessments, measurements, or process monitoring data, for each experimental condition.

5. Analyse Results: Analyse the data collected from the experiments to determine the effects of different parameter settings on the desired outcomes. Statistical analysis techniques, such as analysis of variance (ANOVA), regression analysis, or response surface methodology, can be used to identify significant factors and their interactions.

6. Optimize Parameters: Based on the analysis, identify the optimal parameter settings that lead to the desired outcomes. This may involve finding the parameter combinations that maximize weld strength, minimize defects, optimize process efficiency, or meet other defined objectives. Consider trade-offs between different factors and evaluate the feasibility of implementing the optimized settings in practical production scenarios.

7. Verification and Validation: Validate the optimized parameters by conducting additional experiments or welding trials. Verify that the optimized settings consistently produce the desired results and evaluate their robustness across different operating conditions.

8. Implement and Monitor: Implement the optimized parameters in the production environment. Continuously monitor the process performance, collect data, and analyze the results to ensure that the process remains optimized over time. Adjustments may be necessary based on changing conditions or performance feedback.
Optimization is an iterative process. As new information or requirements arise, it may be necessary to revisit and refine the parameter optimization process to ensure continuous improvement and adaptation to changing needs.

Optimization using a desirability function is a powerful technique to simultaneously optimize multiple process parameters in laser welding. The desirability function combines different response variables into a single objective function, allowing you to find the optimal parameter settings that maximize or minimize the desired outcomes. Here's how you can apply the desirability function approach:

1. Define Response Variables: Identify the response variables that reflect the desired outcomes of the welding process. These could include factors such as weld strength, weld appearance, heat-affected zone (HAZ) size, or porosity level. Each response variable should have a target value or range that represents the desired performance.

2. Normalize Response Variables: Normalize the response variables to a common scale. This step is necessary to ensure that each response variable contributes equally to the desirability function. Normalization can be done using techniques such as z-score normalization or scaling between 0 and 1.

3. Define Desirability Functions: Assign desirability functions to each response variable. A desirability function maps the response variable values to a desirability score between 0 and 1, representing the degree of desirability. Different types of desirability functions can be used depending on the nature of the response variable:

a) Linear: Assigns a linear increase in desirability as the response variable approaches the target value. It can be used when minimizing or maximizing the response is equally desirable.

b) Quadratic: Provides a higher desirability for response values closer to the target value. It is suitable when small deviations from the target are less desirable than larger deviations.

c) Exponential: Emphasizes desirability for response values close to the target and rapidly decreases desirability for larger deviations. It is useful when achieving the exact target value is crucial.

4. Calculate Overall Desirability: Combine the individual desirability scores using a composite desirability function. This function can be a geometric mean, weighted average, or any other aggregation method that suits the specific situation. The composite desirability function provides a single score that represents the overall desirability of a particular combination of process parameters.

5. Optimize using Desirability: Utilize optimization algorithms, such as numerical optimization or evolutionary algorithms, to find the process parameter settings that maximize the overall desirability. These algorithms systematically search the parameter space to identify the optimal combination.

6. Verify and Refine: Validate the optimized parameter settings through experimental verification or additional trials. Assess the welding process using the optimized parameters and evaluate whether the desired outcomes are achieved. If necessary, refine the desirability function or adjust the weighting of response variables to further improve the optimization results.

The desirability function approach allows you to balance multiple objectives and find the optimal compromise among them. It provides a systematic way to optimize process parameters in laser welding, taking into account various response variables and their relative importance.

Optimization algorithms such as Foraging and Hunting algorithms are heuristic search methods commonly used for solving optimization problems. While they may not be specific to laser welding, they can be applied to optimize process parameters in various domains. Here's a brief overview of these algorithms:

1. Foraging Algorithm: The Foraging algorithm is an optimization method inspired by the foraging behaviour of animals. It involves initializing a population of candidate solutions, evaluating their fitness, and simulating foraging behaviour through exploration, exploitation, and communication. The algorithm continues until a termination condition is met, aiming to

find an optimal or near-optimal solution. Ant colony, Particle swarm, Bee colony, Firefly, Cuckoo search algorithms are examples of foraging technique.

2. Hunting Algorithm: The Hunting algorithm is based on the concept of animals hunting for prey. It starts with a population of candidate solutions and simulates the hunting process to iteratively improve the solutions. The algorithm evaluates each solution's fitness or objective value and uses it to guide the search. The hunting process involves selecting the best solutions, applying operators such as mutation or crossover to create new solutions, and replacing the worst solutions with the new ones. This process continues until the termination condition is met. Gray wolf, Golden eagle, Cat swarm, Whale optimization algorithms are examples of hunting technique.

3. Teaching-Learning-Based Optimization (TLBO): This algorithm falls under the category of population-based heuristic algorithms. It is a swarm intelligence algorithm that draws inspiration from the teaching and learning process in a classroom setting. TLBO simulates the interaction between students (individuals) and teachers (guiding forces) to optimize a given problem. It operates on a population of individuals that undergo evolutionary processes, such as selection, crossover, and mutation, to explore and exploit the search space.

Forging, Hunting and Teaching-learning based algorithms are iterative and explore the search space to find the optimal solution. They differ in their exploration strategies and operators used for generating new solutions. These algorithms do not guarantee finding the global optimum but are effective in finding good solutions in a reasonable amount of time.

The search space boundaries and constraints for the parameters are need to be set-up to ensure feasible solutions. The algorithm would then iterate through the search space, evaluating different parameter combinations and updating the solutions based on the objective function. The termination condition can be based on a maximum number of iterations, reaching a satisfactory solution, or other stopping criteria.

It's important to note that the effectiveness of these algorithms depends on various factors such as the problem complexity, search space size, and the selection of appropriate operators. It may require some experimentation and fine-tuning to achieve satisfactory results for the specific laser welding optimization problem.

CHAPTER 2

LITERATURE REVIEW, SCOPE & OBJECTIVES OF PRESENT WORK

2.1. Literature review

Sun Z. et. al [39] stated that flexibility in design and production is substantially increased by the capacity to produce a product utilising a variety of various metals and alloys. Improvements in production economics are frequently made by optimising properties like heat, wear, and corrosion resistance. However, due to the significant variations in physical and chemical properties that may exist, joining dissimilar metal combinations is a difficult process. Primary characteristics of laser welding are precise positioning of the weld bead, quick heating and cooling, low distortion, process flexibility, and chances for product innovation.

Abdel-Monem El-Batahgy [40] different types of austenitic stainless steels with various thicknesses for fusion zone morphology and final solidification structure as a function of laser parameters. A CW mode CO_2 laser with a maximum output of 5 KW was used to create butt welding. In order to generate a weld with complete penetration, a small minimum fusion zone size, and an appropriate weld profile, it is important to carefully choose the laser power, welding speed, defocusing distance, and type of shielding gas combinations based on the thickness of the base metal. The microstructure and mechanical properties of welds are virtually completely unaffected by heat input. A finer solidification structure results from lower laser power and/or faster welding.

Zhao H. et. al [41] variety of viewpoints to analyse and interpret laser welding of automotive aluminium alloys from the 5xxx, 6xxx, and certain 2xxx series. The current state of knowledge about key physical processes such energy absorption, fluid movement and heat transfer in the weld pool, and alloying element vaporisation that occur during laser welding of these alloys is first reviewed. Second, a critical assessment of the structure and attributes of these weldments is made. Third, frequent flaws in laser-welded automotive grade aluminium alloys are described, along with scientific fixes.

Tzeng [42] concentrated on the variables in the pulsed Nd:YAG laser welding process. Pulsed laser seam welding (PLSW) is characterised by a wide number of process variables that affect the welding performance to varying degrees. Strategic control of key process parameters, such as mean laser power, average peak power density, pulse energy, and traversing speed, facilitates the PLSW process. In order to perform regulated pulsed laser welding of materials, a comprehensive investigation of the effects of the aforementioned laser settings on heat flow has also been made in the study.

Reed et. al [43]evaluated the microstructural and mechanical characteristics of the welded V-Cr-Ti alloy sheet materials using a pulsed Nd:YAG laser. An ideal combination of laser characteristics, including lens focal length, pulse energy, pulse repetition rate, beam travel speed, and an inventive shielding gas arrangement, led to deep penetration, defect-free, and oxygen contamination-free welds. The stability of the keyhole and providing an escape route for the gas trapped in the molten weld pool were discovered to be essential for producing welds without defects. Oxygen and nitrogen uptakes were reduced drastically by development of ECB.

Hirose et. al [44]welded age-hardened Al-Mg-Si alloy A6061-T6 plates using a 2.5 KW CO_2 laser and analysed. With comparison to a tungsten inert gas (TIG) weld, the width of the softened zone was substantially smaller in a laser weld. A kinetic equation describing the dissolving of age precipitates was used to quantitatively estimate the hardness distributions and the width of softened patches in HAZ. A high energy density and a fast-welding speed in laser welding produce noticeably narrower softened regions. After an ageing treatment of the softened zone the hardness and tensile strength of butt laser weld were nearly equal to those of the base plate.

Wagner F. et. al [45] demonstrated that laser welding can be employed to join incompatible metals such as Al to steel and Al to Ti due to the welding source's highly localised energy input. The joining process leads to the formation of intermetallic phases. Laser beam welding minimises an excessive development of intermetallic phases due to its locally constrained energy input, rapid joining speed, and concomitant high cooling rates. Intermetallic layer development can be prevented from growing larger than 10 μm, which improves the joint's ductility and other desirable mechanical qualities. Furthermore, Ti/Al and Fe/Al-joint phase development and mechanical characteristics are discussed.

Cao X. et. al [46] employed both CO_2 and Nd:YAG lasers, but welding of 5000 and 6000 series alloys in keyhole mode using latter received special attention. He evaluated the primary laser welding processing parameters, including the influence of the laser, process, and material-related variables on the weld quality. Additionally, the principal flaws found in laser welding Al alloys, including porosity, cracking, oxide inclusions, and loss of alloying elements, are reviewed in terms of their mechanism of development, primary influencing factors, and corrective actions. There is also discussion of the key mechanical characteristics including formability, tensile, and fatigue strength, as well as hardness.

Anawa E. et. al [47] successfully used laser beam welding (LBW) to create ferritic/austenitic (F/A) joints with appropriate mechanical qualities. To improve certain LBW parameters (laser power, welding speed and focus length), a statistical DOE was utilised. The chosen factors, each with five levels, were analysed using the Taguchi method. Using the notched-tensile strength (NTS) method, joint strength was evaluated. Following an analysis of the data using ANOVA and the S/N ratios for the ideal values, the findings were contrasted with the reference material. The Taguchi technique is superior, according to the experimental data.

Gao M. et. al [48] compared single laser and arc welding to the laser-MIG hybrid welded AZ31 magnesium alloy in terms of weld morphology, microstructure features, and mechanical qualities. By using the synergistic effects of the laser arc, hybrid welding can produce stable MIG arcs, reliable droplet transfers, and regular welds that are difficult to achieve with single MIG welding. In comparison to laser welding, hybrid welding has far higher ultimate tensile strength and elongation. The efficiency of hybrid welding is 1.2 times faster than that of single laser welding under these experimental conditions.

G. Padmanaban [49] had taken into account process variables including laser power, welding speed, and focal location in order to construct an empirical relationship that forecasts the tensile strength of the magnesium alloy AZ31B that has been laser welded. A central composite face-cantered design matrix with three factors, three levels, and full replications was used to perform the studies. The tensile strength of joints may be predicted with a 95% degree of confidence using the empirical relationship. The findings suggest that, after laser power and focus position, welding speed has the biggest impact on tensile strength.

Torkamany et. al [50] studied laser welding of low carbon steel to 5754 aluminium alloy in a steel-on-aluminum overlap arrangement, to lessen the production of intermetallic materials

while laser welding. According to the results, the percentage of intermetallic components will grow as peak power, pulse duration, and overlapping factor all increase in constant pulse energy and peak power. Conversely, lowering the aforementioned values will have negative consequences such insufficient penetration depth, spattering, and cavity development. Finally, a peak power, pulse duration, and overlapping factor optimization were provided.

Jiyoung et. al [51] investigated laser welding as an alternative to the conventional bolted connection of the ring gear and differential case in the car's power train. Cast iron and steel with a high carbon content are difficult to weld. The use of laser welding and filler metal with a Ni-base was used to resolve these welding issues. When compared to the bolted connection method, the results of welding with Ni-base filler metal had noise and hardness issues, but they satisfied the requirements for torsional stiffness and durability. Therefore, the penetration depth was reduced. Additionally, fatigue, torsional stiffness, and welding deformation were evaluated using numerical methods.

Acharjee et. al [52] experimented with and researched diode laser transmission welding of dissimilar thermoplastics such as PMMA (polymethyl methacrylate) and ABS (acrylonitrile butadiene styrene). Using RSM, it is determined how different laser welding parameters, including laser power, welding speed, stand-off distance, and clamp pressure, affect weld strength and weld width. To create the mathematical models needed to establish a relationship between the process parameters and the responses, planned tests and analysis are carried out. The sequential F-test, lack-of-fit test, and ANOVA approach are used to assess the suitability of the created models.

Khan et. al [53] looks at laser beam butt welding of dissimilar stainless steels AISI430F and AISI440C. In order to prevent the creation of microcracks, a combined welding and pre- and post-weld treatment technique was created and employed successfully. The effects of line energy and laser welding parameters on weld bead geometry were also investigated, and an optimal laser-welded joint was attempted utilising a full factorial design of experiment technique. Positive changes were observed in all bead properties as laser power increased or welding speed decreased. The ideal parameters for an excellent welded component were laser power of 790-810 W and welding speed of 3.6-4.0 m/min.

Jung et. al [54] used a high-quality continuous wave diode laser with a line-shaped beam to execute laser direct welding of CFRP to Al alloy. The tensile shear test findings showed that an effective lap joint between CFRP (3mm thickness) and Al alloy (2mm thickness) could be

created with a strength of roughly 3 KN. Along the area of CFRP where it melted, the joints cracked. Numerous submillimeter-sized bubbles were found sporadically forming in the wide and shallow melted zone of the CFRP, according to cross sections of the joints. Additionally, a nanometer-thick aluminium oxide coating (k-Al_2O_3) already present on the surface of the aluminium alloy was securely bound to the molten polyamide plastic.

Naeem et. al [55] have utilized CW and quasi-CW fibre lasers in extensive experimental research to weld a variety of diverse material combinations used in the aerospace, electronics, and medical industries. Investigations using various laser and processing settings were conducted, including mechanical and metallurgical tests. It has been made clear that fibre lasers' exceptional beam quality makes it possible to fuse unusual combinations of materials. Controlling the mixing of the different elements is crucial for creating welds with high tensile strength because it prevents the development of brittle intermetallic compounds, which can cause cracking and produce welds with poor mechanical qualities. This study demonstrates that the kind and thickness of intermetallics is significantly influenced by heat input and cooling pace.

Meco et. al [56] made a lap joint configuration with steel on top, 2 mm thick steel (XF350) and 6 mm thick aluminium (AA5083-H22) using the welding-brazing process employing a continuous wave (CW) fibre laser with 8 KW of maximum power. The steel surface was exposed to laser radiation, and the heat was transferred through the steel plate to the steel-aluminum contact, where the aluminium melts and wets the steel surface. The welded samples appeared flawless, and the weld micrographs revealed the presence of a layer of brittle intermetallic compounds (IMC), which was generated when Fe and Al atoms reacted.

Chopde et. al [57] looked into the laser welding of 2 mm thick Al and Cu With the aid of previous literature investigations. Due to the significant physical property misalignment and even worse metallurgical affinity between the two materials, intermetallic phase development and fracture sensitivity during fusion welding of copper and aluminium are induced. The difficulties of the current methods for joining aluminium and copper are discussed, along with the viability of laser welding the same metals more effectively.

Mishra et. al [58] looked into the microstructure and characteristics of deep-penetrated laser-welded joints made of 316 SS and Inconel 625 alloys. Weld microstructures were assessed using optical microscopy, the Brinell Hardness test, the Tensile test, and the stress rupture

properties. According to the experimental findings, the microstructure of the weld zone close to the fusion line in Inconel 625 was primarily cellular, whereas that of SS 316 was columnar dendrites.

Elena-Manuela et. al [59] demonstrated the use of a 1 kW diode laser to weld AISI 321 SS and AISI 1010 carbon steel thin sheets in butt weld. It is addressed how the welding speed affects the joints' shape and microstructure. By using optical, electron, and EDS analysis to structurally characterise the welds, it is possible to see distinct mixed and unmixed zones in the weld bead due to the rapid cooling. The structure of the weld bead is austenitic-martensitic-ferrite. Migration of chromium and nickel was seen in the weld bead area. The dissimilar joints exhibited good tensile behaviour since none of the specimen failures occurred close to the weld zone.

Moharana et. al [60], in their work, copper and AISI 304 stainless steel are joined together without the use of any filler material using pulsed wave Nd-YAG laser welding. To determine the weld penetration depth and metallurgical behaviour within the weld zone, a mechanical and metallurgical examination is conducted. Weld pool geometry confirms that the pulsed wave Nd-YAG laser achieves its maximum penetration depth and that the penetration depth is directly related to pulse energy. Copper solidifies last and flows inside the matrix of the weld zone as it solidifies. The results of the microhardness (MH) investigation indicate that $MH_{SS} > MH_{Weld\ zone} > MH_{Copper}$.

Zhang et. al [61] thoroughly examined and assessed welding technology for ceramics and metals as a research topic with substantial prospects. The current state of this field's research is examined from a variety of process aspects, including fusion welding, brazing welding, and diffusion welding. By addressing the thermal expansion mismatch and lowering the bonding temperature and pressure, it is possible to minimise residual stress and brittle intermetallics close to the interface of the transition joint by employing suitable intermediary materials between these two materials.

Franco et. al [62] demonstrated how power spatial modulation of the laser beam can be used to solve Cu's high thermal conductivity and low absorptivity-related laser welding difficulties. Copper plates are subjected to laser welding with beam oscillation (wobbling effect). Weld surface aspect, bead profile, and the evolution of the microstructure are described in relation to the main welding parameters. The solidification front of the weld metal, which forms as the laser oscillates and moves continually, was seen in the microstructure of the fusion zone as

circular-shaped bands. It is a good option for industrial applications where high thermal and/or electrical conductivities are desired.

Zhang et. al [63] in his work describes the laser welding and brazing of 304 SS and Al_2O_3 ceramic dissimilar metal materials. The outcomes demonstrated that when the laser was directed at the SS side of the junction, filler metal was melted to combine the SS and Al_2O_3. The 1.5 mm thick SS plate would not entirely melt when exposed to a laser beam. The filler metal melted at the SS-Al_2O_3 ceramic contact was due to heat conduction. The contact of the SS and Al2O3 ceramics formed a brazed weld. The joint's response layer ruptured at the ceramic side with a 74 MPa maximum tensile strength.

Hongbo et. al [64] used laser welding to successfully join dual-phase steel DP590 (1.4 mm) and CFRP (3 mm). To further understand the impact of laser power on joint characteristics, bonding mechanisms, and fracture behaviour, experiments and numerical simulations were carried out. According to the findings, increasing laser intensity increased the width and depth of CFRP melting. Compact-bonding was accomplished using a laser with a 400–700 W power range. The additional increase in laser power resulted in the decomposition of CFRP at the interface. With varying laser powers, three separate fracture modes were discovered in the joints: cohesion fracture (CF) in CFRP at 500 W and 600 W, interface fracture at the inner region along with cohesion fracture at the outer region at 700 W and 800 W.

Zapico et. al [65] shows potential applications of laser welding in the e-mobility sector. Particularly, dissimilar welding of thin sheets comprised of various materials, including steel, aluminium, and copper, is increasingly acknowledged as an efficient option for numerous joining applications in the manufacture of batteries and related components. His purpose of research is to assess whether a good lap welding configuration may be used to attach thin copper sheets to thin steel ones. Particularly when cylindrical cells need to be electrically connected to any of the battery's component parts, such as printed circuit boards, busbars, etc. An experimental campaign was conducted using a continuous wave fibre laser and a galvo scanner in order to develop a process window for describing the aforementioned welding application. Metallographic examinations, microhardness measures, electrical conductivity testing, and other methods were used to characterise the results and studies of energy dispersive systems using scanning electron microscopy. It’s seen that the lower steel layer serves as the external housing for a single cell and that a drop through could badly harm the cell itself, special

emphasis was made on the role of process factors in controlling the penetration depth on this layer of steel.

The study of **Antony et. al** [66] primarily examines the mechanical and metallurgical properties of dissimilar joints made by laser welding of commercially pure copper and stainless steel 316L. The tensile test of weldments, Vickers microhardness, and other tests were performed on the laser-welded specimen. Optical metallography, an EDS-based investigation into the chemical make-up of the intermediate layer. The weld area exhibits greatest yield and ultimate tensile strength during the tensile testing. Additionally, the weld zone has a larger degree of elongation. According to the results of the Vickers microhardness test, the copper base had the lowest hardness. While the Cu-SS316L region's weld portion obtained the highest hardness rating. The SEM morphology shows that there is sufficient Cu and SS316L in the weld zone.

Adjusting the processing parameters of welding speed, laser power, offset, and incline angle of the laser beam in the direction of the stainless steel, the microstructures and mechanical properties of stainless steel & copper laser welding were studied by **Chen S et. al** [67]. Fusion welding might be controlled ably changed from the joining mode to welding-brazing. In contrast to the fusion zone mode, which unites stainless steel and copper by melting and mixing both metals, welding-brazing joins liquid stainless steel to solid copper. It is possible to successfully prevent the melting of the copper and ensure that the joining takes place via welding-brazing by offsetting and inclining the laser beam in the direction of the stainless steel. On the copper side, the heat-affected zone (HAZ) grains expand considerably. Spherical particles with copper are produced during liquid separation operations, and some of the larger copper-containing spheres also contain tiny stainless steel-containing spheres. The joint's peak tensile strength is 260 MPa. Depending on the processing parameters applied, the joint showed three typical forms of fracture: the interface, the heat affected zone (HAZ), and the fusion zone. While copper melting only has a negligible impact on tensile strength, it does have an adverse impact on joint toughness.

2.2. Scope of present work

Laser welding of copper and steel is a challenging process due to the different physical properties of the two metals. There are a number of problems that arise when welding steel and copper. These problems include:

a) **Material incompatibility:** Steel and copper have significantly different physical and thermal properties, making their welding challenging. Copper has a melting point of 1085 °C, while steel has a melting point of 1538 °C. This means that when welding steel and copper, it is important to use a heat source that is hot enough to melt both metals, but not so hot that it vaporizes the copper. Copper has a much higher thermal conductivity than steel. This means that heat travels through copper much faster than it travels through steel. This can lead to problems such as heat build-up and cracking. Copper expands and contracts more than steel when it is heated and cooled. This can lead to problems such as gaps and voids in the weld. Copper is not very soluble in iron. This means that when copper is welded to steel, it is difficult to get the two metals to mix properly. This can lead to problems such as poor weld strength and brittleness. These differences in properties can lead to issues such as poor fusion, cracking, and distortion during the welding process. Research is needed to develop welding techniques that ensure proper bonding and minimize these problems [66].

b) **Metallurgical incompatibility:** Steel (BCC) and copper (FCC) have different crystal structures and metallurgical properties. When welded together, the resulting joint can exhibit a range of metallurgical issues, such as brittle intermetallic compounds (IMCs like $Cu_{70}Fe_{30}$, formation of undesirable compounds, and changes in mechanical properties. At room temperature, copper and iron are two separate metals. When they are heated to 1000 degrees Celsius, they begin to react with each other. The atoms of copper and iron break away from their individual crystal structures and start to move around freely. As they move around, they collide with each other and form new bonds. These new bonds create a solid solution of copper and iron atoms. The alloy is now a single, uniform material. The formation of $Cu_{70}Fe_{30}$ is a reversible process. If the alloy is cooled below 1000 degrees Celsius, the copper and iron atoms will start to rearrange themselves into their original crystal structures. The alloy will then revert back to being two separate metals. $Cu_{70}Fe_{30}$ alloy is brittle. The presence of iron atoms in the alloy disrupts the orderly arrangement of copper atoms, which makes the alloy more susceptible to cracking. The alloy has a high yield strength, which means that it can withstand a lot of stress before it begins to deform. However, once it does deform, it is more likely to crack than a more ductile material. The alloy has a low fracture toughness, which means that it is more likely to break when subjected to a sharp impact

[66]. Research is required to understand the metallurgical behaviour of steel-copper joints and develop strategies to mitigate these issues.

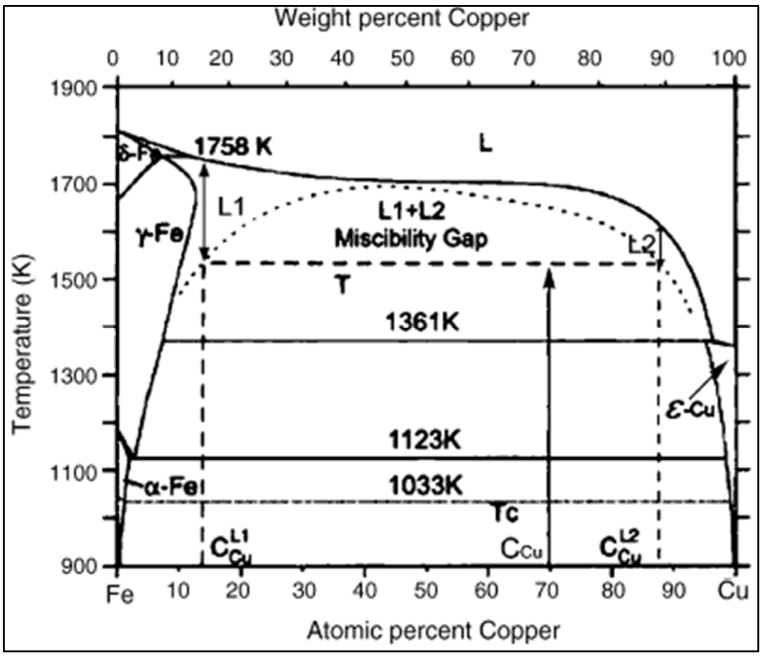

Fig. 2.1. Fe–Cu phase diagram including calculated metastable miscibility dome (dot line) [68]

c) **Joint design and preparation:** Achieving a strong and durable weld between steel and copper requires careful joint design and preparation. The differing coefficients of thermal expansion between the two metals can lead to residual stresses and distortion. Research is needed to optimize joint designs, including considerations such as joint geometry, gap tolerances, and surface preparation techniques, to ensure proper fusion and minimize distortion [66].

d) **Welding process selection:** There are various welding processes available for joining steel and copper, including arc welding (such as TIG and MIG), resistance welding, and laser welding. Each process has its advantages and limitations in terms of heat input, control, and metallurgical outcomes. Research is necessary to evaluate and compare these processes, considering factors like joint strength, efficiency, and cost-effectiveness [66].

e) **Interfacial reactions and corrosion:** Steel and copper are prone to galvanic corrosion when in contact with each other. Welding can accelerate this process, leading to premature joint failure. Research is required to investigate the interfacial reactions between steel and copper during welding and their impact on corrosion resistance. Developing suitable coatings or protective measures to mitigate corrosion in the welded joints is another area of research [66].

This can lead to problems such as:

1) Poor penetration of the laser beam into the copper
2) Hot cracking in the weld zone
3) Corrosion of the weld zone

In some cases, it may be necessary to use a filler metal to improve the strength and corrosion resistance of the weld. The filler metal should be made of a material that has similar physical properties to both copper and steel. With proper care, laser welding of copper and steel can produce high-quality welds that are strong, corrosion-resistant, and aesthetically pleasing.

Here are some ways to get strong laser welds of copper and steel [69], [70]:

1) Use a laser with a wavelength that is well-absorbed by both copper and steel. CO_2 lasers (10600 nm) are a good choice for this application.
2) Use a continuous wave laser rather than a pulsed laser. This will help to prevent hot cracking.
3) Use a high-quality filler metal that is made of a material that has similar physical properties to both copper and steel.
4) Preheating the steel and copper can help to equalize the temperature between the two metals and reduce the risk of cracking.
5) Use a welding process that can heat the copper and steel evenly.
6) Clean the copper and steel surfaces before welding.
7) Use a shielding gas to protect the weld from the elements.
8) Use a filler metal that is compatible with copper and steel that can help to improve the strength and weldability of the joint.
9) Weld slowly and carefully to avoid overheating the copper and steel.
10) Welding in a controlled atmosphere, such as argon or helium, can help to prevent oxidation and improve the quality of the weld.

Here are some additional research problems that are being investigated in the field of steel and copper welding:

1) Developing new welding techniques that can overcome the problems associated with welding steel and copper.
2) Developing new filler metals that are more compatible with steel and copper.
3) Developing new welding procedures that can improve the quality of the weld.
4) Developing new methods for preventing oxidation and brittle IMCs formation that can occur during welding.

To successfully weld copper and steel using a laser, it's important to optimize the laser parameters to accommodate the different materials. Here are some key factors to consider:

1) **Laser wavelength:** Copper has a higher reflectivity at commonly used laser wavelengths, such as those in the near-infrared range. Choosing a laser wavelength that is less reflective to copper, such as green or blue, can help improve the welding process.

2) **Laser power:** Copper requires higher laser power compared to steel due to its higher reflectivity. Adjusting the laser power settings appropriately can ensure sufficient energy is delivered to both materials for effective welding.

3) **Welding speed:** Copper has a lower melting point than steel, so it's crucial to control the welding speed to avoid excessive heat build-up in the copper. Adjusting the welding speed can help achieve a balanced heat input between the two materials.

4) **Filler material:** In some cases, it may be necessary to use a filler material during copper and steel laser welding to enhance the joint strength. The filler material should be compatible with both copper and steel, and its selection depends on the specific application requirements.

5) **Joint design:** Designing the joint between the copper and steel parts is essential for successful laser welding. Proper joint preparation, including fit-up and surface cleanliness, is crucial to achieve strong and reliable welds.

These new techniques have led to significant improvements in the quality of copper steel laser welds. In particular, the formation of IMCs has been significantly reduced, and the mechanical properties of the welds have been improved. As a result, laser welding is now a viable option for joining copper and steel in a variety of applications. These are some specific examples of recent developments in copper steel laser welding:

1) In 2021, researchers at the University of California, Los Angeles (UCLA) developed a new method for laser welding copper and steel that uses a high-power laser and preheating to reduce the formation of IMCs. The resulting welds had excellent mechanical properties and were comparable to welds made using traditional methods.
2) In 2022, researchers at the Technical University of Munich (TUM) developed a new method for laser welding copper and steel that uses a pulsed laser and shielding gas to control the weld pool shape and minimize the heat affected zone. The resulting welds had excellent surface quality and were able to withstand high loads.

These are just a few examples of the recent developments in copper steel laser welding. As research in this area continues, it is likely that even more improvements will be made in the future. This will make laser welding an even more versatile and reliable joining process for a wide range of applications.

2.3. Objectives of present work

Stainless Steel grade 304 (SS 304) and Copper (Cu) has diverse applications in engineering field. This research work aims to investigate and develop a better understanding of the laser weldability of these two metals. Previous researchers have carried out laser welding of these two metals using either filler materials or interlayers or using large wavelength lasers like CO_2 lasers (10600 nm). The main objective of this work is to carry put laser welding of Cu and SS 304 without using any filler material or interlayer and also do it with a lesser wavelength laser like fibre laser (1064 nm). In order to better understanding of the phenomenon, five process parameters i.e., Laser Power (LP), Scanning Speed (SS), Defocus distance (DF), Argon Gas Pressure (GP) & Number of Pass (N) are considered whereas fusion zone or seam width and heat affected zone are considered as quality characteristics of the laser welded joint. The main objectives of this present research work are:

1) To perform the laser butt welding of 1 mm thick Cu and SS 304 using 500W continuous wave Fibre laser.
2) To reduce the formation of longitudinal crack along the weld interface caused by formation of brittle intermetallic compounds (IMCs).
3) To identify the most significant process parameters using statistical DOE based on response surface method.
4) To investigate the effect of laser welding parameters on quality characteristics of welded joint.
5) To develop the empirical relationship between key process parameters and weld quality characteristics.
6) To optimize the process parameters in order to obtain optimum weld quality using desirability function analysis technique.
7) To conduct the confirmation test in order to validate the developed mathematical model
8) To make samples for Tensile strength test of welded joints at particular parameters.
9) To prepare samples for Micro hardness test of joints.
10) To perform Tensile test and micro hardness test.

CHAPTER 3

EXPERIMENTAL SET-UP

3.1. Laser beam welding machine

An image of the experimental setup utilized in this investigation is shown in Fig. 3.1. a system of 1064 nm continuous wave fibre laser powered by a 500W multi-diode Ytterbium doped pump. This Laser system has following main components: (1) Power supply, (2) Stabilizer, (3) Chiller unit, (4) Control panel, (5) Laser source, (6) Air-conditioner panel, (7) DAQ with PLC, (8) Laser head with beam delivery and focusing lens, (9) Fume gas extractor, and (10) Shielding gas supply arrangement.

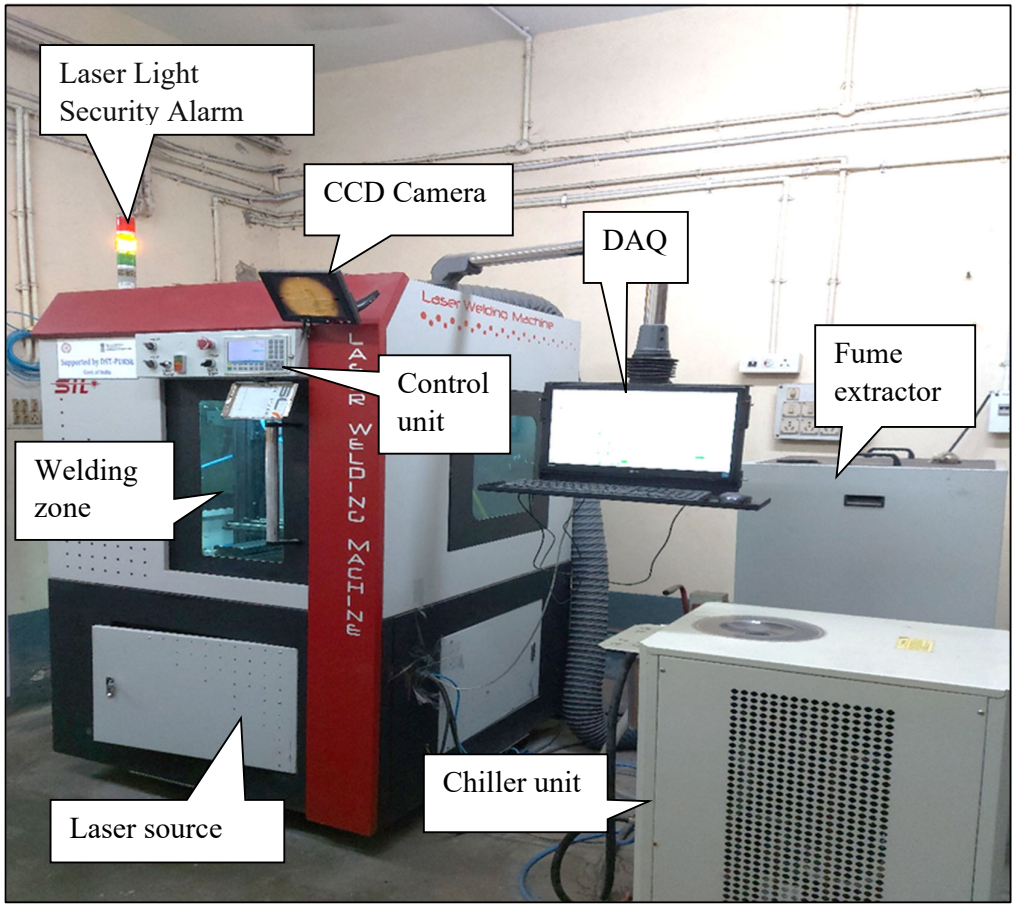

Fig. 3.1. Laser welding machine

3.2. Specification of machine

Table 3.1. Laser specification

Laser type	Multi-diode pump CW Fibre laser
Maximum power	500 Watt
Wavelength	1064 nm
Mode of operation	Continuous mode
Mode of laser beam	Fundamental/Gaussian mode (TEM_{00})
Laser beam spot diameter	500 µm

3.3. Flow chart of procedure

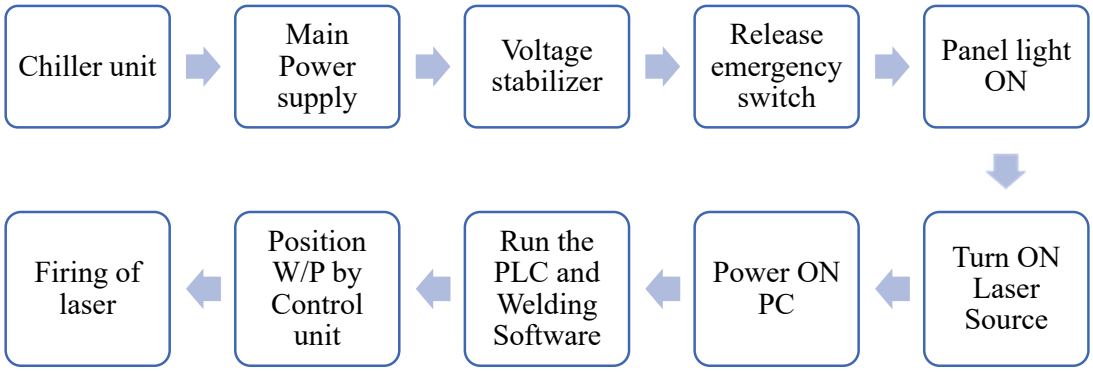

3.4. Components of LBWM

3.4.1. Main power supply

In order to make power accessible at its output in the form of a smooth and constant direct voltage, a mains power supply must convert the power supplied to it at its input by the sinusoidally alternating mains electric supply. A variety of source voltages are necessary for the proper operation of electronic equipment.

Although power supplies have significantly increased in reliability in recent years, modern power supplies are incredibly complicated and can deliver output voltages that are tightly

controlled by feedback mechanisms. Automatic safety circuits are also present in many power-supply circuits to guard against harmful over-voltages or over-current conditions.

3.4.2. Stabilizer

A voltage stabilizer is a tool that automatically keeps the voltage level constant. Regardless the changes in the input, or incoming supply, it is an electrical device that used to deliver a consistent voltage output to a load at its output terminal.

Fig. 3.2. Voltage Stabilizer

Table 3.2. Stabilizer specification

Input voltage	300 to 470 V
Output voltage	415 V
Power	10 KVA
Maximum capacity	139 A

3.4.3. Chiller unit

A laser chiller is the primary element and the most crucial device utilized in managing laser temperature. In order to dissipate heat from laser heat-dissipating components, devices such as laser chillers, portable chillers, rack mounted chillers, water chillers, and heat exchangers are entirely self-contained. De-ionized water is used in chiller.

Fig. 3.3. Chiller Unit

Table 3.3. Chiller unit specification

Power	220 V/50 Hz
Total input	4080 W
Normal cooling capacity	5200 W
Refrigerant	R 22
Refrigerant charge	1580 g
Maximum water volume	25 L

3.4.4. Control panel

The laser beam system's control panel plays a crucial role. We can control and operate the machine manually from here. Positioning of fixture in X-Y space, firing of laser in Z space as needed are frequently used controls. It also facilitates an emergency button which can be used if any problem occurs during operation.

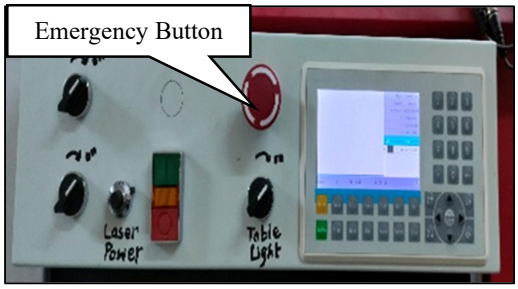

Fig. 3.4. Control Panel

3.4.5. Shielding gas (Ar) supply system

Ultra-High Purity (UHP) Ar (99.99%) is non-toxic, tasteless, odorless, and colorless. 0.93% of the earth's atmosphere is made up of the noble gas Argon (Ar). For rolling and annealing metals and alloys, argon provides an inert, sterile atmosphere, free from nitrogen and oxygen. Argon is used in the casting to remove porosity from molten metals and fix casting flaws. Ar serves the same purpose of providing an inert environment as well in laser welding.

Fig. 3.5.1. Ar Gas Cylinder

Table 3.4. Ar gas cylinder specification

Total Weight (TW)	51.4 Kg
Water Capacity (WC)	46.7 L
TP	250 bar
FP	150 bar

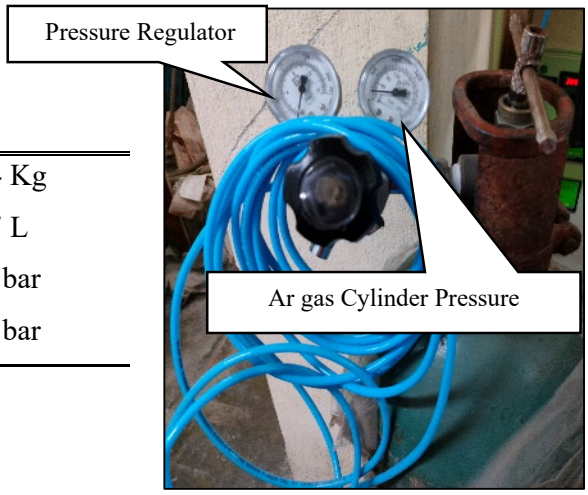

Fig. 3.5.2. Pressure gauges

3.4.6. Air-conditioner panel

Air to air heat exchangers is a relatively inexpensive and energy efficient solution, but they won't safeguard equipment in places where the ambient temperature is higher than the electrical components' maximum functioning temperature.

A refrigerant, which is akin to a heat pipe, is used in air conditioners for electrical control panels. However, to enhance cooling and lower the enclosure's temperature, a compressor pushes the evaporating refrigerant via a condenser coil and an evaporator coil.

Table 3.5. AC panel specification

Capacity	500 W
Voltage	230 V
Current	2.5 A
Refrigerant	R134a
Ambient temperature range	10° C to 45° C
Frequency	50 Hz
Weight	24 Kg

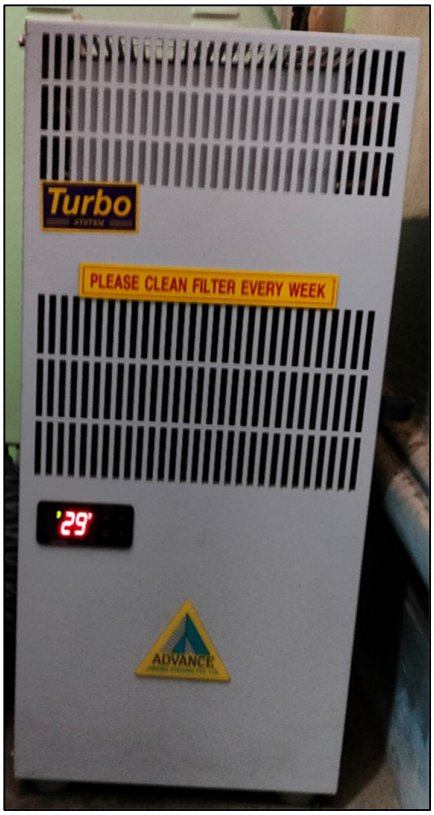

Fig. 3.6. AC Panel

3.4.7. Data acquisition system (DAQ) & Programmable logic controller (PLC)

An ensemble of software and hardware known as a data acquisition system which enables the measurement or control of physical properties of an object in the real world. DAQ hardware, sensors, actuators, signal conditioning gear, and a computer running DAQ software make up a full data acquisition system.

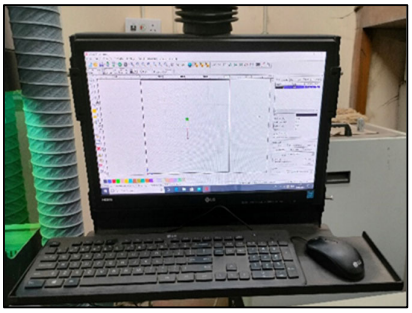

Fig. 3.7.1. DAQ Set up

A programmable logic controller is a small computer that has inputs for data and outputs for sending and receiving commands. A PLC's primary duty is to regulate a system's operations using the underlying logic that has been programmed into it. PLCs are used by businesses all over the world to automate their most crucial procedures.

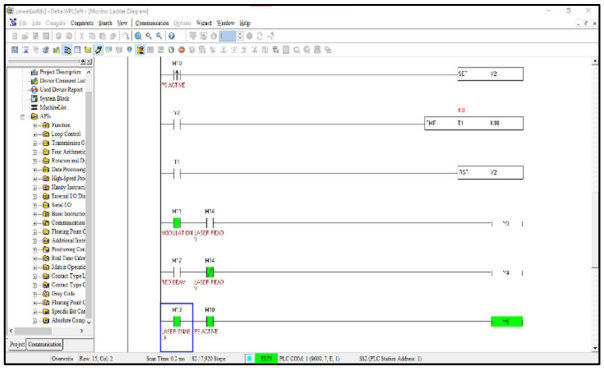

Fig. 3.7.2. PLC Interface

3.4.8. Fume extractor and dust collector

A dust or fume extraction system is an air quality enhancement tool used in commercial and industrial production facilities to enhance the safety and quality of the breathable air by eliminating airborne particulates. Systems for extracting dust operate using the basic principles of capture, transfer, and collection.

A difficult part of plant management is maintaining indoor air quality while reducing energy use and enhancing production efficiency. Dust collectors can have an effect in all these areas, whether they are utilized for product recovery or pollution control.

Fig. 3.8. Fume extractor

Table 3.6. Extractor specification

Frequency	50 Hz
Rotor speed	2880 RPM
Power	2 HP
Input	415 V

3.4.9. Laser source

It operates on the tenet that an atom's electrons become energized when they absorb energy. After some time has passed, it eventually returns to its ground state, at which point a light photon is released. In laser machine wavelength are near-infrared ranging from 0.75 nm to 1.4 nm.

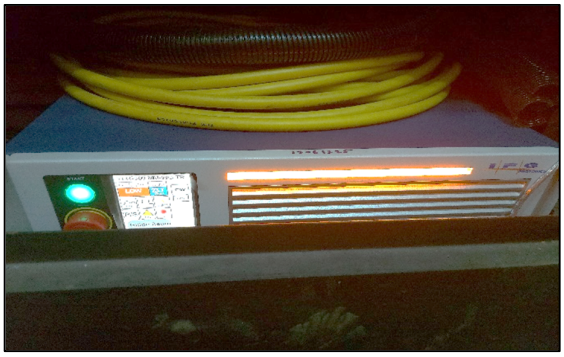

Fig. 3.9. Laser source

3.4.10. Laser head and weld fixture

Fibre cable joins into the laser head to supply the beam from laser source. It is also provided with the supply from shielding gas during welding. F-theta lens is also provided in the head to control the defocus distance. Z-axis movement is facilitated by laser head. A copper nozzle is also provided to concentrate the beam more with high speed. Clamping arrangement holds the workpiece during welding to avoid bending of the job. X and Y-axis movements are provided with the weld bed and facilitated with proximity sensors. CCD camera is used for visualization.

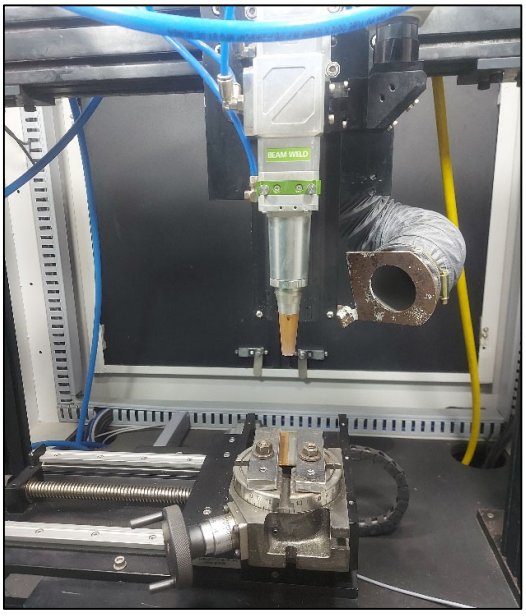

Fig. 3.10. Laser head & weld fixture

3.5. Defocusing

The separation between the focus and the workpiece surface is referred to as defocus. Positive defocus refers to a focus above the workpiece, whereas negative defocus refers to a focus below the workpiece. Due to the excessively high-power density of the spot centre at the laser focus, which readily evaporates into holes, laser welding requires a certain degree of defocus. Greater penetration is attained when negative defocus is applied. Positive defocus should be employed when welding thin materials. The beam focusing mechanism, as well as positive and negative defocus, are shown in Fig. 3.11 [8].

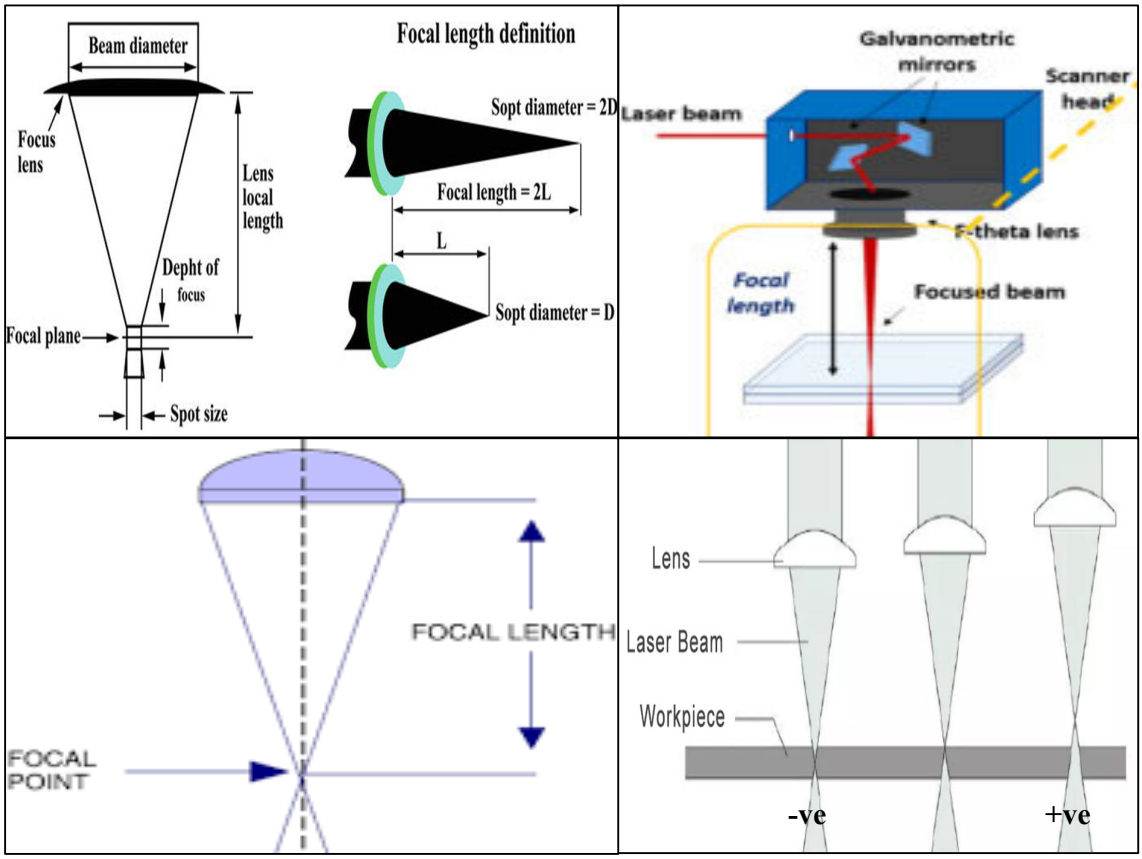

Fig. 3.11. Schematic diagram of laser beam focusing system & defocus [8]

Fig. 3.12 depicts a schematic representation of laser welding system.

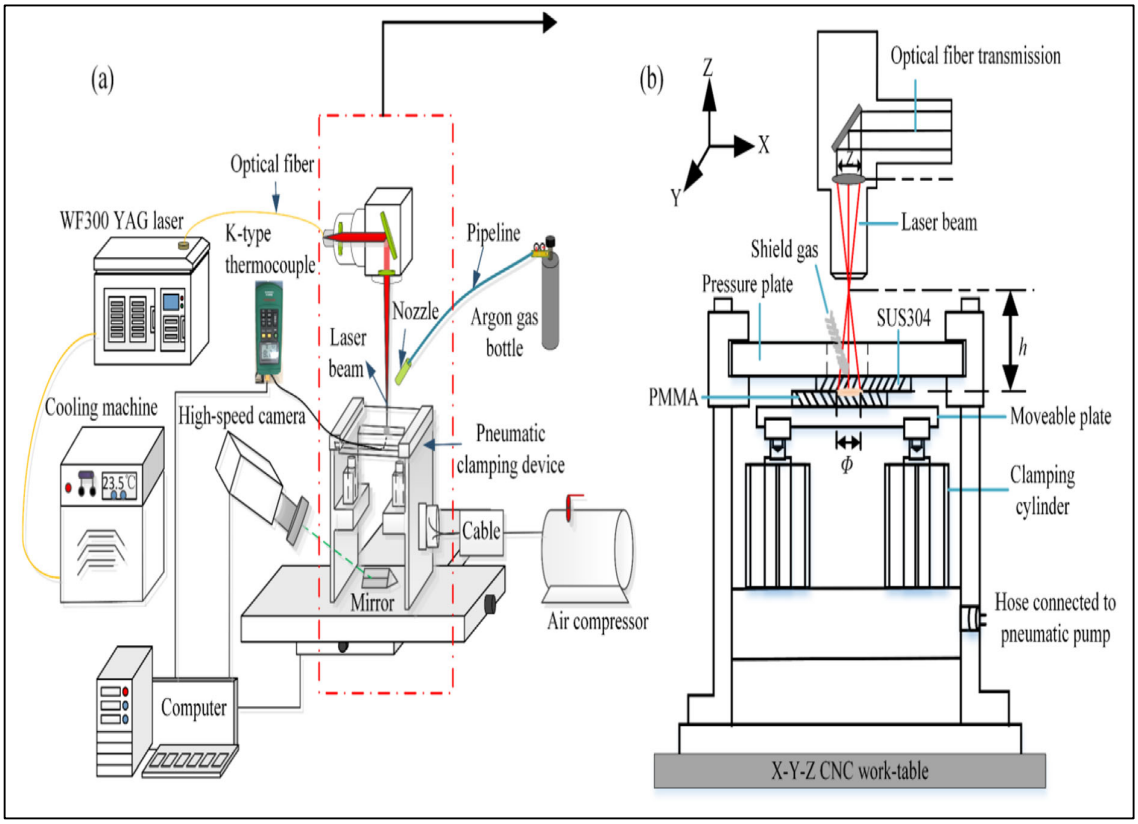

Fig. 3.12. Schematic representation of laser welding setup [71]

CHAPTER 4

MATERIALS, EXPERIMENTAL PLAN & PROCEDURE

In-depth coverage of the work output and the experimental method used for the current study accomplishment is provided in this chapter. The first few paragraphs of this chapter give a quick overview of the experimental planning and the Copper (Cu) & Stainless steel (SS) samples used in the experiment. The details of the experiment are next, including selecting the process parameters and establishing their constraints. The next part goes into great depth on the tools and procedures utilised for the experimental research.

4.1. Workpiece material

Commercially available Pure Copper (Cu) and Stainless-Steel Grade 304 (SS 304) is used as the workpiece materials for laser welding of dissimilar materials. Details of the workpiece materials are provided below:

Table 4.1. Chemical compositions of materials used (wt%) [67]

Name	O	S	Zn	Cu+Ag	Fe	Other
Cu	≤0.06	≤0.005	≤0.005	≥99.9	≤0.005	≤0.1

Name	C	Si	Mn	Cr	N	Ni	P	S	Fe
SS 304	≤0.15	≤0.75	5.5-7.5	16-18	≤0.25	3.5-5.5	≤0.03	≤0.06	Rest

Table 4.2. Physical and mechanical properties of Cu & SS 304 [72], [73]

Properties	Cu	SS 304
Dimension (mm)	65x15x1	65x15x1
Melting point temperature (°C)	1085 °C	1450 °C
Density (Kg/m^3)	8940	8000
Poisson's ratio	0.32-0.34	0.27-0.30

Elastic modulus (GPa)	130	193
Tensile strength (MPa)	210	515
Yield strength (MPa)	33.33	205
Elongation (%)	60	40
Reduction in area (%)	50	50
Hardness (HB)	40	175
Thermal expansion (10^{-6}/°C)	16.7	17.2
Thermal conductivity (W/m-K)	385	16.2
Specific heat (J/kg-K)	389	500
Strain rate (sec^{-1})	10^{-5}-10^{-4}	10^{-3}-10^{-1}

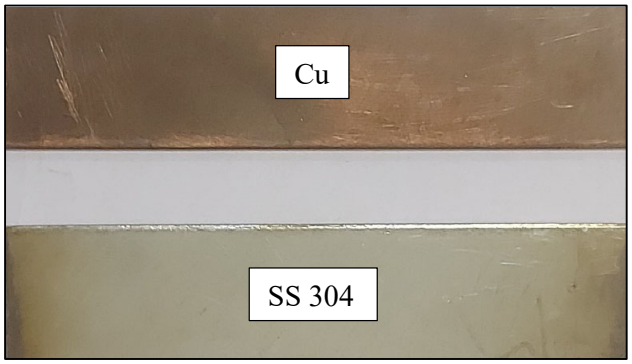

Fig. 4.1. Pictorial view of workpieces

4.2. Experimental plan

The current study has been carried out experimentally using the following experimental approach:

(1) Sample preparation for Cu and SS 304. Rectangular plates measuring 65 x 15 x 1 mm needed to be cleaned, cut, and prepared for laser beam welding.

(2) Making the experimental arrangements like preparing fixtures, edge preparation, proper alignment needed to execute laser beam welding.

(3) Pilot tests are conducted to determine the operating range for Laser Beam Welding studies in order to get the desired value of output responses. For various combinations of input parameters within the available system range, experimental design and

execution of laser welding trials are conducted, and the sub-range within it with desirable qualities and machined features is chosen.

(4) performing laser beam welding experiments using a range of process parameters, including laser power, laser scanning speed, defocus, gas pressure and number of passes. When performing the welding, the appropriate input process parameter combinations are applied.

(5) Using a microscope to examine and quantify the weld sample.

(6) ASTM standard Tensile test sample preparation with the help of wire cut EDM machine.

(7) Micro hardness test sample preparation with various grit size emri paper.

(8) Using a tensile testing equipment to perform pull tests on the prepared samples to ensure the functioning of the joints and using a micro hardness tester machine to find & compare hardness value among the welded joint and parent material.

4.3. Procedure

(a) Turn on the chiller unit switch, then the laser system's power supply and switch on the stabilizer.

(b) Release the emergency switch and turn on the table light, auto homing will begin to go into default configuration.

(c) Switch on the laser source by rotating the key anti clockwise.

(d) Turn on the desktop and set the gas pressure in argon cylinder by manual lever & knob.

(e) On the desktop, choose the power icon to open PLC interface. Run the PLC interface and SET ON the subsequent controls of PS, Modulation and Laser enable which make

the laser source ready to fire laser. Then chose the laser welding program icon to open laser welding control interface.

(f) Fix and align the workpiece in the rotatable fixture and maintain proper contact at the welding interface and place it in the welding zone.

(g) Use continuous or manual mode to manually adjust the location of the workpiece under focussed or defocused conditions.

(h) Set the desired laser power in the PLC interface.

(i) Select a vertical or horizontal line and enter a length in the welding software.

(j) Set the welding process settings in the software, modify the scanning speed, defocus distance, number of passes etc. and start the welding operation after checking all the required parameters are set and good to go.

(k) After the procedure was complete, the reaction was measured, including the weld strength, weld seam width, heat affected zone, micro-hardness, etc.

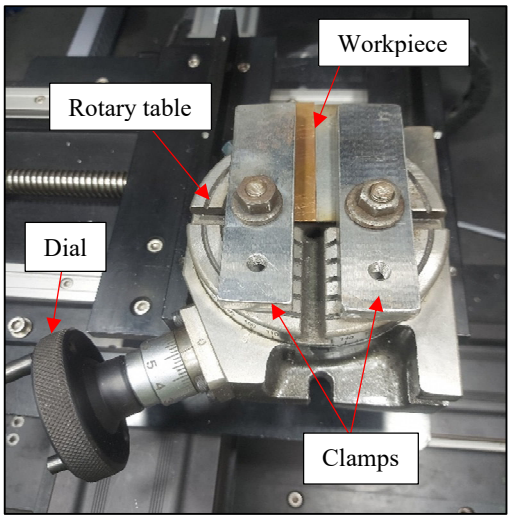

Fig. 4.2. Welding Fixture

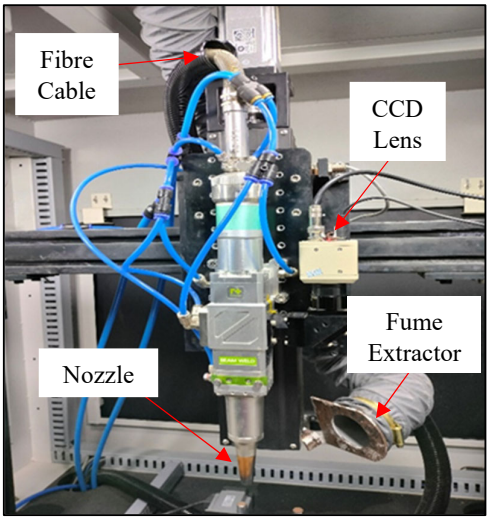

Fig. 4.3. Laser Head

CHAPTER 5

METHODOLOGY

5.1. Response Surface Methodology (RSM)

Response Surface Methodology (RSM) is a statistical technique commonly used in experimental design and optimization. It helps researchers analyse and optimize complex systems by examining the relationship between multiple input variables and their corresponding output/response. The goal of RSM is to create a mathematical model, often represented as a polynomial equation, that describes the relationship between the input variables and the response of interest. This model is then used to predict the optimal combination of input variables that maximizes or minimizes the desired response.
The RSM process typically involves three main steps:

1. **Experimental Design:** RSM starts with the design of a set of experiments, usually based on a factorial design, where different combinations of input variables are tested. The design aims to cover a wide range of input variable values to capture the response behaviour across the design space. This involves selecting the levels of the factors to be tested and the number of experiments to be conducted.

2. **Model Fitting:** The data collected from the designed experiments is used to fit a response surface model. This model represents the mathematical relationship between the input variables and the response. The model can be linear, quadratic, or higher-order, depending on the complexity of the system being studied.

3. **Analysis and Optimization:** Once the response surface model is fitted, it can be analysed to understand the effects of the input variables on the response. Researchers can identify significant factors and interactions, assess the model's adequacy, and perform optimization to find the optimal combination of input variables that maximizes or minimizes the response.

RSM has applications in various fields, such as engineering, chemistry, agriculture, and manufacturing. It allows researchers to gain insights into complex systems, optimize processes, and make data-driven decisions based on the relationships identified through the response surface model.

Central Composite Design (CCD) and Box-Behnken Design (BBD) are the two primary factorial designs for developing second-order polynomial models in RSM and assessing the quadratic response surface. CCD is a fractional factorial design, whereas BBD is a spherical, 2-level fractional factorial design with a centre point and the middle points of the circle's edges engraved on the sphere. Central composite design (CCD) is a statistical experimental design technique used to explore and optimize the response of a system or process to various factors or variables. It is commonly employed in fields such as engineering, chemistry, and industrial research. CCD allows for the assessment of both linear and nonlinear effects of factors, as well as the detection of possible interactions between factors. The design consists of three types of experimental points: factorial points, axial points, and centre points. Factorial points are used to estimate the main effects and interactions of the factors. These points are typically set at the low and high levels of each factor, following a factorial design. The number of factorial points depends on the number of factors being studied. Axial points are added to estimate the curvature of the response surface and provide information about potential interactions. They are typically placed at levels beyond the low and high settings of the factors. Centre points are replicated measurements taken at the centre of the design space. They are used to estimate the error and lack of fit in the model and to check for any experimental drift. By combining these three types of points, CCD allows for the estimation of model parameters and the construction of response surface models that can be used for prediction and optimization.

Box-Behnken design is a statistical experimental design technique that is commonly used in response surface methodology (RSM) for the purpose of optimizing the parameters of a process or system. It was developed by George Box and Donald Behnken in the 1960s. The Box-Behnken design is a type of response surface design that allows for efficient exploration of the design space with a relatively small number of experimental runs. It is particularly useful when the number of factors or variables affecting a process is moderate, as it provides a good balance between the number of experiments required and the amount of information obtained. The design consists of three levels of each factor, typically coded as -1, 0, and +1, which represent the low, medium, and high levels of the factors, respectively. The design also ensures that each

factor is studied at the midpoint of the other two factors, as well as at three other points that form an orthogonal array. The main advantage of the Box-Behnken design is that it allows for fitting a second-order polynomial model to the data, which can be used to estimate the response surface and optimize the process parameters.

$$\boldsymbol{Y = f(X_1, X_2, \dots\dots\dots\dots\dots\dots, X_n) \pm E}$$

Where $X_1, \dots\dots\dots\dots, X_n$ are the independent variables, Y is the response, f is the response function, and E is the experimental error. The type of link between the response and the independent variables heavily influences the response function (f). The polynomial quadratic model is represented by

$$\boldsymbol{Y = \beta_\circ + \sum_{i=1}^{n} \beta_i X_i + \sum_{j=1}^{n} \beta_{ii} X_i^2 + \sum_{i=1}^{n-1} \sum_{i}^{n} \beta_{ij} X_i X_j \pm E}$$

Where, Y is the predicted response; $\beta_\circ$ represents the intercept or regression coefficient β_i, β_{ii} and β_{ij} represents the linear, quadratic and interaction coefficients; X_i and X_j are the coded values of the process variables; and E is the experimental/residual error.

5.2. Response Surface Design

The most popular response surface designs are the central composite design (CCD) and Box-Behnken design. The two primary reaction surface designs are summarised as follows:

5.2.1. Central Composite Design (CCD)

A central composite design (CCD) is an experimental design used in response surface methodology (RSM) to build a second-order (quadratic) model for the response variable without needing to use a complete three-level factorial experiment. After the designed experiment is performed, linear regression is used, sometimes iteratively, to obtain results. Coded variables are often used when constructing this design.

The design matrix for a central composite design experiment involving n factors is derived from a matrix, D, containing the following three different parts corresponding to the three types of experimental runs:

1) The matrix F obtained from the factorial experiment. The factor levels are scaled so that its entries are coded as +1 and −1.

2) The matrix C from the centre points, denoted in coded variables as (0, 0, 0, ..., 0), where there are n zeros.

3) A matrix E from the axial points, with 2n rows. Each factor is sequentially placed at ±α and all other factors are at zero.

Salient points of CCD are as follows:

1) 2^n Factorial design points were used to create it, and numerous centre points were added.

2) The distance of the axial runs from the design centre and the number of centre points are two design characteristics that must be stated.

3) A face-centred central composite design (CCD) with a value $\alpha = 1$ can change the standard central composite design's 5 levels for each factor. For each component, there are just three tiers in the face-centred design.

4) Created for estimating a quadratic model the 2^n factorial points have been used to fit a first order model, this model has exhibited lack of fit, the axial runs are then added to allow the quadratic terms to be incorporated into the model.

5) Near the centre of the design area, replicated centre point offers good prediction capabilities (where the presumed optimum is).

The value of α is a measure of the curvature of the response surface. A smaller value of α will result in a less curved surface, while a larger value of α will result in a more curved surface. The choice of α depends on the amount of curvature that is expected in the response surface.

$$\boldsymbol{\alpha = [Number\ of\ factorial\ runs]^{\frac{1}{4}} = [2^n]^{1/4}}$$

The values of α and the number of center points for different number of factors.

Table 5.1. Central Composite Rotatable Design Points

No. of factor	2	3	4	5	6
Factorial Point	4	8	16	32	64
Axial Point	4	6	8	10	12
Value of α	1.414	1.682	2.000	2.378	2.828
Centre Point	5	6	7	10	15

CCDs are often used in industrial experiments where the response variable is a quality characteristic of a process. CCDs can be used to identify the factors that have the greatest impact on the response variable, to determine the optimal levels of the factors, and to develop a model that can be used to predict the response variable for new combinations of factor levels.

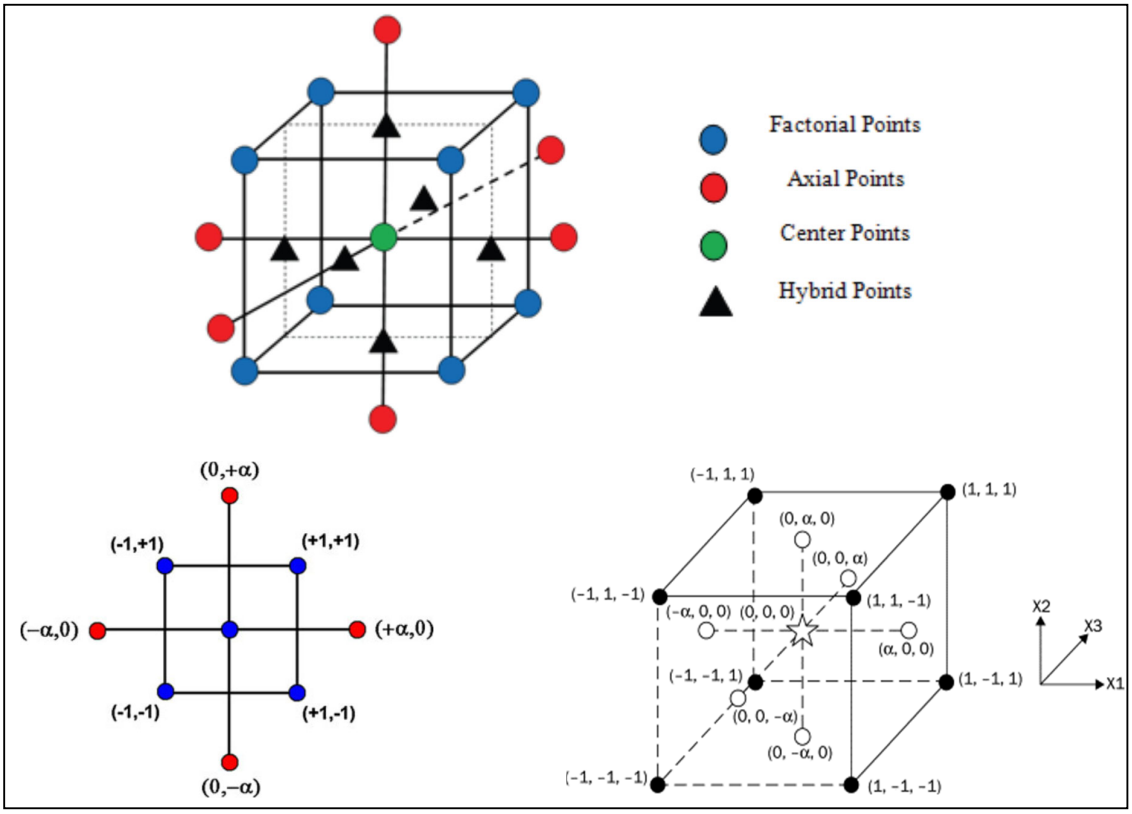

Fig. 5.1. Central Composite Design Points at Design Space for n = 2 & n = 3 [74]

Some of the advantages of using CCDs:

(1) They are more efficient than complete factorial experiments.

(2) They can be used to estimate the curvature of the response surface.

(3) They can be used to identify the factors that have the greatest impact on the response variable.
(4) They can be used to determine the optimal levels of the factors.
(5) They can be used to develop a model that can be used to predict the response variable for new combinations of factor levels.

Some of the disadvantages of using CCDs:

(1) They can be more expensive than complete factorial experiments.
(2) They can be more time-consuming to conduct.
(3) They can be more difficult to analyse.

Overall, CCDs are a powerful tool that can be used to improve the quality of processes. They are a valuable tool for engineers and scientists who are working to optimize the performance of their systems.

5.2.2. Box-Behnken Design (BBD)

A Box-Behnken design is a type of experimental design used in response surface methodology (RSM). A Box-Behnken design is a type of experimental design that is used to fit a quadratic model to a response surface. It is a three-level design, meaning that each factor is tested at three levels: low, medium, and high. The design is created by placing points on the midpoints of the edges of the design space, as well as at the centre. This results in a total of 2n+3 points, where n is the number of factors. Box-Behnken designs are created by placing the independent variables at three equally spaced levels, usually coded as -1, 0, and +1. This results in a design that is rotatable, meaning that the relative positions of the points in the design do not affect the results of the analysis.

Box-Behnken designs are typically used when the response surface is expected to be quadratic. A quadratic response surface is one that is curved, with a minimum or maximum at the centre of the design space. Box-Behnken designs can be used to fit a quadratic model to the data, which can then be used to predict the response variable at any point in the design space.

Some salient points of BBD are as follows:

(1) Has precise placement of design points combines incomplete block design with 2^n factorial.

(2) Every component should always have three levels.

(3) A quadratic estimating model was developed.

(4) Provides a strong estimate in the design space's centre, where the optimum is thought to lie, but is weaker at the cube's corners, where there are no design points.

(5) The accuracy of the remaining runs becomes crucial to the reliability of the model if experimenters wind up missing any experiments. The more initial runs the central composite design has, the more resistant it is to the issue.

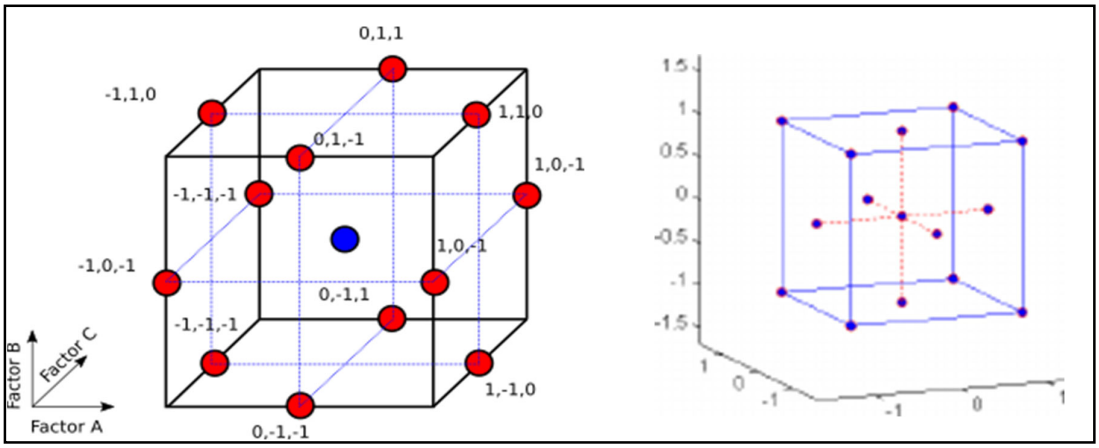

Fig. 5.2. BBD in Design Space for n=3 & FCC Points at Design Space for n=3 [75]

Box-Behnken designs are a good choice for RSM studies when the number of independent variables is relatively small. They are also a good choice when it is important to avoid extreme values of the independent variables.

Some of the advantages of using Box-Behnken designs:

(1) They are rotatable, which means that the relative positions of the points in the design do not affect the results of the analysis.
(2) They are relatively efficient, meaning that they require a smaller number of runs than other types of experimental designs.
(3) They are easy to interpret, making them a good choice for beginners.

Some of the disadvantages of using Box-Behnken designs:

(1) They are not as efficient as other types of experimental designs when the response surface is not quadratic.
(2) They can be difficult to implement in some software packages.
(3) They can be more expensive than other types of experimental designs.

Overall, Box-Behnken designs are a good choice for RSM studies when the number of independent variables is relatively small and the response surface is expected to be quadratic. They are efficient, easy to interpret, and relatively inexpensive.

5.3. Optimization using Genetic Algorithm

5.3.1. Particle Swarm Optimization

Particle Swarm Optimization (PSO) is a nature-inspired population-based metaheuristic algorithm that was first proposed by Kennedy and Eberhart in 1995 [76]. It is a distributed problem-solving method that performs multi-dimensional search in a randomly generated search-space during optimization. It is inspired by the collective behaviour of living organisms like migratory birds, social insect colonies and other animal societies. Like other evolutionary algorithm it uses concept of population and fitness value associated with each particle. In a population or swarm, the behaviour of the particle is affected by either the local best (p_{best}) within a certain neighbourhood or the global best (g_{best}) of the whole population. Advantage of PSO over other evolutionary algorithm is that here particles benefit from their own past experiences and also from the experience of the neighbouring particles. On the contrary, in evolutionary algorithm, individuals use the “memory” of the current population only. Also,

PSO needs fewer user-defined terms to adjust than other traditional algorithms. Fewer user-defined terms improve computational efficiency and lead to faster convergence towards global optima. Two main properties of swarm intelligence behaviour incorporated here are, self-organization, where interactions among the particles are executed on the basis of local information without any global influence and division of labour, where specialized particles perform different tasks simultaneously.

1) Basic PSO Algorithm

The basic PSO algorithm operates in an iterative manner. It starts by initializing a population of particles randomly within the problem space. Each particle has a position and velocity vector, which determine its current location and movement direction, respectively. The algorithm evaluates the fitness of each particle based on a fitness function. Additionally, each particle keeps track of its best position (personal best) and the best position found by the swarm (global best) during the search process.

During each iteration, the particles update their velocities and positions according to the following equations:

Velocity update:

$$v_i(t+1) = w * v_i(t) + c_1 * r_1 * (p_{best,\,i} - x_i(t)) + c_2 * r_2 * (g_{best} - x_i(t))$$

Position update:

$$x_i(t+1) = x_i(t) + v_i(t+1)$$

where $v_i(t)$ represents the velocity of particle i at time t, $x_i(t)$ denotes the position of particle i at time t, $p_{best,\,i}$ represents the personal best position of particle i, g_{best} denotes the global best position found by the swarm, w is the inertia weight, c_1 and c_2 are the acceleration coefficients, and r_1 and r_2 are random values within [0, 1].

2) Particle Representation and Encoding

The representation of particles in PSO depends on the characteristics of the optimization problem. In continuous optimization problems, the particles' positions and velocities are represented by real-valued vectors. For discrete optimization problems, the positions and velocities can be encoded using binary or integer representations. The encoding scheme should ensure the feasibility and consistency of the solutions within the problem domain.

3) Swarm Initialization

The initialization process involves determining the initial positions and velocities of the particles. The positions are usually initialized randomly within the problem space, ensuring that each particle explores a diverse region. The velocities are initialized based on predefined ranges or rules to control the exploration and exploitation trade-off. Proper initialization is crucial for a good exploration of the search space.

4) Update Equations and Velocity Control

The velocity update equation incorporates three components: the inertia term, the cognitive component, and the social component. The inertia term ($w * v_i(t)$) allows particles to maintain their current velocities to encourage exploration. The cognitive component ($c_1 * r_1 * (p_{best,\ i} - x_i(t))$) represents the particle's attraction towards its personal best position, promoting exploitation. The social component ($c_2 * r_2 * (g_{best} - x_i(t))$) guides particles towards the best position found by the swarm, encouraging global exploration.

The inertia weight (w) determines the impact of the previous velocity on the current velocity. It controls the balance between exploration and exploitation during the search process. Commonly used strategies for updating the inertia weight include linear or nonlinear decreasing schemes, adaptive approaches, and dynamic variations.

The population is updated under following conditions:

If $f_i < f_{p\ best,i}$ $\begin{cases} p_{best,i} = x_i \\ f_{p\ best,i} = f_i \end{cases}$ or, if $f_{p\ best,i} < f_{g\ best}$ $\begin{cases} g_{best} = p_{best,i} \\ f_{g\ best} = f_{p\ best,i} = f_i \end{cases}$

Where, $f_{p\ best,i}$ and $f_{g\ best}$ are function associated with $f_{p\ best,i}$ and g_{best} respectively and the goal is to minimize the objective function.

5) Convergence and Termination Criteria

PSO typically terminates when a certain stopping criterion is met. Common termination criteria include reaching a maximum number of iterations, achieving a desired level of fitness, or when the improvement in fitness becomes negligible. The convergence of PSO is influenced by various factors such as the problem complexity, swarm size, parameter settings, and the fitness landscape of the optimization problem.

6) Flowchart

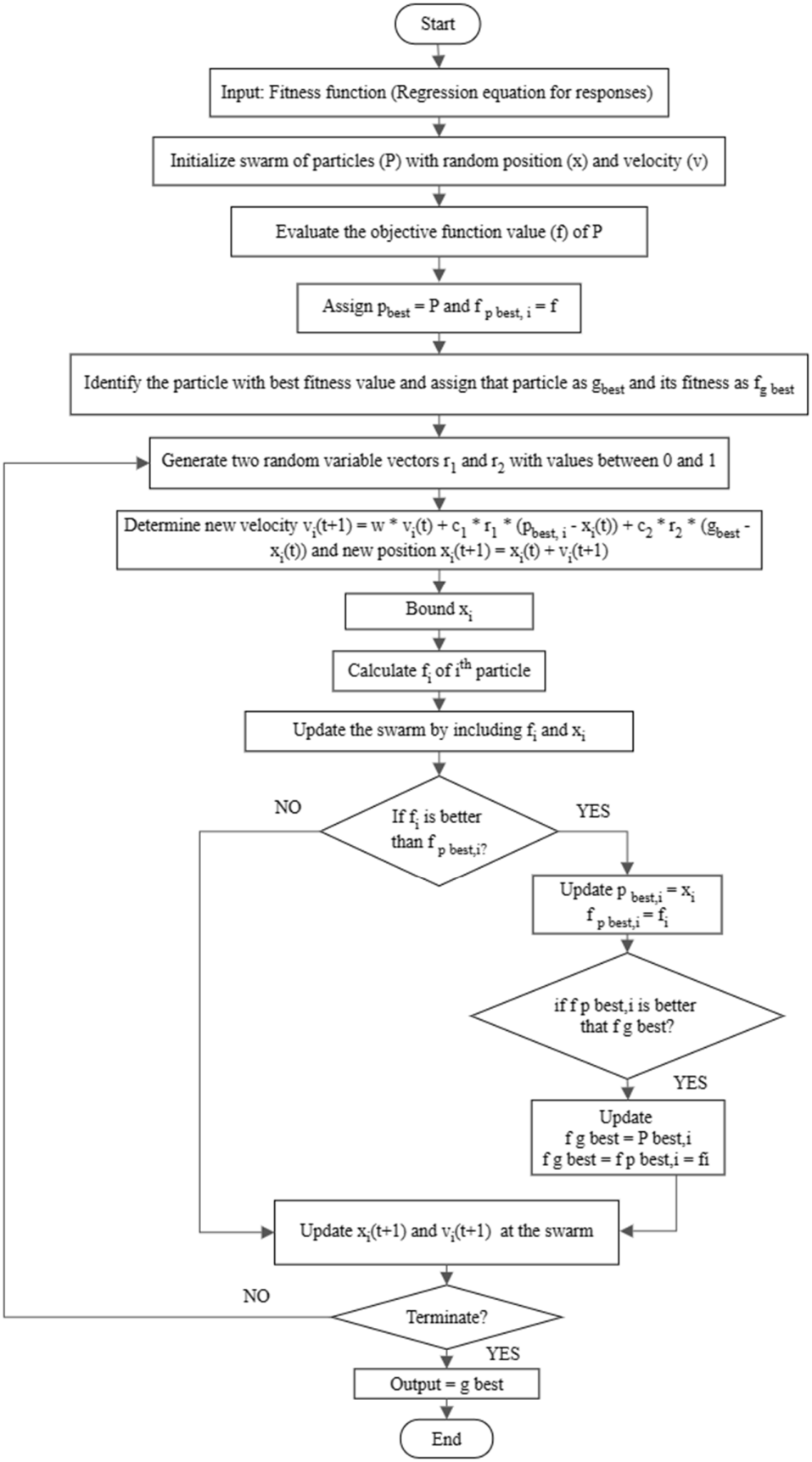
Start
Input: Fitness function (Regression equation for responses)
Initialize swarm of particles (P) with random position (x) and velocity (v)
Evaluate the objective function value (f) of P
Assign p_{best} = P and $f_{p\ best,\ i}$ = f
Identify the particle with best fitness value and assign that particle as g_{best} and its fitness as $f_{g\ best}$
Generate two random variable vectors r_1 and r_2 with values between 0 and 1
Determine new velocity $v_i(t+1) = w * v_i(t) + c_1 * r_1 * (p_{best,\ i} - x_i(t)) + c_2 * r_2 * (g_{best} - x_i(t))$ and new position $x_i(t+1) = x_i(t) + v_i(t+1)$
Bound x_i
Calculate f_i of i^{th} particle
Update the swarm by including f_i and x_i
If f_i is better than $f_{p\ best,i}$?
NO
YES
Update $p_{best,i} = x_i$
$f_{p\ best,i} = f_i$
if f p best,i is better that f g best?
YES
Update
f g best = P best,i
f g best = f p best,i = fi
Update $x_i(t+1)$ and $v_i(t+1)$ at the swarm
NO
Terminate?
YES
Output = g best
End

5.3.2. Teaching-Learning based Optimization (TLBO)

Teaching-Learning-Based Optimization (TLBO) is a relatively recent optimization algorithm that was introduced in 2011 by R.V. Rao, S. Savsani, and D.P. Vakharia [77]. The algorithm was developed as an approach to solve complex optimization problems by simulating the teaching and learning processes observed in nature and human society. The development of TLBO was motivated by the need for efficient optimization algorithms that can handle various real-world problems. Traditional optimization algorithms often face challenges in balancing exploration and exploitation, as well as getting trapped in local optima. TLBO aimed to address these limitations and provide a robust and effective optimization technique.

Teaching-Learning-Based Optimization (TLBO) is an optimization algorithm inspired by the teaching and learning processes observed in nature and human society. TLBO aims to find optimal or near-optimal solutions to a given optimization problem by mimicking the dynamics of teaching and learning.

1) Fundamentals of TLBO:

a) Population-based Optimization: TLBO utilizes a population of candidate solutions to explore and exploit the search space. Each candidate solution represents a potential solution to the optimization problem.

b) Teaching Phase: In the teaching phase, the algorithm identifies the best solution in the population, known as the "teacher." The teacher guides the learning process by influencing the learners in the population towards better solutions. The teacher is usually the solution with the highest fitness or objective value.

Let M_i be the mean and T_i be the teacher at any iteration i. T_i will try to move mean M_i towards its own level, so now the new mean will be T_i designated as M_{new}. The solution is updated according to the difference between the existing and the new mean given by

$$Difference\_Mean_i = r_i\ (M_{new} - TFM_i)$$

Where TF is a teaching factor that decides the value of mean to be changed, and r_i is a random number in the range [0, 1]. The value of TF can be either 1 or 2, which is again a heuristic step and decided randomly with equal probability.

This difference modifies the existing solution according to the following expression

$X_{new,i} = X_{old,i} + Difference\_Mean_i$.

c) Learning Phase: In the learning phase, the learners in the population aim to improve themselves by learning from the teacher. They adjust their positions in the search space based on the guidance provided by the teacher. Learners increase their knowledge by two different means: one through input from the teacher and the other through interaction between themselves. A learner interacts randomly with other learners with the help of group discussions, presentations, formal communications, etc. A learner learns something new if the other learner has more knowledge than him or her. Learner modification is expressed as:

For i = 1 : Pn
Randomly select two learners Xi and Xj , where $i \neq j$
If f(Xi) < f(Xj)
Xnew,i = Xold,i + ri(Xi − Xj)
Else
Xnew,i = Xold,i + ri(Xj − Xi)
End If
End For
Accept Xnew if it gives a better function value

d) Exploration and Exploitation: TLBO aims to balance the exploration of the search space to discover new regions and the exploitation of known promising regions. This is achieved by a combination of global search and local search mechanisms.

2) Initialization: TLBO starts by initializing a population of candidate solutions randomly or using a specific strategy. The population size is typically predefined.

3) Evaluation: Each candidate solution in the population is evaluated using the objective function or fitness measure of the optimization problem. The objective function quantifies the quality or performance of a solution.

4) Teacher Selection: The candidate solution with the highest fitness is selected as the teacher. The teacher's role is to guide the learning process and influence the learners towards better solutions.

5) Learning and Adjustment:

b) Learner Position Update: Each learner solution adjusts its position based on the guidance provided by the teacher. The learners update their positions using a learning equation that incorporates the teacher's information and possibly their own previous positions.

c) Exploration and Exploitation: The learning equation contains parameters that control the exploration and exploitation aspects of the algorithm. These parameters determine the balance between global exploration and local exploitation.

6) Update:

a) **Solution Comparison:** After the learners have adjusted their positions, the fitness of each learner is compared with the fitness of the corresponding teacher. If a learner's fitness is better than its teacher's, it replaces the teacher. Otherwise, the teacher remains unchanged.

b) **Population Update:** The updated population is formed by including the new teacher and the modified learners. The previous generation's teacher is replaced by the learner with the best fitness if it is better than the current teacher.

7) Termination: The algorithm continues the learning process iteratively until a termination criterion is met. This criterion can be a maximum number of iterations, reaching a desired fitness level, or a predefined computational budget.

8) Solution Extraction: Once the algorithm terminates, the best solution found during the optimization process is extracted from the population as the final solution to the problem.

9) Flowchart

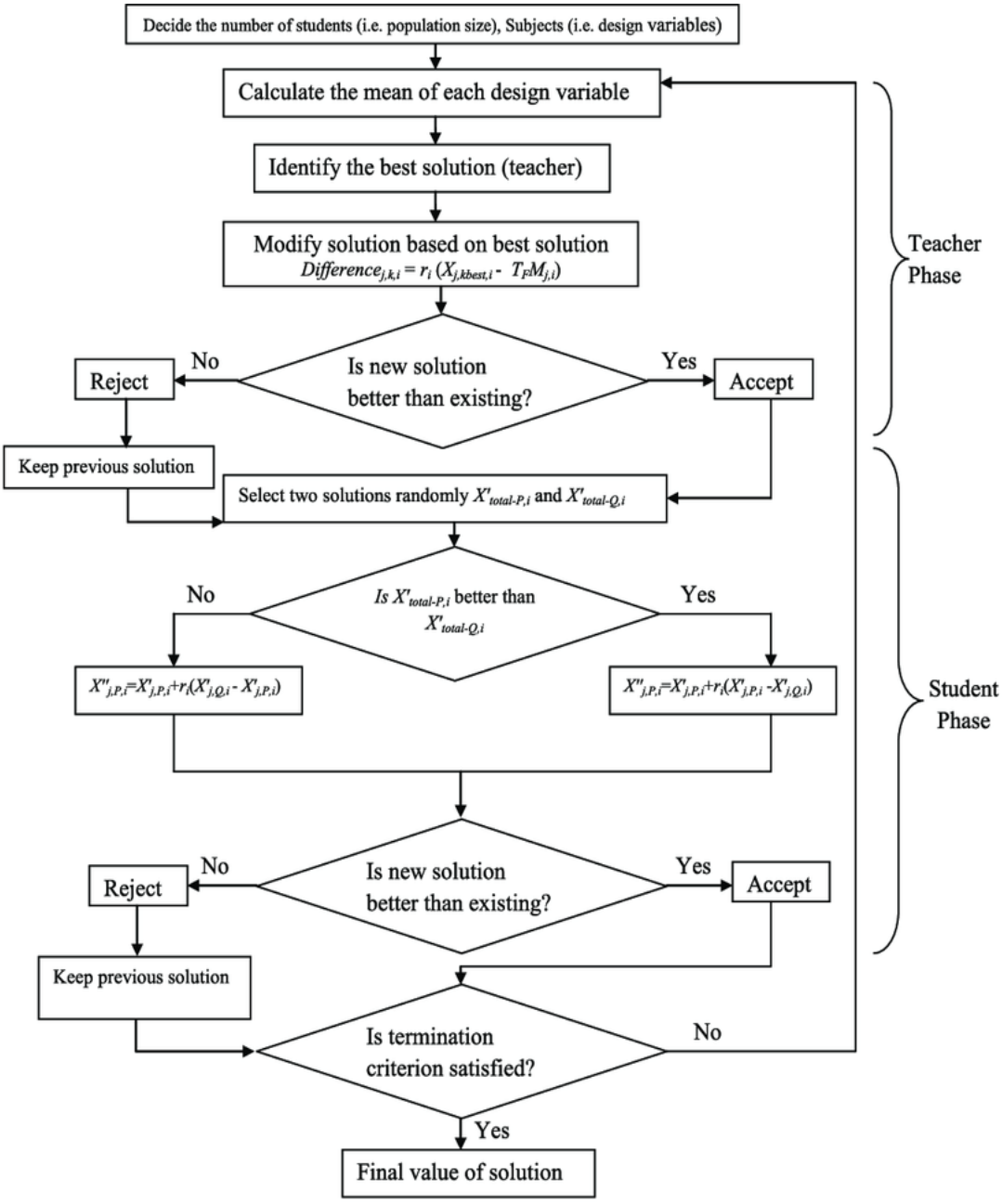

5.3.3. Gray Wolf Optimization (GWO)

Gray Wolf Optimization (GWO) is a nature-inspired metaheuristic algorithm developed by Seyedali Mirjalili in 2014 [78]. It is inspired by the social behaviour and hunting strategies of gray wolves in the wild. GWO belongs to the family of population-based optimization algorithms that mimic the behaviour of animal groups to solve complex optimization problems.

The algorithm draws inspiration from the hierarchical structure and cooperative hunting behaviours of gray wolf packs. Gray wolves are known for their efficient hunting strategies, which involve collaboration, coordination, and adaptive decision-making. The GWO algorithm aims to emulate these behaviours to search for optimal solutions in a given problem space.

The GWO algorithm starts with an initial population of potential solutions, represented as wolves. The position of each wolf corresponds to a candidate solution. The algorithm iteratively updates the positions of the wolves based on a set of predefined rules, which simulate the hunting behaviours observed in gray wolves.

1) Social hierarchy: In order to mathematically model the social hierarchy of wolves when designing GWO, we consider the fittest solution as the alpha (α). Consequently, the second and third best solutions are named beta (β) and delta (δ) respectively. The rest of the candidate solutions are assumed to be omega (ω). In the GWO algorithm the hunting (optimization) is guided by α, β, and δ. The ω wolves follow these three wolves.

2) Encircling prey: As mentioned above, grey wolves encircle prey during the hunt. In order to mathematically model encircling behaviour the following equations are proposed:

$$\vec{D} = \left|\vec{C}.\overrightarrow{X_p}(t) - \vec{X}(t)\right|.$$

$$\vec{X}(t+1) = \overrightarrow{X_p}(t) - \vec{A}.\vec{D}.$$

where t indicates the current iteration, $\vec{A}$ and $\vec{C}$ are coefficient vectors, $\overrightarrow{X_p}$ is the position vector of the prey, and $\vec{X}$ indicates the position vector of a grey wolf. The vectors $\vec{A}$ and $\vec{C}$ are calculated as follows:

$$\vec{A} = 2\vec{a}.\overrightarrow{r_1} - \vec{a}.$$

$$\vec{C} = 2.\overrightarrow{r_2}\,.$$

where components of $\vec{a}$ are linearly decreased from 2 to 0 over the course of iterations and r_1, r_2 are random vectors in [0, 1].

3) Hunting: Grey wolves have the ability to recognize the location of prey and encircle them. The hunt is usually guided by the alpha. The beta and delta might also participate in hunting occasionally. However, in an abstract search space we have no idea about the location of the optimum (prey). In order to mathematically simulate the hunting behaviour of grey wolves, we suppose that the alpha (best candidate solution) beta, and delta have better knowledge about the potential location of prey. Therefore, we save the first three best solutions obtained so far and oblige the other search agents (including the omegas) to update their positions according to the position of the best search agents. The following formulas are proposed in this regard.

$$\overrightarrow{D_\alpha} = \left|\overrightarrow{C_1}.\overrightarrow{X_\alpha} - \vec{X}\right|, \overrightarrow{D_\beta} = \left|\overrightarrow{C_2}.\overrightarrow{X_\beta} - \vec{X}\right|, \overrightarrow{D_\delta} = \left|\overrightarrow{C_3}.\overrightarrow{X_\delta} - \vec{X}\right|.$$

$$\overrightarrow{X_1} = \overrightarrow{X_\alpha} - \overrightarrow{A_1}.\overrightarrow{D_\alpha}, \overrightarrow{X_2} = \overrightarrow{X_\beta} - \overrightarrow{A_2}.\overrightarrow{D_\beta}, \overrightarrow{X_3} = \overrightarrow{X_\delta} - \overrightarrow{A_3}.\overrightarrow{D_\delta}.$$

$$\vec{X}(t+1) = \frac{\overrightarrow{X_1} + \overrightarrow{X_2} + \overrightarrow{X_3}}{3}$$

4) Attacking prey (exploitation): As mentioned above the grey wolves finish the hunt by attacking the prey when it stops moving. In order to mathematically model approaching the prey we decrease the value of $\vec{a}$. Note that the fluctuation range of $\vec{A}$ is also decreased by $\vec{a}$. In other words, $\vec{A}$ is a random value in the interval [-2a, 2a] where a is decreased from 2 to 0 over the course of iterations. When random values of $\vec{A}$ are in [-1,1], the next position of a search agent can be in any position between its current position and the position of the prey. $|A| < 1$ forces the wolves to attack towards the prey.

5) Search for prey (exploration): Grey wolves mostly search according to the position of the alpha, beta, and delta. They diverge from each other to search for prey and converge to attack prey. In order to mathematically model divergence, we utilize $\vec{A}$ with random values greater than 1 or less than -1 to oblige the search agent to diverge from the prey. This emphasizes exploration and allows the GWO algorithm to search globally. $|A| > 1$ forces the grey wolves to diverge from the prey to hopefully find a fitter prey. Another component of GWO that favours exploration is $\vec{A}$. The $\vec{C}$ vector contains random values in [0,2]. This component provides random weights for prey in order to stochastically emphasize ($C > 1$) or deemphasize ($C < 1$) the effect of prey in defining the distance. This assists GWO to show a more random

behaviour throughout optimization, favouring exploration and local optima avoidance. It is worth mentioning here that C is not linearly decreased in contrast to A. We deliberately require C to provide random values at all times in order to emphasize exploration not only during initial iterations but also final iteration. This component is very helpful in case of local optima stagnation, especially in the final iterations. Some points to be noted:

a) The proposed social hierarchy assists GWO to save the best solutions obtained so far over the course of iteration.

b) The proposed encircling mechanism defines a circle-shaped neighbourhood around the solutions which can be extended to higher dimensions as a hyper-sphere.

c) The random parameters A and C assist candidate solutions to have hyper-spheres with different random radii.

d) The proposed hunting method allows candidate solutions to locate the probable position of the prey.

e) Exploration and exploitation are guaranteed by the adaptive values of a and A.

f) The adaptive values of parameters a and A allow GWO to smoothly transition between exploration and exploitation.

g) With decreasing A, half of the iterations are devoted to exploration ($|A| \geq 1$) and the other half are dedicated to exploitation ($|A| < 1$).

h) The GWO has only two main parameters to be adjusted (a and C).

6) Flowchart

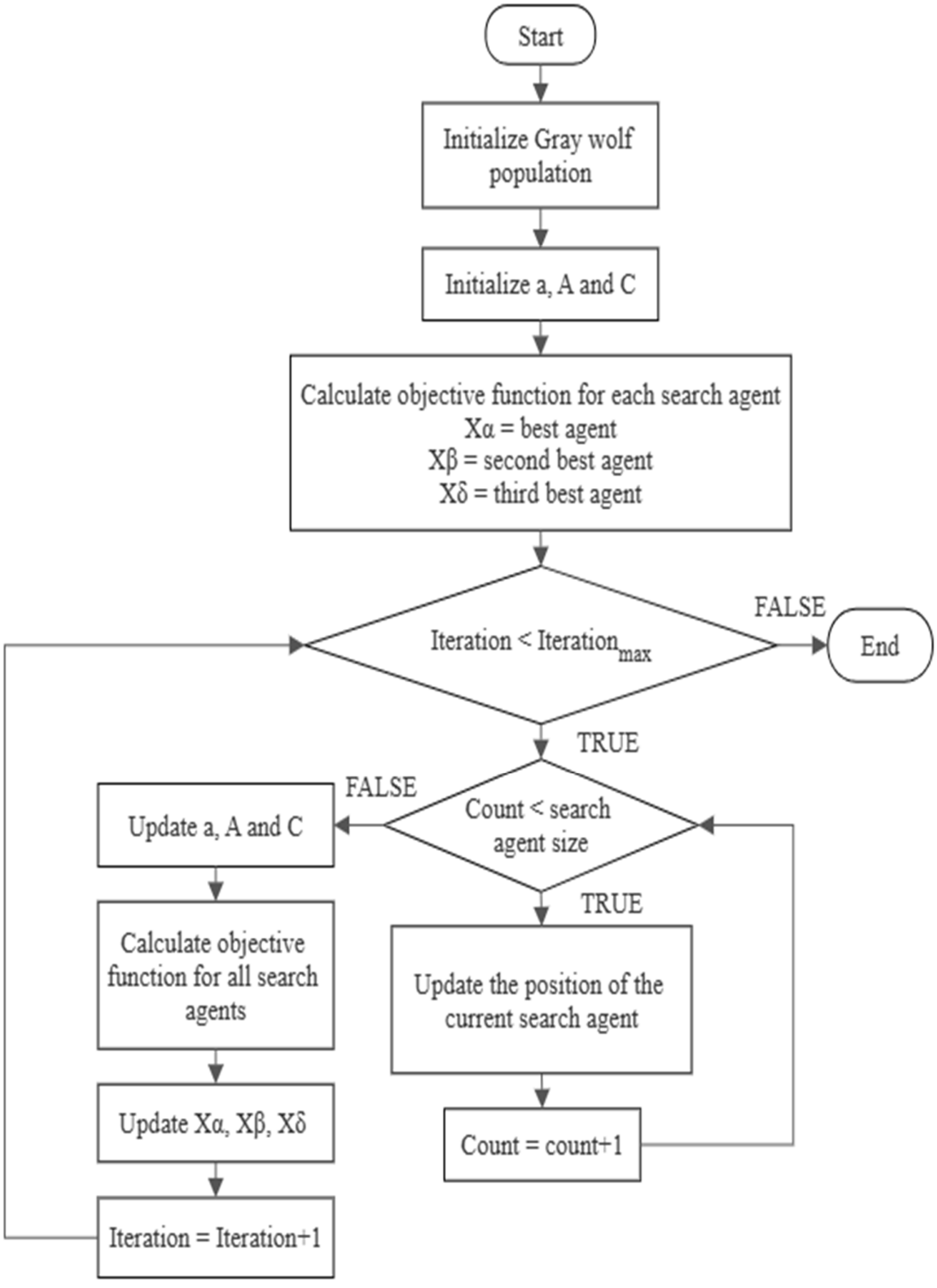
Start
Initialize Gray wolf population
Initialize a, A and C
Calculate objective function for each search agent
Xα = best agent
Xβ = second best agent
Xδ = third best agent
Iteration < Iteration$_{max}$
FALSE
End
TRUE
Count < search agent size
FALSE
Update a, A and C
TRUE
Calculate objective function for all search agents
Update the position of the current search agent
Update Xα, Xβ, Xδ
Count = count+1
Iteration = Iteration+1

5.3.4. Multi-objective optimization using Genetic Algorithm

In single objective optimization, it is observed that all algorithms identify different laser parameter settings for each response, which is very difficult to maintain in a real-time setup. Therefore, it is necessary to create a special mixture of all laser characteristics that results in simultaneous response optimization. The multi-objective function listed below can be developed for this purpose:

$$Min(Y) = \pm w_1 \times \frac{Y_1}{min/\max(Y_1)} \pm w_2 \times \frac{Y_2}{min/\max(Y_2)} \pm w_3 \times \frac{Y_3}{min/\max(Y_3)} \pm$$

$$\ldots\ldots\ldots\ldots\ldots\ldots\ldots \pm w_n \times \frac{Y_n}{min/\max(Y_n)}$$

Where, Y_1, Y_2, Y_3, ……Y_n are objective functions and w_1, w_2, w_3, ……..,w_n are weights assigned to the objectives respectively. (+) sign is for objectives to be minimized and (-) signs for the objectives to be maximized.

CHAPTER 6

EXPERIMENTAL INVESTIGATION

6.1. Experiment

A dissimilar laser welding of Copper (Cu) and Stainless steel 304 (SS 304) is the main focus of this chapter. It's technological datasets as well as an experimental observation or the results of an experimental investigation on the influence of process parameters on welding quality is also discussed in further details. A continuous wave fibre laser was utilised in this experiment.

The goal of this research is to find the best welding variables by linking the key weld quality elements, specifically weld strength along with seam width, to the process parameters included in this study. Using already accessible datasets, the design of experiment (DOE) is applied to analyse & optimise the parameters and increase the weld quality. Empirical mathematical models are developed to determine the relationship between process factors and weld quality attributes. When the quality characteristics are at the desired levels, the created empirical models are used to determine the best welding factors for the targeted optimization criteria. The effect of each parameter on weld quality attributes is investigated, and the best welding conditions are identified.

The experimental design offers a near-perfect value while maintaining the quality of the resources utilised to create process parameters. The impacts of each parameter are utilised to construct empirical models with weld quality attributes. Experimental design using Central Composite Design (CCD) gives a more exact value than Box-Behnken Design (BBD). In addition, due to a limited quantity of workpiece samples, the CCD half-design was chosen.

According to previous studies it is seen that high reflectivity and thermal conductivity of Cu is the major constraint in welding of Cu with other materials. In addition, formation of brittle intermetallic compounds (IMCs) leading to longitudinal crack of weld makes it harder. It is high priority to maintain the laser power in such a range that it provides good weld as well as does not burn the workpiece. Also, it is important to check the cooling rate to omit the crack generation. Keeping these things in mind, Ar gas was used as shielding & chilling medium and to ensure strong weld a number of passes was selected also for every weld. Maintaining gap at

weld interface of two material is also a tricky job. It was ensured that no visible gap is present in the weld interface so that proper melting and fusion of both metals could occur.

6.2. Selection of range of Process parameters

The range of process parameters has been defined based on a number of literature review and machine restrictions. Process variables such as Laser Power (LP), Scanning Speed (SS), Defocus Distance (DF), Number of Passes (N) & Argon Gas Pressure (GP) were chosen to examine their true effects on output parameters such as the fusion zone and heat affected zone on both the metals and ultimately the strength of the welded joint.

Table 6.1. Range of Process parameters

Process Parameter	Symbol	Unit	Level				
			-2	-1	0	+1	+2
Laser Power	LP	Watt	220	240	260	280	300
Scanning Speed	SS	mm/sec	10	14	18	22	26
Defocus Distance	DF	mm	3	4	5	6	7
Number of Passes	N	--	5	7	9	11	13
Argon Gas Pressure	GP	bar	1.25	1.5	1.75	2	2.25

6.3. Experimental observation

The selection of the relevant process parameters was used to generate the design matrix for the experiment using Design-Expert 13 software. Welding is performed using the appropriate input process parameter combinations generated by the Central Composite Design (CCD) of RSM method. The experiment and measurement of responses are carried out subsequently. According to CCD half-design of five process parameters, a design matrix with 32 experiment combinations is generated. Table 6.2 depicts the design matrix with both Actual and Coded values as generated by RSM in Design-Expert 13.

Table 6.2. Design Matrix

Exp No.	Actual Value					Coded Value				
	LP (Watt)	SS (mm/sec)	DF (mm)	N --	GP (bar)	LP	SS	DF	N	GP
1	240	14	4	7	2	-1	-1	-1	-1	1
2	280	14	4	7	1.5	1	-1	-1	-1	-1
3	240	22	4	7	1.5	-1	1	-1	-1	-1
4	280	22	4	7	2	1	1	-1	-1	1
5	240	14	6	7	1.5	-1	-1	1	-1	-1
6	280	14	6	7	2	1	-1	1	-1	1
7	240	22	6	7	2	-1	1	1	-1	1
8	280	22	6	7	1.5	1	1	1	-1	-1
9	240	14	4	11	1.5	-1	-1	-1	1	-1
10	280	14	4	11	2	1	-1	-1	1	1
11	240	22	4	11	2	-1	1	-1	1	1
12	280	22	4	11	1.5	1	1	-1	1	-1
13	240	14	6	11	2	-1	-1	1	1	1
14	280	14	6	11	1.5	1	-1	1	1	-1
15	240	22	6	11	1.5	-1	1	1	1	-1
16	280	22	6	11	2	1	1	1	1	1
17	220	18	5	9	1.75	-2	0	0	0	0
18	300	18	5	9	1.75	2	0	0	0	0
19	260	10	5	9	1.75	0	-2	0	0	0
20	260	26	5	9	1.75	0	2	0	0	0
21	260	18	3	9	1.75	0	0	-2	0	0
22	260	18	7	9	1.75	0	0	2	0	0
23	260	18	5	5	1.75	0	0	0	-2	0
24	260	18	5	13	1.75	0	0	0	2	0
25	260	18	5	9	1.25	0	0	0	0	-2
26	260	18	5	9	2.25	0	0	0	0	2
27	260	18	5	9	1.75	0	0	0	0	0
28	260	18	5	9	1.75	0	0	0	0	0
29	260	18	5	9	1.75	0	0	0	0	0

30	260	18	5	9	1.75	0	0	0	0	0
31	260	18	5	9	1.75	0	0	0	0	0
32	260	18	5	9	1.75	0	0	0	0	0

6.4. Welding operation

Thirty-two samples for each of Cu and SS 304 have been created, cleaned properly and edges are prepared to ensure negligible gap at welding interface. The laser starts to weld the workpiece with all parameters considered as very accurately. At Focus the laser beam spot diameter of 500 µm. As the defocus distance increases spot diameter also increases accordingly. A rotatable special fixture was created to ensure proper clamping during laser operation. Based on the successful laser welding of the 1 mm thick trial samples, these processing parameters were chosen. In trials it was visually observed that at low power the weld strength was not achieved and at very high-power crack was generating due to IMC formation and burn out of weld interface was also evident.

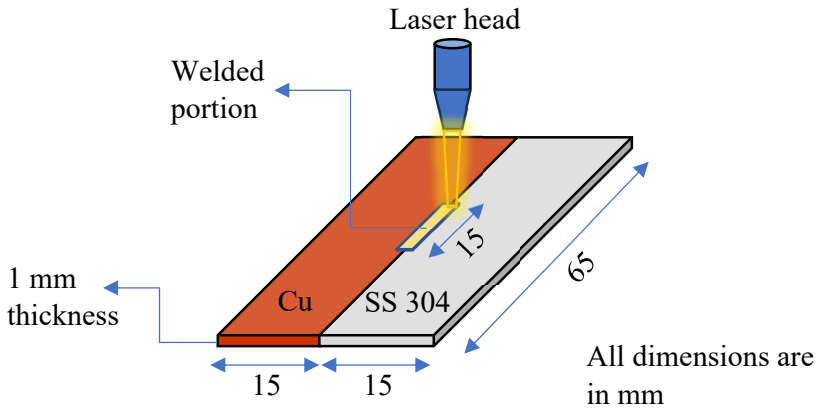

Fig. 6.1. Schematic view of ongoing laser welding on workpiece

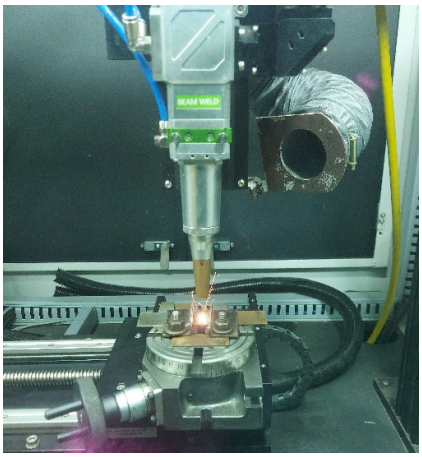

Fig. 6.2. Pictorial view of ongoing laser welding on workpiece

When the laser is turned on, the materials start to fuse with each other and weld bead is generated. It is necessarily a conduction mode of welding and depth of penetration is neither too deep nor too shallow as per visual inspection. The welded workpiece then was precisely measured using a microscope and the data obtained is validated with image analysis software too.

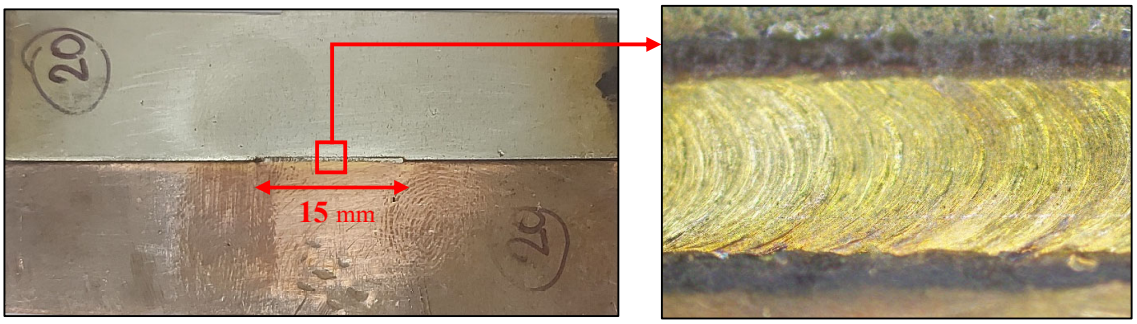

Fig. 6.3. Welded workpiece

6.5. Measuring scope

Weld-seam width / Fusion Zone (FZ) is measured using an Olympus STM 6 measuring microscope. With sub-micron precision (0.1 µm), the STM 6 microscope provides high performance three axis measurements of items. For rejecting coaxial illumination during measurements, an internal LED illuminator is employed. The Olympus STM 6 measuring microscope is seen in Fig. 6.4 and is used to measure the breadth of weld seams.

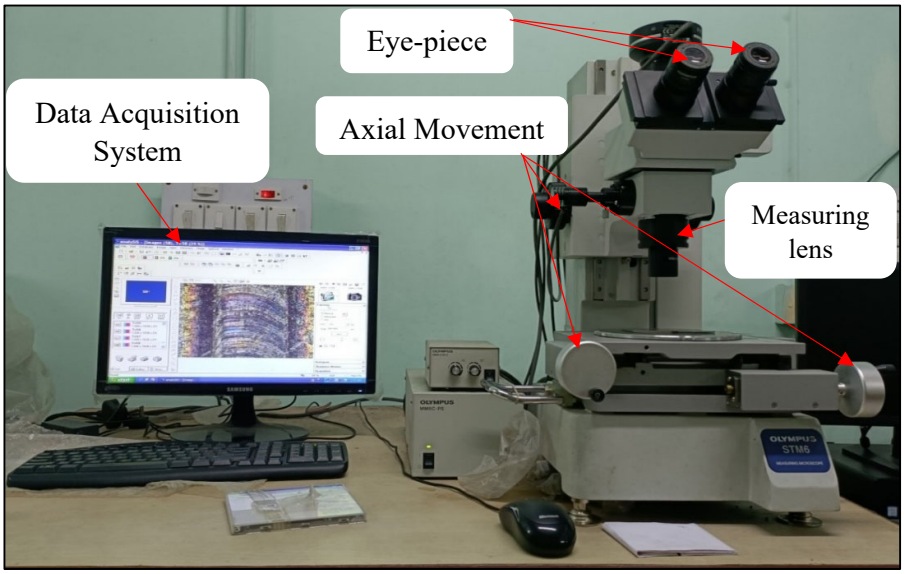

Fig. 6.4. Olympus STM 6 measuring microscope used for measuring FZ, Cu HAZ & SS HAZ

Using a microscope, measure the fusion zone and the heat-affected zone at 200µm. The purpose of this preparatory process was to examine the key elements in the Fusion Zone (FZ) & heat-affected zone in Cu (Cu HAZ) and in SS 304 (SS HAZ). Optical microscopy was used to investigate the microstructure (OM). By correlating the area of the fusion zone in the cross section with the transmission power, the effectiveness of the welding process was assessed.

This led to the introduction of a measure known as Welding Process Efficiency (WPE) to account for the amount of energy used to create a fusion zone in the work-piece. The WPE's definition was provided by

$$\mathbf{WPE} = \frac{\mathbf{A_{FZ}}}{\mathbf{LE}}$$

where A_{FZ} is the area of the fusion zone, while LE is the linear energy.

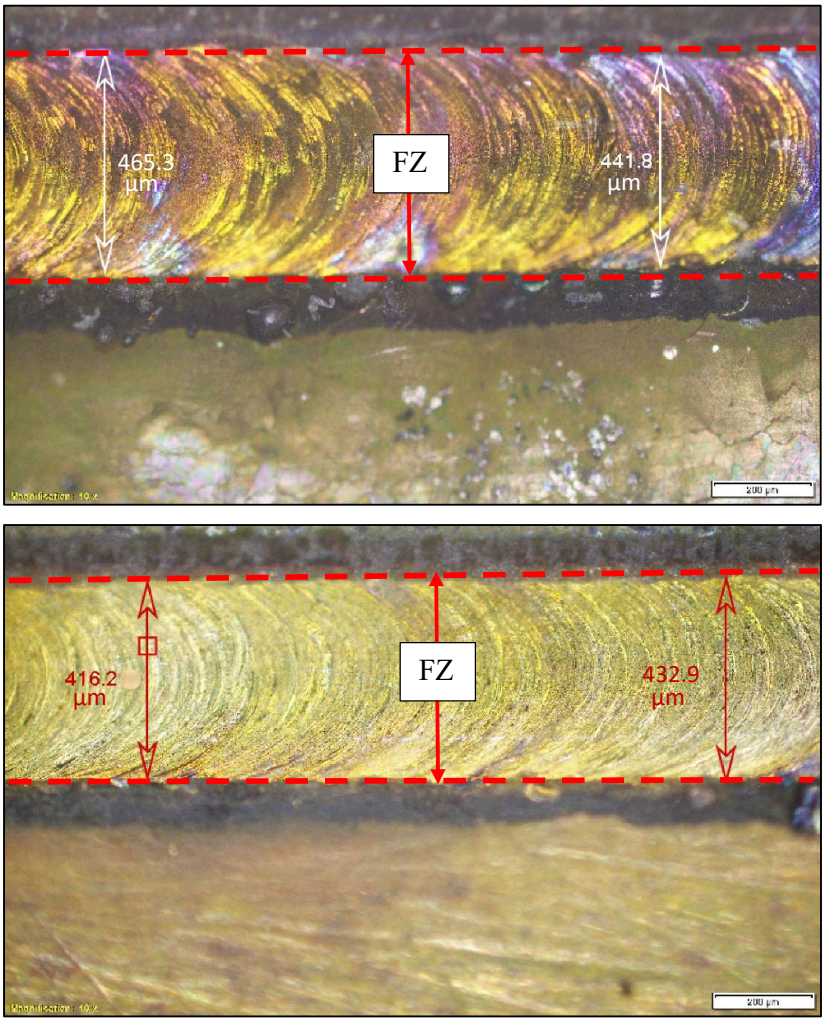

Fig. 6.5. FZ measured by microscope in two samples

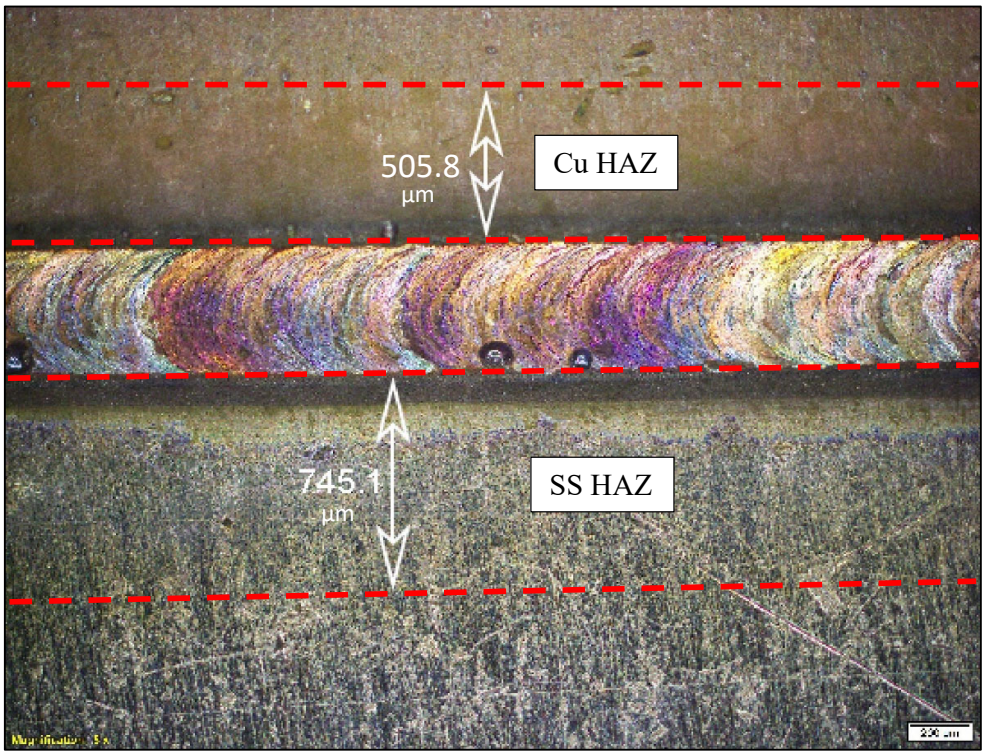

Fig. 6.6. Cu HAZ & SS HAZ measured by microscope

Fig. 6.5 depicts the measured values of fusion zone (seam width) in two different samples. Similarly, Fig. 6.6 shows the measured values of heat affected zone in both copper and SS 304.

CHAPTER 7

RESULTS & DISCUSSION

7.1. Measurement of responses

Fusion zone (FZ) and heat-affected zones i.e., Cu HAZ & SS HAZ are characterised as responses for changes in input parameters such as Laser Power (LP), Scanning Speed (SS), Defocus distance (DF), Number of passes (N) and Argon Gas Pressure (GP).

Table 7.1. Responses of welding process

Exp No.	Factors					Responses		
	LP (Watt)	SS (mm/sec)	DF (mm)	N --	GP (bar)	FZ (µm)	Cu HAZ (µm)	SS HAZ (µm)
1	240	14	4	7	2	414.7	669.67	970.9
2	280	14	4	7	1.5	525.36	826.3	1295.47
3	240	22	4	7	1.5	409.4	520.6	701.34
4	280	22	4	7	2	538.23	810.6	876.3
5	240	14	6	7	1.5	427.07	517.58	747.18
6	280	14	6	7	2	463.2	820.61	961.5
7	240	22	6	7	2	306.57	347.9	563.79
8	280	22	6	7	1.5	428.9	473.33	784.13
9	240	14	4	11	1.5	415.17	741.9	1144.52
10	280	14	4	11	2	482.34	530.8	1028.7
11	240	22	4	11	2	375.34	478.3	825.67
12	280	22	4	11	1.5	454.23	739.38	1158.5
13	240	14	6	11	2	349.3	513.2	871.36
14	280	14	6	11	1.5	511.9	1010.46	1438.82
15	240	22	6	11	1.5	326.53	315.8	544.73
16	280	22	6	11	2	441.83	740.9	894.7
17	220	18	5	9	1.75	331.37	389.14	607.65
18	300	18	5	9	1.75	521.27	832.38	1138.7

19	260	10	5	9	1.75	460.8	695.17	1102.47
20	260	26	5	9	1.75	402.7	358.4	646.9
21	260	18	3	9	1.75	470.63	591.65	1033.33
22	260	18	7	9	1.75	373.1	440.2	687.16
23	260	18	5	5	1.75	434.9	605.4	813.6
24	260	18	5	13	1.75	407.53	640.32	1025.73
25	260	18	5	9	1.25	455.53	701.66	985.93
26	260	18	5	9	2.25	435.8	648.4	838.97
27	260	18	5	9	1.75	447.1	532	786.4
28	260	18	5	9	1.75	437.2	535.13	787.32
29	260	18	5	9	1.75	441.5	536.39	792.81
30	260	18	5	9	1.75	426.27	561.9	797.1
31	260	18	5	9	1.75	441.37	519.22	784.78
32	260	18	5	9	1.75	439.9	505.8	745.1

7.2. Empirical modelling using RSM

Planned testing and subsequent analysis are required for the creation of mathematical models to determine the relationship between the process variables and the weld quality metrics. The adequacy of the developed model is assessed using the sequential F-test, Lack-of-fit test, and Analysis-of-Variance (ANOVA) method. Using Design-Expert 13 software, the measured responses are analysed, and it also determines which mathematical model best fit the data. The effect of each welding parameter on the weld qualities is examined on the basis of the developed mathematical models.

7.2.1. Analysis of Fusion Zone (FZ)

The full-quadratic model, where the extra components are relevant and the model is not aliased, is suggested for the fusion zone by the fit summary shown in Table 7.2. Table 7.3 shows R^2, adjusted R^2, and predicted R^2, indicating that the model is acceptable. ANOVA table is shown in Table 7.4.

The following are the final mathematical model for the Fusion Zone (FZ), as calculated by Design-Expert 13 software:

Regarding the actual variables,

FZ = 930.619 + 0.887795 LP - 23.0561 SS + 41.4656 DF - 22.8088 N - 668.474 GP + 0.0537422 LP x SS + 0.158781 LP x DF + 0.0406406 LP x N + 1.71837 LP x GP - 2.92609 SS x DF - 0.105859 SS x N + 13.3044 SS x GP + 5.13844 DF x N - 34.9875 DF x GP + 1.12625 N x GP - 0.00676619 LP^2 - 0.0843111 SS^2 - 3.82023 DF^2 - 0.995682 N^2 + 34.0764 GP^2

Table 7.2. Fit summary for FZ

Source	Sequential p-value	Lack of Fit p-value	Adjusted R^2	Predicted R^2	
Linear	< 0.0001	0.0073	0.8563	0.7977	
2FI	0.0001	0.1236	0.9631	0.8868	
Quadratic	**0.0163**	**0.4441**	**0.9827**	**0.9015**	**Suggested**
Cubic	0.3421	0.5050	0.9854	0.7095	Aliased

Table 7.3. Model summary for FZ

Std. Dev.	7.28	**R^2**	0.9939
Mean	431.16	**Adjusted R^2**	0.9827
C.V. %	1.69	**Predicted R^2**	0.9015
		Adeq Precision	39.0552

Adeq Precision measures the signal to noise ratio. A ratio greater than 4 is desirable. Model ratio of 39.055 indicates an adequate signal. This model can be used to navigate the design space.

Table 7.4. ANOVA table for FZ

Source	Sum of Squares	Contribution	df	Mean Square	F-value	p-value	
Model	94359.55	99.39%	20	4717.98	89.01	< 0.0001	**Significant**
LP	60171.12	63.38%	1	60171.12	1135.20	< 0.0001	
SS	7498.09	7.90%	1	7498.09	141.46	< 0.0001	
DF	12812.65	13.50%	1	12812.65	241.73	< 0.0001	

N	1864.37	1.96%	1	1864.37	35.17	< 0.0001	
GP	1155.23	1.22%	1	1155.23	21.79	0.0007	
LP x SS	295.75	0.31%	1	295.75	5.58	0.0377	
LP x DF	161.35	0.17%	1	161.35	3.04	0.1089	
LP x N	42.28	0.04%	1	42.28	0.7977	0.3909	
LP x GP	1181.13	1.24%	1	1181.13	22.28	0.0006	
SS x DF	2191.88	2.31%	1	2191.88	41.35	< 0.0001	
SS x N	11.48	0.01%	1	11.48	0.2165	0.6508	
SS x GP	2832.10	2.98%	1	2832.10	53.43	< 0.0001	
DF x N	1689.83	1.78%	1	1689.83	31.88	0.0001	
DF x GP	1224.13	1.29%	1	1224.13	23.09	0.0005	
N x GP	5.07	0.01%	1	5.07	0.0957	0.7628	
LP^2	214.87	0.16%	1	214.87	4.05	0.0692	
SS^2	53.38	0.03%	1	53.38	1.01	0.3372	
DF^2	428.09	0.42%	1	428.09	8.08	0.0160	
N^2	465.29	0.54%	1	465.29	8.78	0.0129	
GP^2	133.05	0.14%	1	133.05	2.51	0.1414	
Residual	583.05	0.61%	11	53.00			
Lack of Fit	339.54	0.36%	6	56.59	1.16	0.4441	**Not significant**
Pure Error	243.51	0.26%	5	48.70			
Total	94942.60	100%	31				

The Model F-value of 89.01 implies the model is significant. There is only a 0.01% chance that an F-value this large could occur due to noise.

P-values less than 0.0500 indicate model terms are significant. In this case LP, SS, DF, N, GP, LP x SS, LP x GP, SS x DF, SS x GP, DF x N, DF x GP, DF^2, N^2 are significant model terms and are also shown in a Pareto chart in Fig. 7.2. Values greater than 0.1000 indicate the model terms are not significant.

The Lack of Fit F-value of 1.16 implies the Lack of Fit is not significant relative to the pure error. Non-significant lack of fit is good, we want the model to fit.

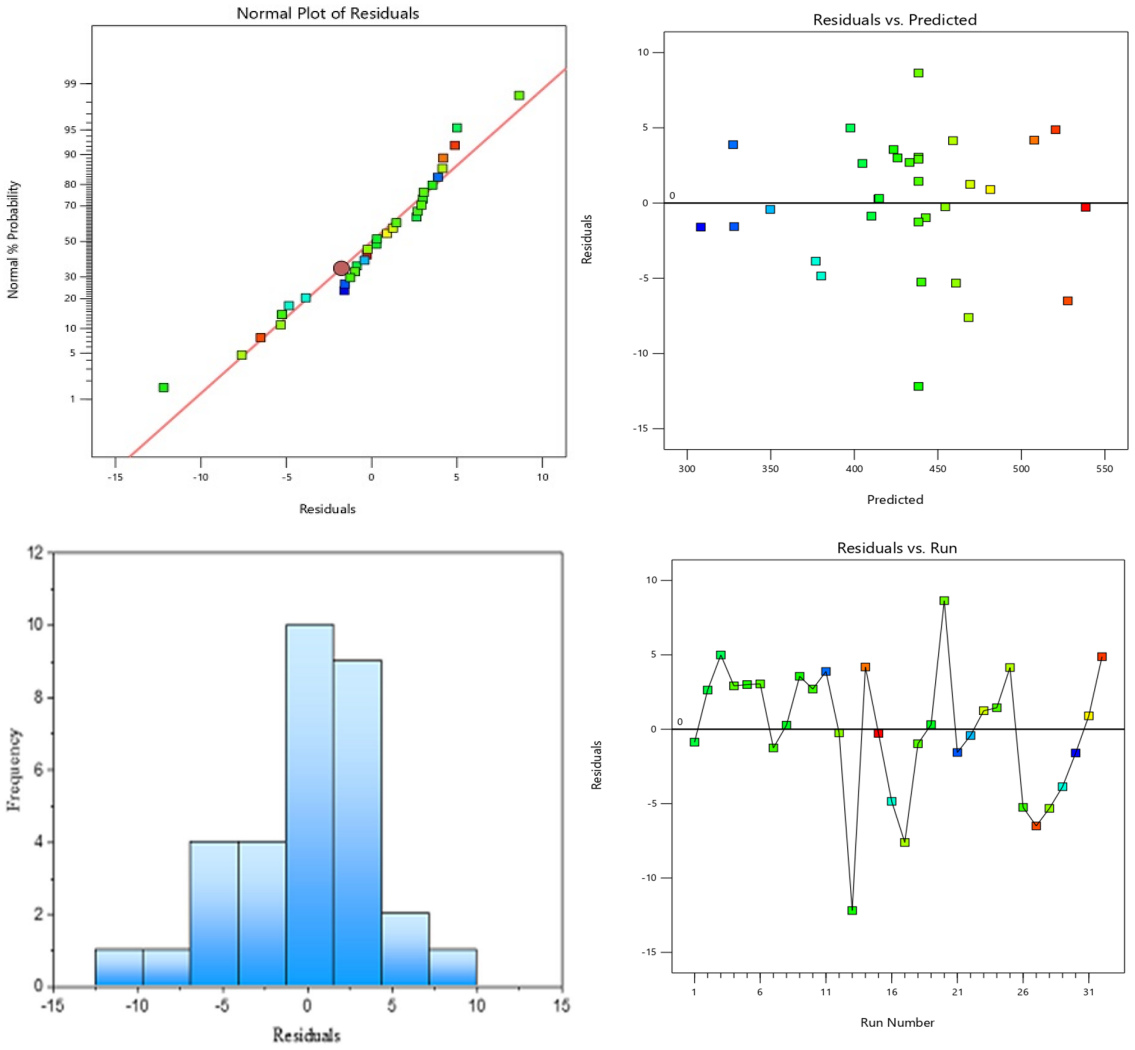

Fig. 7.1. Residual plots for FZ

To determine the error in the residual plot of the fusion zone, the normal distribution is shown. As illustrated in Fig. 7.1, a histogram of residuals, a normal plot of residuals, a plot of residuals vs predicted, and a plot of residuals vs run number have been displayed to indicate both variance constancy and error independence.

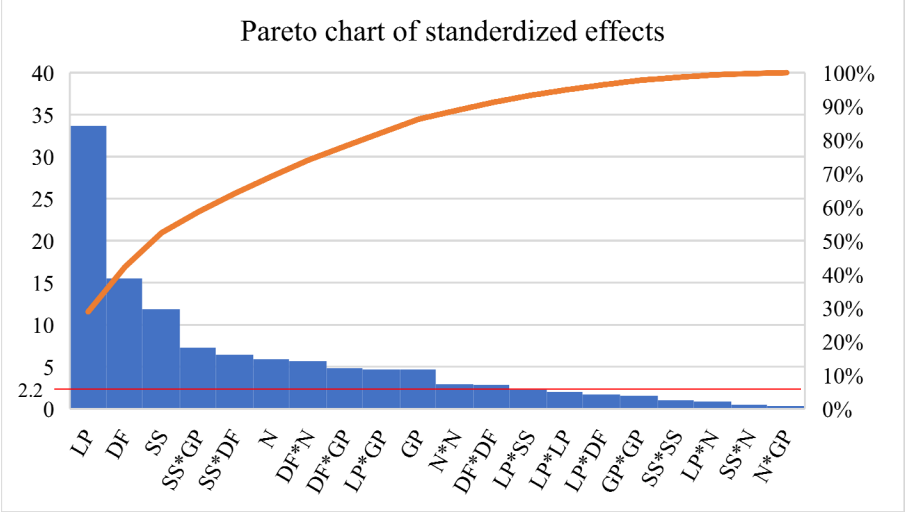

Fig. 7.2. Pareto chart of standardized effects for FZ

7.2.2. Analysis of Cu Heat affected zone (Cu HAZ)

The fit summary in Table 7.5 suggests the full-quadratic model for the heat affected zone of copper, where the additional components are meaningful and the model is not aliased. R^2, adjusted R^2, and predicted R^2 are shown in Table 7.6, suggesting that the model is appropriate. Table 7.7 displays the ANOVA table.

The final mathematical model for the Heat affected zone in copper (Cu HAZ), as estimated by Design-Expert 13 software, is as follows:

Regarding the actual variables,

$$\textbf{Cu HAZ} = 12325.2 - 43.9934\,LP - 147.663\,SS - 926.813\,DF - 111.944\,N - 2704.56\,GP + 0.277961\,LP \times SS + 2.66941\,LP \times DF + 0.151953\,LP \times N - 0.746875\,LP \times GP - 11.9395\,SS \times DF + 1.24805\,SS \times N + 55.6594\,SS \times GP + 23.6791\,DF \times N + 111.062\,DF \times GP - 106.914\,N \times GP + 0.0601503\,LP^2 + 0.191648\,SS^2 + 0.351364\,DF^2 + 6.77128\,N^2 + 642.042\,GP^2$$

Table 7.5. Fit summary for Cu HAZ

Source	Sequential p-value	Lack of Fit p-value	Adjusted R^2	Predicted R^2
Linear	< 0.0001	0.0003	0.5356	0.3577
2FI	0.0032	0.0019	0.8076	-0.0975

Quadratic	**< 0.0001**	**0.3508**	**0.9832**	**0.9073**	**Suggested**
Cubic	0.9602	0.0467	0.9732	-2.2690	Aliased

Table 7.6. Model summary for Cu HAZ

Std. Dev.	21.00	**R^2**	0.9940
Mean	598.45	**Adjusted R^2**	0.9832
C.V. %	3.51	**Predicted R^2**	0.9073
		Adeq Precision	40.9985

Adeq Precision measures the signal to noise ratio. A ratio greater than 4 is desirable. Model ratio of 40.999 indicates an adequate signal. This model can be used to navigate the design space.

Table 7.7. ANOVA table for Cu HAZ

Source	**Sum of Squares**	**Contribution**	**df**	**Mean Square**	**F-value**	**p-value**	
Model	8.082E+05	99.40%	20	40410.43	91.62	<0.0001	**Significant**
LP	3.114E+05	38.30%	1	3.114E+05	706.05	<0.0001	
SS	1.468E+05	18.06%	1	1.468E+05	332.90	<0.0001	
DF	32315.82	3.97%	1	32315.82	73.26	<0.0001	
N	988.04	0.12%	1	988.04	2.24	0.1626	
GP	4813.55	0.59%	1	4813.55	10.91	0.0070	
LP x SS	7911.66	0.97%	1	7911.66	17.94	0.0014	
LP x DF	45604.67	5.61%	1	45604.67	103.39	<0.0001	
LP x N	591.10	0.07%	1	591.10	1.34	0.2715	
LP x GP	223.13	0.03%	1	223.13	0.5059	0.4917	
SS x DF	36493.42	4.49%	1	36493.42	82.74	<0.0001	
SS x N	1595.00	0.20%	1	1595.00	3.62	0.0837	
SS x GP	49567.46	6.10%	1	49567.46	112.38	<0.0001	
DF x N	35884.67	4.41%	1	35884.67	81.36	<0.0001	
DF x GP	12334.88	1.52%	1	12334.88	27.96	0.0003	
N x GP	45722.20	5.62%	1	45722.20	103.66	<0.0001	
LP^2	16980.75	1.38%	1	16980.75	38.50	<0.0001	

SS^2	275.81	0.01%	1	275.81	0.6253	0.4458	
DF^2	3.62	0.08%	1	3.62	0.0082	0.9294	
N^2	21519.03	2.05%	1	21519.03	48.79	<0.0001	
GP^2	47233.28	5.81%	1	47233.28	107.08	<0.0001	
Residual	4851.92	0.60%	11	441.08			
Lack of Fit	3079.47	0.38%	6	513.25	1.45	0.3508	**Not significant**
Pure Error	1772.44	0.22%	5	354.49			
Total	8.131E+05	100%	31				

The model's F-value of 91.62 indicates that it is significant. An F-value this big might arise owing to noise just 0.01 percent, which is insignificant.

Model terms with P-values less than 0.0500 are significant. In this situation, the model elements LP, SS, DF, GP, LP x SS, LP x DF, SS x DF, SS x GP, DF x N, DF x GP, N x GP, LP^2, N^2, GP^2 are relevant and are depicted in a Pareto chart in Fig. 7.3. Values larger than 0.1000 imply that the model terms are unimportant.

The Lack of Fit F-value of 1.45 indicates that the Lack of Fit is insignificant in comparison to the pure error. We want the model to fit, thus a non-significant lack of fit looks Fine.

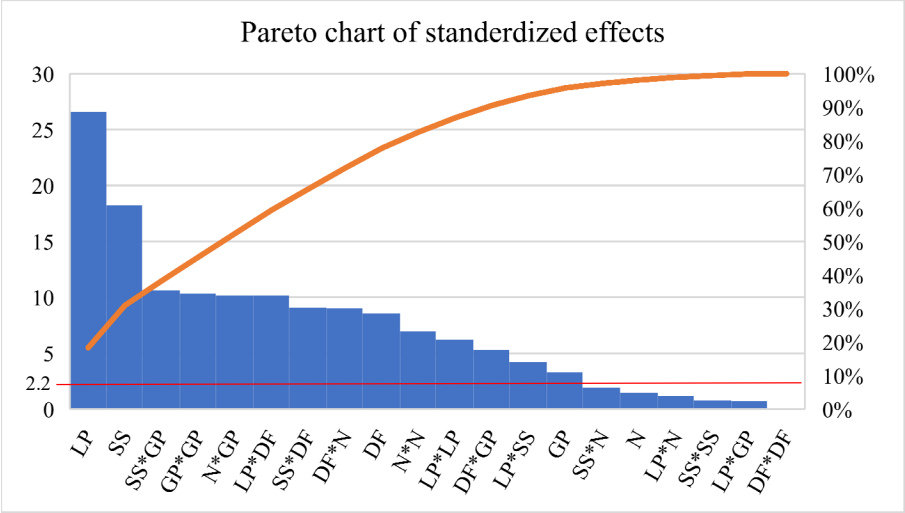

Fig. 7.3. Pareto chart of standardized effects for Cu HAZ

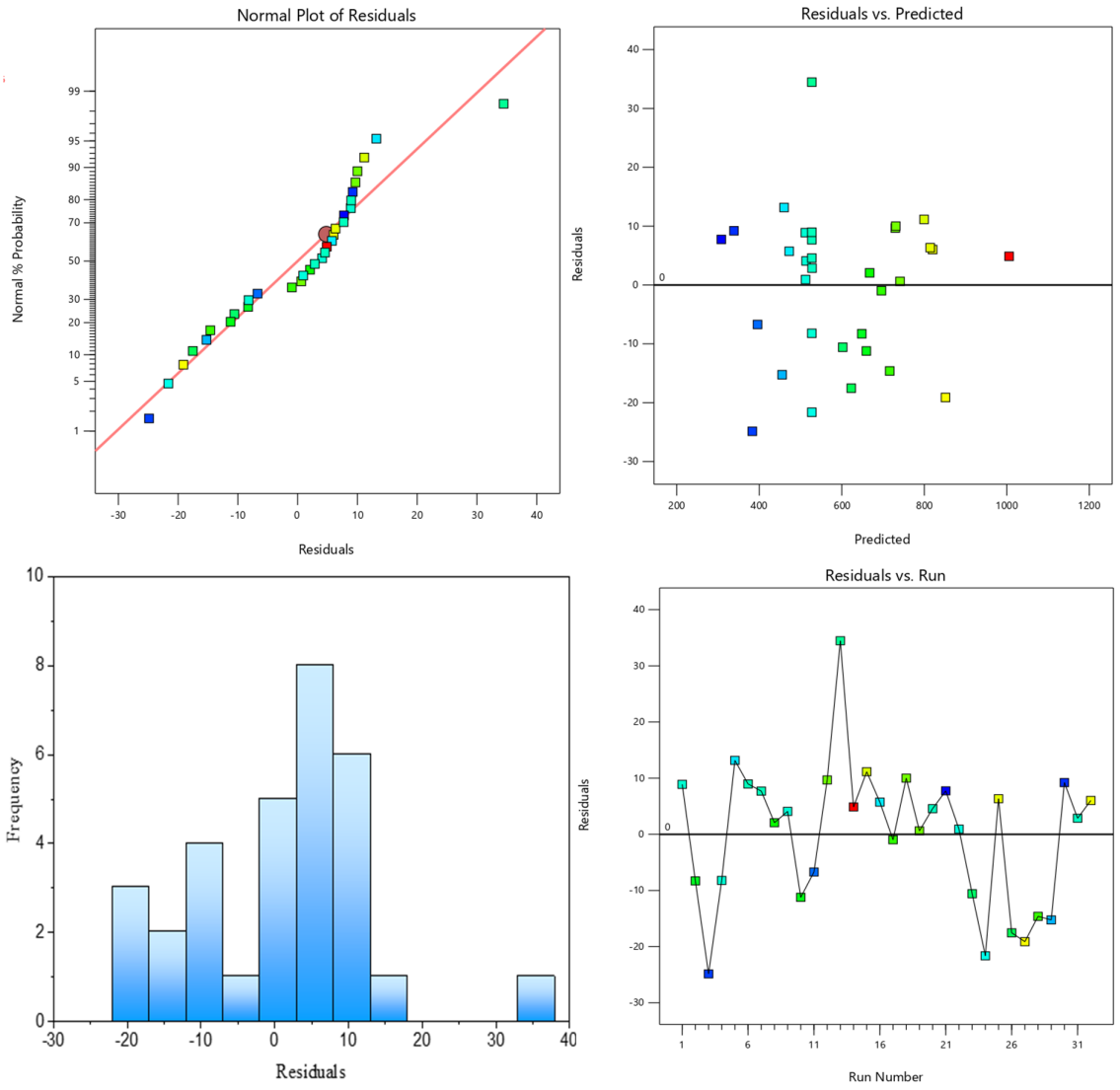

Fig. 7.4. Residual plots for Cu HAZ

The normal distribution is displayed in order to calculate the inaccuracy in the residual plot of the heat affected zone in copper. In order to demonstrate both variance constancy and error independence, as shown in Fig. 7.4, a histogram of residuals, a normal plot of residuals, a plot of residuals versus predicted, and a plot of residuals vs run number have all been presented.

7.2.3. Analysis of SS 304 Heat affected zone (SS HAZ)

For the heat-affected zone of SS 304, the fit summary in Table 7.8 recommends the full-quadratic model, where the extra components are significant and the model is not aliased. Table 7.9's R^2, corrected R^2, and anticipated R^2 values indicate that the model is suitable. The ANOVA table is shown in Table 7.10.

According to estimates made by Design-Expert 13 software, the final mathematical model for the Heat Affected Zone in SS 304 (SS HAZ) is as follows:

Regarding the actual variables,

SS HAZ = 6991.32 - 17.5152 LP - 161.081 SS - 981.222 DF - 161.316 N + 405.805 GP + 0.0684141 LP x SS + 1.98609 LP x DF + 0.312891 LP x N - 12.6209 LP x GP - 5.52703 SS x DF - 0.0805469 SS x N + 47.8306 SS x GP + 11.8634 DF x N + 93.6875 DF x GP - 63.8137 N x GP + 0.0618196 LP^2 + 1.56908 SS^2 + 21.4953 DF^2 + 9.08759 N^2 + 552.745 GP^2

Table 7.8. Fit summary for SS HAZ

Source	Sequential p-value	Lack of Fit p-value	Adjusted R^2	Predicted R^2	
Linear	< 0.0001	0.0004	0.7595	0.6855	
2FI	0.0372	0.0011	0.8545	-0.0834	
Quadratic	**< 0.0001**	**0.1983**	**0.9864**	**0.9057**	**Suggested**
Cubic	0.1830	0.2760	0.9912	0.5735	Aliased

Table 7.9. Model summary for SS HAZ

Std. Dev.	24.26	**R^2**	0.9952
Mean	886.92	**Adjusted R^2**	0.9864
C.V. %	2.74	**Predicted R^2**	0.9057
		Adeq Precision	44.9976

Adeq Precision measures the signal to noise ratio. A ratio greater than 4 is desirable. Model ratio of 44.998 indicates an adequate signal. This model can be used to navigate the design space.

Table 7.10. ANOVA table for SS HAZ

Source	Sum of Squares	Contribut-ion	df	Mean Square	F-value	p-value	
Model	1.339E+06	99.52%	20	66955.23	113.73	<0.0001	**Significant**
LP	4.084E+05	30.35%	1	4.084E+05	693.72	<0.0001	
SS	3.801E+05	28.25%	1	3.801E+05	645.70	<0.0001	
DF	1.484E+05	11.03%	1	1.484E+05	252.16	<0.0001	
N	85281.64	6.34%	1	85281.64	144.86	<0.0001	
GP	51865.17	3.85%	1	51865.17	88.10	<0.0001	
LP x SS	479.28	0.04%	1	479.28	0.8141	0.3862	
LP x DF	25245.24	1.88%	1	25245.24	42.88	<0.0001	
LP x N	2506.25	0.19%	1	2506.25	4.26	0.0635	
LP x GP	63714.59	4.74%	1	63714.59	108.23	<0.0001	
SS x DF	7820.31	0.58%	1	7820.31	13.28	0.0039	
SS x N	6.64	0.00%	1	6.64	0.0113	0.9173	
SS x GP	36604.30	2.72%	1	36604.30	62.18	<0.0001	
DF x N	9007.43	0.67%	1	9007.43	15.30	0.0024	
DF x GP	8777.35	0.65%	1	8777.35	14.91	0.0026	
N x GP	16288.78	1.21%	1	16288.78	27.67	0.0003	
LP^2	17936.34	0.64%	1	17936.34	30.47	0.0002	
SS^2	18488.16	0.76%	1	18488.16	31.40	0.0002	
DF^2	13553.46	0.57%	1	13553.46	23.02	0.0006	
N^2	38759.52	2.46%	1	38759.52	65.84	<0.0001	
GP^2	35008.36	2.60%	1	35008.36	59.47	<0.0001	
Residual	6475.73	0.48%	11	588.70			
Lack of Fit	4714.24	0.35%	6	785.71	2.23	0.1983	**Not significant**
Pure Error	1761.49	0.13%	5	352.30			
Total	1.346E+06	100%	31				

The F-value of 113.73 for the model suggests that it is significant. Only 0.01 percent of the noise could possibly account for an F-value this large, which is negligible.

Significant model terms have P-values under 0.0500. In this case, the important model elements are shown in a Pareto chart in Fig. 7.6 and are as follows: LP, SS, DF, N, GP, LP x DF, LP x GP, SS x DF, SS x GP, DF x N, DF x GP, N x GP, LP^2, SS^2, DF^2, N^2, GP^2. Values over 0.1000 suggest that the model terms are not significant.

The lack of fit is not significant in compared to the pure error, as shown by the lack of fit F-value of 2.23. Since we want the model to fit, an insignificant lack of fit issue is acceptable.

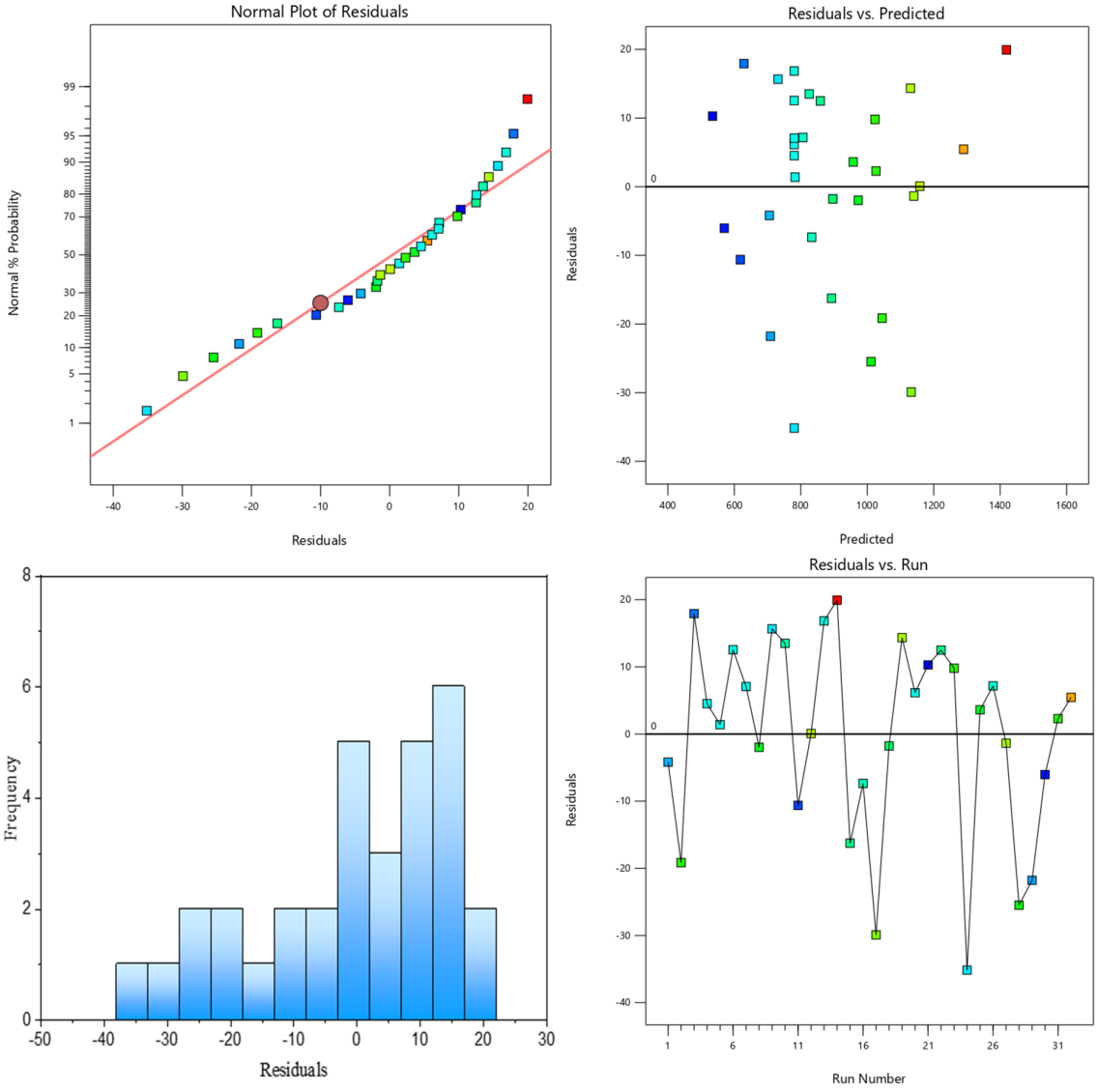

Fig. 7.5. Residual plots for SS HAZ

To determine the reliability of the residual plot of the SS 304 heat-affected zone, the normal distribution is shown. As demonstrated in Fig. 7.5, a histogram of residuals, a normal plot of

residuals, a plot of residuals vs predicted, and a plot of residuals vs run number have all been given to illustrate both variance constancy and error independence.

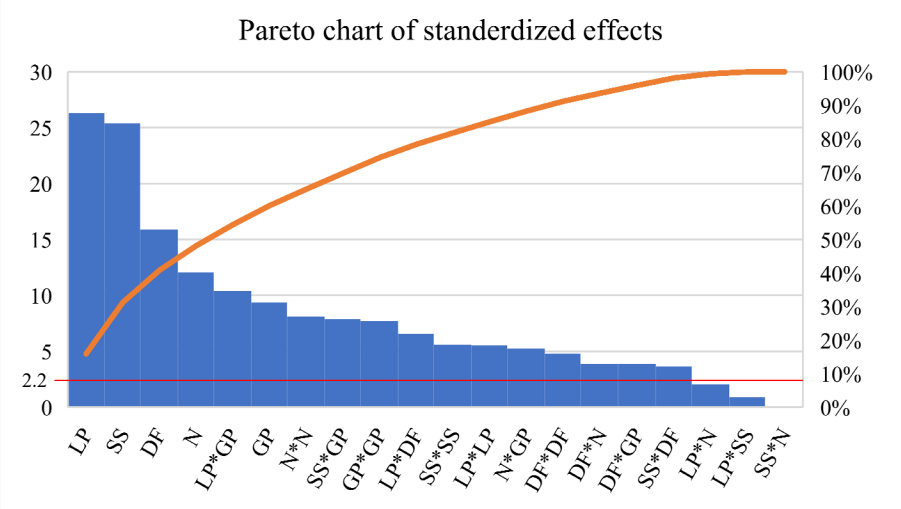

Fig. 7.6. Pareto chart of standardized effects for SS HAZ

7.3. Effects of Process parameters on Responses

The impact of process parameters on the fusion zone and heat affected zone of both Cu & SS 304 of the welded sample is investigated and described here within the constraints of the factors included in this study. The findings are shown graphically using factors interaction plots for the selected material combinations. All key terminology relating to the fusion zone and heat impacted zone are shown, and the factor influence patterns are extensively explored.

7.3.1. Effects of Process parameters on Fusion zone (FZ)

7.3.1.1. Response surface plot and contour plot for the effect of Laser Power (LP) and Scanning Speed (SS) on Fusion zone (FZ)

Effects of the two process parameters named LP and SS on weld quality characteristic i.e., Fusion zone is thoroughly investigated in this section when, other parameters are hold at their respective centres.

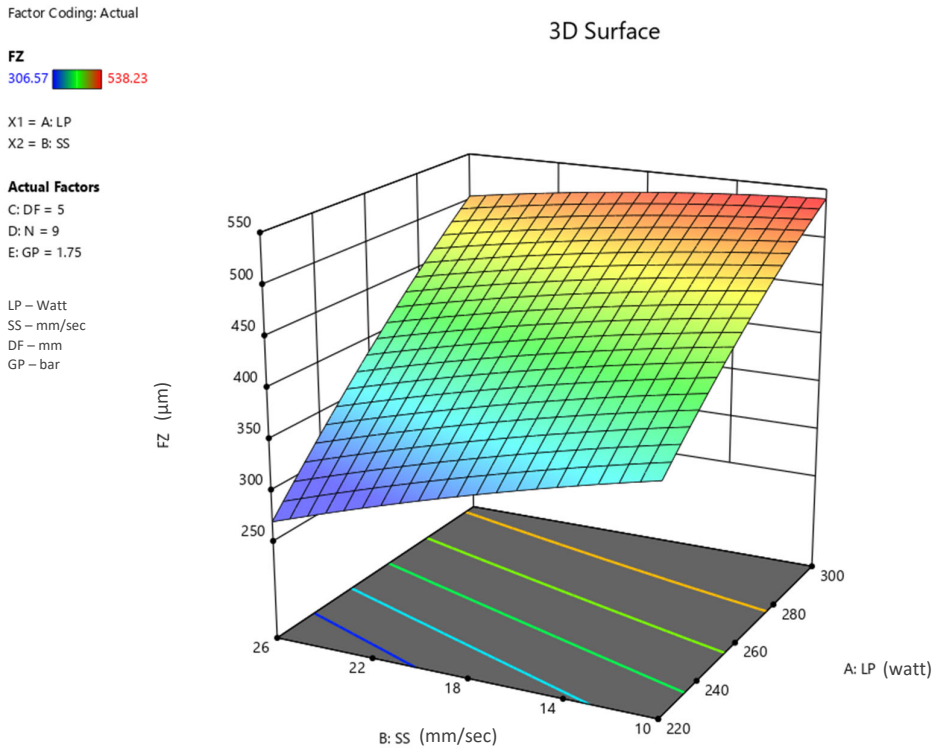

Fig. 7.7. Surface plot showing effects of LP and SS on FZ

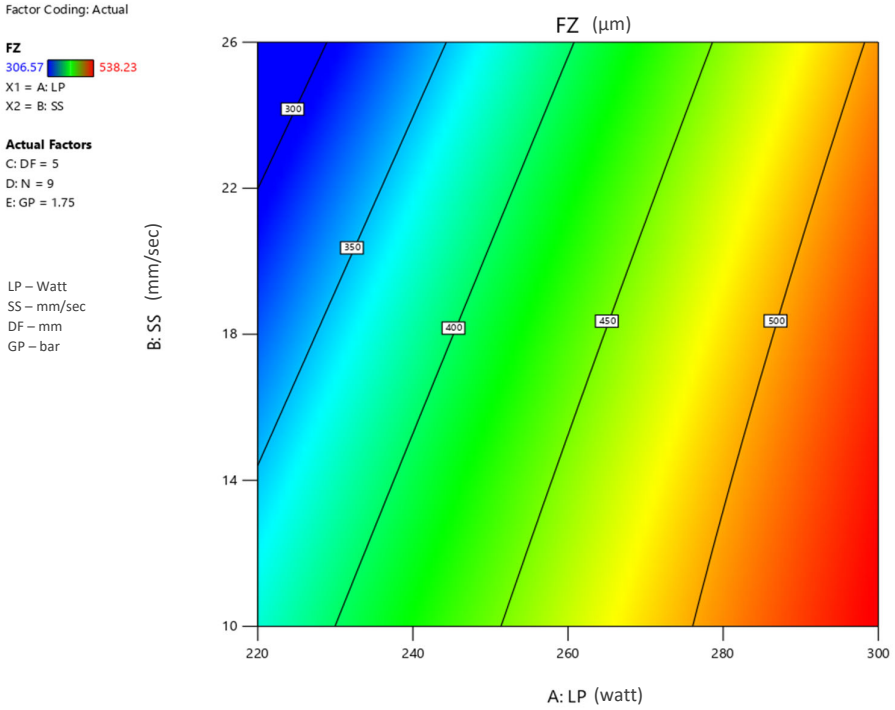

Fig. 7.8. Contour plot showing effects of LP and SS on FZ

Surface plot Fig. 7.7 & Contour plot Fig. 7.8 shows that fusion zone increases with laser power and decreases with scanning speed. Heat input increases with laser power since it directly varies

with line energy; hence, higher energy leads to broader fusion zone. Scanning speed has inverse relationship with line energy and interaction time. Hence scanning speed increases, interaction time decreases then fusion zone also decreases. FZ is seen to be high (538.23 µm) at a combination of high LP (300 W) and low SS (10 mm/sec). Reverse is observed at low LP (220 W) and high SS (26 mm/sec), FZ can go as low as 270 µm.

7.3.1.2. Response surface plot and contour plot for the effect of Laser Power (LP) and Gas Pressure (GP) on Fusion zone (FZ)

Effects of the two process parameters named LP and GP on weld quality characteristic i.e., Fusion zone is thoroughly investigated in this section when, other parameters are hold at their respective centres.

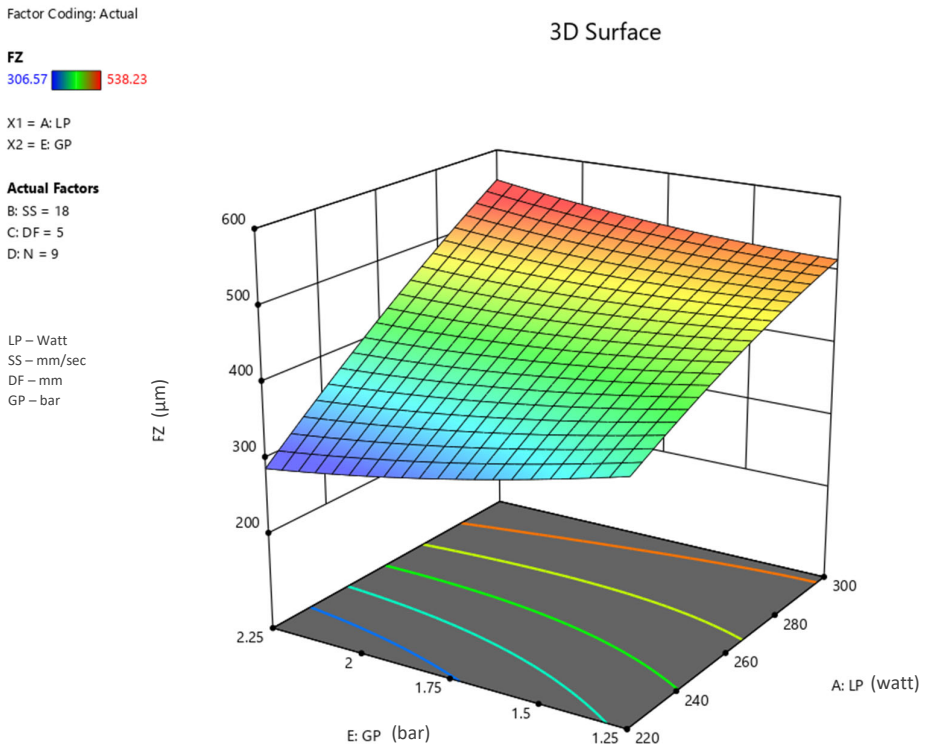

Fig. 7.9. Surface plot showing effects of LP and GP on FZ

Surface plot Fig. 7.9 & Contour plot Fig. 7.10 shows that fusion zone increases with laser power and decreases with gas pressure at low power level but, increases at high power level. Heat input increases with laser power since it directly varies with line energy; hence, higher energy leads to wide fusion zone.

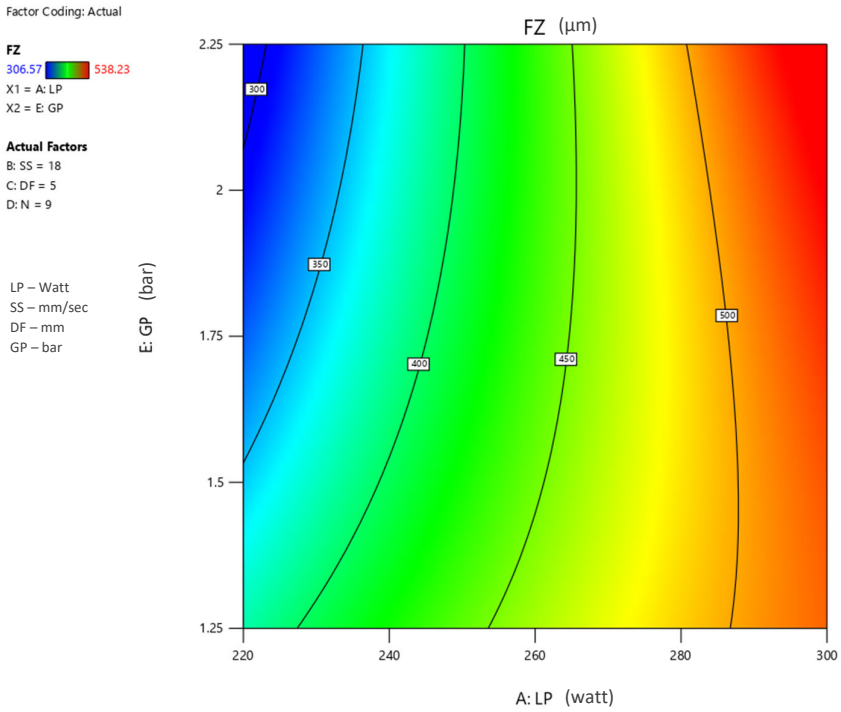

Fig. 7.10. Contour plot showing effects of LP and GP on FZ

A high gas pressure provides better shielding of the weld pool from the surrounding atmosphere, which can help to prevent oxidation and contamination of the weld, results in broad and uniform weld bead. When the LP is high, increasing GP aids the process of fusion. But, at low LP region, lack of fusion is predominant and high cooling rate due to increasing GP in this case reduces the time of fusion & narrow FZ gets developed.

7.3.1.3. Response surface plot and contour plot for the effect of Scanning Speed (SS) and Defocus distance (DF) on Fusion zone (FZ)

Effects of the two process parameters named SS and DF on weld quality characteristic i.e., Fusion zone is thoroughly investigated in this section when, other parameters are hold at their respective centres.

Surface plot Fig. 7.11 & Contour plot Fig. 7.12 shows that fusion zone decreases with increasing scanning speed and defocus distance. As laser speed increases, interaction time decreases. This results into less melting of base metal and poor fusion. Laser spot diameter increases as defocus increases, also the laser power intensity decreases along with it. FZ decreases with this decrease of effective laser power. At 7 mm defocus distance and 26 mm/sec

scanning speed FZ is minimum as seen and reaches a maximum zone at lower speed and lees defocus range.

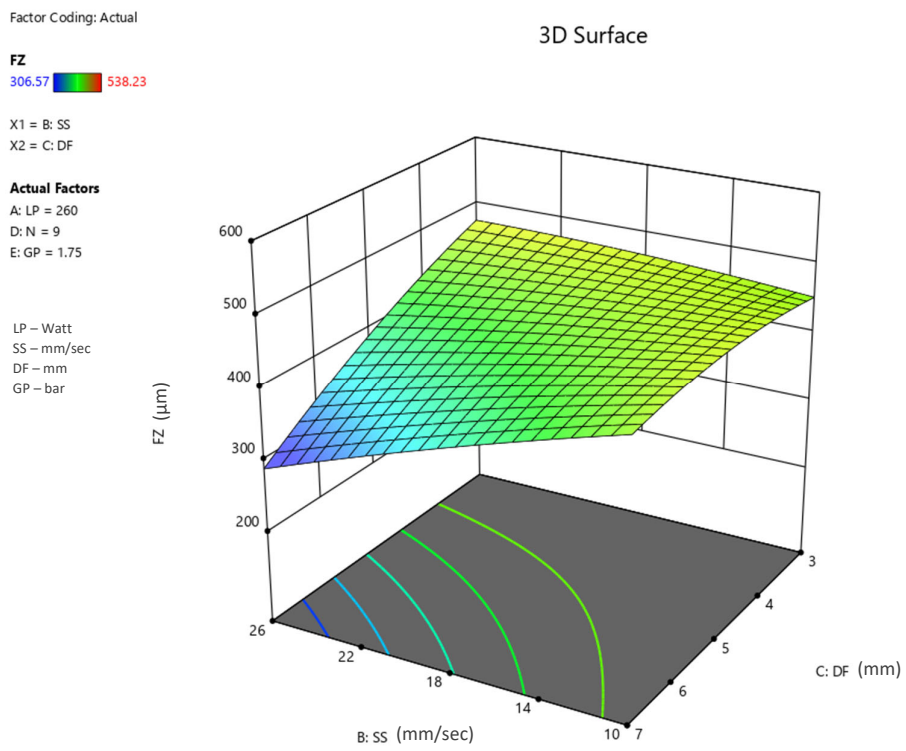

Fig. 7.11. Surface plot showing effects of SS and DF on FZ

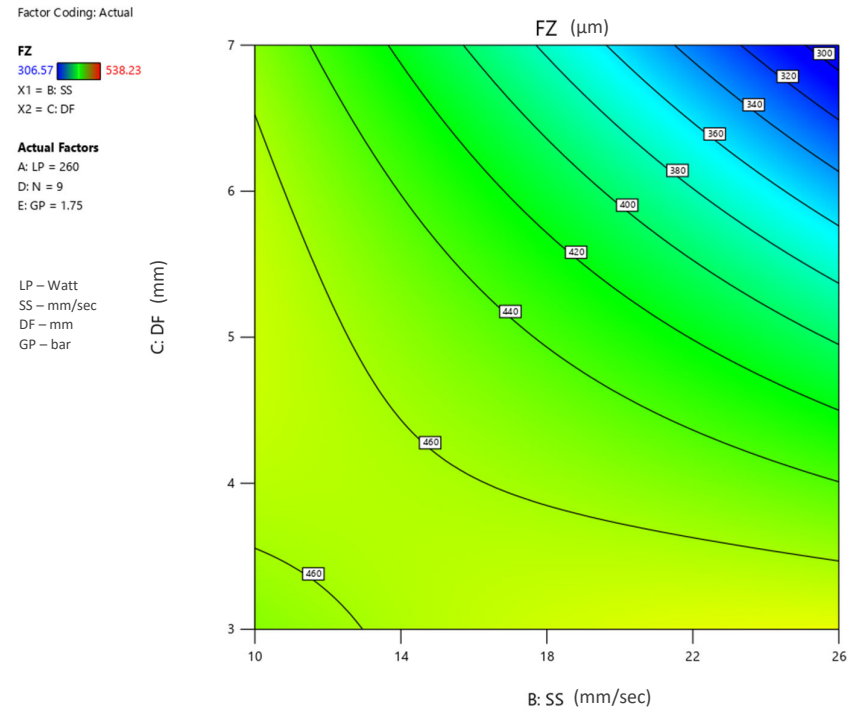

Fig. 7.12. Contour plot showing effects of SS and DF on FZ

7.3.1.4. Response surface plot and contour plot for the effect of Scanning Speed (SS) and Gas Pressure (GP) on Fusion zone (FZ)

Effects of the two process parameters named SS and GP on weld quality characteristic i.e., Fusion zone is thoroughly investigated in this section when, other parameters are hold at their respective centres.

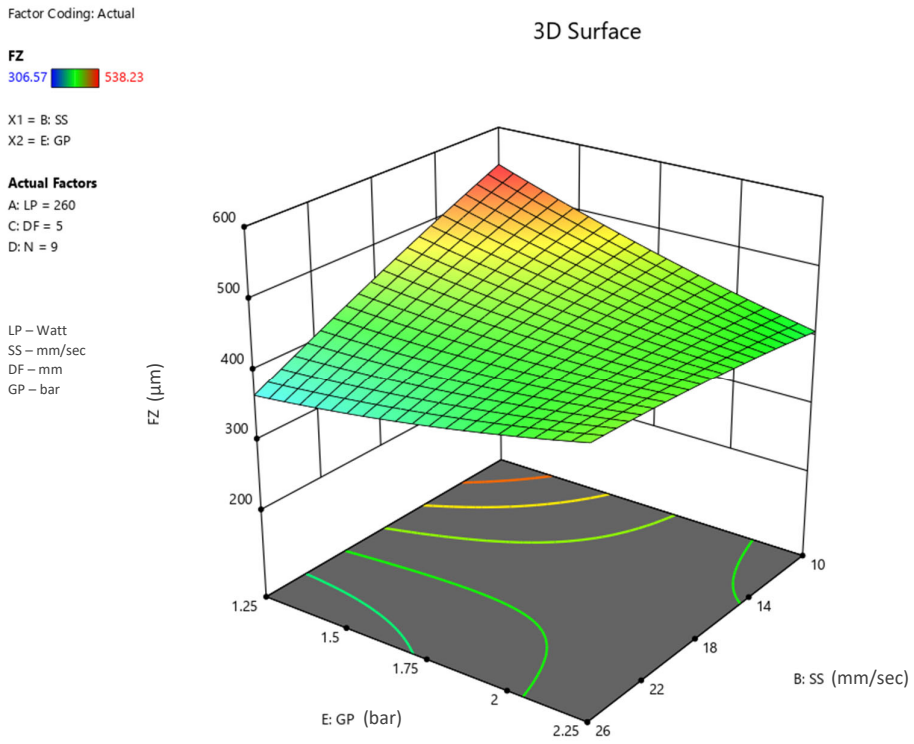

Fig. 7.13. Surface plot showing effects of SS and GP on FZ

Surface plot Fig. 7.13 & Contour plot Fig. 7.14 shows that fusion zone decreases with increasing scanning speed and gas pressure. As laser speed increases, interaction time decreases. This results into less melting of base metal and poor fusion. High gas pressure causes turbulence in the weld pool, which can lead to spatter and poor penetration. It can also increase the heat loss from the weld, which can lead to a narrower weld bead. Scanning speed has greater influence on FZ than gas pressure as seen on the plot. As SS increases from 10 to 26 mm/sec, FZ reaches a lower value compared to when the gas pressure increases from 1.25 to 2.25 bar.

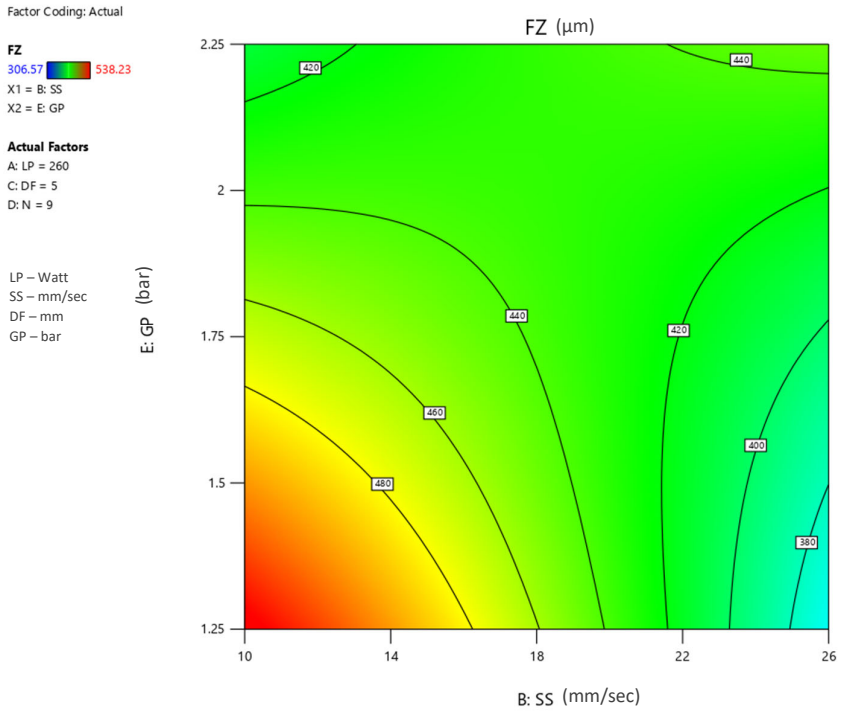

Fig. 7.14. Contour plot showing effects of SS and GP on FZ

7.3.1.5. Response surface plot and contour plot for the effect of Defocus distance (DF) and Number of passes (N) on Fusion zone (FZ)

Effects of the two process parameters named DF and N on weld quality characteristic i.e., Fusion zone is thoroughly investigated in this section when, other parameters are hold at their respective centres.

Surface plot Fig. 7.15 & Contour plot Fig. 7.16 shows that fusion zone decreases with increasing defocus distance and number of passes. Laser power intensity decreases with the increase in defocus distance. This results into less melting of base metal and narrow seam of weld. In case of number of passes, fusion zone is wider in the range of 5 to 7 passes, but after that as number of passes increases, redeposition of material starts occurring, in some cases burnout of base metal also. This results into a good penetration but narrow weld bead.

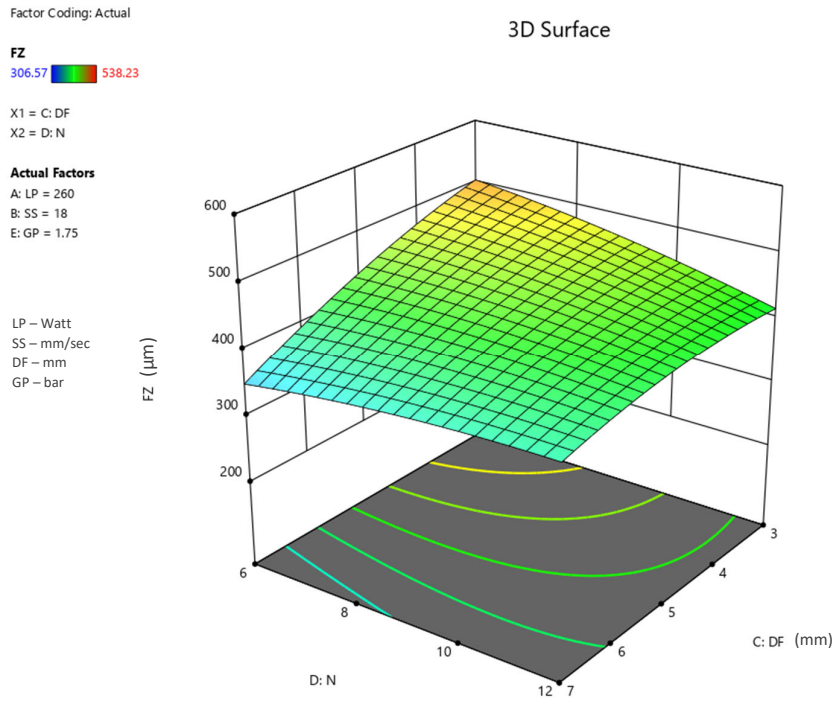

Fig. 7.15. Surface plot showing effects of DF and N on FZ

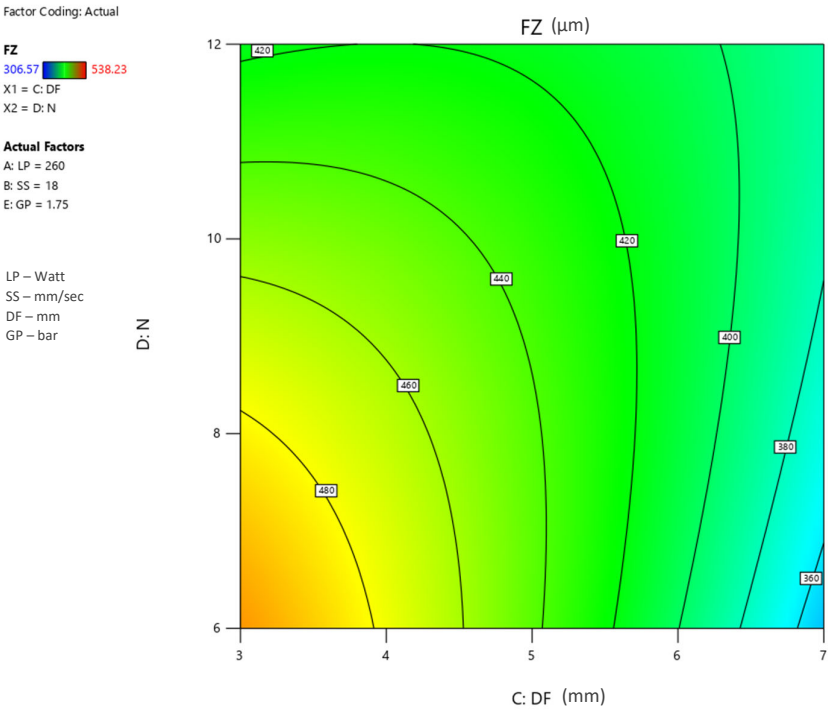

Fig. 7.16. Contour plot showing effects of DF and N on FZ

7.3.1.6. Response surface plot and contour plot for the effect of Defocus distance (DF) and Gas pressure (GP) on Fusion zone (FZ)

Effects of the two process parameters named DF and GP on weld quality characteristic i.e., Fusion zone is thoroughly investigated in this section when, other parameters are hold at their respective centres.

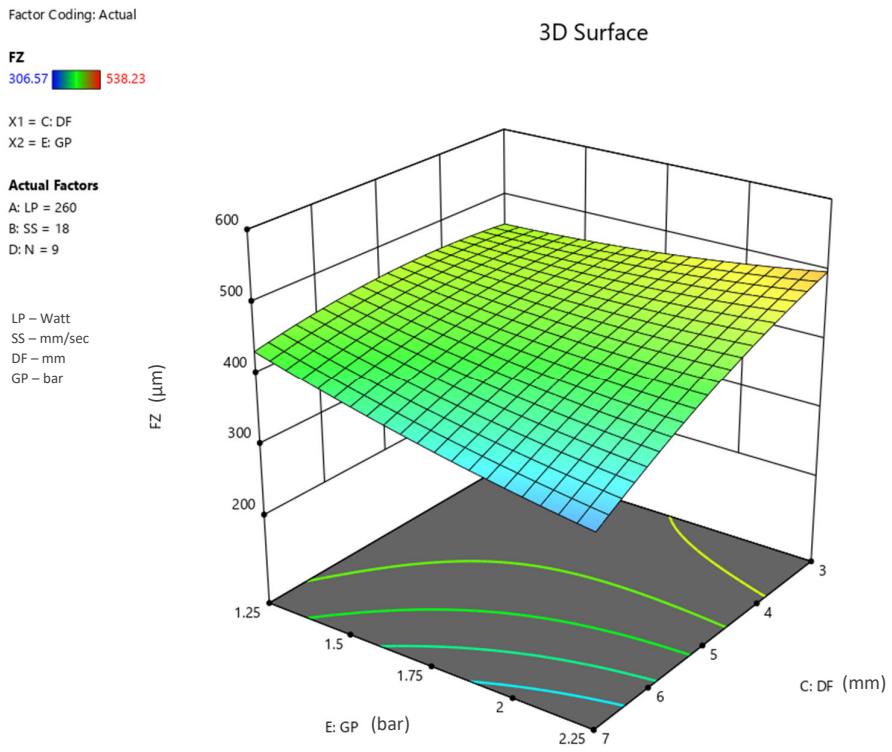

Fig. 7.17. Surface plot showing effects of DF and GP on FZ

Surface plot Fig. 7.17 & Contour plot Fig. 7.18 shows that fusion zone decreases with increasing defocus distance and gas pressure. Turbulence in the weld pool caused by high gas pressure might result in spatter and poor penetration. It can also enhance heat loss from the weld, resulting in a smaller weld bead. The intensity of laser power diminishes as the defocus distance increases. This results in less melting of the base metal and a thin weld seam. At a lower range of defocus, laser intensity is pretty high. At high laser intensity, a high gas pressure provides better shielding of the weld pool from the surrounding atmosphere and turbulence effect gets diminished, which can help to prevent oxidation and contamination of the weld, results in broad and uniform weld bead.

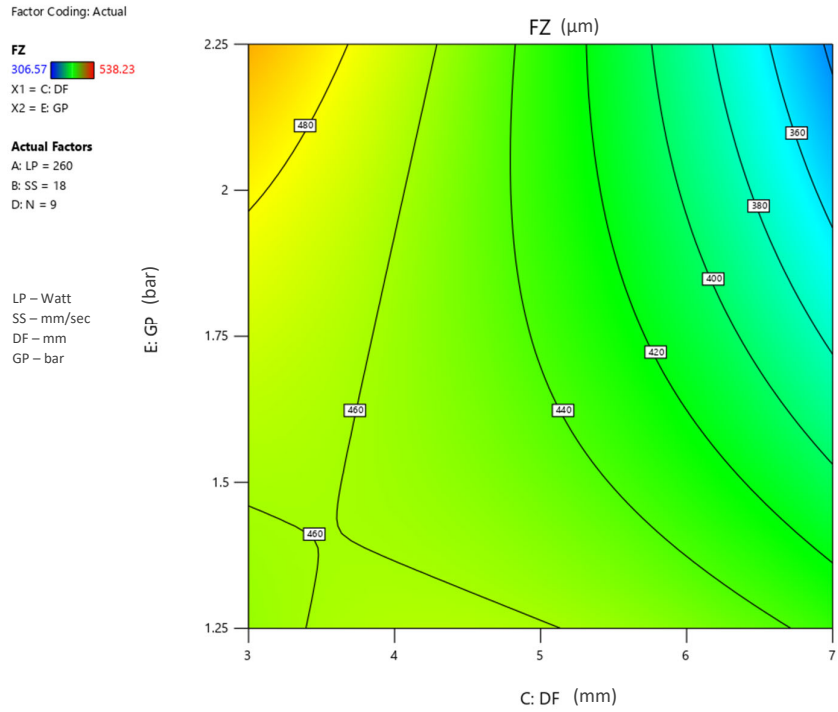

Fig. 7.18. Contour plot showing effects of DF and GP on FZ

A single factor interaction of all parameters is also shown in Fig. 7.19.

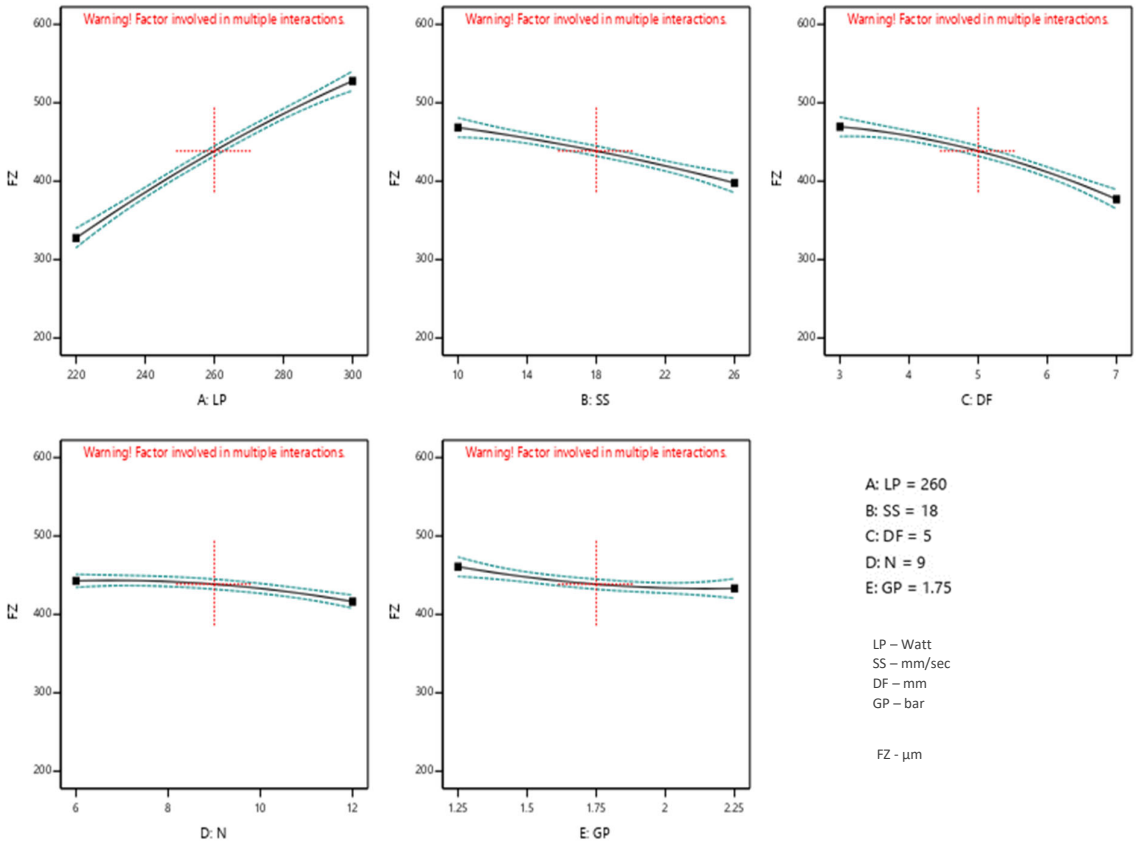

Fig. 7.19. Single factor interaction of all parameters with FZ

7.3.2. Effects of Process parameters on Heat affected zone of Copper (Cu HAZ)

7.3.2.1. Response surface plot and contour plot for the effect of Laser Power (LP) and Scanning Speed (SS) on Copper Heat affected zone (Cu HAZ)

Effects of the two process parameters named LP and SS on weld characteristic i.e., Copper heat affected zone is thoroughly investigated in this section when, other parameters are hold at their respective centres.

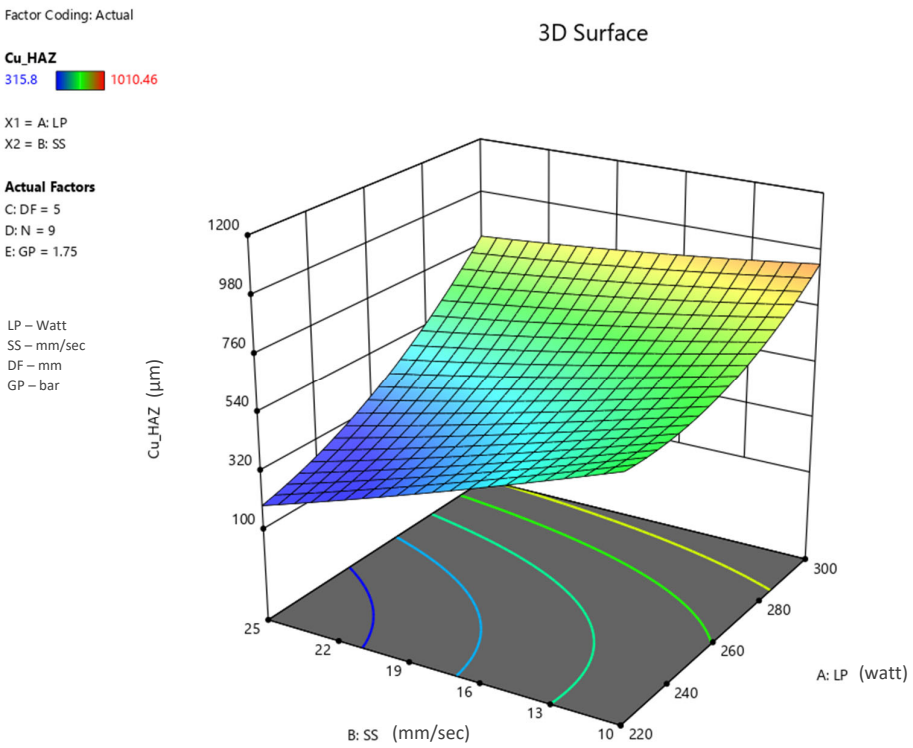

Fig. 7.20. Surface plot showing effects of LP and SS on Cu HAZ

Surface plot Fig. 7.20 & Contour plot Fig. 7.21 shows that heat affected zone increases with increasing laser power and decreasing scanning speed. As the laser power increases, the heat input into the material increases, and the HAZ becomes larger. This is because the higher laser power causes the material to heat up to a higher temperature. A faster scanning speed will result in a smaller HAZ. This is because the metal is heated for a shorter period of time, which allows it to cool more quickly. It can be seen that at 220W LP & 25 mm/sec SS, Cu HAZ attains a minimum value whereas at 300W LP & 10 mm/sec SS, Cu HAZ reaches its maximum value.

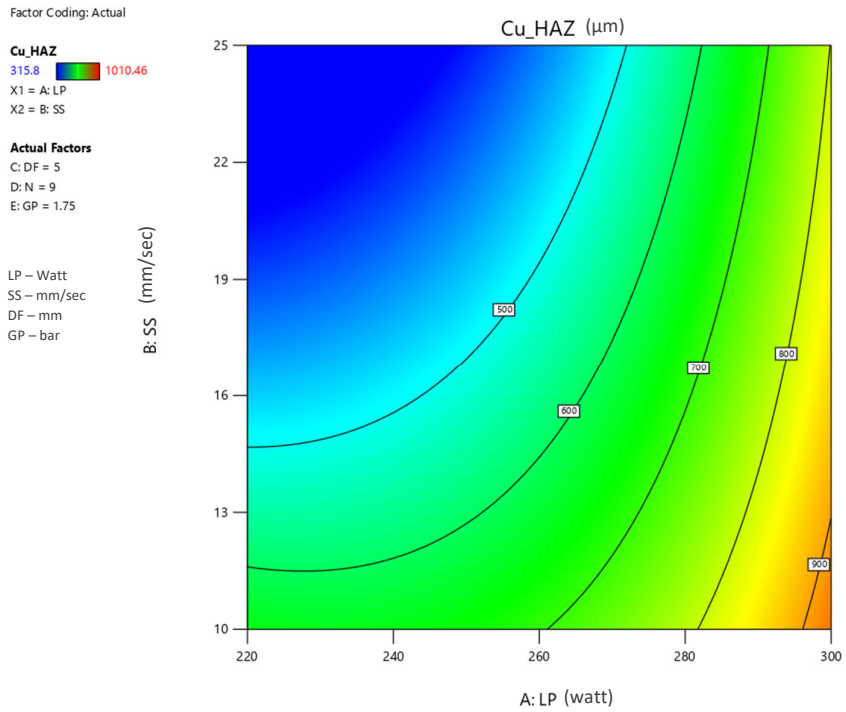

Fig. 7.21. Contour plot showing effects of LP and SS on Cu HAZ

7.3.2.2. Response surface plot and contour plot for the effect of Laser Power (LP) and Defocus distance (DF) on Copper Heat affected zone (Cu HAZ)

Effects of the two process parameters named LP and DF on weld characteristic i.e., Copper heat affected zone is thoroughly investigated in this section when, other parameters are hold at their respective centres.

Surface plot Fig. 7.22 & Contour plot Fig. 7.23 shows that heat affected zone increases with increasing laser power and increases with defocus at high power region but decreases at low power region with increasing defocus. As the laser power increases, so does the heat input into the material, and the HAZ grows bigger. This is because the stronger the laser power, the higher the temperature of the material. At higher range of laser power (260W-300W) HAZ increases as defocus increases due to bigger laser spot diameter in defocused condition. HAZ decreases at lower laser power range (220W- 240W) with increase in defocus as laser intensity becomes very low at low power and high defocus.

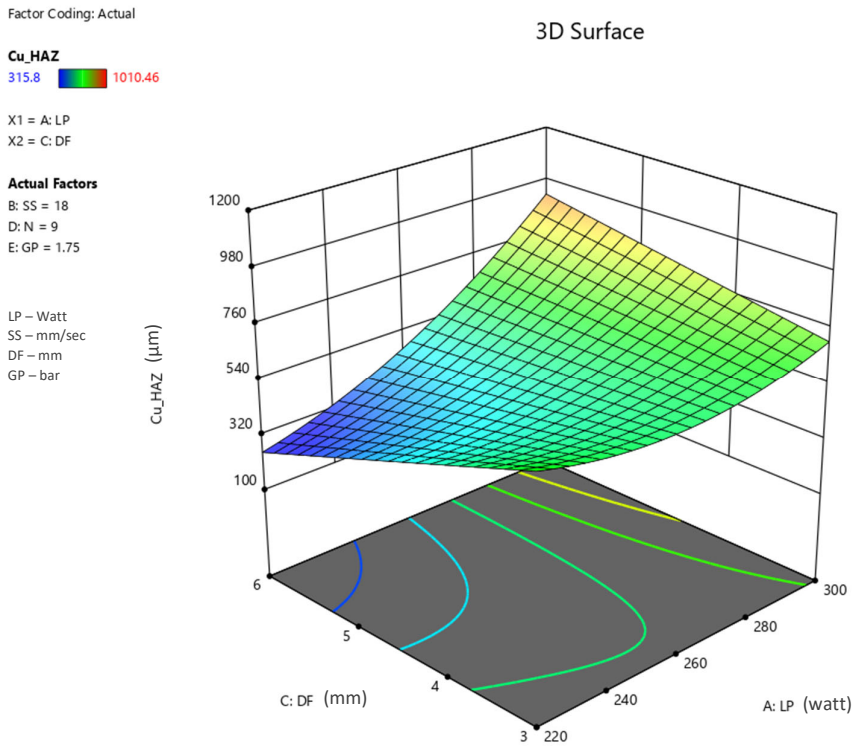

Fig. 7.22. Surface plot showing effects of LP and DF on Cu HAZ

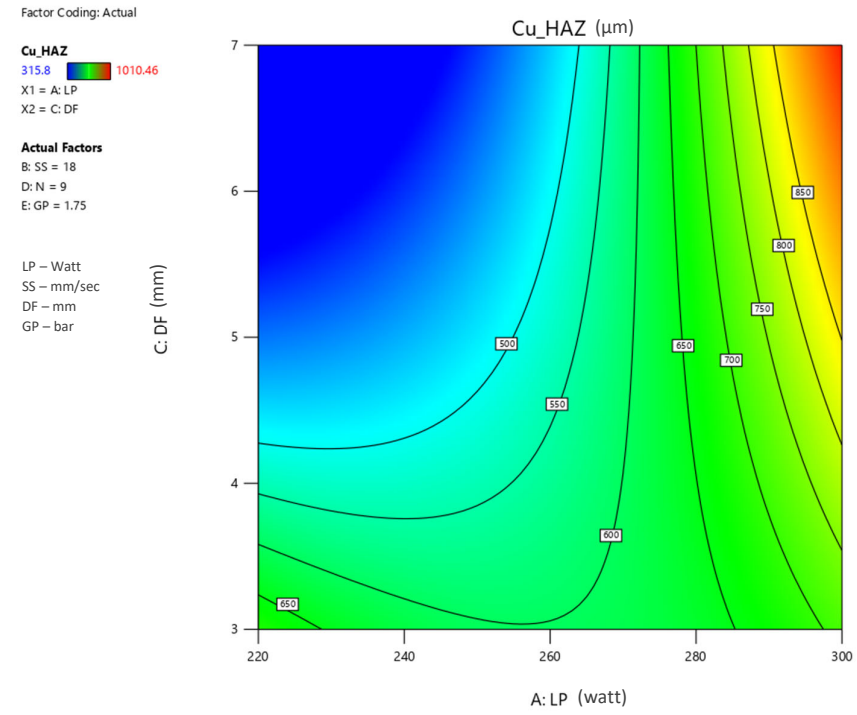

Fig. 7.23. Contour plot showing effects of LP and DF on Cu HAZ

7.3.2.3. Response surface plot and contour plot for the effect of Scanning Speed (SS) and Defocus distance (DF) on Copper Heat affected zone (Cu HAZ)

Effects of the two process parameters named SS and DF on weld characteristic i.e., Copper heat affected zone is thoroughly investigated in this section when, other parameters are hold at their respective centres.

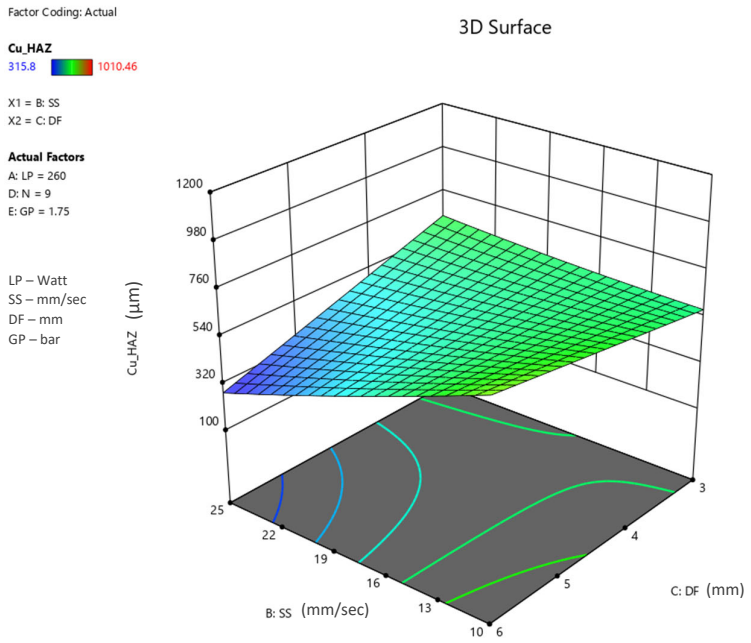

Fig. 7.24. Surface plot showing effects of SS and DF on Cu HAZ

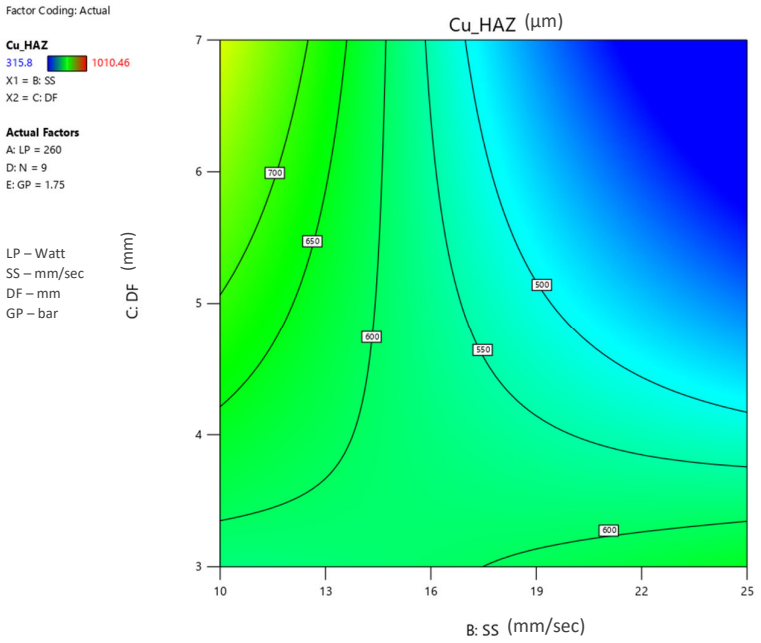

Fig. 7.25. Contour plot showing effects of SS and DF on Cu HAZ

Surface plot Fig. 7.24 & Contour plot Fig. 7.25 shows variation of heat affected zone with scanning speed and defocus. A smaller HAZ will come from a rapid scanning speed. This is because the metal is heated for a shorter duration of time, allowing it to cool faster. At low defocus region intensity of laser is high. So, speed has very minimal effect on HAZ. For the same reason of low intensity of laser HAZ decreases with increase of DF for a range of SS.

7.3.2.4. Response surface plot and contour plot for the effect of Scanning Speed (SS) and Gas Pressure (GP) on Copper Heat affected zone (Cu HAZ)

Effects of the two process parameters named SS and GP on weld characteristic i.e., Copper heat affected zone is thoroughly investigated in this section when, other parameters are hold at their respective centres.

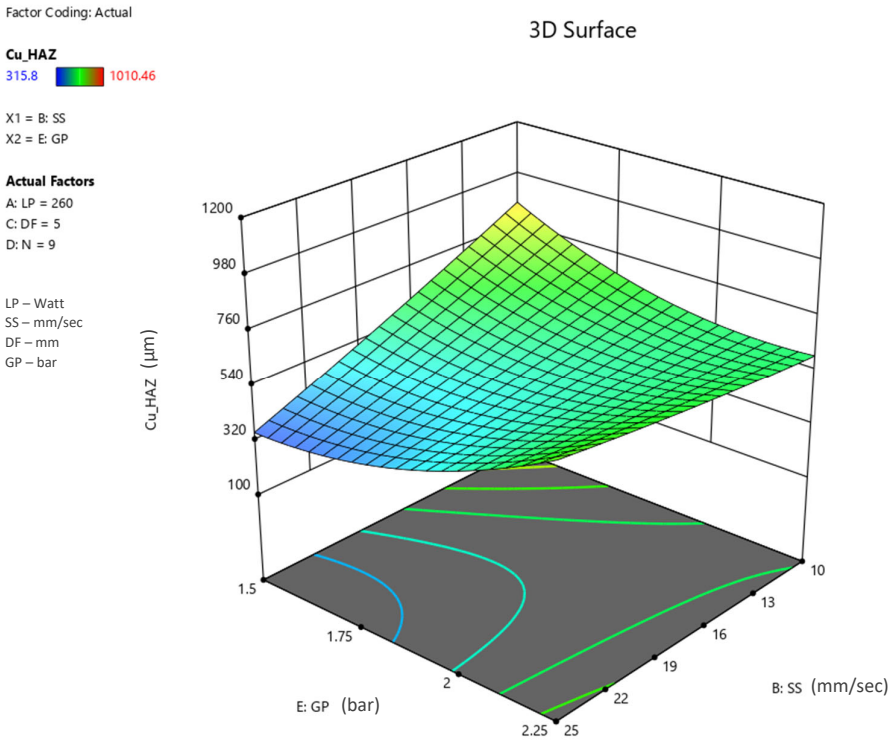

Fig. 7.26. Surface plot showing effects of SS and GP on Cu HAZ

Surface plot Fig. 7.26 & Contour plot Fig. 7.27 shows variation of heat affected zone with scanning speed and gas pressure. Faster welding will result in a smaller HAZ. This is due to the metal being heated for a shorter amount of time, which allows it to cool more quickly. At high gas pressure region, helps in dissipating the heat generated during welding and can enhance the convective heat transfer, leading to faster cooling. This can result in a narrower

HAZ with a smaller grain size. As gas pressure decreases from 2.25 bar to 1.25 bar, HAZ also increases drastically to maximum value when the speed is on the lower side. At high-speed range (20 to 25 mm/sec) where the influence pf speed is negligible, the higher the pressure, the more gas molecules there are to absorb heat. Also, at the higher the pressure, the more turbulent the gas flow, which can help to mix the shielding gas with the surrounding air. This can help to prevent oxidation of the metal, but it can also transfer more heat to the surrounding metal which increases HAZ.

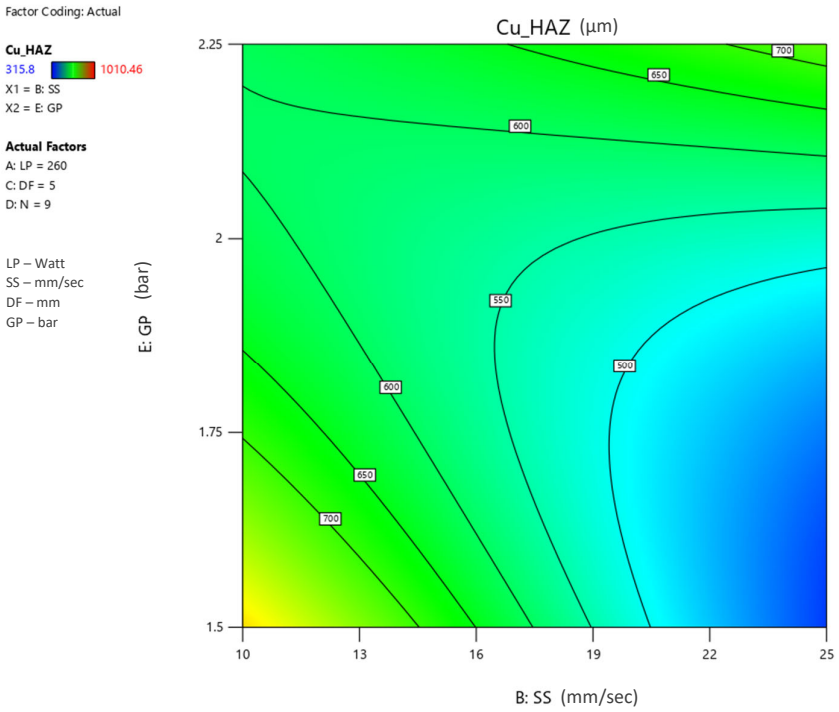

Fig. 7.27. Contour plot showing effects of SS and GP on Cu HAZ

7.3.2.5. Response surface plot and contour plot for the effect of Defocus distance (DF) and Number of passes (N) on Copper Heat affected zone (Cu HAZ)

Effects of the two process parameters named DF and N on weld characteristic i.e., Copper heat affected zone is thoroughly investigated in this section when, other parameters are hold at their respective centres.

Surface plot Fig. 7.28 & Contour plot Fig. 7.29 shows variation of heat affected zone with defocus distance and number of passes. At a range of 3 to 4 mm defocus, laser intensity is high. When the number of passes is increased from 5 to 13, penetration increases but HAZ gets narrower. Within the range of 5 to 7 mm defocus, laser intensity is less but spot diameter gets

bigger. In this case as number of passes increases, penetration gets shallow but forms a wider HAZ.

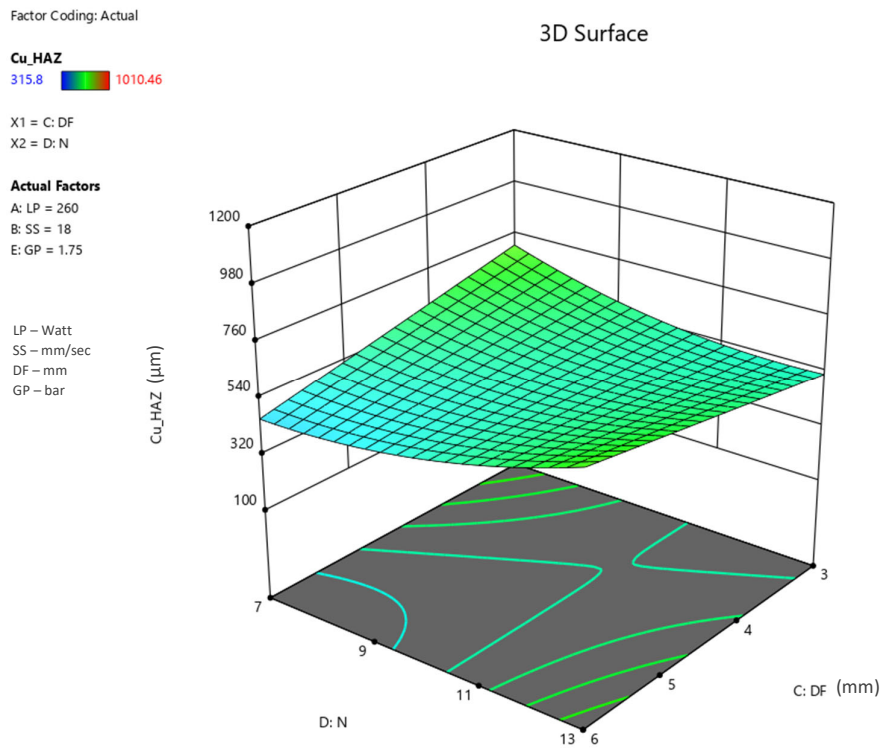

Fig. 7.28. Surface plot showing effects of DF and N on Cu HAZ

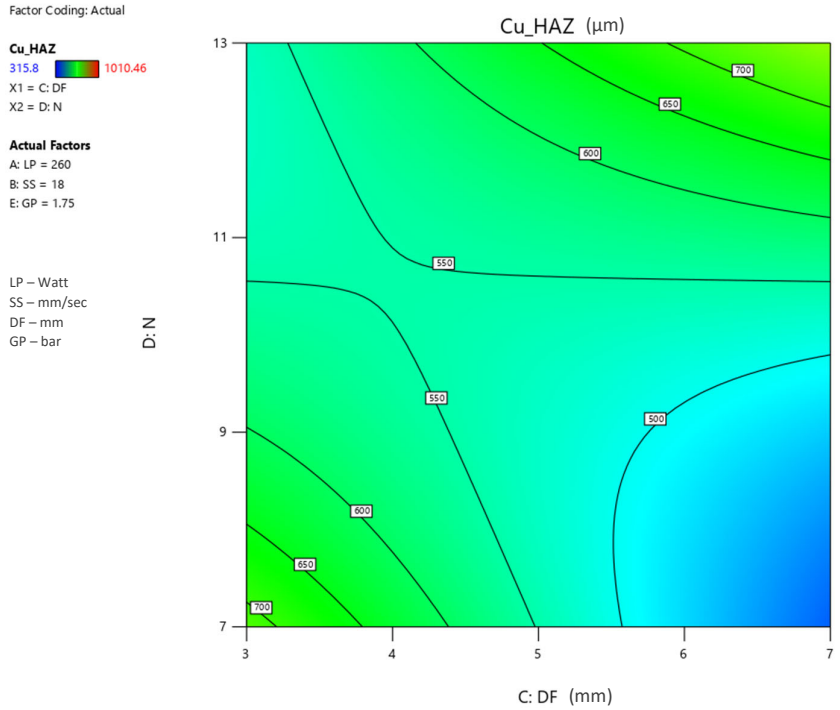

Fig. 7.29. Contour plot showing effects of DF and N on Cu HAZ

7.3.2.6. Response surface plot and contour plot for the effect of Defocus distance (DF) and Gas pressure (GP) on Copper Heat affected zone (Cu HAZ)

Effects of the two process parameters named DF and GP on weld characteristic i.e., Copper heat affected zone is thoroughly investigated in this section when, other parameters are hold at their respective centres.

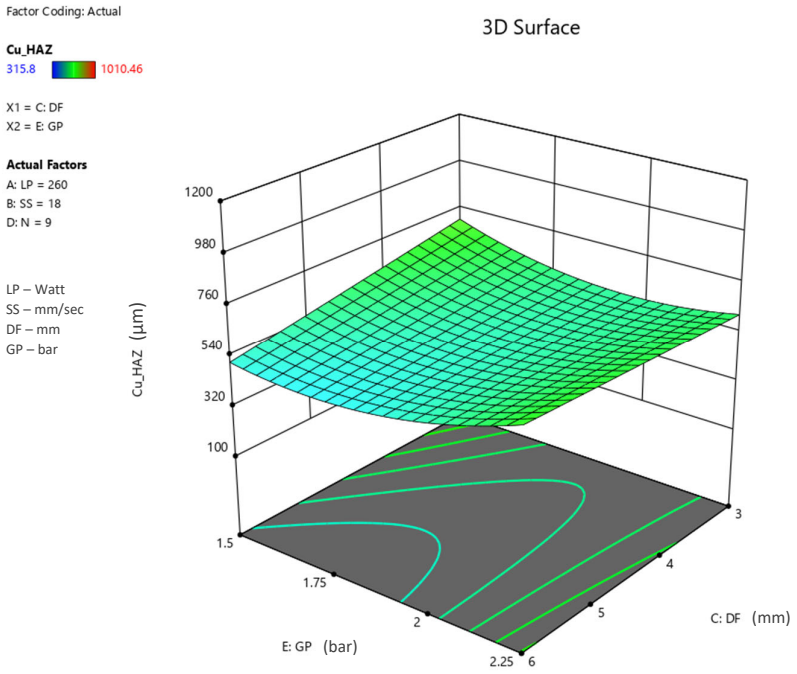

Fig. 7.30. Surface plot showing effects of DF and GP on Cu HAZ

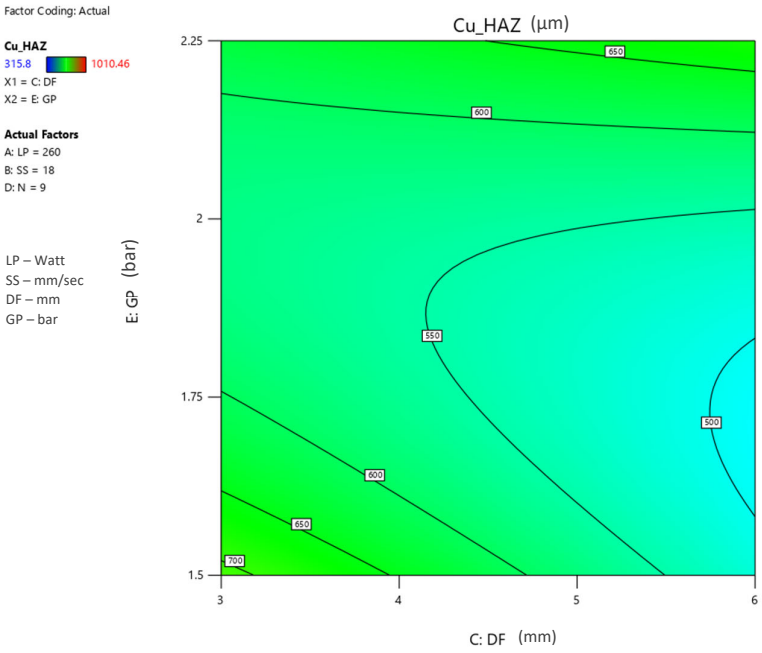

Fig. 7.31. Contour plot showing effects of DF and GP on Cu HAZ

Surface plot Fig. 7.30 & Contour plot Fig. 7.31 shows variation of heat affected zone with defocus distance and gas pressure. Laser intensity decreases drastically with increase in defocus. Even though laser spot diameter gets bigger with increasing defocus, if other parameters does not aid the power intensity HAZ always decrease. With increasing gas pressure HAZ first decreases due to chilling effect. But after a certain GP (1.85 – 1.9 bar) it starts increasing due to turbulence effect at high pressure. The more turbulent the gas flow, the better chance there is for the shielding gas and ambient air to mix. The metal may not oxidise as much as a result, but more heat may be transferred to the surrounding metal.

7.3.2.7. Response surface plot and contour plot for the effect of Number of passes (N) and Gas pressure (GP) on Copper Heat affected zone (Cu HAZ)

Effects of the two process parameters named N and GP on weld characteristic i.e., Copper heat affected zone is thoroughly investigated in this section when, other parameters are hold at their respective centres.

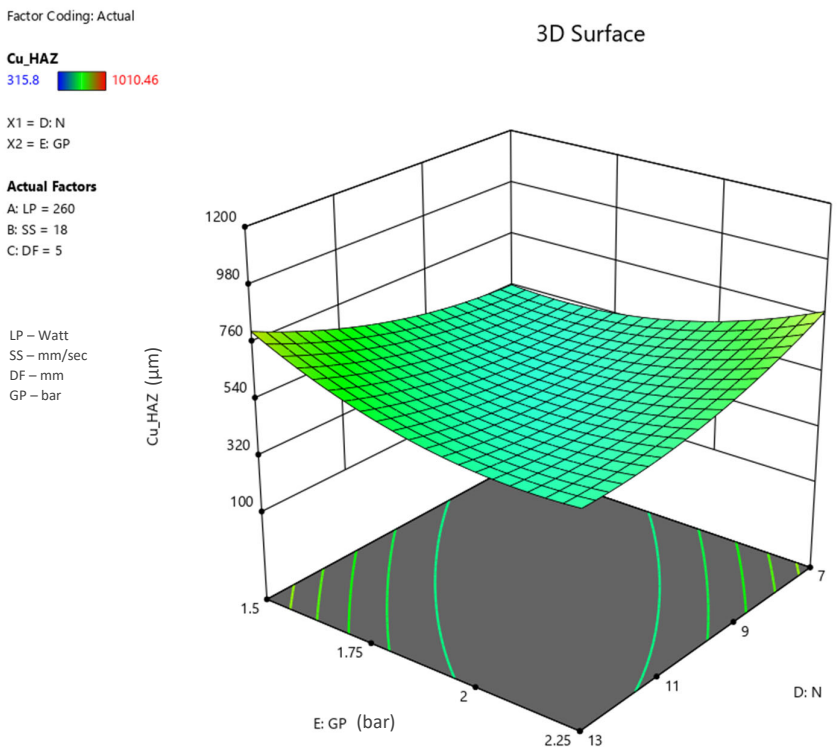

Fig. 7.32. Surface plot showing effects of N and GP on Cu HAZ

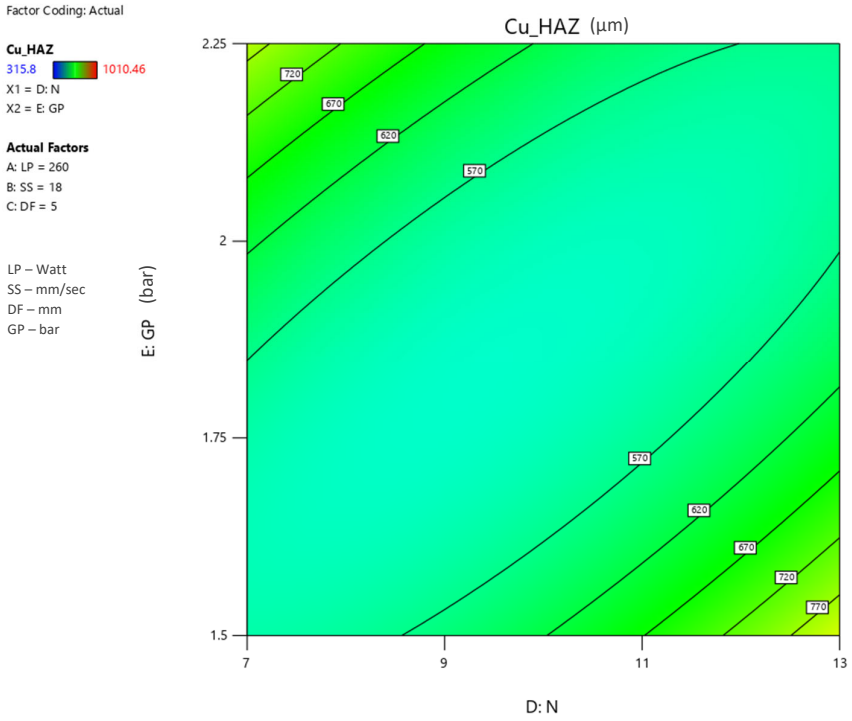

Fig. 7.33. Contour plot showing effects of N and GP on Cu HAZ

Surface plot Fig. 7.32 & Contour plot Fig. 7.33 shows variation of heat affected zone with number of passes and gas pressure. At lower gas pressure region (1.25 – 1.75 bar) the chilling effect of gas is predominant. HAZ increases with the number of passes as heat input to base metal increases with each pass. HAZ starts to increase again after GP of 1.75 bar due to the turbulence at weld pool. The chance of a mixing between the shielding gas and surrounding air increases with the intensity of gas flow turbulence. As a result, the metal may not oxidise as much, but more heat may be passed to the metal around it. At low GP and low N, HAZ is minimum as cooling rate is high. Also, at high GP and high N, HAZ is minimum as all the heat energy goes into melting the base metal and achieve greater penetration.

A single factor interaction of all parameters is also shown in Fig. 7.34.

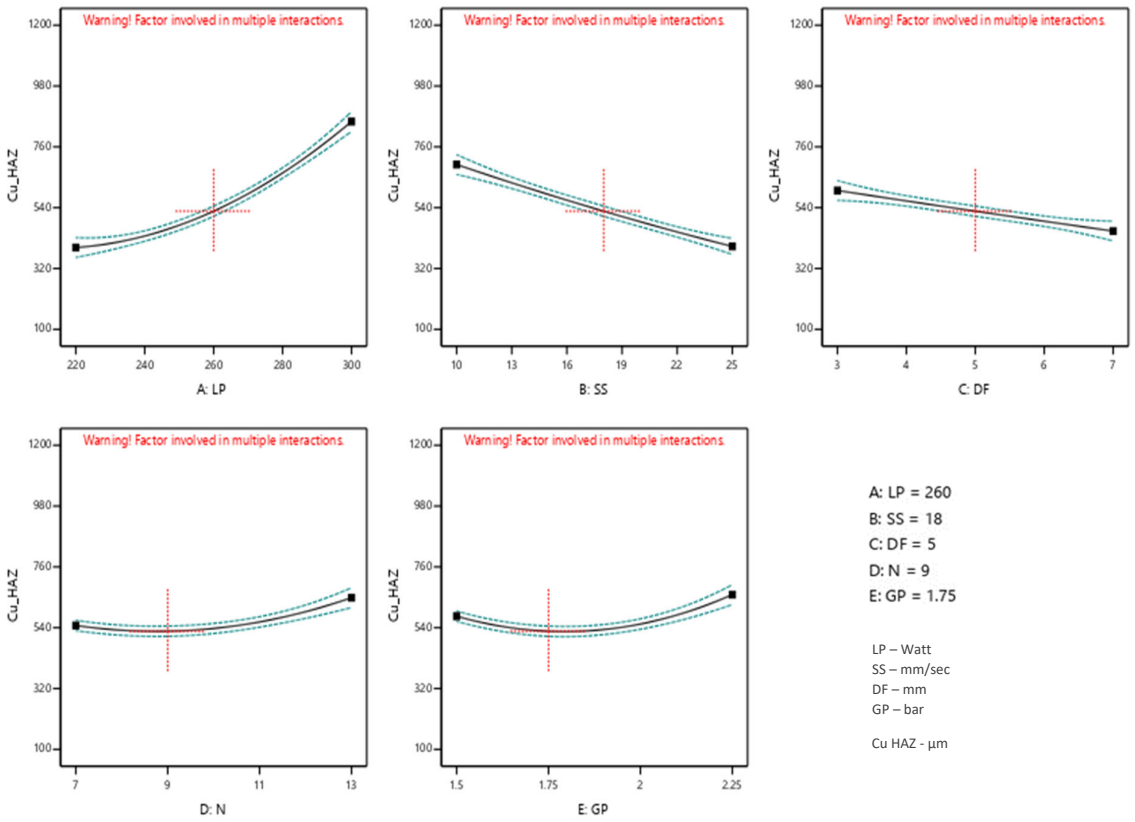

Fig. 7.34. Single factor interaction of all parameters with Cu HAZ

7.3.3. Effects of Process parameters on Heat affected zone of SS 304 (SS HAZ)

7.3.3.1. Response surface plot and contour plot for the effect of Laser Power (LP) and Defocus distance (DF) on SS 304 Heat affected zone (SS HAZ)

Effects of the two process parameters named LP and DF on weld characteristic i.e., SS 304 heat affected zone is thoroughly investigated in this section when, other parameters are hold at their respective centres.

Surface plot Fig. 7.35 & Contour plot Fig. 7.36 shows that heat affected zone increases with increasing laser power and decreases with increasing defocus. The HAZ expands as the laser power rises because the material absorbs more heat. This is due to the fact that the temperature of the material increases with increasing laser power. As laser intensity gets extremely low at low power and high defocus, HAZ drops with increasing defocus.

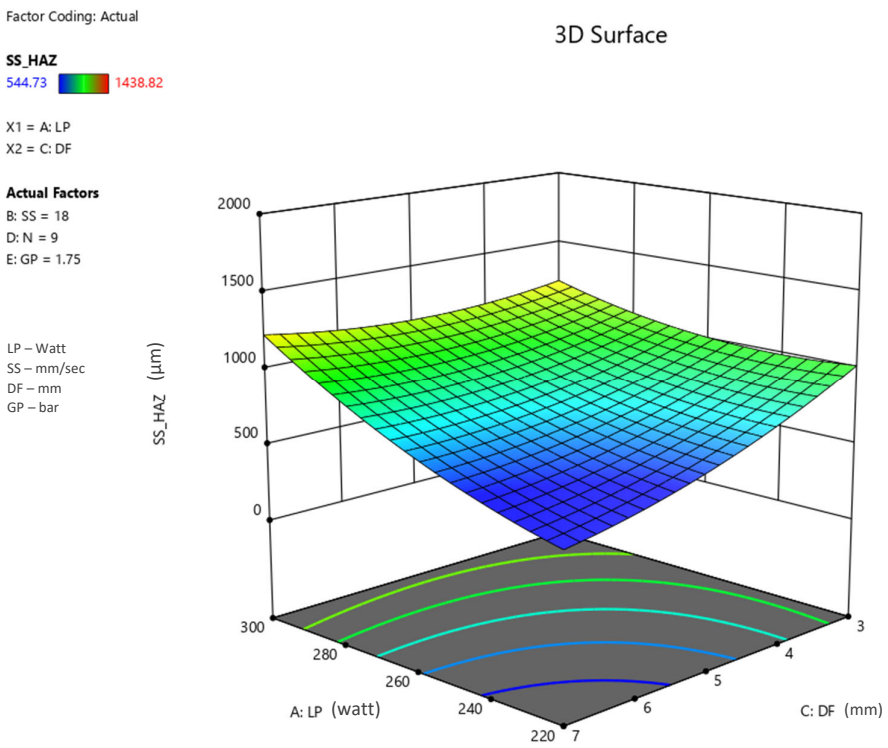

Fig. 7.35. Surface plot showing effects of LP and DF on SS HAZ

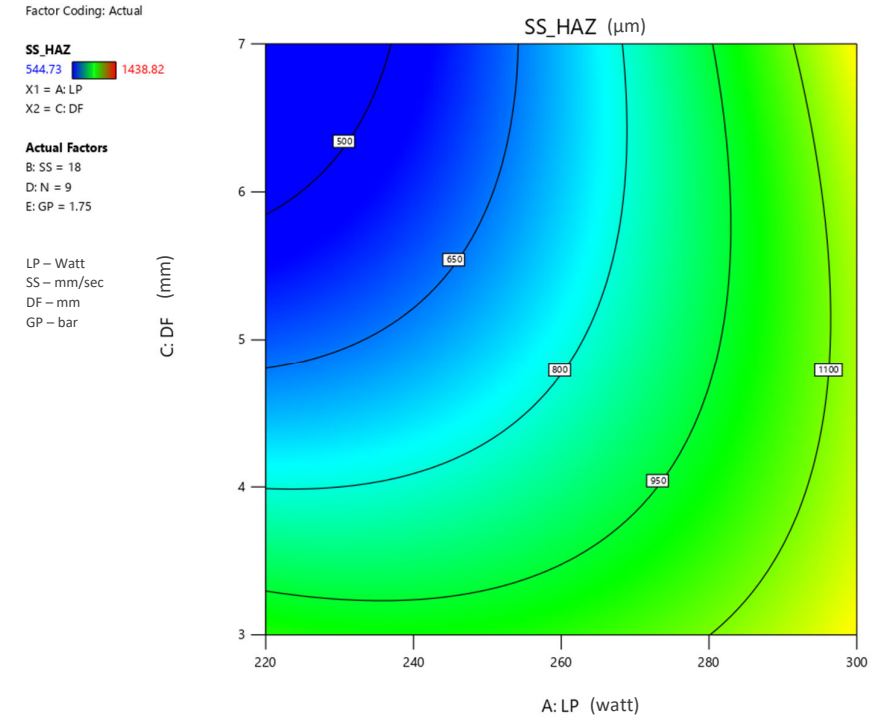

Fig. 7.36. Contour plot showing effects of LP and DF on SS HAZ

7.3.3.2. Response surface plot and contour plot for the effect of Laser Power (LP) and Gas Pressure (GP) on SS 304 Heat affected zone (SS HAZ)

Effects of the two process parameters named LP and GP on weld characteristic i.e., SS 304 heat affected zone is thoroughly investigated in this section when, other parameters are hold at their respective centres.

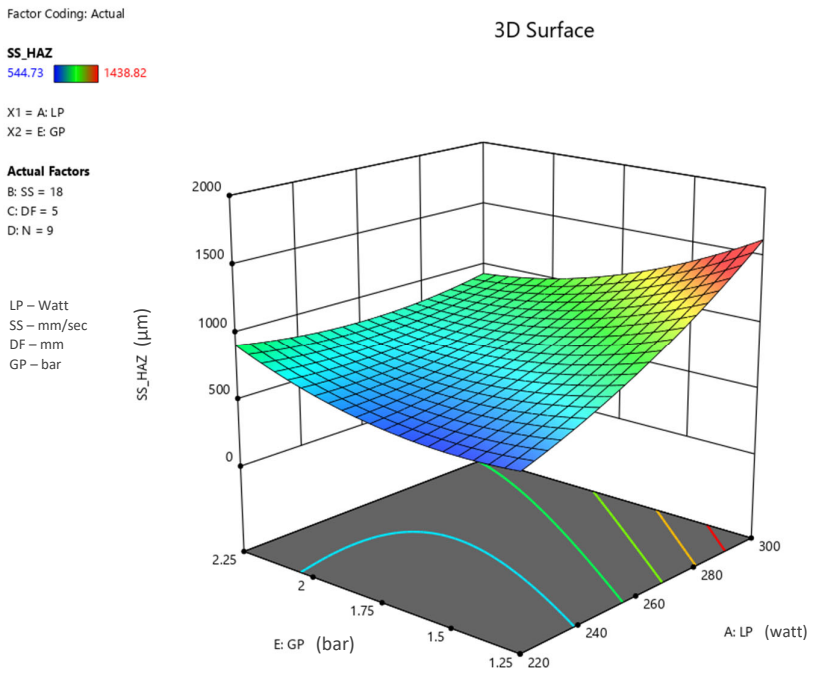

Fig. 7.37. Surface plot showing effects of LP and GP on SS HAZ

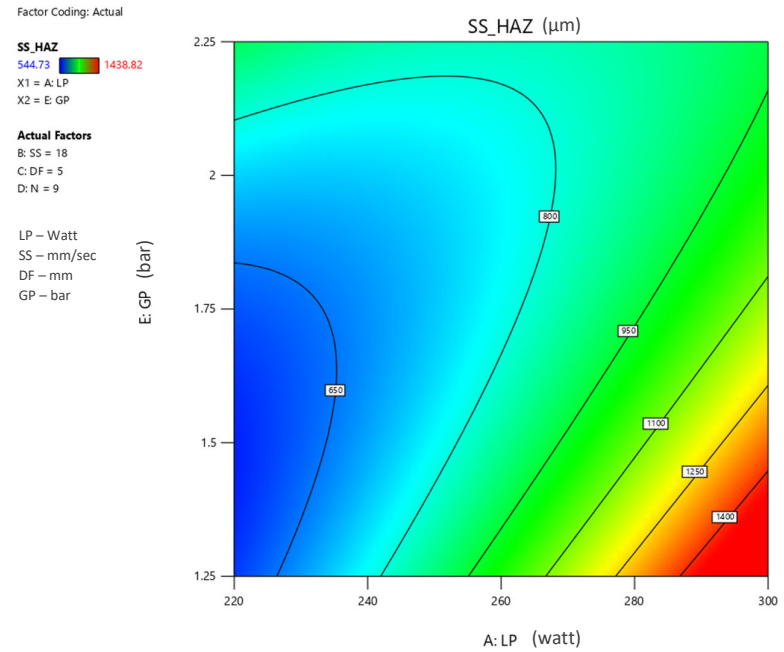

Fig. 7.38. Contour plot showing effects of LP and DF on SS HAZ

Surface plot Fig. 7.37 & Contour plot Fig. 7.38 shows that heat affected zone increases with increasing laser power and decreases with increasing defocus. As the laser power increases, the material absorbs more heat, causing the HAZ to grow. This occurs as a result of the material's temperature rising with increased laser power. In the low power zone (220–240W), the number of gas molecules available to absorb heat increases with increasing pressure. Additionally, when pressure increases, the gas flow becomes more turbulent, which might aid in blending the shielding gas with the air around it. The metal may not oxidise as much as a result, but more heat may be transferred to the surrounding metal. GP can only affect a quicker cooling rate in the high-power zone (260-300W). A higher GP might result in faster cooling. So, when LP is 300W, HAZ is minimal at 2.25 bar GP.

7.3.3.3. Response surface plot and contour plot for the effect of Scanning Speed (SS) and Defocus distance (DF) on SS 304 Heat affected zone (SS HAZ)

Effects of the two process parameters named SS and DF on weld characteristic i.e., SS 304 heat affected zone is thoroughly investigated in this section when, other parameters are hold at their respective centres.

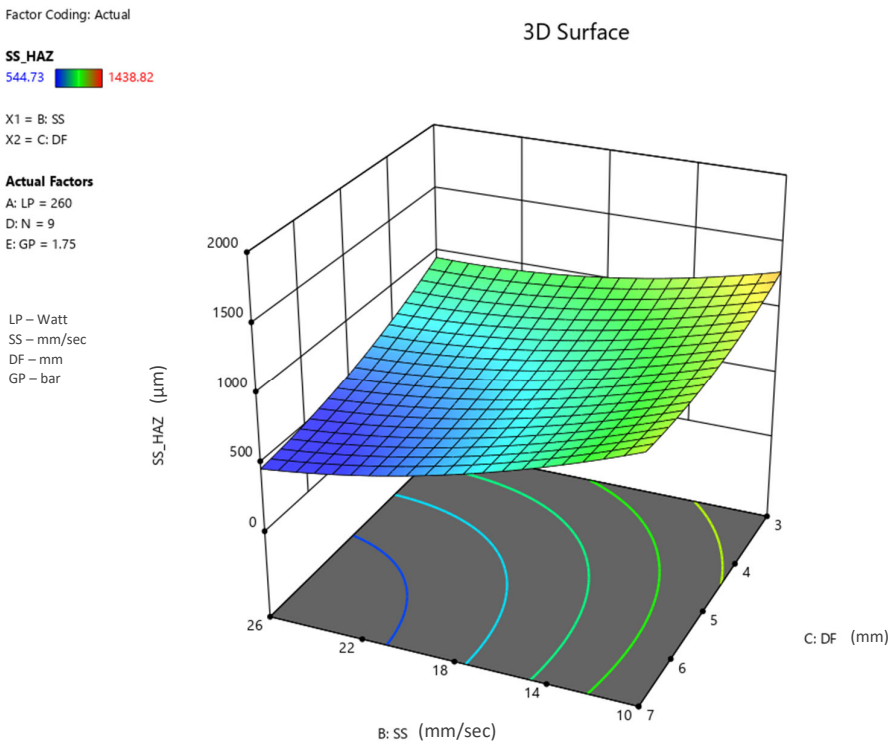

Fig. 7.39. Surface plot showing effects of SS and DF on SS HAZ

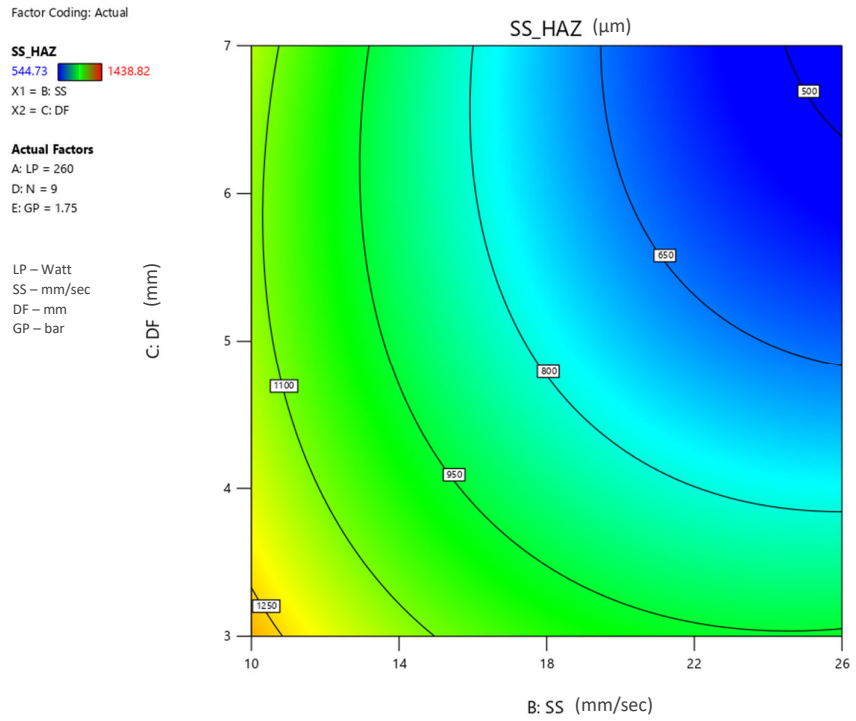

Fig. 7.40. Contour plot showing effects of SS and DF on SS HAZ

Surface plot Fig. 7.39 & Contour plot Fig. 7.40 shows variation of heat affected zone with scanning speed and defocus. Fast scanning will result in a smaller HAZ. This is due to the metal being heated for a shorter period of time, which allows it to cool more quickly. The laser has a high intensity in the low defocus zone. Speed therefore minimally affects HAZ. For the same reason that HAZ drops with increasing DF for a range of SS.

7.3.3.4. Response surface plot and contour plot for the effect of Scanning Speed (SS) and Gas Pressure (GP) on SS 304 Heat affected zone (SS HAZ)

Effects of the two process parameters named SS and GP on weld characteristic i.e., SS 304 heat affected zone is thoroughly investigated in this section when, other parameters are hold at their respective centres.

Surface plot Fig. 7.41 & Contour plot Fig. 7.42 shows variation of heat affected zone with scanning speed and gas pressure. Faster welding will result in a smaller HAZ. This is due to the metal being heated for a shorter amount of time, which allows it to cool more quickly. A

higher GP might result in faster cooling, as GP only has Chilling effect at lower welding speeds. So, when SS is in the low to mid-range (10 to 20 mm/sec), HAZ decreases with increase in GP.

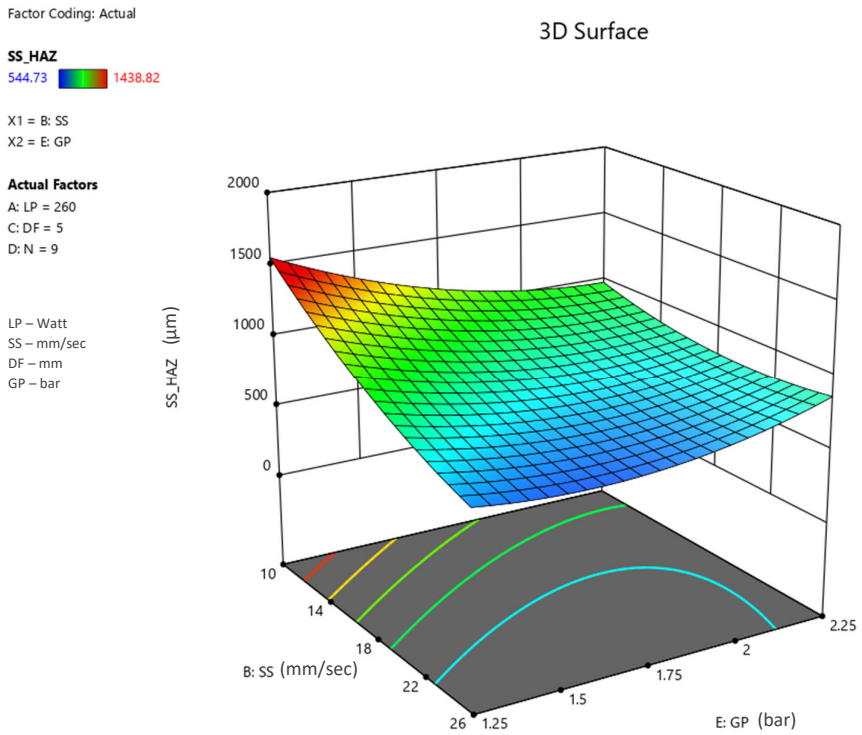

Fig. 7.41. Surface plot showing effects of SS and GP on SS HAZ

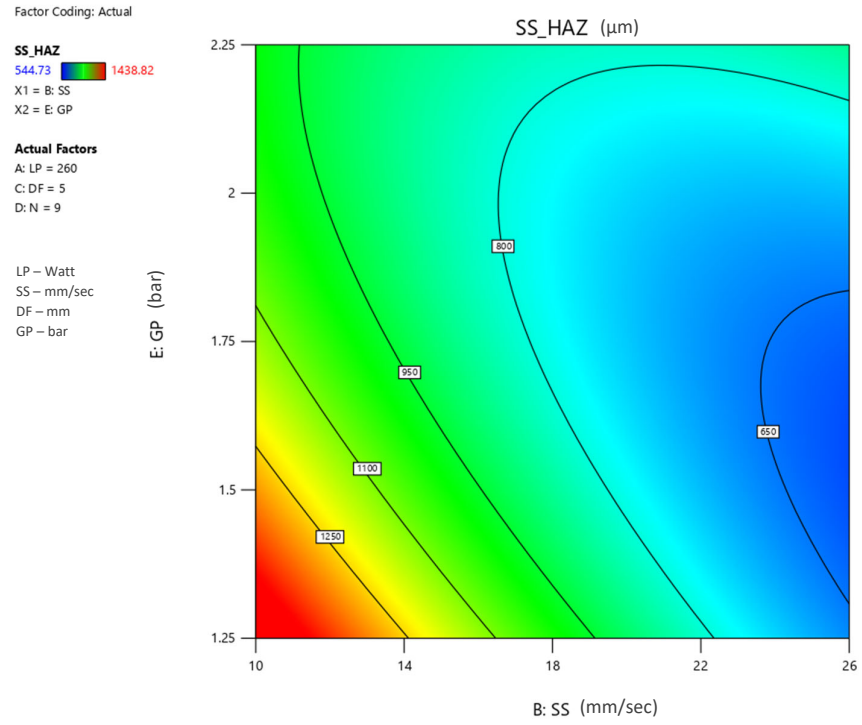

Fig. 7.42. Contour plot showing effects of SS and GP on SS HAZ

7.3.3.5. Response surface plot and contour plot for the effect of Defocus distance (DF) and Number of passes (N) on SS 304 Heat affected zone (SS HAZ)

Effects of the two process parameters named DF and N on weld characteristic i.e., SS 304 heat affected zone is thoroughly investigated in this section when, other parameters are hold at their respective centres.

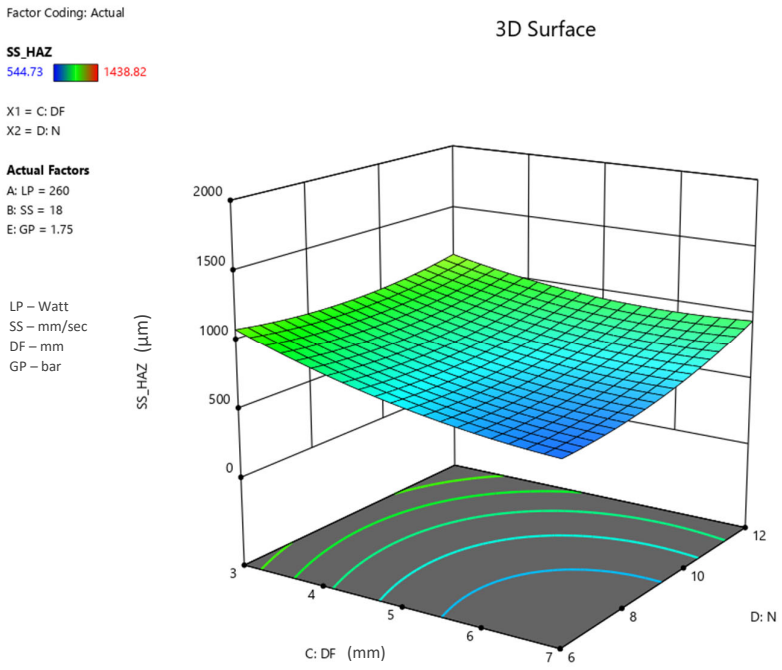

Fig. 7.43. Surface plot showing effects of DF and N on SS HAZ

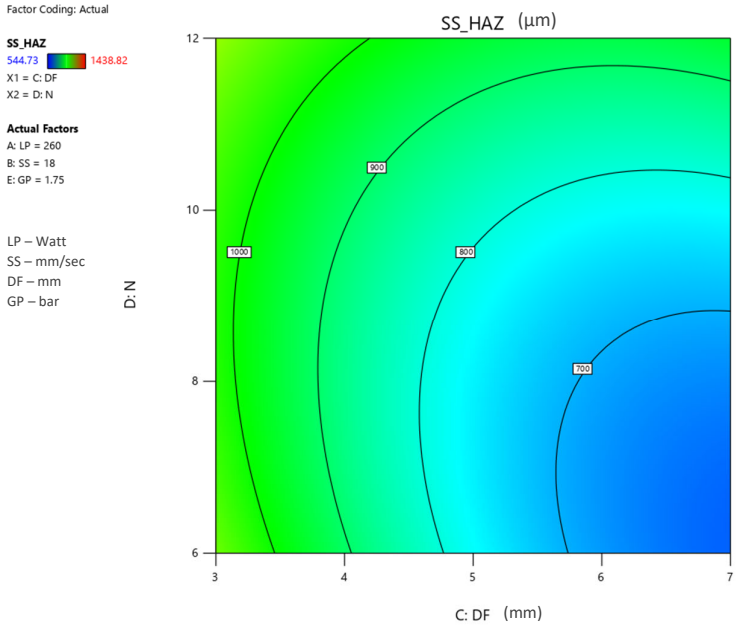

Fig. 7.44. Contour plot showing effects of DF and N on SS HAZ

Surface plot Fig. 7.43 & Contour plot Fig. 7.44 shows variation of heat affected zone with defocus distance and number of passes. Laser intensity is strong at a defocus distance of 3 to 4 mm. The HAZ grows narrower yet penetration rises as the number of passes rises from 5 to 13. The laser power is lower but the spot width increases in the 5 to 7 mm defocus range. In this instance, penetration becomes shallow as the number of passes rises yet a larger HAZ is formed. Defocus causes the laser's intensity to decrease, which causes a narrow HAZ.

7.3.3.6. Response surface plot and contour plot for the effect of Defocus distance (DF) and Gas pressure (GP) on SS 304 Heat affected zone (SS HAZ)

Effects of the two process parameters named DF and GP on weld characteristic i.e., Copper heat affected zone is thoroughly investigated in this section when, other parameters are hold at their respective centres.

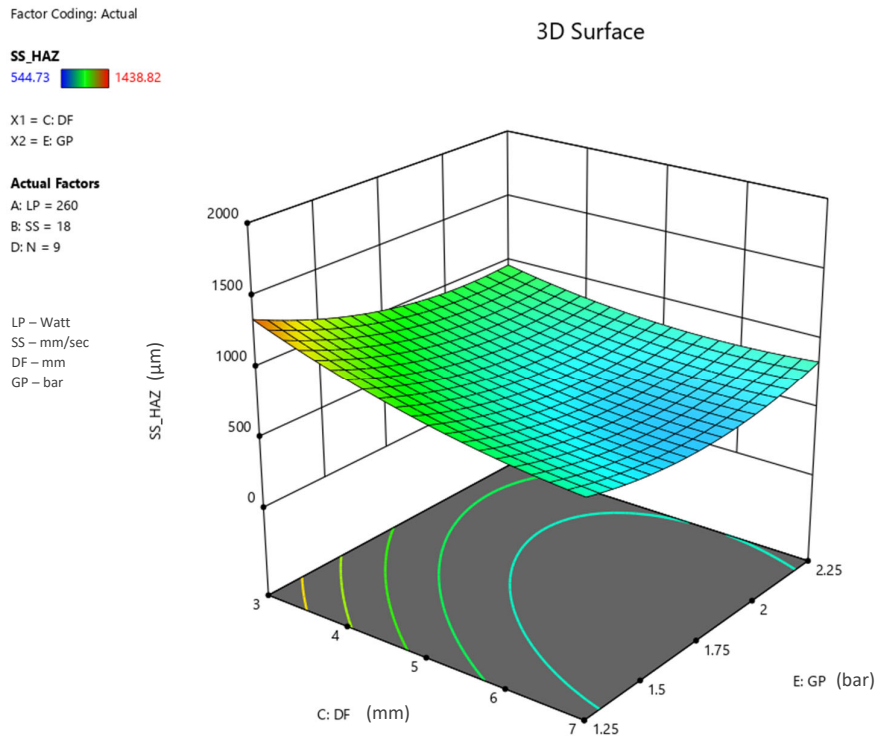

Fig. 7.45. Surface plot showing effects of DF and GP on SS HAZ

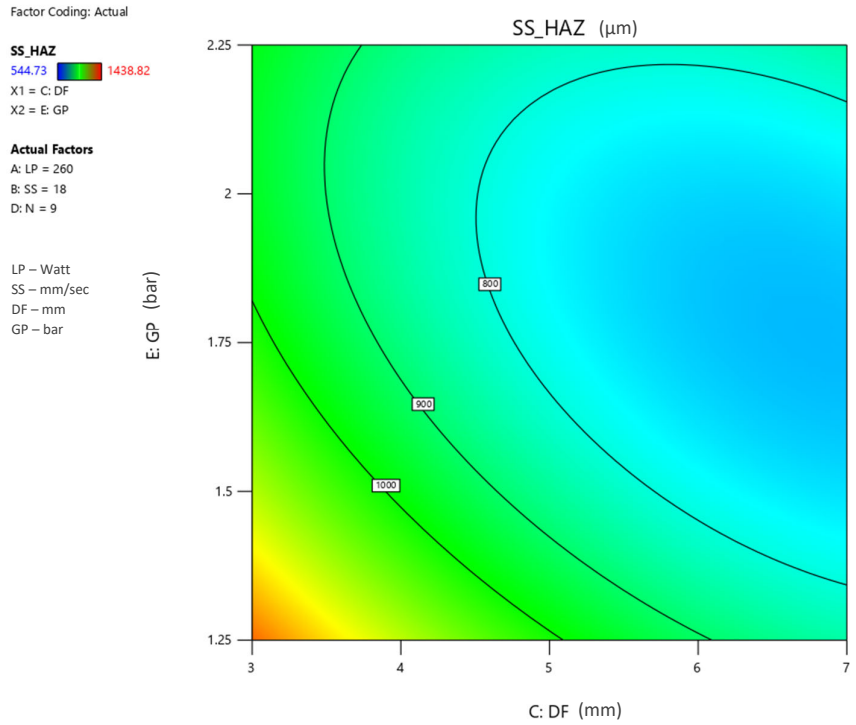

Fig. 7.46. Contour plot showing effects of DF and GP on SS HAZ

Surface plot Fig. 7.45 & Contour plot Fig. 7.46 shows variation of heat affected zone with defocus distance and gas pressure. As defocus increases, laser intensity dramatically drops. Even if the laser spot diameter grows as the defocus distance increases, the HAZ always decreases if other factors are not helping. Faster cooling is provided by high GP. After receiving heat input from the laser, base metal rapidly cools, resulting in a reduced HAZ.

7.3.3.7. Response surface plot and contour plot for the effect of Number of passes (N) and Gas pressure (GP) on SS 304 Heat affected zone (SS HAZ)

Effects of the two process parameters named N and GP on weld characteristic i.e., Copper heat affected zone is thoroughly investigated in this section when, other parameters are hold at their respective centres.

Surface plot Fig. 7.47 & Contour plot Fig. 7.48 shows variation of heat affected zone with number of passes and gas pressure. At lower gas pressure region, the cooling effect of gas is less and as gas pressure increases cooling becomes faster. As the effect of heat input becomes less due to faster cooling, HAZ decreases with increase in GP. HAZ increases with the number

of passes as heat input to base metal increases with each pass and the heat is conducted throughout the base material and affects its microstructure.

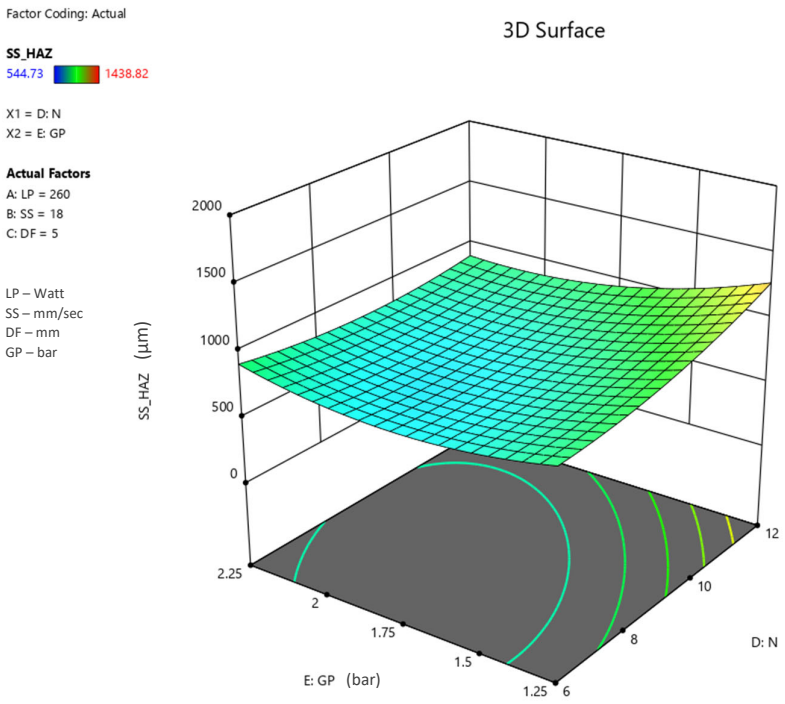

Fig. 7.47. Surface plot showing effects of N and GP on SS HAZ

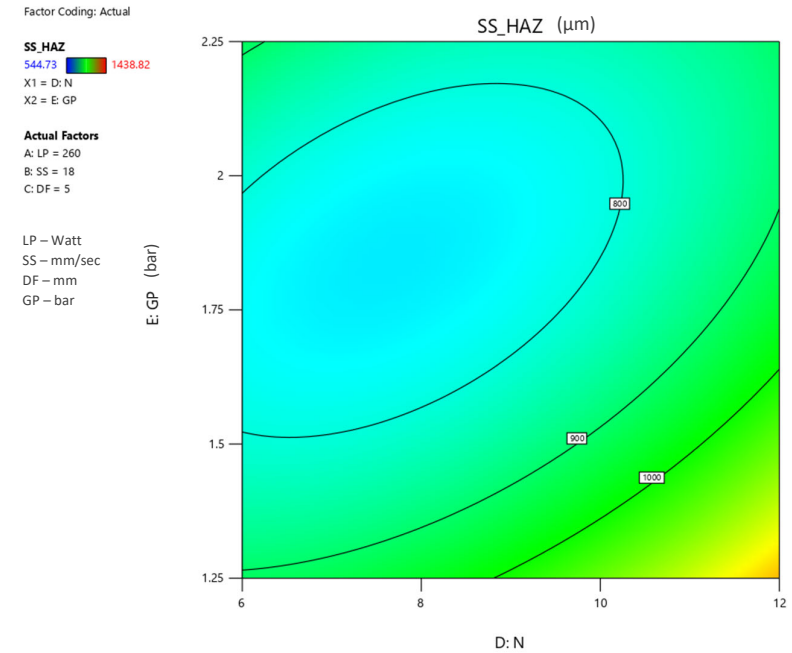

Fig. 7.48. Contour plot showing effects of N and GP on SS HAZ

A single factor interaction of all parameters is also shown in Fig. 7.49.

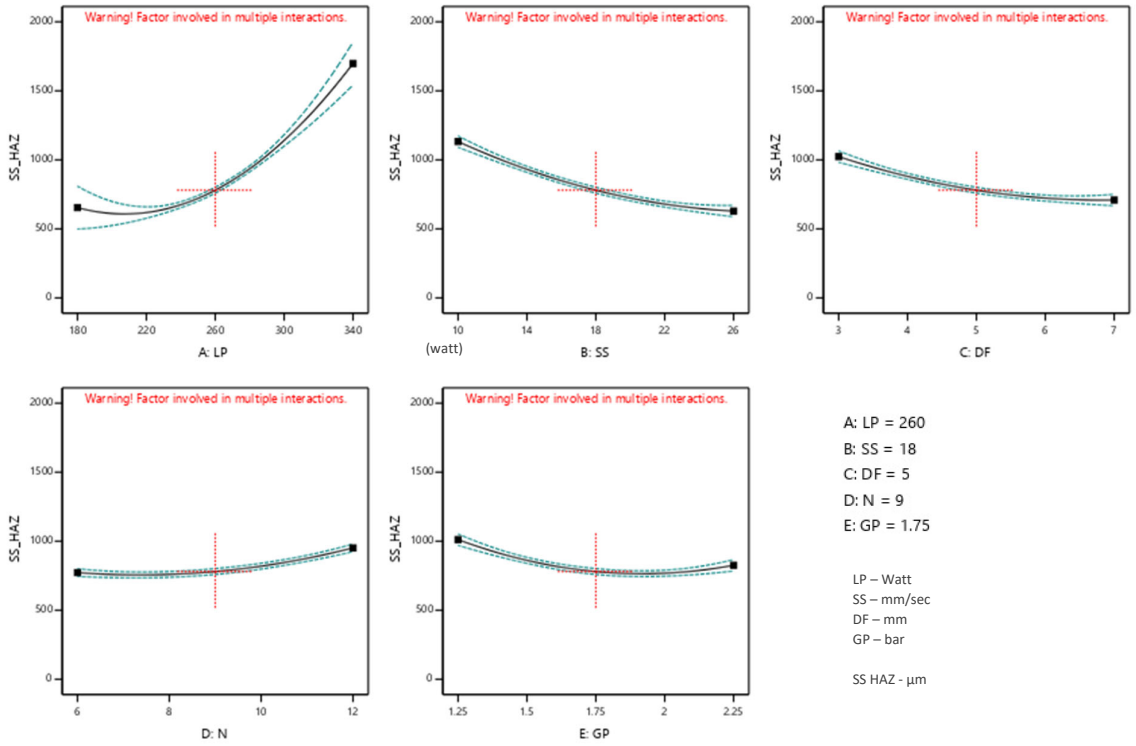

Fig. 7.49. Single factor interaction of all parameters with SS HAZ

7.4. Optimization of process parameters

For Cu & SS 304 laser welding, this part tries to simultaneously enhance the fusion zone and minimize the heat-impacted zone. In order to get the best answers, a numerical multi-response surface methodology and the necessary optimization criteria are included into an objective optimization strategy. From the experimental results and research papers it is evident that more fusion zone (seam width) leads to better tensile strength. Attaining a particular tensile strength of the welded zone is our primary criteria along with reducing the HAZ to an extent possible within the parameter ranges is our secondary criteria for optimization.

7.4.1. Desirability function-based optimization technique

The optimization module in the Design-Expert 13 seeks for a combination of factor values that simultaneously satisfy the constraints placed on each of the responses and factors. In numerical optimization, the created regression model is used to investigate the design space in search of the factor values that best satisfy any combination of one or more goals. The goals are combined into a general desirability function. A location where this desirability function value hits 1 is found by numerical optimization.

Two criteria are introduced by this numerical optimization. The first need is to accomplish the target fusion zone in an area determined by experimental findings and observing the response values and taking the mean of most practical range in which majority of the values are lying in order to obtain the necessary weld strength without putting any constraints on the process parameters or the heat affected zone. Achieving the least heat affected zone for both copper and SS 304 separately is the goal of the second criterion, which has no constraints on the process variables or the fusion zone. Achieving the desired fusion zone and reducing the heat-affected zone while retaining a low operating cost is the goal of the final criteria.

7.4.1.1. Optimization results for targeted Fusion zone (FZ)

Table 7.11 lists the restrictions that were used in the optimization results for the intended fusion zone in accordance with the mathematical model developed for the fusion zone. The solution has been optimized by giving equal weight to the lower, target, and upper boundaries of the linear desirability function. One option with a near-targeted FZ and a respectably low HAZ was selected from a series of solutions offered by Design-Expert with a desirability value of 1. The fusion zone has been found to be 494.999 μm, which is close to the intended value. Cu HAZ value is 584.207 μm and SS HAZ is 897.203 μm which are also low compared to their maximum values. After optimization, the additional process parameters, LP (268.726 ≈ 269 W), SS (19.762 mm/sec), DF (3.5 mm), N (9.491 ≈ 9) and GP (1.985 ≈ 2 bar) are adjusted to their optimal parametric settings. The anticipated setting falls within the experimental performance window that reflects the choice of parametric ranges. Fig. 7.50 and Fig. 7.51 depicts the contour plot of desirability and optimization results for targeted FZ respectively.

Table 7.11. Constraints for optimization of FZ

Name	Goal	Lower Limit	Upper Limit	Lower Weight	Upper Weight	Importance
LP (Watt)	is in range	220	300	1	1	3
SS (mm/sec)	is in range	10	26	1	1	3
DF (mm)	is in range	3	7	1	1	3
N	is in range	5	13	1	1	3
GP (bar)	is in range	1.25	2.25	1	1	3
FZ (μm)	is target = 495	490	530	1	1	3
Cu HAZ (μm)	none	550	1010.46	1	1	3
SS HAZ (μm)	none	750	1438.82	1	1	3

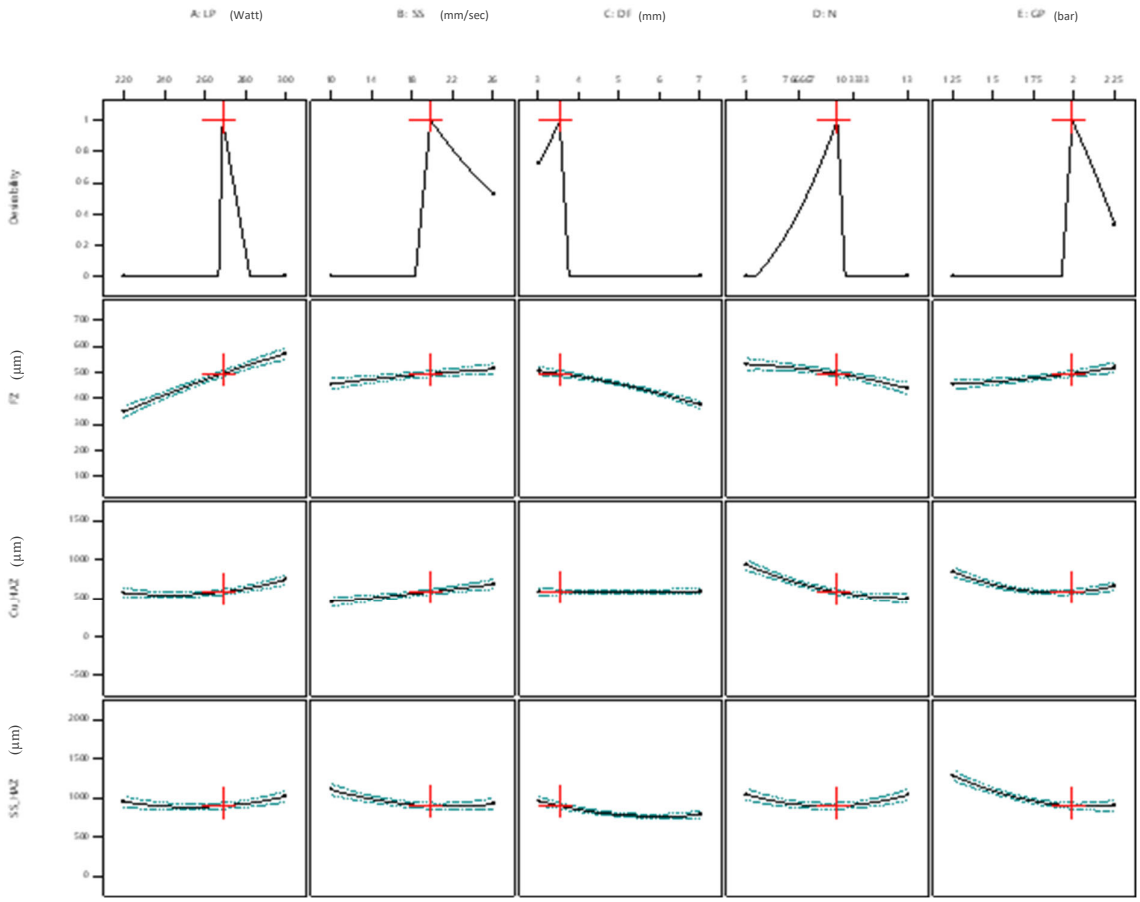

Fig. 7.50. Optimization results for targeted FZ

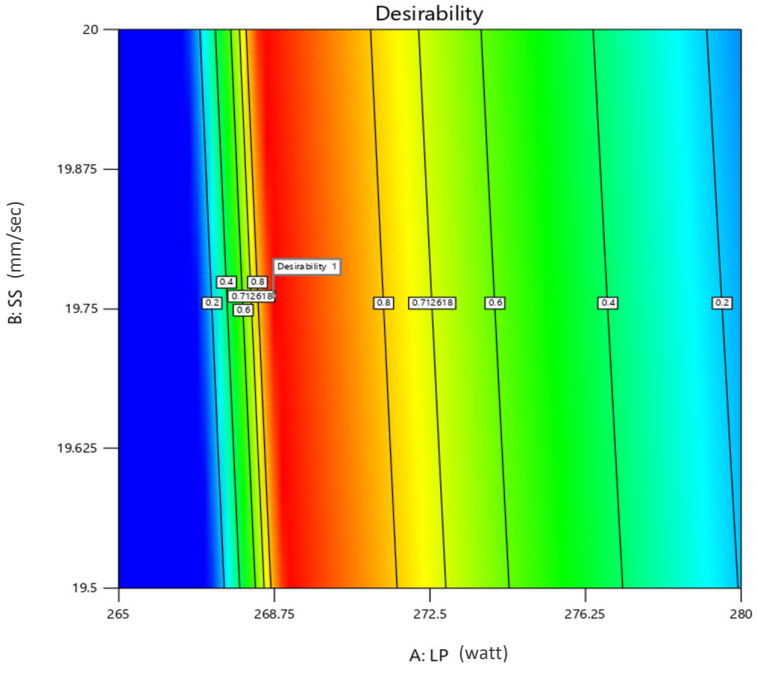

Fig. 7.51. Contour plot of desirability for LP & SS on FZ

7.4.1.2. Optimization results for minimizing Copper Heat affected zone (Cu HAZ)

According to the mathematical model created for the Cu HAZ, Table 7.12 provides the constraints that were used in the optimization outcomes for the smallest heat affected zone in a usable range. Giving the lower, target, and higher limits of the linear desirability function equal weight has optimised the answer. A solution with a desirability value of 1 was chosen from a set of options presented by Design-Expert that had a minimal HAZ and a respectably decent FZ.

The fusion zone has been found to be 449.607 µm. Cu HAZ value is 423.656 µm and SS HAZ is 967.953 µm which are also low compared to their maximum values. After optimization, the additional process parameters, LP (269.832 ≈ 270 W), SS (14.87 mm/sec), DF (3.766 mm), N (11.8 ≈ 12) and GP (2.115 ≈ 2.1 bar) are adjusted to their optimal parametric settings. The anticipated setting falls within the experimental performance window that reflects the choice of parametric ranges. The contour plots for the optimization and desirability findings for the minimum Cu HAZ are shown in Fig. 7.52 and Fig. 7.53, respectively.

Table 7.12. Constraints for optimization of Cu HAZ

Name	Goal	Lower Limit	Upper Limit	Lower Weight	Upper Weight	Importance
LP (Watt)	is in range	220	300	1	1	3
SS (mm/sec)	is in range	10	26	1	1	3
DF (mm)	is in range	3	7	1	1	3
N	is in range	5	13	1	1	3
GP (bar)	is in range	1.25	2.25	1	1	3
FZ (µm)	none	306.57	538.23	1	1	3
Cu HAZ (µm)	minimize	450	1010.46	1	1	3
SS HAZ (µm)	none	544.73	1438.82	1	1	3

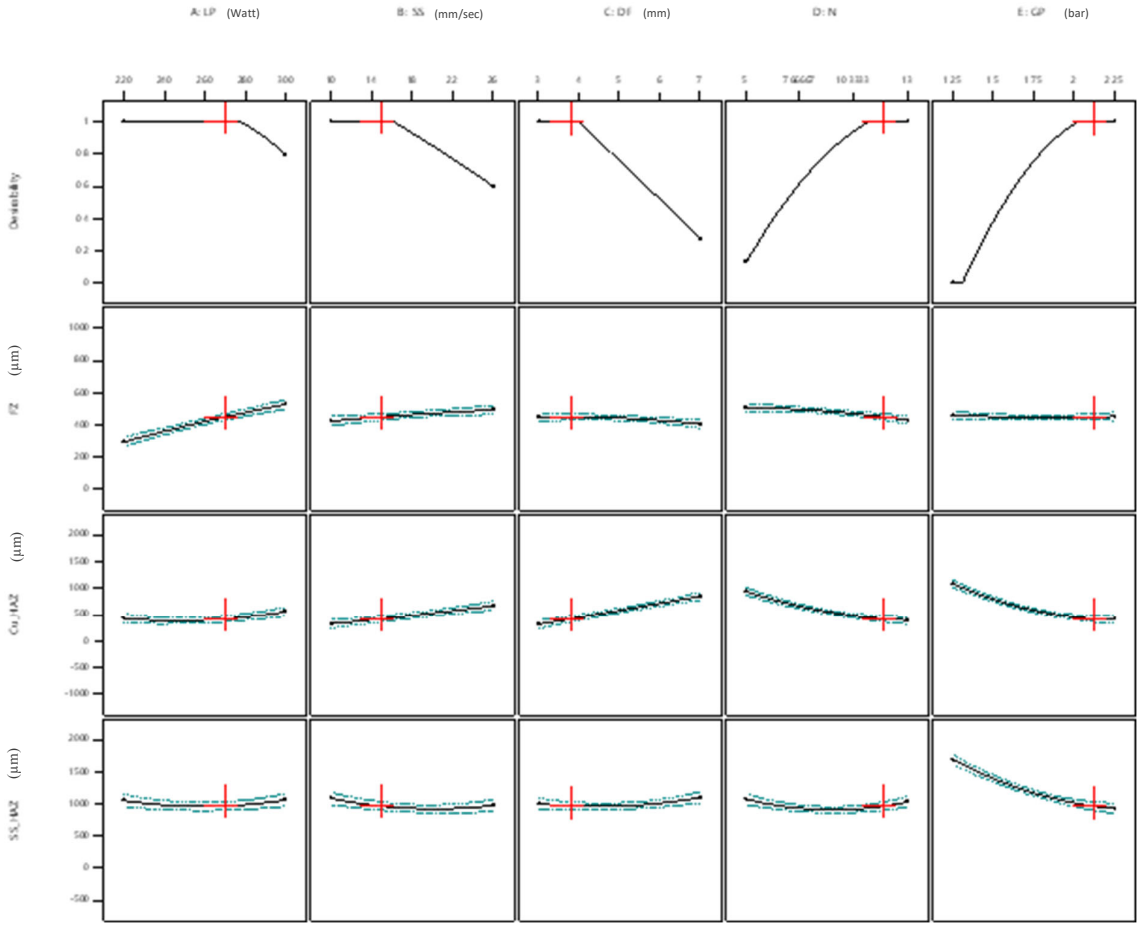

Fig. 7.52. Optimization results for minimizing Cu HAZ

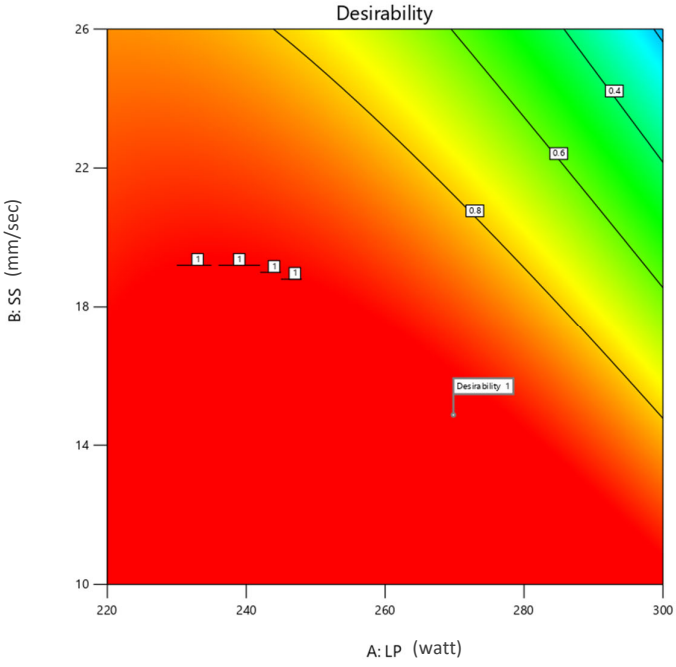

Fig. 7.53. Contour plot of desirability for LP & SS on Cu HAZ

7.4.1.3. Optimization results for minimizing SS 304 Heat affected zone (SS HAZ)

Table 7.13 shows the constraints that were applied in the optimization results for the smallest heat affected zone in a workable range based on the mathematical model produced for the SS HAZ. Giving equal weight to the lower, target, and upper limits of the linear desirability function has optimised the solution. A solution with a desirability value of one was picked from a set of possibilities suggested by Design-Expert that had a low HAZ and a reasonable FZ.

The fusion zone has been found to be 435.752 µm. Cu HAZ value is 510.646 µm and SS HAZ is 704.809 µm which are also low compared to their maximum values. After optimization, the additional process parameters, LP (261.877 ≈ 262 W), SS (23.557 mm/sec), DF (4.774 mm), N (8.736 ≈ 9) and GP (1.896 ≈ 1.9 bar) are adjusted to their optimal parametric settings. The anticipated setting falls within the experimental performance window that reflects the choice of parametric ranges. The contour plots for the optimization and desirability findings for the minimum SS HAZ are shown in Fig. 7.54 and Fig. 7.55, respectively.

Table 7.13. Constraints for optimization of SS HAZ

Name	Goal	Lower Limit	Upper Limit	Lower Weight	Upper Weight	Importance
LP (Watt)	is in range	220	300	1	1	3
SS (mm/sec)	is in range	10	26	1	1	3
DF (mm)	is in range	3	7	1	1	3
N	is in range	5	13	1	1	3
GP (bar)	is in range	1.25	2.25	1	1	3
FZ (µm)	none	306.57	538.23	1	1	3
Cu HAZ (µm)	none	315.8	1010.46	1	1	3
SS HAZ (µm)	minimize	750	1438.82	1	1	3

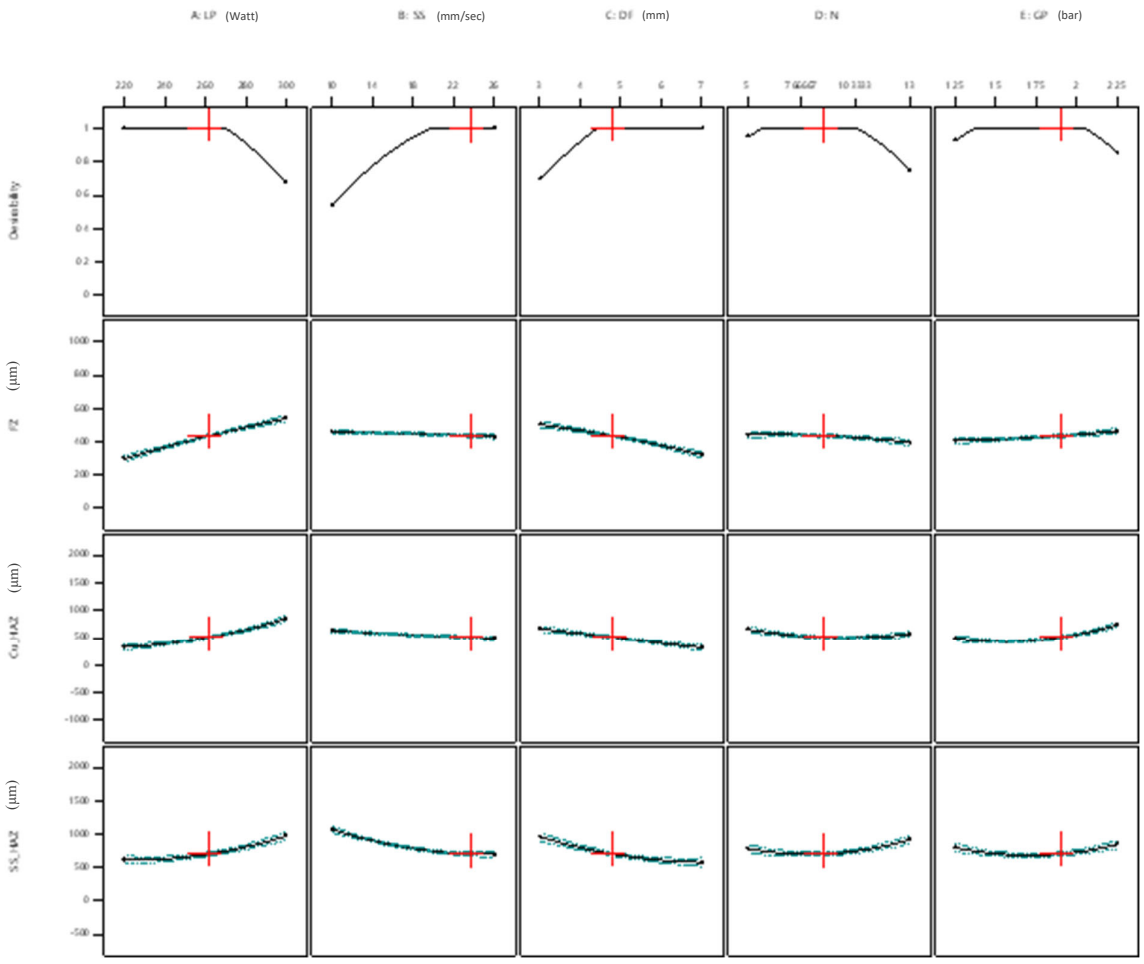

Fig. 7.54. Optimization results for minimizing SS HAZ

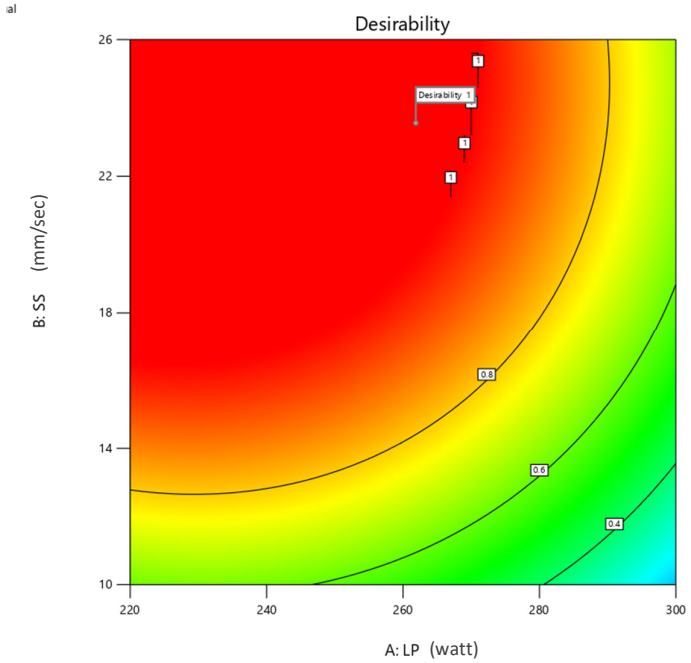

Fig. 7.55. Contour plot of desirability for LP & SS on SS HAZ

7.4.1.4. Multiple optimization results for targeted FZ and minimum Cu HAZ & SS HAZ

Table 7.14 shows the constraints that were applied in the optimization results for the smallest heat affected zone for both the material and a targeted FZ to attain desired weld strength in a workable range based on the mathematical model produced for the FZ & HAZ of Cu and SS 304. Giving equal weight to the lower, target, and upper limits of the linear desirability function has optimised the solution. A solution with a desirability value of one was picked from a set of possibilities suggested by Design-Expert that had a minimum HAZ and a near target FZ.

The fusion zone has been found to be 494.999 µm. Cu HAZ value is 690.166 µm and SS HAZ is 800.899 µm which are also low compared to their maximum values. After optimization, the additional process parameters, LP (275.01 ≈ 275 W), SS (22.626 mm/sec), DF (4.598 mm), N (7.99 ≈ 8) and GP (2.001 ≈ 2 bar) are adjusted to their optimal parametric settings. The anticipated setting falls within the experimental performance window that reflects the choice of parametric ranges. The contour plots for the optimization and desirability findings for the minimum SS HAZ are shown in Fig. 7.56 and Fig. 7.57, respectively.

Table 7.14. Constraints for optimization of targeted FZ and minimum Cu HAZ & SS HAZ

Name	Goal	Lower Limit	Upper Limit	Lower Weight	Upper Weight	Importance
LP (Watt)	is in range	220	300	1	1	3
SS (mm/sec)	is in range	10	26	1	1	3
DF (mm)	is in range	3	7	1	1	3
N	is in range	5	13	1	1	3
GP (bar)	is in range	1.25	2.25	1	1	3
FZ (µm)	is target = 495	490	530	1	1	3
Cu HAZ (µm)	minimize	710	1010.46	1	1	3
SS HAZ (µm)	minimize	800	1438.82	1	1	3

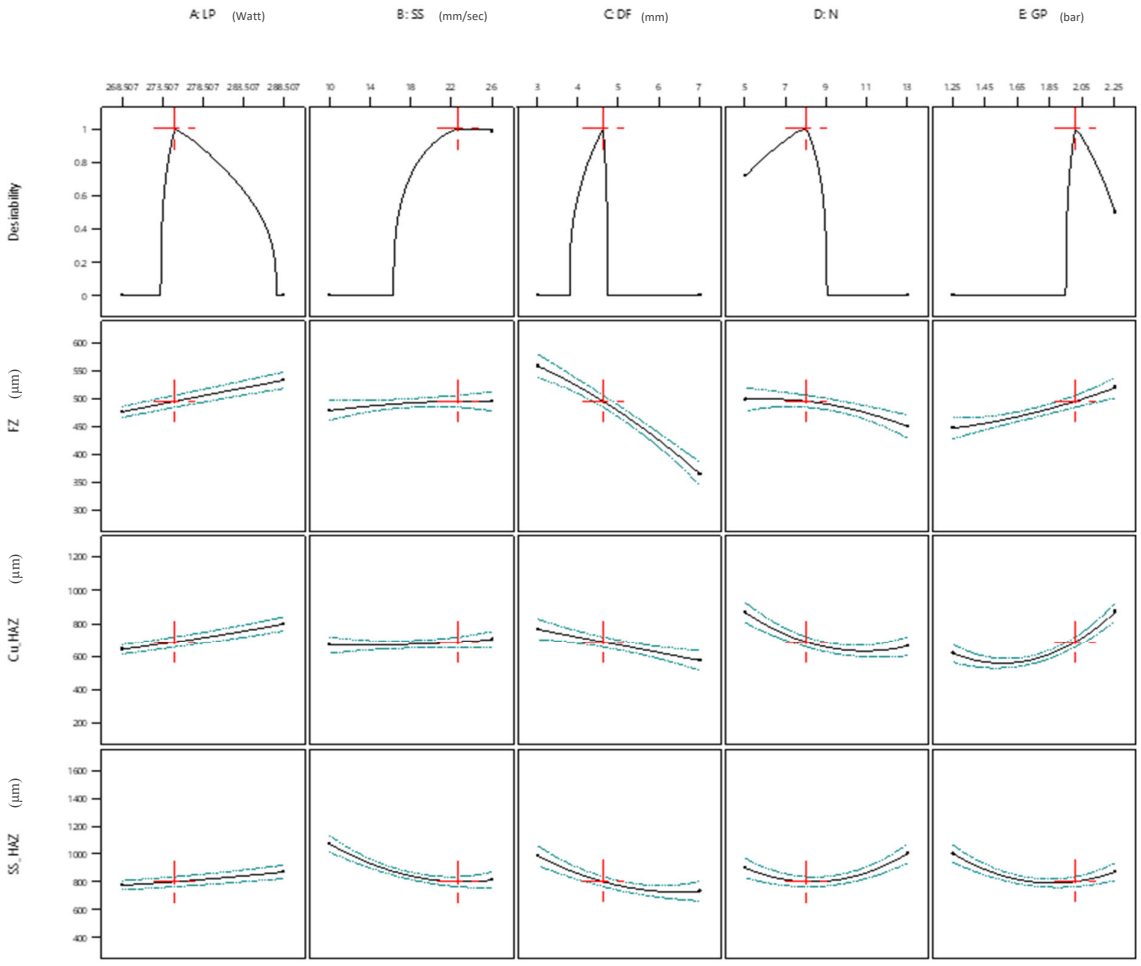

Fig. 7.56. Optimization results for targeted FZ and minimum Cu HAZ & SS HAZ

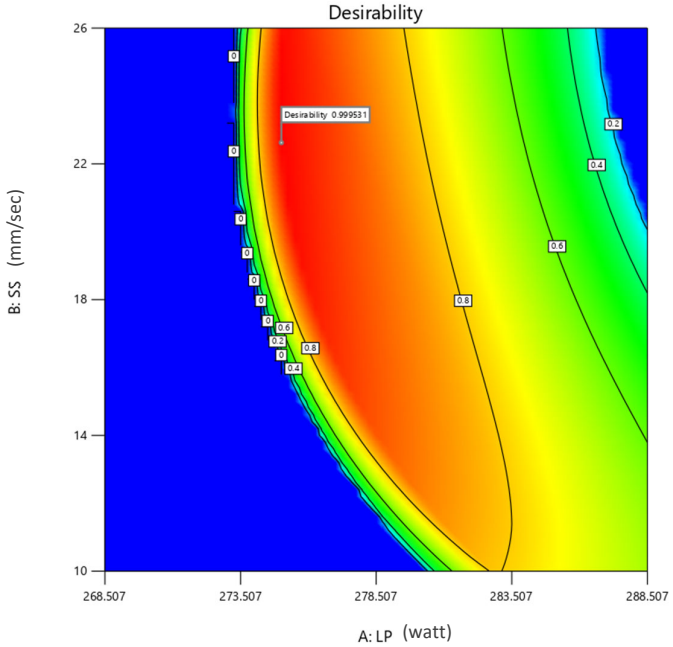

Fig. 7.57. Contour plot of desirability for LP & SS on multi-objective optimization

From these optimized results, parameters are chosen for preparation of tensile test samples. As laser power has the highest influence on responses, only this is changed in a certain range keeping all other parameters at constant optimized value as shown in Table 7.14. Also, the tensile test samples are shown in Fig. 7.58. These samples are also used to carry out the validation check of the mathematical model.

Table 7.15. Parameters for tensile test samples and validation check

Exp. No.	LP (Watt)	SS (mm/sec)	DF (mm)	N --	GP (bar)	FZ (µm)	Cu HAZ (µm)	SS HAZ (µm)
T1	265	22.6	4.6	8	2	465.233	620.474	762.261
T2	270	22.6	4.6	8	2	480.106	652.824	779.77
T3	275	22.6	4.6	8	2	494.642	688.182	800.37
T4	280	22.6	4.6	8	2	508.839	726.548	824.061
T5	285	22.6	4.6	8	2	522.697	767.921	850.843

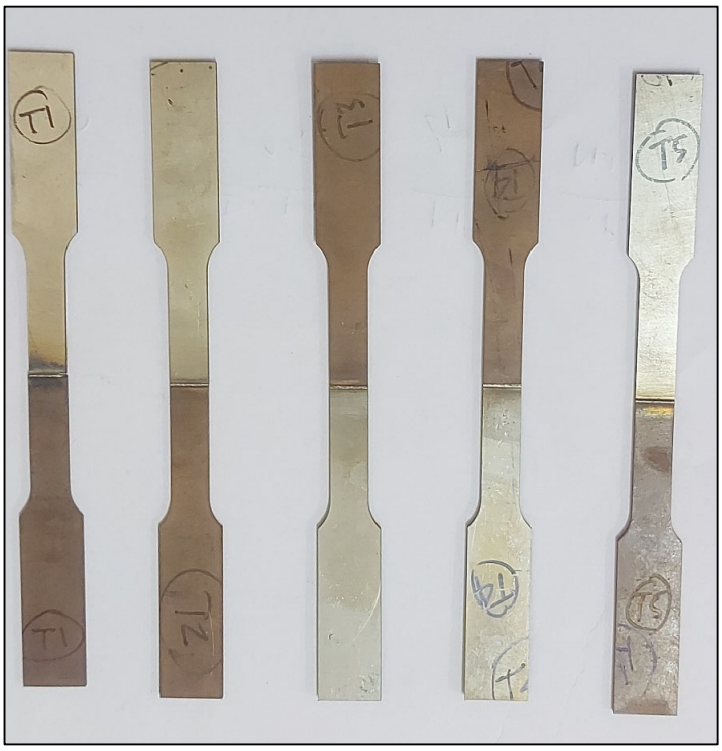

Fig. 7.58. Tensile test samples

7.4.2. Optimization using PSO, TLBO & GWO

7.4.2.1. Single objective optimization

Given that this is the range where the welding is found to be most reliable, the lower and upper boundaries of the [LP, SS, DF, N, GP] population space are assigned as [260, 14, 4, 7, 1.5] and [290, 22, 6, 11, 2], respectively. The algorithm is run through 100 iterations with a population size of 100.

1) PSO

The FZ is chosen as the fitness function to be maximised in order to produce the Maximum Fusion Zone (FZ) utilising the regression equation. For the following parameters: LP = 280 W, SS = 14 mm/sec, DF = 5.07 mm, N = 9, GP = 1.5 bar, and the maximum fusion zone is 511.64 µm, the optimum solution has been found. The fitness vs. iteration curve in Fig. 7.59 quickly converged after the 10^{th} iteration and became saturated over the 22^{nd} iterations to obtain the best fitness value, which is the maximum fusion zone.

Using the regression equation, the Cu HAZ is chosen as the fitness function to be minimised in order to obtain the Minimum Heat Affected Zone of Copper (Cu HAZ). The optimum solution has been established for the following parameters: LP = 260 W, SS = 20 mm/sec, DF = 6 mm, N = 9, GP = 1.62 bar, and the smallest heat affected zone is 418.14 µm. The fitness vs. iteration curve in Fig. 7.60 converged promptly after the 16^{th} iteration and got saturated over the 23^{rd} iterations to produce the best fitness value, which is the minimum heat affected zone.

The SS HAZ is chosen as the fitness function to be minimised using the regression equation in order to achieve the Minimum Heat Affected Zone of SS (SS HAZ). The best solution has been found for the following parameters: The LP is 260 W, the SS is 20 mm/sec, the DF is 6 mm, the N is 9, the GP is 1.80 bar, and the smallest heat affected zone is 698.55 µm. The fitness vs. iteration curve in Fig. 7.61 converged quickly after the 25^{th} iteration and became saturated during the 33^{rd} iteration to produce the ideal fitness value, which is the least heat affected zone.

2) TLBO

The FZ is chosen as the fitness function to be maximised in order to produce the Maximum Fusion Zone (FZ) utilising the regression equation. For the following parameters: LP = 280 W, SS = 14 mm/sec, DF = 4 mm, N = 7, GP = 1.5 bar, and the maximum fusion zone is 520.48 µm, the optimum solution has been found. The fitness vs. iteration curve in Fig. 7.59 quickly converged after the 8^{th} iteration and became saturated over the 24^{th} iterations to obtain the best fitness value, which is the maximum fusion zone.

Using the regression equation, the Cu HAZ is chosen as the fitness function to be minimised in order to obtain the Minimum Heat Affected Zone of Copper (Cu HAZ). The optimum solution has been established for the following parameters: LP = 265 W, SS = 21 mm/sec, DF = 6 mm, N = 7, GP = 1.5 bar, and the smallest heat affected zone is 410.10 µm. The fitness vs. iteration curve in Fig. 7.60 got saturated over the 5^{th} iterations to produce the best fitness value, which is the minimum heat affected zone.

The SS HAZ is chosen as the fitness function to be minimised using the regression equation in order to achieve the Minimum Heat Affected Zone of SS (SS HAZ). The best solution has been found for the following parameters: The LP is 265 W, the SS is 18 mm/sec, the DF is 7 mm, the N is 7, the GP is 1.75 bar, and the smallest heat affected zone is 689.11 µm. The fitness vs. iteration curve in Fig. 7.61 became saturated during the 4^{th} iteration to produce the ideal fitness value, which is the least heat affected zone.

3) GWO

The FZ is chosen as the fitness function to be maximised in order to produce the Maximum Fusion Zone (FZ) utilising the regression equation. For the following parameters: LP = 280 W, SS = 22 mm/sec, DF = 4 mm, N = 7, GP = 2 bar, and the maximum fusion zone is 538.51 µm, the optimum solution has been found. The fitness vs. iteration curve in Fig. 7.59 quickly became saturated over the 8^{th} iterations to obtain the best fitness value, which is the maximum fusion zone.

Using the regression equation, the Cu HAZ is chosen as the fitness function to be minimised in order to obtain the Minimum Heat Affected Zone of Copper (Cu HAZ). The optimum solution has been established for the following parameters: LP = 265 W, SS = 14 mm/sec, DF = 4 mm, N = 11, GP = 2 bar, and the smallest heat affected zone is 474.87 µm. The fitness vs. iteration curve in Fig. 7.60 got saturated over the 7th iterations to produce the best fitness value, which is the minimum heat affected zone.

The SS HAZ is chosen as the fitness function to be minimised using the regression equation in order to achieve the Minimum Heat Affected Zone of SS (SS HAZ). The best solution has been found for the following parameters: The LP is 270 W, the SS is 20 mm/sec, the DF is 6 mm, the N is 7, the GP is 1.75 bar, and the smallest heat affected zone is 695.09 µm. The fitness vs. iteration curve in Fig. 7.61 became saturated during the 9th iteration to produce the ideal fitness value, which is the least heat affected zone.

7.4.2.2. Multi-objective optimization

The multi-objective function developed for this purpose is:

$$Min(Y) = -w_1 \times \frac{FZ}{FZ_{max}} + w_2 \times \frac{Cu\ HAZ}{Cu\ HAZ_{min}} + w_3 \times \frac{SS\ HAZ}{SS\ HAZ_{min}}$$

Here, w1, w2 and w3 all are taken as the weightage to each objective maximization of FZ and minimization of Cu HAZ & SS HAZ respectively. All objectives are given same weightage (w1 = w2 = w3 = $\frac{1}{3}$) as all are equally important.

Given that this is the range where the welding is found to be most reliable, the lower and upper boundaries of the [LP, SS, DF, N, GP] population space are assigned as [260, 14, 4, 7, 1.5] and [290, 22, 6, 11, 2], respectively. The algorithm is run through 100 iterations with a population size of 100.

1) PSO

The FZ is chosen as the fitness function to be maximised in order to produce the Maximum Fusion Zone (FZ), Cu HAZ and SS HAZ chosen as fitness function to be minimized in order to produce minimum heat affected zones utilising the regression equation. For the following

parameters: LP = 275 W, SS = 17.05 mm/sec, DF = 4 mm, N = 10.35 ≈ 10, GP = 2 bar, and the maximum fusion zone is 489.64 µm, minimum Cu HAZ is 569.66 µm and minimum SS HAZ is 909.22 µm, the optimum solution has been found.

2) TLBO

The FZ is chosen as the fitness function to be maximised in order to produce the Maximum Fusion Zone (FZ), Cu HAZ and SS HAZ chosen as fitness function to be minimized in order to produce minimum heat affected zones utilising the regression equation. For the following parameters: LP = 277 W, SS = 18 mm/sec, DF = 4 mm, N = 10, GP = 2 bar, and the maximum fusion zone is 497.32 µm, minimum Cu HAZ is 569.66 µm and minimum SS HAZ is 909.22 µm, the optimum solution has been found.

3) GWO

The FZ is chosen as the fitness function to be maximised in order to produce the Maximum Fusion Zone (FZ), Cu HAZ and SS HAZ chosen as fitness function to be minimized in order to produce minimum heat affected zones utilising the regression equation. For the following parameters: LP = 275 W, SS = 17.03 mm/sec, DF = 4 mm, N = 10.34 ≈ 10, GP = 2 bar, and the maximum fusion zone is 489.58 µm, minimum Cu HAZ is 569.43 µm and minimum SS HAZ is 909.54 µm, the optimum solution has been found.

Fig. 7.62 depicts the comparison of three optimization algorithms PSO, TLBO and GWO used in single objective optimization of responses i.e., maximize FZ, minimize Cu HAZ & SS HAZ. It is observed that GWO predicts the maximum FZ among three and TLBO gives the minimum Cu HAZ and SS HAZ. PSO predicts very close to the optimum values for all three responses. Also, GWO predicts well for minimum SS HAZ but deviates in case of Cu HAZ.

In case of multi-objective optimization as shown in Fig. 7.63, PSO and GWO gives almost same optimal values, whereas TLBO gives the best results when it comes to maximizing FZ and minimizing SS HAZ. But Cu HAZ is slightly more in case of TLBO w.r.t. PSO & GWO which can be ignored.

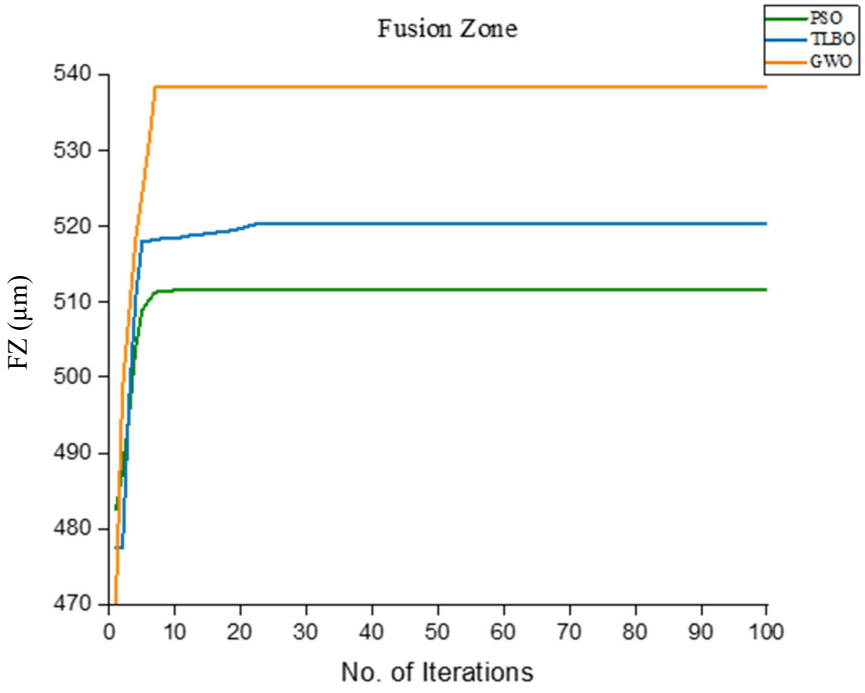

Fig. 7.59. Convergence diagram of max. FZ vs iteration for PSO, TLBO and GWO

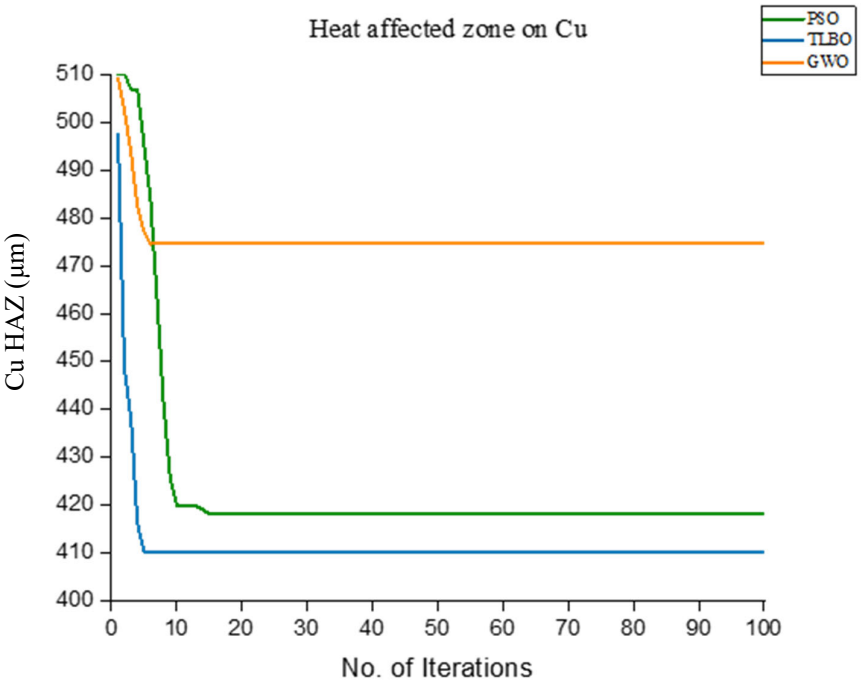

Fig. 7.60. Convergence diagram of min. Cu HAZ vs iteration for PSO, TLBO and GWO

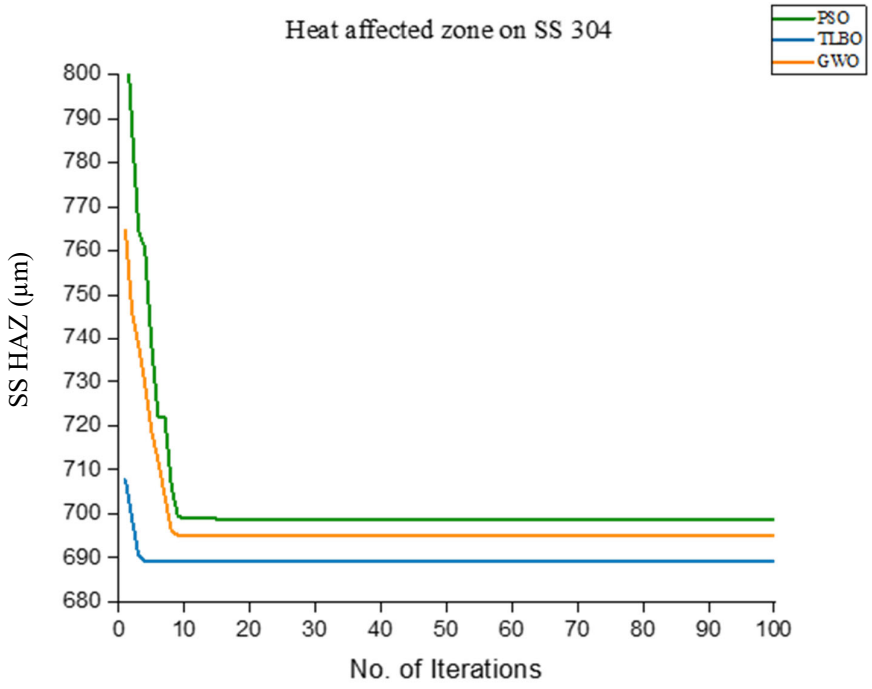

Fig. 7.61. Convergence diagram of min. SS HAZ vs iteration for PSO, TLBO and GWO

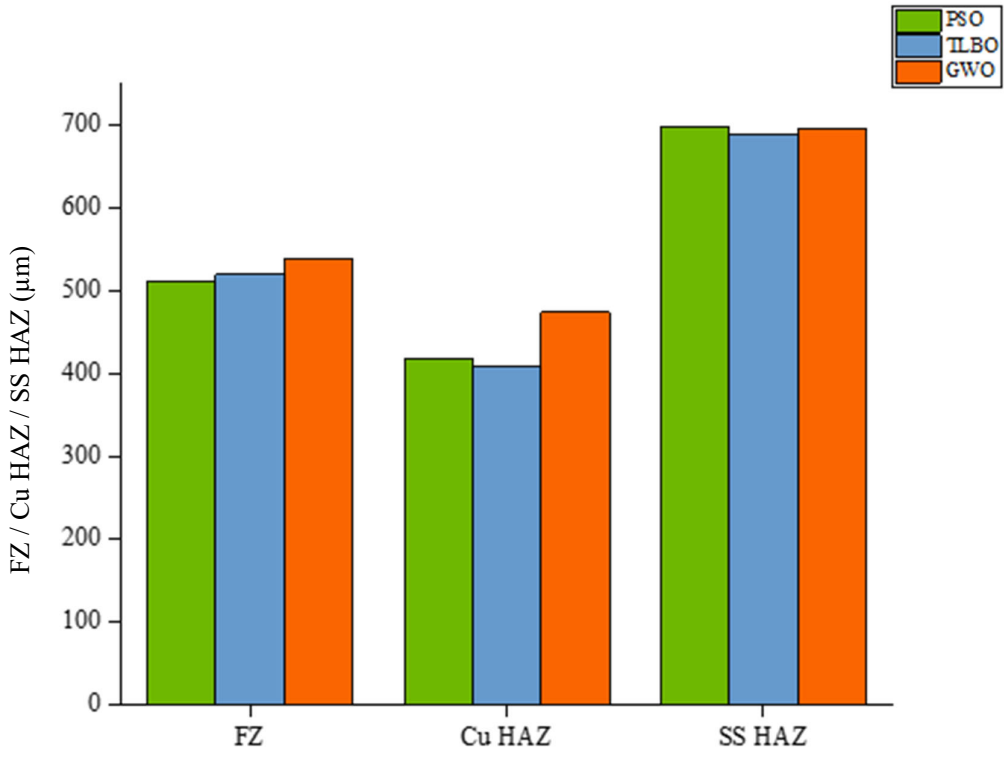

Fig. 7.62. Comparison of PSO, TLBO and GWO w.r.t. single objective optimization of FZ, Cu HAZ and SS HAZ

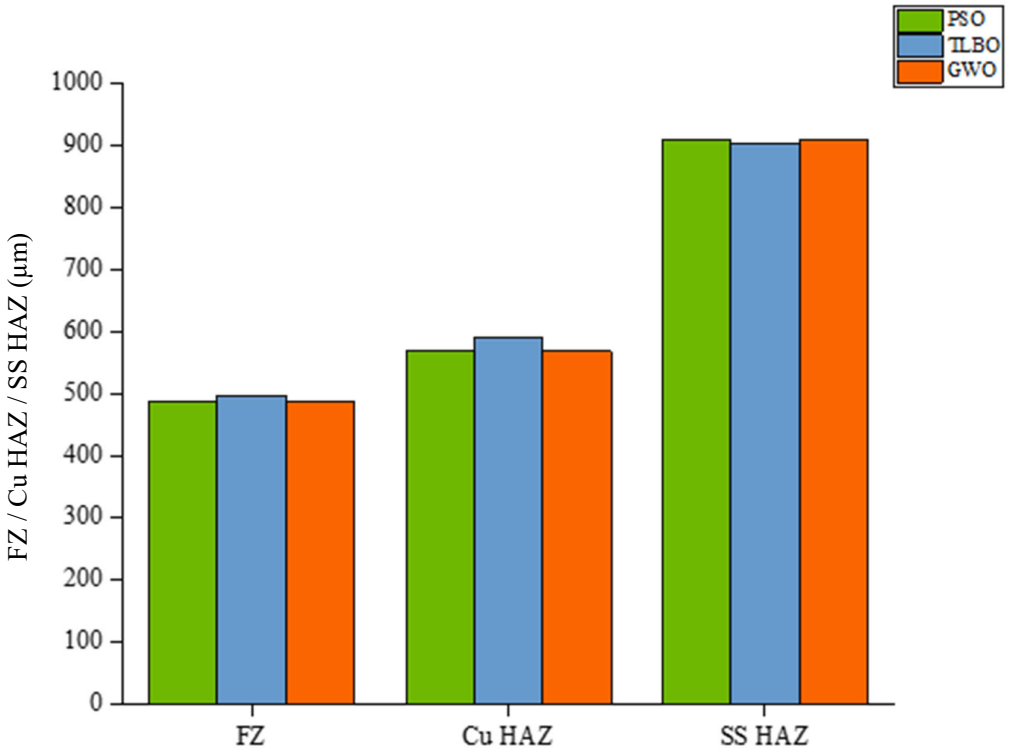

Fig. 7.63. Comparison of PSO, TLBO and GWO w.r.t. multi-objective optimization of FZ, Cu HAZ and SS HAZ

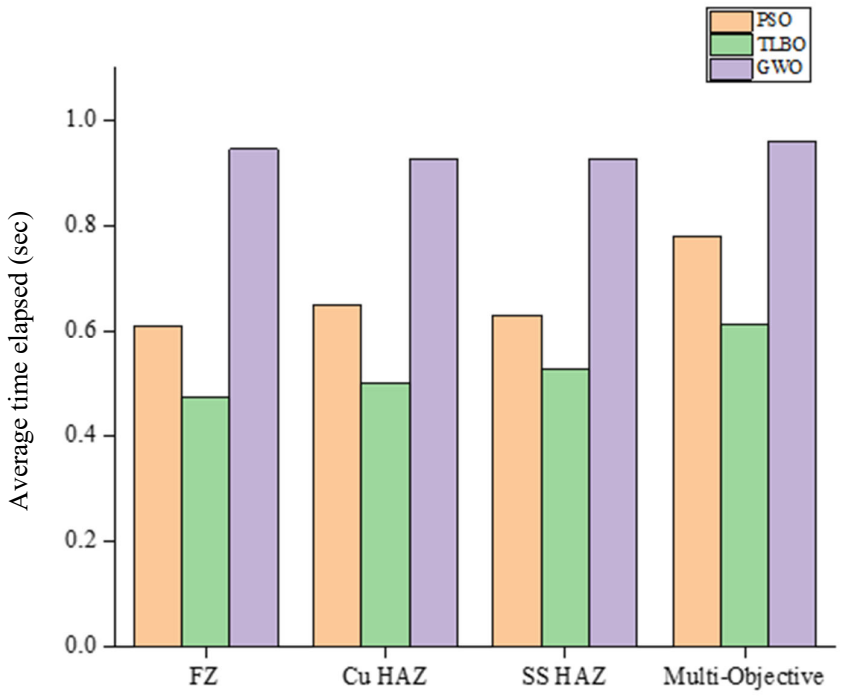

Fig. 7.64. Comparison of PSO, TLBO and GWO w.r.t. average time elapsed for optimization

Table 7.16. Comparison of PSO, TLBO & GWO w.r.t. optimal values obtained

Algorithm	Max. FZ (µm)	Min. Cu HAZ (µm)	Min. SS HAZ (µm)	Multi-objective		
				Max. FZ (µm)	Min. Cu HAZ (µm)	Min. SS HAZ (µm)
PSO	511.64	418.14	698.55	489.64	569.66	909.22
TLBO	520.48	410.10	689.11	497.32	590.46	902.76
GWO	538.51	474.87	695.09	489.58	569.43	909.54

Table 7.17. Comparison of PSO, TLBO & GWO w.r.t. average time elapsed for optimization

Algorithm	FZ	Cu HAZ	SS HAZ	Multi-objective
PSO	0.610437	0.651227	0.631636	0.781298
TLBO	0.473596	0.499395	0.527073	0.613576
GWO	1.245939	1.281887	1.272548	1.316256

The comparison of three algorithms i.e., PSO, TLBO & GWO with respect to optimal results obtained in single & multi-objective optimization and average time elapsed to perform these optimization runs in MATLAB R2021a is shown in tabular form in Table. 7.16 and Table 7.17.

Fig. 7.64 shows the average time elapsed during the 100 iterations performed for all three-optimization algorithm along with multi-objective optimization using these. Average time taken by TLBO is minimum for all the cases and for GWO is maximum. PSO lies in between them. Therefore, according to optimization performance and average time elapsed, TLBO is best suited for our purpose followed by PSO and GWO.

CHAPTER 8

CONCLUSION & FUTURE SCOPE

8.1. Conclusion

In this study, laser beam welding of 1 mm thick dissimilar materials, Cu and SS 304 in butt configuration, is performed using a continuous wave fibre laser under various welding conditions to investigate the effect of process parameters on weld bead geometry, i.e., FZ and HAZ of both metals. The statistical DOE using ANOVA response surface methodology is used to find the most significant process parameters and their percentage contribution to output responses. To plot their individual and combined effect, a regression equation is used. Following that, a few validation experiments are carried out at selected points in the study of desirability function-based optimization within the range of process parameters. The process parameters are optimized to obtain a certain targeted width of FZ as well as minimal HAZ of Cu & SS in a practically specified range for producing necessary welding strength. The following conclusions can be reached from research:

1. A 500 W CW Fiber laser was used to successfully perform laser butt welding of 1 mm thick Cu and SS 304. Smooth, uniform, and acceptable micropore sizes, as well as a gleaming bead with no spatters and a crack-free weld bead, have all been achieved.

2. Weld defects were greatly decreased in an adequate shielding gas environment with optimal process parameter selection. Using response surface methods, an empirical mathematical model was built between major laser welding process parameters and weld quality attributes.

3. ANOVA results shows that laser power has highest impact on fusion zone width followed by defocus distance, scanning speed, number of passes and gas pressure. Laser power has positive impact on fusion zone width, but all other parameters are having negative impact. The fusion zone has been found to be 494.999 μm, which is close to the intended value (495 μm). It is achieved at optimal process parameters, LP of 268.726 ≈ 269 W, SS of 19.762 mm/sec, DF of 3.5 mm, N of 9.491 ≈ 9 and GP of 1.985 ≈ 2 bar using single objective DFA based optimization method.

4. According to ANOVA results, laser power has the greatest impact on copper heat affected zone width, followed by scanning speed and laser beam defocusing distance. The impact of laser power, number of passes, and gas pressure on Cu HAZ width is positive, whereas scanning speed and defocus distance are negative. Minimum copper heat affected zone of 423.656 μm inside a reasonable range is achieved at optimal process parameters, LP of 269.832 ≈ 270 W, SS of 14.87 mm/sec, DF of 3.766 mm, N of 11.8 ≈ 12 and GP of 2.115 ≈ 2.1 bar using single objective DFA based optimization method.

5. According to the ANOVA results, laser power has the highest influence on the size of the stainless-steel heat affected zone, followed by scanning speed, laser beam defocusing distance, and gas pressure. Laser power and number of passes have a positive effect on SS HAZ width, but scanning speed, defocus distance, and gas pressure all have a negative effect. At optimal process parameters, LP of 261.877 ≈ 262 W, SS of 23.557 mm/sec, DF of 4.774 mm, N of 8.736 ≈ 9 and GP of 1.896 ≈ 1.9 bar, a minimum stainless-steel heat affected zone of 704.809 μm within a feasible range is reached utilizing a single objective DFA based optimization technique.

6. Targeted fusion zone has been found to be 494.999 μm. Cu HAZ value is 690.166 μm and SS HAZ is 800.899 μm which are also minimum inside a specified range. Optimal process parameters, LP of 275.01 ≈ 275 W, SS of 22.626 mm/sec, DF of 4.598 mm, N of 7.99 ≈ 8 and GP of 2.001 ≈ 2 bar using multi objective DFA based optimization method.

7. PSO, TLBO and GWO algorithms are used to compare the compatibility of GA in optimization of process parameters. GA gave very close and similar results to the desirability-based optimization. According to optimization performance and average time elapsed the best suitable algorithm is as follows: TLBO > PSO > GWO.

8. Using the optimal process parameters of multi-objective optimization, a total 5 sets of experiments are conducted and samples for tensile test are made.

8.2. Future scope

In the future, more emphasis should be placed on the development of more efficient technologies for the manufacturing of inexpensive but complex dissimilar junctions of metals such as Cu and SS 304. More research should be done in this field, which is still unexplored in many aspects for diverse and numerous vital uses, particularly welding, which has a promising future in many industrial-based domains with significant applications such as fuel lines, brake systems, and electrical connections in the automotive industry, refrigeration units, aircraft components, missile systems, space vehicles, electrical transmission systems, electronic components, and many more.

1. More methodologies and types of lasers should be used to directly join Cu and SS without any interlayer.

2. To ensure the strength of the welded joint tensile testing and micro-hardness tests have to be carried out using the samples prepared.

3. Future advancements can explore welding of high-strength copper alloys and high-alloy steels. Understanding the metallurgical interactions using X-ray diffraction (XRD) and optimizing the process parameters to reduce formation of brittle IMCs for these materials will open up new applications and industries.

4. More advancements in FEM modelling and simulation using software like ANSYS or ABAQUS will emphasize the results obtained from experiments.

5. Innovations in joint design and geometry can enhance the effectiveness of laser welding for copper and steel. Researchers can explore new joint configurations, such as lap joints, butt joints, or T-joints, to improve the strength and durability of the welds. Additionally, investigating the impact of different surface preparations, such as coatings, pre-treatments or pre-heats, can lead to improved bonding between copper and steel. Also, effect of clamping pressure to restrict thermal expansion can also be studied.

6. Various Machine Learning methods like Artificial Neural Network (ANN) can be used to create the mathematical model and analyse it.

REFERENCES

[1] K. Shimoda, *Introduction to laser physics*. 2013.

[2] Y. Yang, S. L.-J. of M. P. Technology, and undefined 1999, "A study on the joining strength of laser spot welding for automotive applications," *Elsevier*.

[3] S. P.-B. dental journal and undefined 2007, "Introduction, history of lasers and laser light production," *nature.com*.

[4] "Trends in welding research : proceedings of the 5th International Conference, Pine Mountain, Georgia, USA, June 1-5, 1998 | WorldCat.org.".

[5] S. C. Singh, H. Zeng, C. Guo, and W. Cai, "Nanomaterials: Processing and Characterization with Lasers," *Nanomaterials: Processing and Characterization with Lasers*, Aug. 2012, doi: 10.1002/9783527646821.

[6] L. C. preprint arXiv:2008.03940 and undefined 2020, "Introduction to Laser Physics," *arxiv.org*.

[7] S. Katayama, *S. Katayama, Very easy book of laser processing*.

[8] S. Katayama, *Fundamentals and details of laser welding*. 2020.

[9] A. Weld Tech Inc, "Laser Welding Fundamentals."

[10] F. I. Hussein *et al.*, "Evaluation of PMMA joining to stainless steel 304 using pulsed Nd:YAG laser," *Opt Laser Technol*, vol. 49, pp. 143–152, Jul. 2013, doi: 10.1016/J.OPTLASTEC.2012.12.028.

[11] "Conduction and Keyhole Welding | EB Industries." https://ebindustries.com/conduction-mode-and-keyhole-mode-welding/ (accessed May 14, 2023).

[12] "Laser Welding Fundamentals – Laser Chirp." https://www.laserchirp.com/2016/07/laser-welding-fundamentals/ (accessed May 14, 2023).

[13] "Laser Plastic Welding Procedures | LPKF." https://www.lpkf.com/en/industries-technologies/laser-plastic-welding/technology-welding-procedures/ (accessed May 16, 2023).

[14] S. Chiang and C. E. Albright, "The Effect of Welding Parameters on the Mechanical Properties of Stainless Steel," *Weld J*, vol. 72, no. 3, pp. 117–121, 1993.

[15] C. Limmaneevichitr and S. Kou, "Experiments to simulate effect of Marangoni convection on weld pool shape," *Welding Journal (Miami, Fla)*, vol. 79, pp. 231s–237s, Aug. 2000.

[16] P. Peças, Henrique, R. M. Miranda, and L. Quintino, "P. PEÇAS, M. HENRIQUE, R. M. MIRANDA E L. QUINTINO, 'Laser welding of low thickness zinc coated and

uncoated carbon steel sheets', Optical and Quantum Electronics, 27, 1995, 1193-1201 DOI: 10.1007/BF00326475," *Opt Quantum Electron*, vol. 27, pp. 1193–1201, Jan. 1995, doi: 10.1007/BF0032647.

[17] "Continuous Wave vs. Pulsed Laser Welding | EB Industries," *https://ebindustries.com/*, Accessed: May 16, 2023.

[18] C. Kumar, M. Das, C. P. Paul, and B. Singh, "Experimental investigation and metallographic characterization of fiber laser beam welding of Ti-6Al-4V alloy using response surface method," *Opt Lasers Eng*, vol. 95, pp. 52–68, Aug. 2017, doi: 10.1016/J.OPTLASENG.2017.03.013.

[19] K. Seiji, "Laser Welding," *JOURNAL OF THE JAPAN WELDING SOCIETY*, vol. 78, no. 2, pp. 124–138, 2009, doi: 10.2207/JJWS.78.124.

[20] Katayama and Seiji, "Recent progress in Laser Welding Technology," *JVSJ*, vol. 55, no. 11, pp. 471–480, 2012, doi: 10.3131/JVSJ2.55.471.

[21] E. L.-L. focus world and undefined 1998, "Carbon dioxide lasers deliver flexibility and power," *laserfocusworld.com*, Accessed: May 17, 2023.

[22] "Carbon Dioxide Laser Construction and Working, 5 Application, 5 Advantage, Disadvantages." https://physicswave.com/carbon-dioxide-laser-construction-and-working/ (accessed May 17, 2023).

[23] M. Yadegari, M. Asadian, H. Saeedi, … Y. K.-J. of crystal, and undefined 2013, "Formation of gaseous cavity defect during growth of Nd: YAG single crystals," *Elsevier*, Accessed: May 18, 2023.

[24] K. Semwal, S. B.-I. J. of Physics, and undefined 2013, "Study of Nd3+ ion as a dopant in YAG and glass laser," *researchgate.net*, vol. 1, no. 1, pp. 15–21, 2013, doi: 10.12691/ijp-1-1-3.

[25] W. Pfleging, "A review of laser electrode processing for development and manufacturing of lithium-ion batteries," *Nanophotonics*, vol. 7, no. 3, pp. 549–573, Dec. 2017, doi: 10.1515/NANOPH-2017-0044/HTML.

[26] Y. Chen *et al.*, "A review of lithium-ion battery safety concerns: The issues, strategies, and testing standards," *Elsevier*.

[27] L. Nong, C. Shao, T. Kim, S. H.-J. of M. Systems, and undefined 2018, "Improving process robustness in ultrasonic metal welding of lithium-ion batteries," *Elsevier*.

[28] S. Leuthner, "Lithium-ion battery overview," *Lithium-Ion Batteries: Basics and Applications*, pp. 13–19, Aug. 2018, doi: 10.1007/978-3-662-53071-9_2.

[29] R. Fish, L. G.- Eplasty, and undefined 2009, "Conduction of electrical current to and through the human body: a review," *ncbi.nlm.nih.gov*.

[30] M. Hamed, A. El-Tayeb, I. Moukhtar, … A. E. D.-R. in, and undefined 2022, "A review on recent key technologies of lithium-ion battery thermal management: External cooling systems," *Elsevier*.

[31] "Notes, E. (2020). Lithium-ion battery advantages." Electronic Notes Website (accessed May 18, 2023).

[32] G. Zubi, R. Dufo-López, … M. C.-… and S. E., and undefined 2018, "The lithium-ion battery: State of the art and future perspectives," *Elsevier*.

[33] "Diode Laser: The Most Versatile and Convenient Coherent Light Source." https://www.findlight.net/blog/diode-laser/ (accessed May 18, 2023).

[34] E. Snitzer, "Proposed fiber cavities for optical masers," *J Appl Phys*, vol. 32, no. 1, pp. 36–39, 1961, doi: 10.1063/1.1735955.

[35] "Fibre Lasers - Working Principles, Applications & More | Fractory." https://fractory.com/fibre-lasers-explained/ (accessed May 18, 2023).

[36] "Advantages and Disadvantages of Fiber Lasers – Laser News, Laser articles, Laser reviews." https://www.lucklaser.com/news/advantages-and-disadvantages-of-fiber-lasers-1384 (accessed May 19, 2023).

[37] H. Wandera Okumu, "CLEANING OF METAL SURFACES BY LASER IRRADIATION; MATHEMATICAL MODELING AND EXPERIMENTAL ANALYSIS," 2022.

[38] R. Brockmann and K. Mann, "Disk Lasers Enable Industrial Manufacturing – What Was Achieved and What Are the Limits?," *Laser Technik Journal*, vol. 4, no. 3, pp. 50–53, Jun. 2007, doi: 10.1002/LATJ.200790166.

[39] Z. Sun and J. C. Ion, "Laser welding of dissimilar metal combinations," *J Mater Sci*, vol. 30, no. 17, pp. 4205–4214, 1995, doi: 10.1007/BF00361499.

[40] A. M. El-Batahgy, "Effect of laser welding parameters on fusion zone shape and solidification structure of austenitic stainless steels," *Mater Lett*, vol. 32, no. 2–3, pp. 155–163, Aug. 1997, doi: 10.1016/S0167-577X(97)00023-2.

[41] H. Zhao, D. R. White, and T. DebRoy, "Current issues and problems in laser welding of automotive aluminium alloys," *International Materials Reviews*, vol. 44, no. 6, pp. 238–266, Jun. 1999, doi: 10.1179/095066099101528298.

[42] Y. F. Tzeng, "Parametric analysis of the pulsed Nd:YAG laser seam-welding process," *J Mater Process Technol*, vol. 102, no. 1–3, pp. 40–47, May 2000, doi: 10.1016/S0924-0136(00)00447-7.

[43] C. B. Reed, K. Natesan, Z. Xu, and D. L. Smith, "The effect of laser welding process parameters on the mechanical and microstructural properties of V–4Cr–4Ti structural materials," *Journal of Nuclear Materials*, vol. 283–287, no. PART II, pp. 1206–1209, Dec. 2000, doi: 10.1016/S0022-3115(00)00348-2.

[44] A. Hirose, K. F. Kobayashi, H. Yamaoka, and N. Kurosawa, "Evaluation of properties in laser welds of A6061-T6 aluminium alloy," *Welding International*, vol. 14, no. 6, pp. 431–438, 2000, doi: 10.1080/09507110009549207.

[45] F. Wagner, I. Zerner, M. Kreimeyer, T. Seefeld, and G. Sepold, "Characterization and properties of dissimilar metal combinations of Fe/Al and Ti/Al-sheet materials,"

International Congress on Applications of Lasers & Electro-Optics, vol. 2001, no. 1, pp. 365–374, Oct. 2001, doi: 10.2351/1.5059885.

[46] X. Cao, W. Wallace, C. Poon, and J.-P. Immarigeon, "Research and Progress in Laser Welding of Wrought Aluminum Alloys. I. Laser Welding Processes," *Materials and Manufacturing Processes*, vol. 18, no. 1, pp. 1–22, Jan. 2003, doi: 10.1081/AMP-120017586.

[47] E. M. Anawa and A. G. Olabi, "Optimization of tensile strength of ferritic/austenitic laser-welded components," *Opt Lasers Eng*, vol. 46, no. 8, pp. 571–577, 2008, doi: https://doi.org/10.1016/j.optlaseng.2008.04.014.

[48] M. Gao, X. Y. Zeng, B. Tan, and J. C. Feng, "Study of laser MIG hybrid welded AZ31 magnesium alloy," *Science and Technology of Welding and Joining*, vol. 14, no. 4, pp. 274–281, May 2009, doi: 10.1179/136217109X406929.

[49] G. Padmanaban and V. Balasubramanian, "Optimization of laser beam welding process parameters to attain maximum tensile strength in AZ31B magnesium alloy," *Opt Laser Technol*, vol. 42, no. 8, pp. 1253–1260, Nov. 2010, doi: 10.1016/J.OPTLASTEC.2010.03.019.

[50] M. J. Torkamany, S. Tahamtan, and J. Sabbaghzadeh, "Dissimilar welding of carbon steel to 5754 aluminum alloy by Nd:YAG pulsed laser," *Mater Des*, vol. 31, no. 1, pp. 458–465, Jan. 2010, doi: 10.1016/J.MATDES.2009.05.046.

[51] J. Yu, T. Jung, S. Kim, and S. Rhee, "Laser welding of cast iron and carburized steel for differential gear," *Journal of Mechanical Science and Technology*, vol. 25, no. 11, pp. 2887–2893, 2011, doi: 10.1007/s12206-011-0809-x.

[52] B. Acherjee, A. S. Kuar, S. Mitra, D. Misra, and S. Acharyya, "Experimental investigation on laser transmission welding of PMMA to ABS via response surface modeling," *Opt Laser Technol*, vol. 44, no. 5, pp. 1372–1383, 2012, doi: https://doi.org/10.1016/j.optlastec.2011.12.029.

[53] M. M. A. Khan, L. Romoli, and G. Dini, "Laser beam welding of dissimilar ferritic/martensitic stainless steels in a butt joint configuration," *Opt Laser Technol*, vol. 49, pp. 125–136, Jul. 2013, doi: 10.1016/J.OPTLASTEC.2012.12.025.

[54] K.-W. Jung, Y. Kawahito, M. Takahashi, and S. Katayama, "Laser direct joining of carbon fiber reinforced plastic to aluminum alloy," *J Laser Appl*, vol. 25, no. 3, p. 032003, Mar. 2013, doi: 10.2351/1.4794297.

[55] M. Naeem, A. Montello, and C. Rasmussen, "Experimental Studies of Fiber Laser Welding of a Range of Dissimilar Material Combinations," 2015.

[56] S. Meco, G. Pardal, S. Ganguly, S. Williams, and N. McPherson, "Application of laser in seam welding of dissimilar steel to aluminium joints for thick structural components," *Opt Lasers Eng*, vol. 67, pp. 22–30, Apr. 2015, doi: 10.1016/J.OPTLASENG.2014.10.006.

[57] R. S. Chopde, “Study on Laser beam Welding of Copper and Aluminum joint,” *IOSR Journal of Mechanical and Civil Engineering*, vol. 17, no. 10, pp. 65–74, Mar. 2017, doi: 10.9790/1684-17010056574.

[58] A. GMishra, D. Dixit, and A. K. Sharma, “Study on microstructural and mechanical properties of dissimilar joint of laser beam welded Inconel 625 and SS 316,” *International Journal of Advance Industrial Engineering*, vol. 6, no. 01, Apr. 2018, doi: 10.14741/IJAIE/V.6.1.2.

[59] E. M. Stanciu *et al.*, “Dissimilar Laser Welding of AISI 321 and AISI 1010,” *Tehnicki Vjesnik - Technical Gazette*, vol. 25, no. 2, pp. 344–350, Apr. 2018.

[60] B. R. Moharana, S. K. Sahu, A. Maiti, S. K. Sahoo, and T. K. Moharana, “An experimental study on joining of AISI 304 SS to Cu by Nd-YAG laser welding process,” *Mater Today Proc*, vol. 33, pp. 5262–5268, Jan. 2020, doi: 10.1016/J.MATPR.2020.02.953.

[61] Y. Zhang, Y. K. Chen, D. S. Yu, D. Q. Sun, and H. M. Li, “A review paper on effect of the welding process of ceramics and metals,” *Journal of Materials Research and Technology*, vol. 9, no. 6, pp. 16214–16236, Nov. 2020, doi: 10.1016/J.JMRT.2020.11.088.

[62] D. Franco, J. P. Oliveira, T. G. Santos, and R. M. Miranda, “Analysis of copper sheets welded by fiber laser with beam oscillation,” *Opt Laser Technol*, vol. 133, p. 106563, Jan. 2021, doi: 10.1016/J.OPTLASTEC.2020.106563.

[63] Y. Zhang, Y. K. Chen, J. P. Zhou, D. Q. Sun, and H. M. Li, “Laser welding-brazing of alumina to 304 stainless steel with an Ag-based filler material,” *Metallurgical Research & Technology*, vol. 118, no. 1, p. 104, 2021, doi: 10.1051/METAL/2020086.

[64] H. Xia *et al.*, “Influence of laser welding power on steel/CFRP lap joint fracture behaviors,” *Compos Struct*, vol. 285, p. 115247, Apr. 2022, doi: 10.1016/J.COMPSTRUCT.2022.115247.

[65] E. Pérez Zapico, A. Ascari, V. Dimatteo, and A. Fortunato, “Laser dissimilar welding of copper and steel thin sheets for battery production,” *J Laser Appl*, vol. 33, no. 1, p. 012016, Feb. 2021, doi: 10.2351/7.0000309.

[66] K. Antony and T. R. Rakeshnath, “Dissimilar laser welding of commercially pure copper and stainless steel 316L,” in *Materials Today: Proceedings*, Elsevier Ltd, 2019, pp. 369–372. doi: 10.1016/j.matpr.2019.12.043.

[67] S. Chen, J. Huang, J. Xia, X. Zhao, and S. Lin, “Influence of processing parameters on the characteristics of stainless steel/copper laser welding,” *J Mater Process Technol*, vol. 222, pp. 43–51, 2015, doi: 10.1016/j.jmatprotec.2015.03.003.

[68] Y. Y. Chuang, R. Schmid, and Y. A. Chang, “Thermodynamic analysis of the iron-copper system I: The stable and metastable phase equilibria,” *Metallurgical Transactions A*, vol. 15, no. 10, pp. 1921–1930, Oct. 1984, doi: 10.1007/BF02664905/METRICS.

[69] Z. Gao, Y. Yang, L. Wang, B. Zhou, and F. Yan, "Formation Mechanism and Control of Solidification Cracking in Laser-Welded Joints of Steel/Copper Dissimilar Metals," *Metals 2022, Vol. 12, Page 1147*, vol. 12, no. 7, p. 1147, Jul. 2022, doi: 10.3390/MET12071147.

[70] A. Mannucci, I. Tomashchuk, V. Vignal, P. Sallamand, and M. Duband, "Parametric study of laser welding of copper to austenitic stainless steel," *Procedia CIRP*, vol. 74, pp. 450–455, Jan. 2018, doi: 10.1016/J.PROCIR.2018.08.160.

[71] Y. Huang, X. Gao, B. Ma, and Y. Zhang, "Interface Formation and Bonding Mechanisms of Laser Welding of PMMA Plastic and 304 Austenitic Stainless Steel," *Metals 2021, Vol. 11, Page 1495*, vol. 11, no. 9, p. 1495, Sep. 2021, doi: 10.3390/MET11091495.

[72] K. Lingadurai, B. Nagasivamuni, M. Muthu Kamatchi, and J. Palavesam, "Selection of Wire Electrical Discharge Machining Process Parameters on Stainless Steel AISI Grade-304 using Design of Experiments Approach," *Journal of The Institution of Engineers (India): Series C*, vol. 93, no. 2, pp. 163–170, Jun. 2012, doi: 10.1007/s40032-012-0020-6.

[73] İ. Ay and S. Çelik, "COMPARISON OF PROPERTIES OF FRICTION AND DIFFUSION WELDED JOINTS MADE BETWEEN THE PURE ALUMINIUM AND COPPER BARS Micro-Computed Tomography based modelling for composites View project COMPARISON OF PROPERTIES OF FRICTION AND DIFFUSION WELDED JOINTS MADE BETWEEN THE PURE ALUMINIUM AND COPPER BARS," 1999.

[74] F. J. Pontes, M. B. Silva, J. R. Ferreira, A. P. De Paiva, P. P. Balestrassi, and G. B. Schönhorst, "A DOE based approach for the design of RBF artificial neural networks applied to prediction of surface roughness in AISI 52100 hardened steel turning," *Journal of the Brazilian Society of Mechanical Sciences and Engineering*, vol. 32, no. 5 SPEC. ISSUE, pp. 503–510, 2010, doi: 10.1590/s1678-58782010000500010.

[75] J. D. Kechagias and N. Vidakis, "Parametric optimization of material extrusion 3D printing process: an assessment of Box-Behnken vs. full-factorial experimental approach," *International Journal of Advanced Manufacturing Technology*, vol. 121, no. 5–6, pp. 3163–3172, Jul. 2022, doi: 10.1007/S00170-022-09532-2.

[76] J. Kennedy and R. Eberhart, "Particle swarm optimization," *Proceedings of ICNN'95 - International Conference on Neural Networks*, vol. 4, pp. 1942–1948, doi: 10.1109/ICNN.1995.488968.

[77] R. V. Rao, V. J. Savsani, and D. P. Vakharia, "Teaching–learning-based optimization: A novel method for constrained mechanical design optimization problems," *Computer-Aided Design*, vol. 43, no. 3, pp. 303–315, Mar. 2011, doi: 10.1016/J.CAD.2010.12.015.

[78] S. Mirjalili, S. M. Mirjalili, and A. Lewis, "Grey Wolf Optimizer," *Advances in Engineering Software*, vol. 69, pp. 46–61, Mar. 2014, doi: 10.1016/J.ADVENGSOFT.2013.12.007.